



UNIVERSITAT  
POLITÈCNICA  
DE VALÈNCIA

---

# Multi-objective Control on Inverter-based Microgrids

Valencia, February 2024

---

Author: Óscar Gonzales-Zurita

Director: Guillermo Escrivá Escrivá

Codirector: Jean-Michel Clairand



# Acknowledgements

Firstly, I express my deepest gratitude to Dr. Guillermo Escrivá Escrivá, my esteemed thesis director, and Dr. Jean-Michel Clairand, my invaluable thesis codirector. Their help and guidance were crucial throughout this difficult journey filled with many challenges. I always felt their unwavering support. With their valuable knowledge, experience, and advice, they encouraged me to achieve one of my personal goals: achieving a doctoral degree.

During the challenging process of publication, I was fortunate to receive invaluable assistance from Dr. Oscar Lasso Andino. His unwavering support to guide me through various uncertainties greatly improved my publication. I extend my heartfelt gratitude for his outstanding cooperation and mentorship.

Thanks to Dr. José Manuel Aller Castro from Universidad Politécnica Salesiana, Dr. Damià Gomila Villalonga from Universitat de les Illes Balears, and Dr. Mattia Ricco from Università di Bologna for serving as thesis reviewers. Their feedback was invaluable and significantly enhanced the quality of the final version of my doctoral thesis.

I extend my gratitude to Dr. Carlos Roldán Porta from Universitat Politècnica de València, as well as Dr. Damià Gomila Villalonga and Dr. Pere Colet Rafecas from Universitat de les Illes Balears, for agreeing to serve on the thesis defense committee. Without a doubt, their insights following the doctoral defense have greatly contributed to my professional growth.

---

I want to express my gratitude to Universidad de las Américas for their willingness to fund the implementation of a microgrid as part of the process of my doctoral thesis.

Finally, I want to extend my deepest gratitude to my family. To my parents for their support; to my wife, Verónica, and my son, Santiago, who were the main motivation to fulfill this great dream.

# Abstract

The increasing use of fossil fuels for energy generation has contributed significantly to the global warming crisis. Different places far from electrical infrastructure employ oil-based generators that increase environmental contamination. In this context, the massive introduction of microgrids into society has brought opportunities for distributed energy generation, benefiting people worldwide. For example, microgrids can provide electricity to those vulnerable populations living in remote areas with limited access to transmission and distribution infrastructures. Additionally, microgrids promote renewable resources, reducing the environmental impact compared to traditional electricity generation methods like thermal power plants or nuclear facilities. Moreover, microgrids enable small-scale electricity generation, allowing families to achieve energy independence and sell excess energy to the local power company.

Various benefits have been analyzed concerning the widespread implementation of microgrids. However, this adoption has also brought about some associated problems. For instance, efficient energy management is crucial in regions with limited energy resources. Microgrids manage energy through devices called inverters, which operate using traditional closed-loop regulation algorithms such as the proportional-integral (PI) control. It has been demonstrated that the PI control has several disadvantages compared to newer control proposals. These drawbacks include instability under certain operating conditions, loss of precision in non-linear operating regions, and difficulties in tuning the algorithm properly, leading to increased time delays in response or decreased accuracy in tracking the steady-state reference operation.

---

One promising approach to address the closed-loop energy management problems in microgrids is the utilization of multi-objective control algorithms. These algorithms enable the simultaneous optimization of multiple objectives, such as minimizing power loss, maximizing efficiency, and ensuring voltage stability. Implementing such algorithms in microgrid inverters can significantly improve the energy management system. This thesis explores how multi-objective control algorithms implemented in microgrid inverters can improve energy management problems, ensuring more efficient and sustainable operations.

The application of multi-objective techniques to microgrid inverters can yield several benefits. For instance, optimizing conflicting objectives like rise time reduction and overshoot minimization can significantly enhance the voltage signal output from the inverter. This optimization improves system performance, stability, and reliability, ultimately contributing to more efficient energy management within microgrids.

Any inverter in a microgrid needs a control algorithm to perform closed-loop regulation. In this context, the second-order sliding mode control is a robust control strategy that has gained attention in microgrid inverter applications. Using this approach, the inverter can achieve precise and fast control, even in the presence of uncertainties and disturbances. Using robust control strategies enhances the overall stability and performance of the microgrid system, ensuring optimal energy management. The tuning process is essential for closed-loop control algorithms because it modifies the controller response to achieve control objectives.

Particle Swarm Optimization (PSO) is an efficient optimization algorithm employed in closed-loop controllers that can effectively solve multi-objective problems formulated into a single cost function. The microgrid inverter's control parameters can be optimized using PSO to achieve desired objectives, efficiently tuning a control strategy. For sliding mode controllers, some tuning strategies are based on heuristic techniques. The single cost function solves various problems in a microgrid, but there are problems when different objectives in a process can not be improved simultaneously due to their conflicting relation.

The multi-objective algorithms employed in this thesis, such as Multi-Objective Genetic Algorithms (MOGA), Multi-Objective Differential Evolution (MODE), and Multi-Objective Artificial Sheep Algorithm (MOASA), have demonstrated their ability to enhance inverter performance by optimizing conflicting objectives. These algorithms can effectively balance objectives such as reducing rise

---

time and minimizing overshoot in the inverter output signal. Consequently, the overall performance and efficiency of microgrid inverters can be improved.

Integrating multi-objective control algorithms in microgrid inverters holds great potential for addressing energy management challenges and optimizing performance. Microgrid inverters can achieve enhanced stability, efficiency, and reliability using techniques like second-order sliding mode control and optimization algorithms such as PSO, MOGA, MODE, and MOASA. By adopting these approaches, there is a new methodology for a more sustainable and resilient energy future while mitigating the adverse effects of global warming caused by fossil fuel consumption in conventional power generation.





# Resumen

El aumento en el uso de combustibles fósiles para la generación de energía ha contribuido significativamente a la crisis del calentamiento global. Diferentes lugares alejados de la infraestructura eléctrica emplean generadores a base de gasolina que aumentan la contaminación ambiental. En este contexto, la introducción masiva de microrredes en la sociedad ha traído oportunidades para la generación de energía de forma distribuida, beneficiando a personas en todo el mundo. Por ejemplo, las microrredes pueden brindar electricidad a poblaciones vulnerables que viven en áreas remotas con acceso limitado a infraestructuras de transmisión y distribución. Además, las microrredes promueven el uso de recursos renovables, reduciendo el impacto ambiental en comparación con los métodos tradicionales de generación de electricidad, como las plantas de energía térmica o las instalaciones nucleares. Además, las microrredes permiten la generación de electricidad a pequeña escala, lo que permite que las familias logren la independencia energética y vendan el exceso de energía a la compañía eléctrica local.

Se han analizado diversos beneficios respecto a la amplia implementación de microrredes. Sin embargo, esta adopción también ha generado algunos problemas asociados. Por ejemplo, una gestión eficiente de la energía es crucial en regiones con recursos energéticos limitados. Las microrredes administran la energía a través de dispositivos llamados inversores, que operan mediante algoritmos tradicionales de regulación en lazo cerrado, como el control proporcional-integral (PI). Se ha demostrado que el control PI tiene varias desventajas en comparación con propuestas de control más recientes. Estos inconvenientes incluyen inestabilidad bajo ciertas condiciones de operación, pérdida de precisión

---

en regiones de trabajo no lineales y dificultades para sintonizar adecuadamente el algoritmo, lo que resulta en mayores retardos en el tiempo de respuesta o una menor precisión en el seguimiento del estado estable de la referencia de operación.

Un enfoque prometedor para abordar los problemas de gestión de energía en lazo cerrado en las microrredes es la utilización de algoritmos de control multiobjetivo. Estos algoritmos permiten la optimización simultánea de múltiples objetivos, como la minimización de pérdidas de potencia, la maximización de la eficiencia y la garantía de la estabilidad de voltaje. La implementación de dichos algoritmos en inversores de microrred puede mejorar significativamente el sistema de gestión de energía. Esta tesis explora cómo los algoritmos de control multiobjetivo implementados en inversores de microrred pueden mejorar los problemas de gestión de energía, garantizando operaciones más eficientes y sostenibles.

La aplicación de técnicas multi-objetivo a los inversores de las microrredes puede tener varios beneficios. Por ejemplo, optimizar objetivos conflictivos como la reducción del tiempo de respuesta y la minimización del sobrepico puede mejorar en gran medida la señal de voltaje de salida del inversor. Esta optimización mejora el rendimiento, la estabilidad y la confiabilidad del sistema, contribuyendo en última instancia a una gestión de energía más eficiente en las microrredes.

Cualquier inversor en una microrred necesita un algoritmo de control para realizar una regulación en bucle cerrado. En este contexto, el control por modos deslizantes de segundo orden es una estrategia de control robusta que ha ganado atención en las aplicaciones de inversores de microrredes. Mediante el uso de este enfoque, el inversor puede lograr un control preciso y rápido, incluso en presencia de incertidumbres y perturbaciones. El uso de estrategias de control robustas mejora la estabilidad y el rendimiento general del sistema de microrredes, asegurando una gestión de energía óptima. El proceso de ajuste es esencial para los algoritmos de control en bucle cerrado, ya que modifica la respuesta del controlador para alcanzar los objetivos de control.

La optimización por enjambre de partículas (PSO por sus siglas en inglés) es un eficiente algoritmo de optimización empleado en controladores en lazo cerrado que puede resolver de manera efectiva problemas multi-objetivo formulados en una sola función de costo. Los parámetros de control del inversor de la microrred pueden ser optimizados mediante la utilización de PSO para lograr los objetivos deseados, ajustando de manera eficiente una estrategia de control. Para controladores por modos deslizantes, algunas estrategias de

---

ajuste se basan en técnicas heurísticas. La función de costo única resuelve varios problemas en una microrred, pero existen dificultades cuando diferentes objetivos en un proceso no pueden ser mejorados simultáneamente debido a su relación conflictiva.

Estrategias como Algoritmos Genéticos Multi-Objetivo (MOGA por sus siglas en inglés), Evolución Diferencial Multi-Objetivo (MODE por sus siglas en inglés) y Algoritmo Artificial de Ovejas Multi-Objetivo (MOASA por sus siglas en inglés), han demostrado su capacidad para mejorar el rendimiento del inversor mediante la optimización de objetivos conflictivos. Estos algoritmos pueden equilibrar de manera efectiva objetivos como la reducción del tiempo de respuesta y la minimización del sobreimpulso en la señal de salida del inversor. En consecuencia, el rendimiento general y la eficiencia de los inversores de la microrred pueden mejorar.

La integración de algoritmos de control multi-objetivo en los inversores de la microrred tiene un gran potencial para abordar los desafíos de gestión de energía y optimizar el rendimiento. Los inversores de la microrred pueden lograr una mayor estabilidad, eficiencia y confiabilidad utilizando técnicas como el control por modos deslizantes de segundo orden y algoritmos de optimización como PSO, MOGA, MODE y MOASA. Al adoptar estos enfoques, se presenta una nueva metodología para un futuro energético más sostenible y resiliente, al tiempo que se mitigan los efectos adversos del calentamiento global causado por el consumo de combustibles fósiles en la generación convencional de energía.



# Resum

L'augment en l'ús de combustibles fòssils per a la generació d'energia ha contribuït significativament a la crisi de l'escalfament global. Diferents llocs allunyats de la infraestructura elèctrica empren generadors a base de gasolina que augmenten la contaminació ambiental. En aquest context, la introducció massiva de microrredes en la societat ha portat oportunitats per a la generació d'energia de forma distribuïda, beneficiant a persones arreu del món. Per exemple, les microrredes poden proporcionar electricitat a poblacions vulnerables que viuen en àrees remotes amb accés limitat a infraestructures de transmissió i distribució. A més, les microrredes promouen l'ús de recursos renovables, reduint l'impacte ambiental en comparació amb els mètodes tradicionals de generació d'electricitat, com les plantes de potència tèrmica o les instal·lacions nuclears. A més a més, les microrredes permeten la generació d'electricitat a petita escala, la qual cosa permet que les famílies aconseguisquen la independència energètica i venguen l'excés d'energia a la companyia elèctrica local.

S'han analitzat diversos beneficis respecte a l'àmplia implementació de microrredes. No obstant això, aquesta adopció també ha generat alguns problemes associats. Per exemple, una gestió eficient de l'energia és crucial en regions amb recursos energètics limitats. Les microrredes administren l'energia a través de dispositius anomenats inversors, que operen mitjançant algorismes tradicionals de regulació en bucle tancat, com el control proporcional-integral (PI). S'ha demostrat que el control PI té diversos inconvenients en comparació amb propostes de control més recents. Aquests inconvenients inclouen inestabilitat sota certes condicions d'operació, pèrdua de precisió en regions de treball no lineals i dificultats per a sintonitzar adequadament l'algoritme, la qual cosa

---

resulta en majors retards en el temps de resposta o una menor precisió en el seguiment de l'estat estable de la referència d'operació.

Un enfocament prometedor per a abordar els problemes de gestió d'energia en bucle tancat en les microrredes és la utilització d'algoritmes de control multi-objectiu. Aquests algoritmes permeten l'optimització simultània de múltiples objectius, com la minimització de pèrdues de potència, la maximització de l'eficiència i la garantia de l'estabilitat de voltatge. La implementació d'aquests algoritmes en inversors de microrred pot millorar significativament el sistema de gestió d'energia. Aquesta tesi explora com els algoritmes de control multi-objectiu implementats en inversors de microrred poden millorar els problemes de gestió d'energia, garantint operacions més eficients i sostenibles.

L'aplicació de tècniques multi-objectiu als inversors de les microxarxes pot tindre diversos beneficis. Per exemple, optimitzar objectius conflictius com la reducció del temps de resposta i la minimització del sobrepico pot millorar en gran manera el senyal de voltatge d'eixida de l'inversor. Aquesta optimització millora el rendiment, l'estabilitat i la confiabilitat del sistema, contribuint en última instància a una gestió d'energia més eficient en les microxarxes.

Qualsevol inversor en una microxarxa necessita un algorisme de control per a realitzar una regulació en bucle tancat. En aquest context, el control per maneres lliscants de segon ordre és una estratègia de control robusta que ha guanyat atenció en les aplicacions d'inversors de microxarxes. Mitjançant l'ús d'aquest enfocament, l'inversor pot aconseguir un control precís i ràpid, fins i tot en presència d'incerteses i pertorbacions. L'ús d'estratègies de control robustes millora l'estabilitat i el rendiment general del sistema de microxarxes, assegurant una gestió d'energia òptima. El procés d'ajust és essencial per als algorismes de control en bucle tancat, ja que modifica la resposta del controlador per a aconseguir els objectius de control.

L'optimització per eixam de partícules (PSO per les seues sigles en anglés) és un eficient algorisme d'optimització emprat en controladors en llaç tancat que pot resoldre de manera efectiva problemes multi-objectiu formulats en una sola funció de cost. Els paràmetres de control de l'inversor de la microxarxa poden ser optimitzats mitjançant la utilització de PSO per a aconseguir els objectius desitjats, ajustant de manera eficient una estratègia de control. Per a controladors per maneres lliscants, algunes estratègies d'ajust es basen en tècniques heurístiques. La funció de cost única resol diversos problemes en una microxarxa, però existeixen dificultats quan diferents objectius en un procés no poden ser millorats simultàniament a causa de la seua relació conflictiva.

---

Estratègies com a Algorismes Genètics Multi-Objectiu (MOGA per les seues sigles en anglés), Evolució Diferencial Multi-Objectiu (MODE per les seues sigles en anglés) i Algorisme Artificial d'Ovelles Multi-Objectiu (MOASA per les seues sigles en anglés), han demostrat la seua capacitat per a millorar el rendiment de l'inversor mitjançant l'optimització d'objectius conflictius. Aquests algorismes poden equilibrar de manera efectiva objectius com la reducció del temps de resposta i la minimització del sobreimpulso en el senyal d'eixida de l'inversor. En conseqüència, el rendiment general i l'eficiència dels inversors de la microxarxa poden millorar.





# Contents

Abstract	vii
Contents	xvii
1 Introduction	1
1.1 Introduction	1
1.2 Justification	3
1.3 Objectives	5
1.4 Outlines of the Thesis	6
2 Background of Inverter-based Microgrids	9
2.1 Introduction	9
2.2 Overview of Inverter-based Microgrids	10
2.3 Components of the Inverter-based Microgrid	17
2.4 Overview of Single-Phase Inverters Topologies	27
2.5 Microgrid Energy Management	33
2.6 Microgrid's Opportunity on Environmental Concerns	39
2.7 Microgrid Management and Operation Standards	43

2.8	Conclusions of the Chapter	50
3	State of the Art: Multi-objective Control Approach	53
3.1	Introduction	53
3.2	Multi-objective Functions Approach on IBMGs	54
3.3	Multi-objective Optimization Methods	77
3.4	Evaluation Indexes on Multi-objective Optimization	82
3.5	Conclusions of the Chapter	85
4	New Methodology: Multi-objective Approach for Optimizing the Closed-loop Control of Active Power in Inverter-based Microgrids	87
4.1	Introduction	87
4.2	Microgrid Modelling	89
4.3	Sliding Mode Controller Approach	97
4.4	Single Function Optimization Approach	107
4.5	Multiple Function Optimization Approach	113
4.6	Performance Indexes	121
4.7	Conclusions of the Chapter	122
5	Case Study: Analysis of an Experimental Inverter-based Microgrid for Active Power Management	125
5.1	Introduction	125
5.2	Experimental Microgrid at Universitat Politècnica de València	126
5.3	Meteorological Data	129
5.4	Proposal of a Microgrid at Universidad de Las Américas	135
5.5	Conclusions of the Chapter	149
6	Results of Multi-objective Approach for Active Power Management on Microgrids	151
6.1	Introduction	151
6.2	Simulation Proposal Under SMC-2 + PSO Method	152
6.3	Experimental Microgrid Improvement Under SMC-2 + PSO Methodology	168

6.4	Experimental Microgrid Improvement Under SMC-2 + MOO Methodology . . .	176
6.5	Conclusions of the Chapter . . . . .	200
7	Thesis Conclusions	203
7.1	Conclusions of the Dissertation. . . . .	203
7.2	Main Contributions . . . . .	206
7.3	Future Developments . . . . .	207
7.4	Publications . . . . .	208
A	Microgrid at Universitat Politècnica de València	209
B	HOQ for microgrid implementation	213
C	Microgrid at Universidad de Las Américas	215
	Bibliography	219



# List of Figures

2.1	Basic MG environment. . . . .	12
2.2	Typical interconnected microgrid scheme, adapted from (Roosa 2020a). . . . .	14
2.3	PV panel, adapted from (Shaikh 2017). . . . .	18
2.4	Components of a PV cell, adapted from (Guerra et al. 2018). . . . .	19
2.5	Changes in I–V curve due to temperature, adapted from (Cubas, Pindado, and De Manuel 2014) . . . . .	21
2.6	Changes in I–V curve due to solar radiation, adapted from (Cubas, Pindado, and De Manuel 2014). . . . .	22
2.7	Typical charge-discharge voltage for a sealed PB-Acid battery, adapted from (Hariprakash et al. 2001). . . . .	25
2.8	Single-phase inverter in islanding operation, adapted from (Vásquez et al. 2017). . . . .	29
2.9	Single-phase inverter in islanding operation, adapted from (Vásquez et al. 2017). . . . .	30
2.10	SPWM for a single-phase full-bridge inverter, adapted from (Ye et al. 2020). . . . .	32

2.11	Single-phase inverter in islanding operation, adapted from (Shen et al. 2019).	33
2.12	Microgrid scheme from different inverter-based sources adapted from (Miveh et al. 2016).	34
2.13	Hierarchical scheme for control a PV-battery-diesel MG, adapted from (Shi et al. 2018b).	37
2.14	Global carbon dioxide emissions, adapted from (Peters et al. 2020).	40
2.15	Dioxide of carbon emissions per capita by 2016, adapted from (Fuller 2018).	41
2.16	Targets for renewable energy from 2020 to 2030 in the European Union, adapted from (Liobikienė and Butkus 2017).	47
3.1	Multi-objective trade-off optimization methods, adapted from (Cui et al. 2017).	57
3.2	Evaluation mapping of a multi-objective problem, adapted from (Van Veldhuizen, Lamont, et al. 1998).	67
3.3	Pareto front for two objectives, adapted from (Van Veldhuizen, Lamont, et al. 1998).	67
3.4	Flow diagram of MOSOS multi-objective control, adapted from (Teekaraman, Kuppusamy, and Nikolovski 2019).	69
3.5	Multi-objective control on Hierarchical-based micro-grid application, adapted from (Zeng et al. 2016).	70
3.6	Bumpless control structure of MGs with two mode controllers, adapted from (Wu et al. 2019).	71
4.1	SPVSI scheme.	90
4.2	Grid connected SPVSI scheme.	92
4.3	Grid connected SPVSI with step-up transformer scheme.	94
4.4	Reduced equivalent circuit of an inverter-based microgrid.	95
4.5	Super-twisting phase trajectory.	99

4.6	Decoupling model for SPVSI control. . . . .	104
4.7	SPVSI control scheme. . . . .	110
4.8	Scheme for controller’s tuning. . . . .	112
5.1	Microgrid system at Universitat Politècnica de València. . . . .	127
5.2	Setting the place and time for climatology data. . . . .	130
5.3	Getting the radiation and temperature data. . . . .	131
5.4	Radiation in fall season from 2017 to 2021 in València city. . . . .	131
5.5	Temperature in fall season from 2017 to 2021 in València city. . . . .	132
5.6	Radiation in Valencia from 29 October to 02 November 2022. . . . .	133
5.7	Variotrack VT-80 (Fadlallah and Benhadji Serradj 2020) . . . . .	140
5.8	Studer XTM-4000 (Stanev and Nakov 2020) . . . . .	141
5.9	Siemens S7-1200 CPU 1214C AC/DC/RLY (Santos and da Silva 2021) . . . . .	143
5.10	Sentron PAC 3220 (Sarmiento Paute 2020). . . . .	144
5.11	Flow diagram of the closed-loop regulation. . . . .	146
5.12	Flow diagram of the closed-loop regulation. . . . .	147
5.13	Implemented topology of an inverter-based microgrid . . . . .	148
6.1	Active power rate tracking. . . . .	154
6.2	Grid and SPVSI voltages in the time domain. . . . .	155
6.3	Grid current in the time domain. . . . .	155
6.4	SPVSI currents in axes D and Q. . . . .	156
6.5	Scenario of sag and swell disturbances on the grid. . . . .	157
6.6	Scenario of active power tracking with disturbances. . . . .	158
6.7	Scenario of active power response against disturbances in axis D. . . . .	158

6.8	Load profile tracking. . . . .	160
6.9	Grid, SPVSI, and load currents in the time domain. . . . .	162
6.10	Grid, SPVSI, and load current segments in the time domain. . . . .	163
6.11	SPVSI currents in axes D and Q with load demand. . . . .	163
6.12	$V_{rms}$ voltage and frequency on the grid for SMC-2 controller. . . . .	164
6.13	Calculation time performance of the control law. . . . .	166
6.14	Experimental data from an inverter-based microgrid at Universitat Politècnica de València. . . . .	168
6.15	Comparison between the real and emulated model. . . . .	169
6.16	Current values of the grid, load, and SPVSI. . . . .	171
6.17	Sections under the analysis of currents from the grid, load, and SPVSI. . . . .	171
6.18	Currents in DQ reference frame of SPVSI. . . . .	172
6.19	$V_{rms}$ voltage and frequency on the grid for the SMC-2 controller. . . . .	173
6.20	Active power performance comparison between SMC-2 and PI. . . . .	173
6.21	Active power performance comparison between SMC-2 and PI. . . . .	175
6.22	Pareto front from MOGA in simulation #1. . . . .	177
6.23	Pareto front from MOGA in simulation #2. . . . .	177
6.24	Pareto front from MOGA in simulation #3. . . . .	178
6.25	Pareto front from MODE in simulation #1. . . . .	178
6.26	Pareto front from MODE in simulation #2. . . . .	179
6.27	Pareto front from MODE in simulation #3. . . . .	179
6.28	Pareto front from MOASA in simulation #1. . . . .	180
6.29	Pareto front from MOASA in simulation #2. . . . .	180
6.30	Pareto front from MOASA in simulation #3. . . . .	181



---

6.31 Step response for MOGA simulations. . . . .	184
6.32 Step response for MODE simulations. . . . .	184
6.33 Step response for MOASA simulations. . . . .	185
6.34 Radar plot for MOGA simulations. . . . .	186
6.35 Radar plot for MODE simulations. . . . .	186
6.36 Radar plot for MOASA simulations. . . . .	187
6.37 Comparison between PSO and MOGA applied to SMC-2. . . .	188
6.38 Current values of the grid, load, and SPVSI. . . . .	188
6.39 Sections under the analysis of currents from the grid, load, and SPVSI. . . . .	189
6.40 Currents in DQ reference frame of SPVSI. . . . .	189
6.41 $V_{rms}$ voltage and frequency on the grid for SMC-2+MOGA controller. . . . .	190
6.42 Comparison between PSO and MODE applied to SMC-2. . . .	191
6.43 Current values of the grid, load, and SPVSI. . . . .	191
6.44 Sections under the analysis of currents from the grid, load, and SPVSI. . . . .	192
6.45 Currents in DQ reference frame of SPVSI. . . . .	193
6.46 $V_{rms}$ voltage and frequency on the grid for SMC-2+MODE controller. . . . .	193
6.47 Comparison between PSO and MOASA applied to SMC-2. . . .	194
6.48 Current values of the grid, load, and SPVSI. . . . .	195
6.49 Sections under the analysis of currents from the grid, load, and SPVSI. . . . .	195
6.50 Currents in DQ reference frame of SPVSI. . . . .	196
6.51 $V_{rms}$ voltage and frequency on the grid for SMC-2+MOASA controller. . . . .	196

6.52 Radar plot between MOO algorithms and PSO. . . . .	198
A.1 Battery bank. . . . .	209
A.2 Charge controller. . . . .	210
A.3 PV panels. . . . .	211
A.4 Inverter. . . . .	211
B.1 HOQ of the inverted-based microgrid project . . . . .	214
C.1 Elements from the SPVSI scheme at Universidad de Las Américas. . . . .	216
C.2 Elements from the SPVSI part 1. . . . .	217
C.3 Elements from the SPVSI part 2. . . . .	218
C.4 Elements from the SPVSI (power meters). . . . .	218

# List of Tables

2.1	Types of PV panels (Yang et al. 2018). . . . .	20
2.2	Example of life of use of a Pb-acid battery, adapted from (Hariprakash et al. 2001). . . . .	24
2.3	Study from McKinsey to GHG reductions in USA. . . . .	42
2.4	Main energy polices for MG development from 2010 (Ali et al. 2017). . . . .	44
2.5	Power quality requirements on IEEE Std 1547-2018. . . . .	46
3.1	Multi-objective optimization approaches . . . . .	73
3.2	Resume of advanced controllers objectives . . . . .	75
3.3	Objectives presented on IBMG regulation . . . . .	76
4.1	States of power switches on the SPVSI. . . . .	90
5.1	Parameters of the inverter-based microgrid at Universitat Politècnica de València. . . . .	128
5.2	Radiation data validation . . . . .	133

5.3	Morphological chart of the inverted-based microgrid . . . . .	138
6.1	PSO scenario for tuning the control method. . . . .	153
6.2	SMC-2 tuning based in PSO. . . . .	153
6.3	Performance comparison between SMC-2 and PI. . . . .	164
6.4	Time performance comparison between SMC-2 and PI. . . . .	166
6.5	Performance scenarios of the inverter-based microgrid . . . . .	170
6.6	Performance indexes values between SMC-2 and PI . . . . .	174
6.7	Parameters for MOO simulations . . . . .	181
6.8	SMC-2 parameters from MOO methods . . . . .	182
6.9	IGD results from MOO simulations . . . . .	183
6.10	Response parameters from MOO simulations for a step input . . . . .	185
6.11	Performance indexes between PSO and MOO methods for various scenarios of SPVSI . . . . .	197

# List of Acronyms

<b>AC</b>	Alternate Current
<b>ANN</b>	Artificial Neural Network
<b>CG</b>	Centralized Generation
<b>CH<sub>4</sub></b>	Methane
<b>CO<sub>2</sub></b>	Carbon Dioxide
<b>COA</b>	Chaotic Optimization Algorithm
<b>CSI</b>	Current Source Inverter
<b>DC</b>	Direct Current
<b>DE</b>	Differential Evolution
<b>DER</b>	Distributed Energy Resource
<b>DG</b>	Distributed Generation
<b>EA</b>	Evolution-based algorithms
<b>EP</b>	Evolutionary Programming
<b>EPC</b>	Electronic Power Converters
<b>ES</b>	Evolutionary Strategy

<b>FACTS</b>	Flexible Alternating Current Transmission System
<b>GA</b>	Genetic Algorithm
<b>GHG</b>	Greenhouse Gases
<b>GSA</b>	Gravitational Search Algorithm
<b>HOSMC</b>	High Order Sliding Mode Control
<b>HSA</b>	Harmony Search Algorithm
<b>IAE</b>	Integral of Absolute Error
<b>IBMG</b>	Inverter-based Microgrid
<b>ICA</b>	Imperialistic Competition Algorithm
<b>IEEE</b>	Institute of Electrical and Electronics Engineers
<b>IGBT</b>	Insulated-gate Bipolar Transistor
<b>ISE</b>	Integral of Square Error
<b>ITAE</b>	Integral of Time Absolute Error
<b>ITSE</b>	Integral of Time Square Error
<b>IWD</b>	Intelligent Water Drops Algorithm
<b>LQR</b>	Linear Quadratic Regulator
<b>MG</b>	Microgrid
<b>MLM</b>	Multilevel Modulation
<b>MOA</b>	Magnetic Optimization Algorithm
<b>MOASA</b>	Multi-objective Artificial Sheep Algorithm
<b>MODE</b>	Multi-objective Differential Evolution
<b>MOEA</b>	Multi-objective Evolutionary Algorithm
<b>MOGA</b>	Multi-objective Genetic Algorithm
<b>MOSFET</b>	Metal-oxide-semiconductor Field-effect Transistor

<b>MOSOS</b>	Multi-objective Symbiotic Organism Search
<b>MPC</b>	Model Predictive Control
<b>NDE</b>	Non-delivered Energy
<b>NSGA</b>	Non-dominated Sorting Genetic Algorithm
<b>PCC</b>	Point of Common Coupling
<b>PD+I</b>	Proportional-derivative plus Integral
<b>PES</b>	Power Electrical System
<b>PESA</b>	Pareto Envelope-based Selection Algorithm
<b>PI</b>	Proportional-integral
<b>PID</b>	Proportional-integral-derivative
<b>PSO</b>	Particle Swarm Optimization
<b>PWM</b>	Pulse Width Modulation
<b>RES</b>	Renewable Energy Resource
<b>SA</b>	Simulated Annealing
<b>SMC</b>	Sliding Mode Control
<b>SMC-2</b>	Second Order Sliding Mode Control
<b>SPEA</b>	Strength Pareto Evolutionary Algorithm
<b>SPVSI</b>	Single-phase Voltage Source Inverter
<b>SPWM</b>	Sinusoidal Pulse Width Modulation
<b>SVPWM</b>	Space Vector Pulse Width Modulation
<b>THD</b>	Total Harmonic Distortion
<b>TSA</b>	Tabu Search Algorithm
<b>UPS</b>	Uninterruptible Power Supply
<b>VEGA</b>	Vector Evaluation Genetic Algorithm

**VSG**      Voltage Source Generator

**VSI**      Voltage Source Inverter



# Nomenclature

## Parameters

$V_{DC}$	DC voltage at inverter's input [V]
$S_1 - S_4$	Power switches at H-bridge topology
$R$	Resistor from SPVSI [ $\Omega$ ]
$L$	Inductor from SPVSI filter [ $H$ ]
$C$	Capacitor from SPVSI filter [ $F$ ]
$V_g$	Grid voltage [V]
$R_g$	Resistor from grid side [ $\Omega$ ]
$L_g$	Inductor from grid side [ $H$ ]
$R_L$	Load resistor [ $\Omega$ ]
$f_s$	Switching frequency [ $kHz$ ]
$k_p$	Proportional constant for PI controller
$k_i$	Integral constant for PI controller
$K_p$	Proportional constant for PI sliding surface at SMC-2
$K_i$	Integral constant for PI sliding surface at SMC-2

$K_{pd/q}$	Proportional constant for PI sliding surface in $d/q$ axes at SMC-2
$K_{id/q}$	Integral constant for PI sliding surface in $d/q$ axes at SMC-2
$\sigma$	Sliding surface
$\lambda$	Constant parameter from SMC-2's control law
$W$	Constant parameter from SMC-2's control law
$I_{dref}$	SPVSI reference current in D-axis [A]
$I_{qref}$	SPVSI reference current in Q-axis [A]
$r_r$	Ramp rate
$N_P$	Number of turns at primary coils in a transformer
$N_S$	Number of turns at secondary coils in a transformer
$N$	Ratio of transformer number of coils
$v_{g'}$	Grid's voltage reflected to primary side [V]
$R_{g'}$	Resistor from grid reflected to primary side [ $\Omega$ ]
$L_{g'}$	Inductor from grid reflected to primary side [H]
$V_{PV}$	Rated maximum voltage of PV panels [V]
$I_{PV}$	Rated maximum current of PV panels [A]
$n$	Number of PV panels
$L_m$	Transformer's magnetization inductor [H]
$R_c$	Transformer's core losses resistor [ $\Omega$ ]
$S_b$	Transformer's base apparent power [VA]
$VLL_b$	Transformer's base voltage line-line [V]
$V_{bat}$	Battery rated voltage [V]
$C_{bat}$	Battery capacity [Ah]
$\eta$	PV panel efficiency [%]

$E$	Solar radiation [ $W/m^2$ ]
$A$	PV panel surface [ $m^2$ ]
$P_{max}$	Maximum active power produced per panel [ $W$ ]

**Variables**

$v_o$	SPVSI's output voltage [ $V$ ]
$v_L$	SPVSI's inductor output voltage [ $V$ ]
$v_R$	SPVSI's resistor output voltage [ $V$ ]
$v_C$	SPVSI's capacitor output voltage [ $V$ ]
$i_L$	SPVSI's inductor output current [ $A$ ]
$i_R$	SPVSI's resistor output current [ $A$ ]
$i_C$	SPVSI's capacitor output current [ $A$ ]
$v_{PCC}$	Voltage at point of common coupling [ $V$ ]
$v_{Lg}$	Grid's inductor output voltage [ $V$ ]
$v_{Rg}$	Grid's resistor output voltage [ $V$ ]
$i_{Lg}$	Grid's inductor output current [ $A$ ]
$i_{Rg}$	Grid's resistor output current [ $A$ ]
$x$	Vector of variable states
$P_o$	SPVSI output power [ $W$ ]
$u$	Control signal
$X$	Vector of particle's position at PSO
$X_{ipbest}$	Previous best position of particles in the swarm at PSO
$X_{inbest}$	Previous best global position of particles in the swarm at PSO
$V$	Vector of particle's velocity at PSO
$c_1 - c_2$	Learning coefficients at PSO

$r_1 - r_2$	Random numbers at PSO
$\Omega$	Inertial constant at PSO
$J$	Fitness function
$V^*$	Lyapunov's candidate function
$e$	Error signal for closed-loop control
$u_{SMC-2}$	Control law for second-order SMC
$X_a$	Signals in alpha reference frame
$X_b$	Signals in beta reference frame
$X_d$	Signals in D reference frame
$X_q$	Signals in Q reference frame
$u_{d*}$	Decoupled control signal in D-axis
$u_{q*}$	Decoupled control signal in Q-axis
$\sigma_d$	Sliding surface in D-axis
$\sigma_q$	Sliding surface in Q-axis
$t_r$	Rising time [s]
$e_A$	Absolute error in percentage [%]
$\varepsilon\%$	Relative error [%]
$V_{real}$	Values obtained from experimental microgrid
$V_{sim}$	Values obtained from PSCAD microgrid
$P$	Deviation values for radar plot [%]
$F$	Vector of optimization functions
$f$	Optimization function
$J_1$	Optimization index for rising time
$t_{10}$	Time when SPVSI signals reaches 10% of final value

$t_{90}$	Time when SPVSI signals reaches 90% of final value
$J_2$	Optimization index for overshoot
$r_{ef}$	Reference (final) value for SPVSI response
$y_{max}$	Maximum value for SPVSI response
$J_{min}$	Optimized index
$N_P$	Number of particles in a population at MOO
$l_b$	Lower bound of search at MOO
$l_u$	Upper bound of search at MOO
$G$	Particle's generation at MOO
$X_{opt}$	Optimum value from particles swarm at MOO
$J_{opt}$	Optimum index value from particles swarm at MOO
$P_0$	Initial population at MOO
$P_{parent}$	Parent population at MOO
$P_{child}$	Child population at MOO
$X_{child}$	Value from child particles at MOO
$J_{child}$	Optimum index value from child particles at MOO
$\mathcal{P}^*$	Pareto optimal set
$\mathcal{P}\mathcal{F}^*$	Pareto front
$\mathcal{P}\mathcal{F}$	True-Pareto front
$d$	Euclidean distance employed in IGD index

**General indexes**

$t$	Time
$i$	i-esim element
$j$	j-esim element

$k$	Time step
$m$	Number of equality constraints
$p$	Number of inequality constraints

# Chapter 1

# Introduction

## 1.1 Introduction

In recent years, renewable energy applications are no longer a novelty in science and technology. This trend is growing due to the depletion of conventional energy sources such as oil and natural gas. These fossil fuels have reached critical levels and the implementation of renewable energy is imperative to maintain industrial activities around the world. Furthermore, the use of conventional energy sources has devastated the atmosphere, leading to significant carbon dioxide emissions and a substantial decrease in air quality, negatively impacting the natural environment. Given these challenges, there is an urgent need to prioritize developing and implementing sustainable energy solutions.

A microgrid is an alternative for electricity generation without the major user of fossil fuels. Microgrids have emerged as systems that have been extensively analyzed and studied to support electrical production on the grid. These systems consist of different sources, power converters, and loads that collaborate as agents, working synergistically to achieve efficient energy management.

The transition from conventional energy generation to microgrids has encountered various technical and economic challenges. Currently, the dominant oil industry possesses advanced infrastructure and technology that, unfortunately,

contributes significantly to pollution. To promote renewable energy, it is essential to enhance collaboration between companies and researchers. This will lead to reduced material and equipment costs and to improved energy conversion efficiency. By bringing together expertise from both sectors, the energy field can make significant strides in making renewable energy sources more accessible and economically viable for a sustainable future. Moreover, the growing demand for cleaner production underscores the need for energy systems heavily influenced by renewable energy generation in the future.

Given these factors, electricity companies are inclined toward the widespread adoption of microgrids in the coming years. This technology offers superior advantages over existing renewable energy applications, particularly in remote areas far from major cities. Inverters, which convert direct current (DC) into alternate current (AC), play a crucial role in microgrids due to the predominance of AC loads in residential and industrial areas. Significant progress has been achieved in integrating loads with varying energy consumption and combining multiple microgrids to create larger electricity production systems. However, continuous efforts are needed to ensure the stability of these microgrids under diverse operating conditions. Moreover, it is crucial to address the issue of high tariffs linked to these technologies to make microgrid implementation more attractive and feasible.

In other aspects, the massive involvement of inverters in industrial applications has brought about the adoption of simple yet effective control algorithms in the power generation process. However, these algorithms have limitations both in their mathematical structure and in their applicability.

One of the most commonly used controllers in managing energy in inverter-based microgrids is the proportional-integral controller. This algorithm is known for its mathematical simplicity and effective tracking of references. However, several issues are associated with its use, such as its inability to fully control non-linear processes. Another problem is the prioritization of conflicting objectives, for example, the speed of the response signal and its overshoot. There are also concerns about responding to transients generated by abrupt changes in the reference signal. These problems negatively impact the quality of energy generated by the microgrid, affecting the generation of active power, and having implications for the efficiency of the inverter, which must make the most of the energy from distributed sources in areas with limited access to electricity.



## 1.2 Justification

Energy management is the key aspect of microgrids. In this thesis, the analysis of an inverter-based microgrid is performed. This type of microgrid lies in the use of an inverter, which is a power electronic converter that transforms energy from DC to AC. The conventional electricity transportation scheme employs a big infrastructure where energy is transferred through distribution power plants in diverse cities. Microgrids are on-site generation systems where multiple sources produce energy for the final consumer.

In this research, the aim is to contribute proposals that enhance the field of energy management in microgrids, further reducing the dependence on fossil fuels for energy generation.

Given that the transition from conventional power generation to microgrids presents challenges in inverter control, this project proposes an alternative approach employing a more robust control method to enhance energy conversion efficiency in the inverter. Emphasis is placed on the inverter's energy transformation process, as most of the load consumption, especially in residential cases, occurs in AC.

This thesis suggests using multi-objective algorithms to enhance the performance of advanced controllers through an intelligent tuning process that incorporates the concepts of particle swarm optimization and genetic algorithms. The goal is to improve the transient response of the inverter and its steady-state reference tracking compared to conventional controllers. For instance, a current issue in control is the complex tuning of processes with conflicting objectives. This thesis underscores an appropriate tuning process considering conflicting objectives such as rise time and overshoot. Consequently, the efficiency of electronic equipment will also be enhanced compared to current proposals, and it is anticipated that the results could serve as input for manufacturers of industrial inverters to embrace new closed-loop control techniques.

The choice of multi-objective techniques is novel in energy management processes. In addition, the following advantages are demonstrated:

Multi-objective algorithms can enable optimal power dispatch and scheduling in microgrids. Considering energy demand, available renewable and conventional energy generation, and storage capacities. These algorithms determine the most cost-effective and sustainable way to distribute energy within the microgrid. This optimization can lead to significant energy savings, reduced costs, and improved efficiency.

Moreover, multi-objective algorithms can enhance the resilience and reliability of microgrids. These algorithms can continuously monitor the state of the microgrid, detect any abnormalities or failures, and autonomously reconfigure the system to isolate faults and restore the power supply. This self-healing capability is crucial in ensuring uninterrupted power delivery and mitigating the impact of outages or disturbances.

Microgrids often operate decentralized, with multiple distributed energy resources and loads interconnected. Multi-objective algorithms can facilitate effective coordination and control of these distributed elements. By dynamically adjusting the power flow and voltage levels, these algorithms can optimize the utilization of available resources, balance supply and demand, and minimize losses.

Furthermore, as microgrids become increasingly interconnected with the main grid, multi-objective algorithms play a vital role in achieving grid integration and managing interactions between the microgrid and the conventional power system. These algorithms can enable seamless energy exchange, support grid stability, and ensure smooth transitions between grid-connected and islanded modes of operation. In this context, new policies are being developed to complain requirements of energy quality and security of electrical devices as detailed for the following reasons:

- **Improve energy management:** The operation of microgrids contains essential aspects such as maintaining stable values of voltage and frequency under different operating values. The constant variation of loads on the grid tends to change voltage and frequency values. This variability on the demand site might affect critical equipment, especially electronic ones.
- **Support conventional grid:** The microgrid structure is coupled to other similar schemes. These systems help the generation side produce more energy if much electricity is needed. The key advantage is the implementation of these structures in places far from cities that still need to have a distribution power plant aside.
- **Improve energy quality:** General problems such as reactive power compensation can be improved to obtain higher-quality electricity on the consumer's side. Governments worldwide are implementing policies to effectively manage energy quality and provide optimal benefits to final consumers.

All these aspects converge to maintain a high level of reliability to produce electricity without interruptions, without distortions, and with better tariffs.

The proposal of multi-objective algorithms to replace traditional microgrid techniques is widely understood.

### 1.3 Objectives

The main objective of this thesis is to propose a new methodology scheme of a multi-objective algorithm applied to an inverter-based microgrid to establish operational values of different electrical magnitudes. Operational values such as voltage, frequency, active, and reactive power must comply with standard parameters of policies on the integration of inverter-based microgrids into the grid. The specific objectives are listed as follows:

- To analyze the background of inverter-based microgrids and the state of the art on microgrid's closed-loop regulation. The background will present the components' analysis and functions in a microgrid, while the state of the art will present the main research and proposals on microgrid energy management.
- To propose and design a non-conventional control algorithm to improve energy management in a microgrid. The proposed methodology includes a new scheme for reducing active power tracking error and proposes an innovative tuning process based on the multi-objective optimization approach.
- To validate the effectiveness of the new control approach, various experiments will be carried out in a laboratory microgrid at the Universitat Politècnica de València. The active power management will be tested under various microgrid, grid, and load interaction scenarios. These results will be compared with current microgrid data, providing numerical performance indexes that will support this thesis proposal.
- To develop an experimental microgrid in Universidad de Las Américas from Ecuador employing the knowledge learned from the microgrid at Universitat Politècnica de València. The microgrid will include all components for power management between the inverter, grid, and load.

## 1.4 Outlines of the Thesis

To accomplish the objectives of this work, the thesis is organized as follows:

Chapter 2 describes the background of inverter-based microgrids. A summary of the most significant parameters, types, and characteristics of inverters are studied. The main component of the microgrid is detailed, which is the single-phase voltage source inverter (SPVSI). The complementary components of the microgrid, such as PV panels, batteries, charge controller, and so forth, are studied to understand the microgrid operation. In addition, some standards that regulate the performance of inverter-based microgrids are identified to analyze the context of the microgrid improvement proposal.

Then, Chapter 3 presents the literature review of the multi-objective control approach. The challenges and perspectives of multi-objective algorithms are presented. This chapter constitutes a key source of information to establish a methodology for multi-objective optimization to manage active power in an inverter-based microgrid.

Based on the analysis performed in the previous sections, chapter 4 is presented for the multi-objective formulation to improve active power management in an inverter-based microgrid. It relies on specifications that will prove the objectives proposed in this thesis. The second-order sliding mode control (SMC-2) is presented as the regulation method. Then, it is improved by tuning its control law constants from the multi-objective algorithms proposed.

Chapter 5 is devoted to the analysis of the different microgrid elements at the Universitat Politècnica de València. In this scenario, a case study is proposed for the new methodology of active power management from the multi-objective perspective. Also, the climate conditions show the irradiance values of the experimental microgrid to propose different control scenarios of active power. Once the microgrid is analyzed and understood, a proposal for the design of a microgrid at the Universidad de Las Américas in Ecuador is presented.

In Chapter 6, the results of the SMC-2 control scheme with a multi-objective approach are implemented on a model based on a microgrid using real data. The microgrid in this analysis contains all the basic elements found in a microgrid applied to a residential environment. These elements are photovoltaic panels, a charge controller, and storage batteries. These elements are connected to the inverter and its output is connected to a common coupling point between the inverter, load, and grid. Different scenarios are analyzed in which the grid delivers and/or receives power from the inverter. The data obtained

are analyzed with performance indexes to evaluate the SMC-2 under the multi-objective approach. Conversely, the conventional PI controller is evaluated to compare the new methodology against a conventional control method used majorly on industrial inverters.

Chapter 7 summarizes the conclusions of this thesis and some suggestions for further works are given. The publications in this Ph.D. document are also presented.



# Background of Inverter-based Microgrids

### 2.1 Introduction

This chapter presents the fundamental concepts of inverter-based microgrids for a better understanding of the scope of this thesis. Firstly, the voltage source inverters are analyzed since they play a crucial role in microgrids by converting electrical energy generated from renewable and non-renewable sources into electricity for final consumers. This technology is used in major decentralized generation (DG) applications, which involve energy generation from different resources apart from the main grid. Power electronics topologies inside the inverters can be configured in various ways, such as half-bridge or full-bridge connections, depending on grid requirements and available resources. Additionally, the microgrid contains elements such as photovoltaic panels, batteries, charge controllers, and so forth to perform energy conversion. Furthermore, implementing standards and regulations for inverter installation is essential to ensure these systems' safety, efficiency, and reliability. These regulations establish quality standards, protection measures, and grid connection guidelines, promoting the adoption and sustainable development of microgrids.

The chapter begins by describing the overview of inverter-based microgrids in section 2.2. Section 2.3 shows the different components and their functions for the operation of an inverted-based microgrid. Subsequently, the general concepts of single-phase inverters, their topologies, and modulation signals are explained in section 2.4. Section 2.5 details the power generation structure for hierarchical control purposes in a microgrid. Section 2.6 details the environmental concerns to approach from the microgrid's perspective. Section 2.7 shows the main management and operation standards applied to microgrids, and, finally, in section 2.8, the main conclusions drawn from the content of this chapter are presented.

## 2.2 Overview of Inverter-based Microgrids

### 2.2.1 Basic definitions

Currently, conventional power plants are heavily relying on centralized energy sources such as gas, coal, and nuclear power to meet the electricity demands of a large consumer base. However, the transmission of electrical energy over long distances necessitates costly infrastructure. In contrast, microgrids (MGs) operate on a smaller scale, utilizing diverse energy sources and loads. Moreover, MGs have the advantage of integrating with similar systems.

MGs represent a modern and innovative approach to fulfilling residential and commercial electrical needs. These systems offer a reliable and resilient power supply with exceptional performance metrics. Moreover, the widespread adoption of decentralized energy sources has driven the rapid expansion of microgrids, especially in remote locations. MGs consist of small-scale power systems that leverage renewable and fossil fuel resources, providing numerous advantages for electricity generation. Additionally, microgrids have evolved to meet diverse customer demands, exhibiting variations in size, generation sources, and the type of current produced. This allows them to be tailored to specific customer requirements.

Generally, the energy generated by MGs is consumed locally. While there is no universally standardized definition for MGs, the U.S. Department of Energy defines an MG as *a group of interconnected loads and distributed energy resources within clearly defined electrical boundaries that operate as a single controllable entity about the grid* (Lenhart and Araújo 2021). Another definition, provided by the International Council on Large Electric Systems (CIGRR) C6.22 Working Group, describes an MG as an *electricity distribution system that com-*

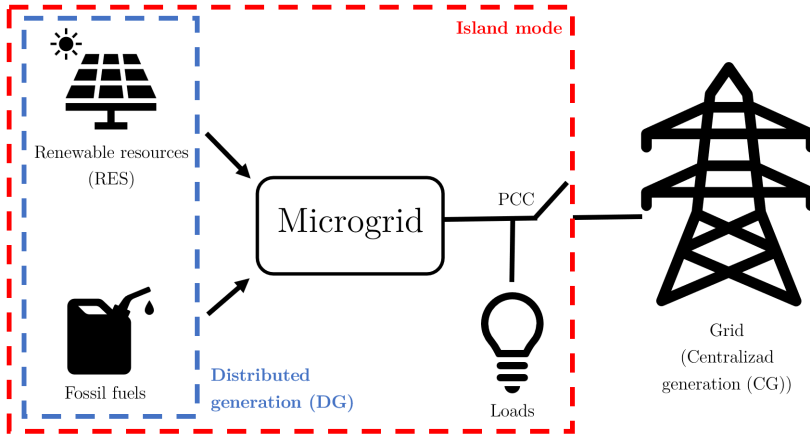


prises loads and distributed energy resources (such as distributed generators, storage devices, or controllable loads) capable of operating in a controlled and coordinated manner, whether connected to the main power grid or operating autonomously (Bhutto, Bak, and Ali 2017). Furthermore, more comprehensive definitions exist, such as *Microgrids are modern, small-scale versions of the centralized electricity system. They serve specific local objectives, such as enhancing reliability, reducing carbon emissions, diversifying energy sources, and reducing costs, as determined by their community. Like the bulk power grid, smart microgrids generate, distribute, and regulate the flow of electricity to consumers, but they do so at the local level* (What is a microgrid? 2015).

### 2.2.2 Energy Cycle Generation in a Microgrid

Distributed generation (DG) has emerged as a critical electricity production system, offering numerous advantages for final energy consumers (Murty and Kumar 2020). It addresses challenges associated with centralized generation (CG), which refers to the traditional energy generation, transmission, and distribution from large infrastructures in specific locations. CG faces limitations in achieving management objectives, and the transition to DG aims to optimize installation costs, extend power access to remote areas, and establish a resilient energy consumption system that is less vulnerable to blackouts (Clairand et al. 2019b). Additionally, the shift to DG contributes to reducing carbon dioxide (CO<sub>2</sub>) emissions by replacing fossil fuels with renewable energy sources (RES) (Katircioğlu et al. 2019).

MGs are renowned for their ability to produce electricity from DG sources and integrate electrical storage systems. These sources engage with a cluster of loads connected at the Point of Common Coupling (PCC) within the grid. The PCC serves as the electrical point of interaction for power management, encompassing the grid, microgrid, and loads. MGs facilitate the reliable integration of distributed energy resources (DER), which include small renewable and fossil fuel resources, thereby mitigating CO<sub>2</sub> emissions (Olivares et al. 2014). DER elements support electricity production from sources around the microgrid, providing electricity to areas where conventional electrical infrastructure is unavailable. Consequently, MGs are known for their high-quality service, robustness, and sustainability. They can either inject energy into the traditional grid or operate independently in *island mode* to meet the local consumption demands of end consumers (Sood and Abdelgawad 2019). These key concepts are illustrated in Figure 2.1.



**Figure 2.1:** Basic MG environment.

The current trend in electricity production indicates a significant increase in electricity generation from DG. MGs currently include generation plants with capacities of up to 300 MW and are projected to experience further growth (Akinyele, Belikov, and Levron 2018). This growth brings additional benefits to energy consumption, such as serving as crucial support for implementing electric mobility on a large scale (Clairand et al. 2019a)

MGs can be implemented in either DC (direct current) or AC (alternate current) schemes. DC schemes significantly impact research due to their simpler electrical control system structures (Benamar et al. 2020). They offer advantages such as the absence of devices like DC/AC power converters, eliminating variables like reactive power and harmonics, and achieving high efficiency and reliability compared to AC generation (Lakshmi and Hemamalini 2017). However, AC remains the dominant power generation method due to its extensive demand in residential and industrial applications (Abhinav et al. 2017). Some approaches explore hybrid MGs to leverage the production and distribution trends of DC while still addressing the predominant demand for AC (Khaticbzadeh et al. 2017). In this context, the voltage source inverter (VSI) plays a vital role in supporting these sources of electrical generation within a concept known as inverter-based microgrids (IBMGs). The VSI is an electronic device that converts DC energy into AC using a power electronic device-based electronic scheme.

While IBMGs offer advantages in terms of local resiliency and improved operation and stability of distribution systems, they also present challenges re-

garding reliability and stability. One notable issue is the instability caused by low inertia resulting from VSIs, as discussed in (Kerdphol, Rahman, and Mitani 2018). These resources lack the inertia provided by traditional synchronous generators used in CG. Additionally, (Rodrigues, Souza, and Ribeiro 2018) mentions the occurrence of voltage and frequency deviations when MGs are disconnected from the main grid and operate in island mode. This phenomenon can critically impact loads that rely on stable voltage and frequency values.

The critical problem of imbalanced loads arising from different line and output impedance values is addressed in (Ghosh and Chattopadhyay 2020). To stabilize a multivariable system, a sophisticated control technique is required. Non-linear loads represented by power converters with total harmonic distortion (THD), as discussed in (Mohapatra and Agarwal 2019), also contribute to these effects. This study emphasizes the need for a robust controller to handle sudden demand changes and reject disturbances effectively. Addressing these issues requires considering inertia, voltage and frequency control, load balancing, and effective control strategies for non-linear loads.

Considering the challenges mentioned earlier, researchers have focused on enhancing the performance of IBMGs through closed-loop control systems. Several proposals have emerged in the design of feedback regulators, such as using droop power control to maintain voltage and frequency values, as proposed by (Ziouani et al. 2018). Advanced control systems have been implemented to address robustness in IBMGs, including the application of linear quadratic regulator (LQR) as suggested by (Patarroyo-Montenegro, Salazar-Duque, and Andrade 2018), or sliding mode control (SMC) as presented in (Safa et al. 2018), to mitigate the effects of non-linear loads on grid management. Other researchers, such as (Andishgar, Gholipour, and Hooshmand 2017), have explored broader objectives, including power flow control, voltage, and frequency regulation, unbalanced load conditions, and harmonic generation.

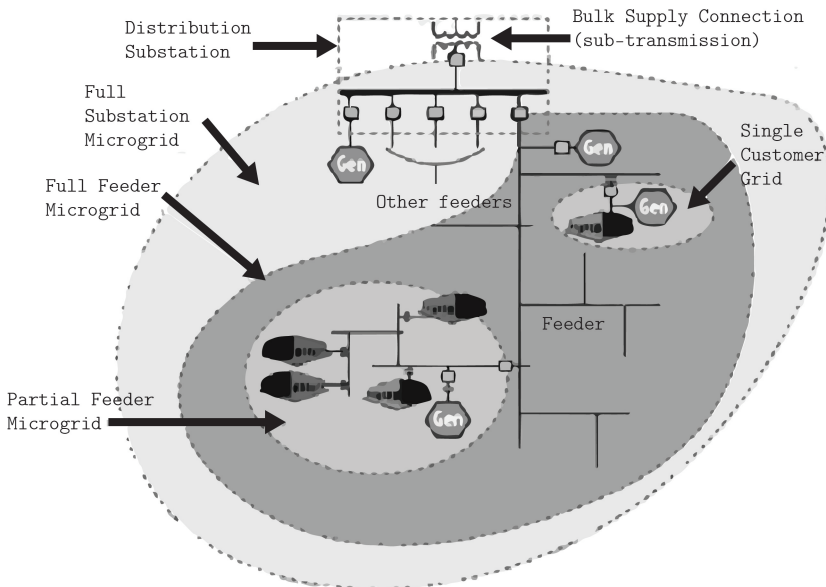
### ***2.2.3 Approach of electricity generation***

Despite significant electrical infrastructure and technology advancements, numerous regions worldwide still need access to reliable electricity. While overall electricity production has increased due to the implementation of various electrical grids, there remains an imbalance in energy distribution. Regrettably, many people in these underserved areas struggle to meet basic needs such as access to dependable lighting, heating, and communication devices.

Furthermore, the absence of electricity access has far-reaching consequences beyond daily living. In regions where education is a priority, the inability to employ technology for a more efficient learning process can result in significant disadvantages. Students in these areas often require assistance accessing the internet or using digital resources to enhance their learning activities, which puts them at a disadvantage compared to their peers in more connected and centralized areas.

Even with advancements in electricity production and infrastructure worldwide, it remains crucial to guarantee universal access to this essential resource. Individuals in underdeveloped areas will continue to encounter obstacles that limit their ability to achieve their maximum educational potential.

One of the primary goals of MGs is to generate electricity locally, with a strong emphasis on high reliability. Moreover, the decentralized nature of MGs enables the integration of a broader range of device components, which is often challenging with conventional grids. Upgrading the infrastructure of conventional grids frequently leads to disruptions for a significant number of consumers. Conversely, when MGs are connected to the main grid, they can be disconnected and operate independently in island mode in the event of a grid failure, as seen in Figure 2.2 (Roosa 2020a).



**Figure 2.2:** Typical interconnected microgrid scheme, adapted from (Roosa 2020a).

The terminology associated with MGs frequently incorporates concepts such as *resiliency*. This term is widely employed to depict the capacity of a generation system to restore its original state after experiencing one or multiple failure conditions. MGs are recognized for their uninterrupted energy flow, which draws upon diverse energy sources and storage equipment. The main advantages and disadvantages are shown below for a more comprehensive explanation of MGs features.

#### ***2.2.4 Advantages and disadvantages of microgrids***

MGs have emerged as a new trend in electricity generation, offering several advantages and certain disadvantages ([Al-Ismail 2021](#)). The key advantages of MGs include:

- High flexibility: MGs integrate various energy sources, reducing the need for extensive transmission infrastructure as local energy generation becomes possible.
- Dispatchable energy: MGs feature robust energy storage systems, allowing energy to be dispatched on demand.
- Island mode operation: In the event of a main grid failure, MGs can continue operating in island mode, providing an uninterrupted energy supply. This is particularly beneficial for industrial processes.
- Redundancy: MGs exhibit redundancy and can restart their functions using the black start method, enabling electric generation without relying on external power transmission systems.
- Cost-effective expansion: MGs require less infrastructure investment than conventional grid upgrades, reducing costs for future electrical service expansions. Additionally, MGs can prioritize energy sources based on pricing.
- Revenue generation: Excess energy produced by MGs can be sold to the main grid, generating revenue for the MG owner.

However, MGs also have some disadvantages, which include:

- Infrastructure costs: Development and maintenance of multiple energy sources in MGs can be expensive.

- Intermittency and balancing challenges: Multiple energy sources in MGs can lead to intermittency and balancing issues, especially in remote areas with high maintenance costs.
- Policy complexities: MGs often face policy challenges that impose specific requirements on their operation. A clear explanation of policies is needed to facilitate the widespread implementation of MGs.

Despite these disadvantages, the numerous benefits offered by MGs make them an attractive option for future electricity generation and distribution. The advantages of implementing MGs far outweigh the weaknesses that have been analyzed. This antecedent explains the increasing trend in the adoption of MGs. The following section will deepen into the various types of microgrids currently available.

### 2.2.5 *Types of microgrids*

The classification of MGs is determined by the type of electricity generation, whether it is alternating current (AC) or direct current (DC). While most residential and commercial appliances rely on AC energy, specific loads require DC energy. Therefore, DC generation can enhance efficiency by reducing the need for multiple converters when the primary energy source is DC.

Another important feature is flexibility, a crucial aspect of MGs, as these systems incorporate heat generation sources alongside their main focus on electrical generation. Experts in the electrical field often categorize MGs as true microgrids and minigrids. True microgrids involve on-site installations similar to the main grid, where nearby consumers use energy near the generation system. On the other hand, minigrids employ multiple energy sources and are preferable for supplying energy to critical loads during outages ([Chang et al. 2021](#)).

Another classification of MGs is based on their features and applications, distinguishing them as off-grid or grid-interconnected systems. Off-grid systems, such as those found in the Canary Islands in Spain and Bonaire in the Caribbean, rely on photovoltaic panels, wind power, pumped hydro storage, biodiesel, and battery storage without taking the grid's energy. Grid-interconnected systems, like the one in Fort Bliss, Texas, serve various utilities, including communities, industries, and military bases interconnected to the main grid ([Groppi et al. 2021](#)).

Roosa (Roosa 2020b) proposes an interesting alternative classification for MGs, which includes the following categories:

- Development grids: Infrastructure designed for small-scale commercial operations.
- Motivational grids: Infrastructure that caters to non-essential needs.
- Hidden microgrids: Local generators used for emergencies.
- Isolated microgrids: Systems employed in remote locations far from major cities.
- Mobile microgrids: Deployed in military applications where immediate access to electricity is performed on demand.

Advancements in MGs have led to various improvements in their operation, incorporating features for large-scale integration. These systems prioritize energy density balancing from multiple sources, scheduled dispatching, and high grid reliability. The flexibility of advanced MGs enables plug-and-play interoperability for users.

Lastly, a new trend called virtual microgrids integrates multiple nonadjacent resources and can operate in island mode remotely. Connectivity is ensured through cloud-based software, allowing proper coordination of all components in the extended grid (Anoh et al. 2019).

The different types of MGs analyzed comprise elements that achieve energy production objectives. To appropriately adapt a power management controller, it is essential to understand these elements' characteristics clearly. Below is a concise overview of a microgrid's main components and key features.

## 2.3 Components of the Inverter-based Microgrid

This section offers a detailed description of the components that comprise a microgrid. Each element possesses specific functions and characteristics that support the operation of the microgrid. Understanding the process of each component is crucial in determining their appropriate sizing, selection, implementation, and control. The following components represent the general structure of a microgrid.

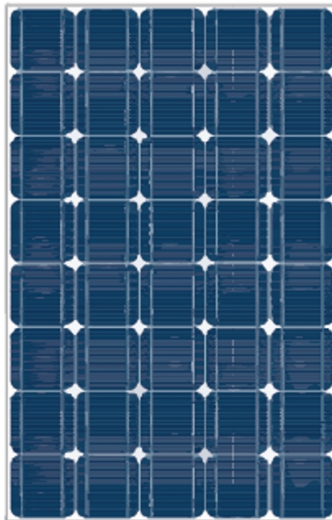
### 2.3.1 Photovoltaic panels

Photovoltaic (PV) panels comprise multiple small cells that convert solar radiation into electricity (Fontenot and Dong 2019). The following sections detail the main characteristics of PV panels.

#### 2.3.1.1 Components of PV panels

A PV panel, also known as a PV module, consists of interconnected cells that are electrically connected and protected from the weather. These panels are commonly encased in tempered glass and framed with tempered aluminum, facilitating their transportation and installation.

The solar cells within the panel are electrically linked together, and the entire assembly is tightly sealed and protected using vacuum sealing techniques, as illustrated in Figure 2.3.

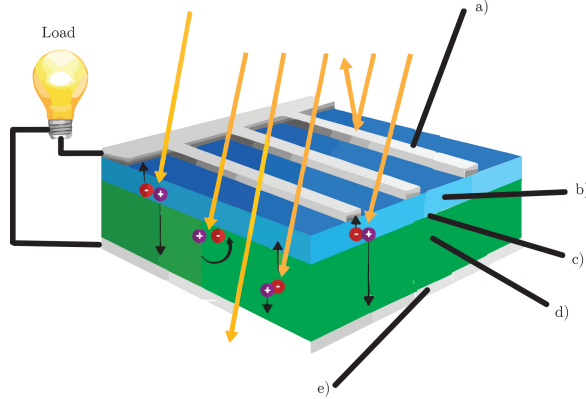


**Figure 2.3:** PV panel, adapted from (Shaikh 2017).

A solar cell is a small component that converts sunlight into electricity by the PV effect. It is essentially a diode semiconductor capable of developing a voltage of  $0.5 - 1.0V$  and a density of current of  $20 - 40mA/cm^2$  depending on the materials used for its elaboration and sunlight conditions (Yang et al. 2018).



Every modern solar cell usually consists of the following components (Figure 2.4):



**Figure 2.4:** Components of a PV cell, adapted from (Guerra et al. 2018).

- a) Glass plate. It allows light to enter the cells and protects the semiconductors.
- b) Anti-reflective layer. It is placed between the glass plate and the semiconductor, minimizing the light loss by reflection.
- c) The n-type semiconductor layer. It contains a concentration of excited electrons greater than the p-type shell. The electrical charges are transported from the n-type layer to the p-type layer causing a voltage in the solar cell.
- d) Semiconductor plates. These sections are placed for type n and p layers. It offers a pathway for electrons to go from the n-type semiconductor to the p-type, generating an electric field.
- e) The p-type semiconductor layer. It has an electron deficiency, attracting excited electrons from the n-type shell. As a result, a potential difference (voltage) between both layers is presented.

### 2.3.1.2 Types of photovoltaic cells

There are different technologies on the market. The most used cells are silicon-based technologies representing 90% of global photovoltaic production (Yang et al. 2018). In this sense, there are three types of cells as described in Table 2.1.

### 2.3.1.3 Electrical characteristics of a PV panel

Each PV panel manufacturer offers documentation and labeling that provide comprehensive product information. These specifications typically include

Type of cell	Efficiency [%]	Characteristics
Crystalline silicon	22	Made of a crystal of vastly high purity silicon with homogeneous blue color. They have outstanding performance and a life of up to 25 years of use. They represent the highest price on the market.
multi-crystalline silicon	18	Made of silicon mixed with Arsenic and Gallium. Lower price compared to the previous one. Life of use is less than 20 years. Different shades of blue color.
Amorphous	13	Made of a thin layer of silicon. Low performance and prices. Homogeneous brown color.

**Table 2.1:** Types of PV panels (Yang et al. 2018).

electrical terminology, general product details, cell type, physical characteristics (such as width, length, thickness, and weight), and the type of junction box used, among other relevant information.

One important characteristic is the I–V curve of a PV panel, which indicates the range of current and voltage values the PV panel provides. This curve is derived from standard test conditions (STC), which involve an irradiance level of  $1000 \text{ W/m}^2$  and a cell temperature of  $25 \text{ }^\circ\text{C}$ . The I–V curve provides valuable insights into the performance and capabilities of the PV panel for electricity production (Steiner and Siefer 2023).

#### 2.3.1.4 I–V curve of a PV panel

The I–V curve provides the current-voltage ratio for different loads (Steiner and Siefer 2023).

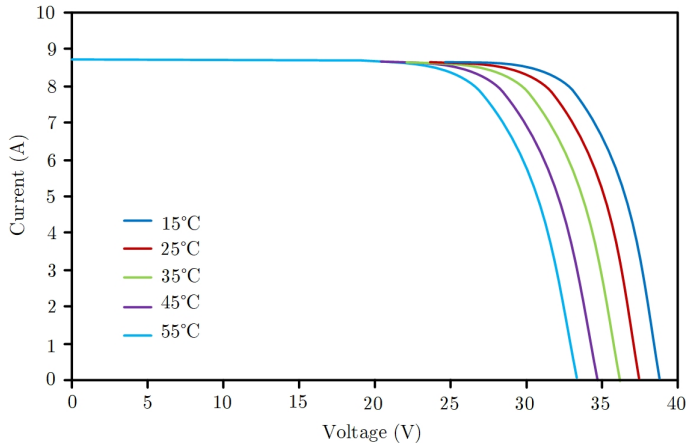
The following parameters are identified from the I–V curve:

- Open circuit voltage ( $V_{oc}$ ). It represents the maximum voltage in volts obtained from the PV panel in the STC conditions from open circuit operation.

- Short circuit current ( $I_{sc}$ ). It is the maximum intensity in amperes that can be obtained from the PV panel in STC conditions, causing a short circuit.
- Maximum voltage ( $V_{PV}$ ). It is the voltage value corresponding to the maximum power point ( $MPP$ ). It is about 80% of the open circuit voltage.
- Maximum current ( $I_{PV}$ ). It is the current value corresponding to the  $MPP$ .
- Peak power or maximum power ( $P_{max}$ ). This parameter of power is also called  $MPP$ . It is the maximum power in watts supplied by a PV panel when the product of the voltage by the intensity is maximum.

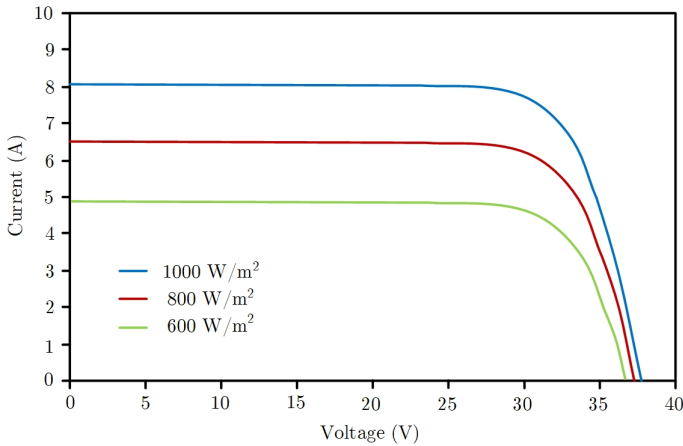
### 2.3.1.5 Environmental effects on solar panels

The operational temperature range for PV panels is typically 20 °C to 25 °C higher than the surrounding environmental temperature. However, this elevated temperature adversely affects the efficiency of electronic devices. As the temperature rises, the PV current remains relatively constant. Still, there is a substantial decrease in voltage, resulting in a reduction in the  $MPP$  as illustrated in Figure 2.5.



**Figure 2.5:** Changes in I–V curve due to temperature, adapted from (Cubas, Pindado, and De Manuel 2014)

Conversely, as the solar radiation increases, the short circuit current of PV cells also increases, although there is a moderate decrease in the open circuit voltage (Li et al. 2021). The greater the amount of radiation the PV system receives, the higher the power that can be extracted, as depicted in Figure 2.6.



**Figure 2.6:** Changes in I–V curve due to solar radiation, adapted from (Cubas, Pindado, and De Manuel 2014).

### 2.3.1.6 Solar radiation

Solar radiation is quantified using irradiance units, which measure the luminous power received in a surface area of  $1 \text{ m}^2$  at a given moment. The unit of irradiance is expressed as watts per square meter ( $\text{W}/\text{m}^2$ ). Irradiance can be categorized into three components based on its behavior: direct, diffuse, and albedo radiation. Together, these three types of irradiance represent the total incident radiation the sun produces. Furthermore, the accumulation time of solar irradiance (such as days, months, or years) is called solar insolation. This metric represents the total amount of solar energy the sun produces in a given time. Its unit is expressed as kilowatt-hours per square meter ( $\text{kWh} - \text{h}/\text{m}^2$ ) (Li et al. 2021).

### 2.3.2 Batteries

Batteries are energy storage devices that rely on chemical reactions to produce electricity. The key characteristics of a battery include its capacity in ampere-hours and the depth of discharge (Kong et al. 2019). The features as explained as follows:

#### 2.3.2.1 Charge and discharge capacity

Capacity refers to the current a battery can deliver/receive over a specified number of hours at its nominal voltage, typically at 25 °C. Capacity is measured in ampere-hours (Ah).

The charging and discharging regime can be determined by dividing the rated battery capacity ( $C_{bat}$ ) by the nominal current the battery can deliver ( $I_N$ ), as illustrated in Equation 2.1.

$$Ch/Dis\ time(h) = \frac{C_{bat}(Ah)}{I_N(A)}. \quad (2.1)$$

Where  $Ch$  means the charge time and  $Dis$  means the discharge time of the battery. Typically, the capacity of a battery is presented employing the letter  $C$  followed by indexes between 5 to 100 that represent the time in hours. For instance, the indexes  $C_5$  and  $C_{100}$  show the battery will be discharged in 5 and 10 hours, respectively. The working point temperature influences the battery capacity. If the temperature decreases, the capacity decreases as well. On the other side, an elevated temperature causes a reduction in battery life. For example, one of the batteries widely used in PV applications is the lead-acid (Pb-Acid) battery due to its low costs compared to similar technologies (Charles et al. 2019). Table 2.2 shows the characteristics of a lead-acid (Pb-Acid) battery between temperature and its life of use.

#### 2.3.2.2 Battery life

The lifespan of a battery is commonly measured in cycles, which refers to the number of charge and discharge cycles it undergoes. The battery's usable capacity and overall lifespan can decrease with each cycle. Therefore, it is crucial to carefully manage the number of cycles that batteries in PV systems experience to maximize their lifetime and performance.

Two important metrics related to battery performance are the state of charge (SOC) and the depth of discharge (DOD). The state of charge indicates

Electrolyte temperature [ $^{\circ}C$ ]	Reduced life of use [%]
25	0
30	30
35	50
40	65
45	77
50	87
55	95

**Table 2.2:** Example of life of use of a Pb-acid battery, adapted from (Hariprakash et al. 2001).

the remaining capacity of the battery as a percentage of its nominal capacity, providing valuable information about the current charge level. On the other hand, the depth of discharge represents the percentage of the battery's nominal capacity that has been discharged, indicating the extent to which the battery's total capacity has been utilized (Lee et al. 2020). The following equations show the capacities  $SOC$  and  $DOD$ :

$$SOC(\%) = \frac{C_{bat}(Ah) - Used\ C_{bat}(Ah)}{C_{bat}(Ah)}, \quad (2.2)$$

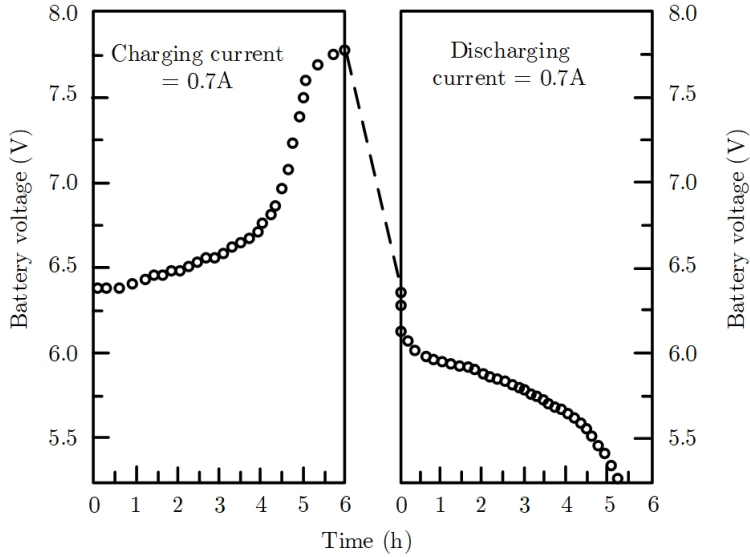
$$DOD(\%) = \frac{Used\ C_{bat}(Ah)}{C_{bat}(Ah)}. \quad (2.3)$$

Where  $C_{bat}$  refers to battery capacity, the voltage of the batteries varies according to the  $SOC$ . Figure 2.7 shows the  $SOC$  and  $DOD$  characteristics for a lead-acid battery with a nominal voltage of 12 V and an electrolyte temperature of 25  $^{\circ}C$ .

### 2.3.2.3 Types of Batteries

PV systems utilize various types of batteries that possess different characteristics and costs. The main types of batteries used in PV systems are summarized below (Saha et al. 2022).

The first battery type is *lead-acid batteries*, consisting of two positive and one negative electrode. These batteries employ an electrolyte solution of sulfuric acid mixed with distilled water. Lead batteries function based on a chemical



**Figure 2.7:** Typical charge-discharge voltage for a sealed PB-Acid battery, adapted from (Hariprakash et al. 2001).

reaction between lead and sulfuric acid, which generates a potential difference between the battery terminals. When electricity is applied to the battery, this reaction is reversed, allowing the energy to be stored for later use.

Furthermore, *gel batteries* use a gel form of acid. This gel eliminates the presence of liquid that could be lost due to poor battery usage. As a result, corrosion is reduced. Gel batteries offer advantages such as higher resistance to low temperatures, extended lifespan, and durability in deep discharge cycles. However, they have slightly higher internal resistance, limiting the maximum current flow, and they tend to be more expensive than other battery types.

### 2.3.3 Charge Controller

A charge controller is a device that regulates batteries' charging and discharging cycles in PV systems (Yang et al. 2020). Its main features are summarized as follows:

- It prevents overcharging of batteries once they reach full charge, suspending the charging process to avoid gas production and excessive temperature increase.

- It safeguards against over-discharging during insufficient sunlight, preventing premature battery degradation.
- It ensures the PV system operates at its maximum power point (*MPP*).

Most commonly used charge controllers have nominal voltage values of 12, 24, or 48 V to interconnect an external battery. The selection of these devices depends on the load's demand, considering the maximum current and power requirements.

The operational principle of the charge controllers is based on the load conditions, and it can be described through the following stages:

1. Equalization: This stage equalizes the charge among the battery cells after a low state of charge. Balancing the charges minimizes gassing and ensures balanced battery performance.
2. Deep charge: Following the equalization stage, the system allows uninterrupted charging of the batteries until the nominal battery voltage value is reached. Then, the system switches to the float stage, indicating that the battery has reached approximately 90% of its capacity. In the next phase, the charging process will be completed.
3. Final charge and float: The final charging phase involves setting a Dynamic Flotation Band (DFB), which defines a voltage range. This range spans approximately 10% between the final load and nominal voltage. The system operates within this band to perform the last charge, ensuring optimal battery performance.

Upon reaching a full charge, the controller injects a small, floating current. This current serves two purposes: it keeps the battery fully charged and compensates for the self-discharge of the battery when no energy is consumed.

These stages and control mechanisms ensure efficient charging, proper maintenance, and extended lifespan of the batteries in the PV system.

### 2.3.4 Voltage Source Inverter

The voltage source inverter is crucial for converting the energy in a PV system. This device was extensively discussed in the *basic definitions* from Section 2.2.



### 2.3.5 Programmable Logic Controller

A Programmable Logic Controller (PLC) is an industrial computer used in various automation applications. These devices execute activities programmed by users in code. The PLC is a fundamental component of a microgrid as it controls the closed-loop regulation of the PV system, interpreting the measurements performed by different sensors and transmitters (Wang et al. 2020).

### 2.3.6 Energy Meter

The energy meter allows the acquisition of essential parameters in an electrical system, including voltage, current, power, and harmonic content. This equipment receives feedback signals for monitoring any electrical system (Wang et al. 2020).

The energy meter enables the measurement of relevant parameters in an electrical system, such as voltage, current, power, and harmonic content. This equipment receives feedback signals used to monitor and analyze the electrical system.

As previously mentioned, numerous studies have considered MGs' parameters and performance characteristics. These studies have been mentioned in a general sense to provide context for analyzing the MG and its components. So, it is essential to analyze the electrical operation at one of the primary components of the microgrid responsible for the energy conversion process: the voltage source inverter for single-phase applications.

## 2.4 Overview of Single-Phase Inverters Topologies

Inverters can be adapted to single-phase or three-phase electrical systems. The choice of which system to employ depends on the specific functionalities desired for a particular working area. While this work primarily focuses on single-phase systems, it is important to note that there are no marked differences between single-phase and three-phase systems due to their very similar principles of energy generation.

As mentioned earlier, inverters are electronic devices that convert energy from DC into AC. Initially, these prototypes faced challenges adapting to industrial applications due to their complexity and high cost, as mentioned in (Luo and Ye 2017). However, a significant breakthrough occurred before the 1960s

when a new era of robust and affordable inverter technology was introduced, revolutionizing several industrial applications.

By the 1970s, inverters had gained widespread use in AC applications like speed control in AC motors, surpassing the popularity of DC motors in previous decades. This shift emphasizes the numerous advantages of inverters, including compact size, cost-effectiveness, and reduced maintenance requirements to perform various industrial applications. The development of semiconductor technology in the 1980s further enhanced the performance of electrical converters. Introducing devices such as MOSFETs and IGBTs produced robust and reliable inverters, widely adopted across various industrial improvements (Luo and Ye 2017).

Presently, inverters are utilized in diverse technological domains, employing a range of topologies. The control of semiconductors in inverters is based on various techniques, ranging from pulse width modulation (PWM) to multilevel modulation (MLM). Among these techniques, PWM stands as the most commonly used modulation technique and finds extensive application in topologies such as voltage source inverters (VSIs), current source inverters (CSIs), impedance source inverters (ZSIs), and multistage PWM inverters (Periyamayagam et al. 2020).

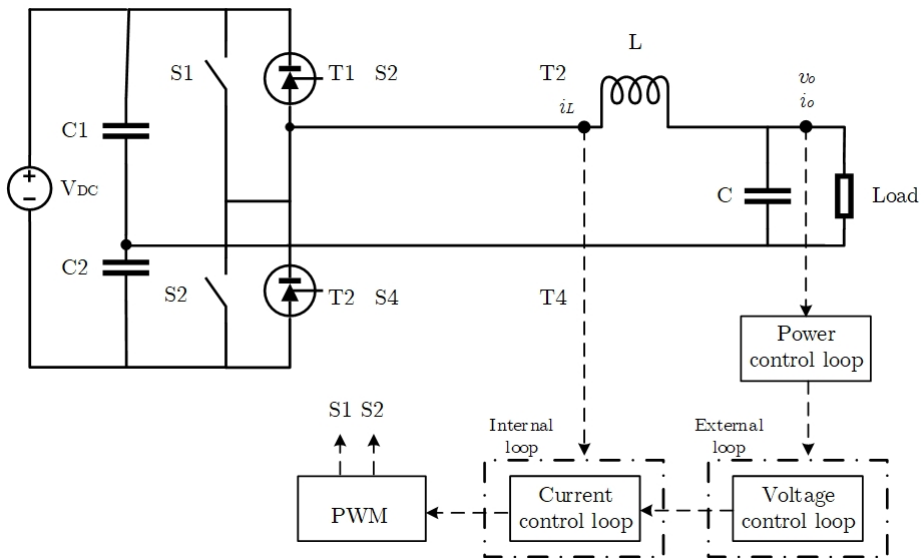
Inverters are broadly employed in the following applications (Fontenot and Dong 2019):

- AC machines that utilize Voltage and frequency control mechanisms to regulate their speed.
- Stabilized AC power sources that provide a constant voltage, such as uninterruptible power supplies (UPSs).
- Implementation of flexible AC transmission systems (FACTS).
- Employment of passive and active filters to mitigate unwanted signals or harmonics.
- Devices used for compensating reactive power.

The existing literature comprises various VSIs, finding different topologies and switching methods to enhance the output voltage. The following section will discuss the common topologies used in single-phase inverters, as this thesis highlights the applications of a single-phase electrical system. However, the principles and considerations outlined in single-phase configurations can be applied to three-phase systems commonly found in industrial applications.

### 2.4.1 Single-Phase Half-Bridge Voltage Source Inverter

This topology as seen in Figure 2.8, represents the simplest form to perform DC to AC energy conversion. In this scheme, S1 and S2 (power switches) switch in different instants. A key consideration is avoiding switching S1 and S2 simultaneously to prevent short circuits. The two anti-parallel thyristors (T1 and T2) provide reverse voltage control if a bi-directional power converter is needed. Two capacitors (C1 and C2) are added to balance energy and establish a neutral point. These capacitors must be similar to each other to ensure a balanced performance.



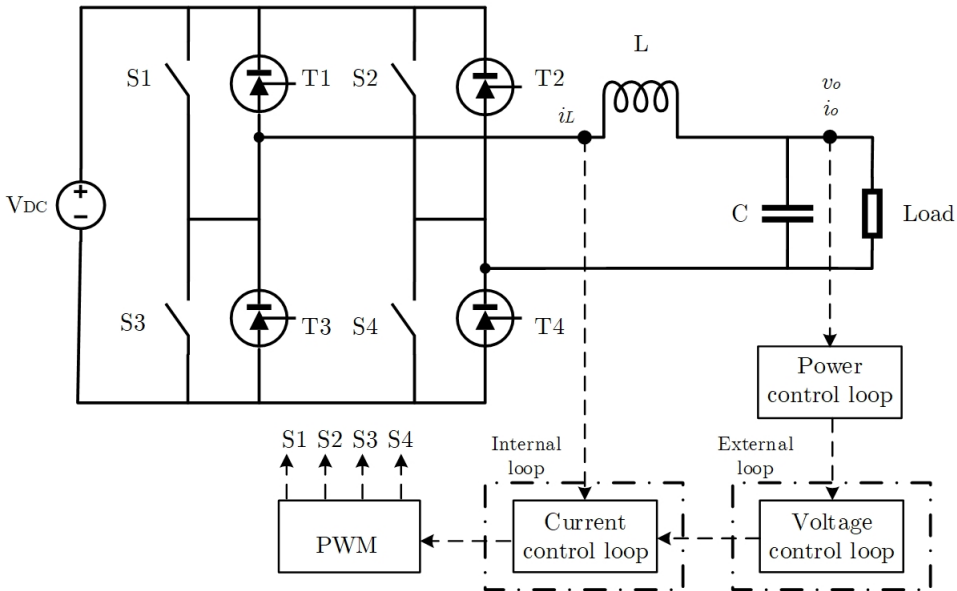
**Figure 2.8:** Single-phase inverter in islanding operation, adapted from (Vásquez et al. 2017).

Even though the half-bridge scheme is one of the simplest VSI models, several works use this topology due to the versatility of two power switches, the generation of two control signals, and the use of a floating reference on the DC bus formed by two capacitors ( $C1$  and  $C2$ ). In solar systems, these schemes demonstrate flexibility and fast energy control. Several half-bridge VSIs form symmetric and asymmetric topologies for adapting a single DC source. The symmetry will depend on the capacitance values of the parallel capacitors; if the capacitance values are equal, the voltage generation is symmetric. In this context, the energy density is high because of various topologies adapted in series and parallel arrays to achieve applications of high energy values. How-

ever, drawbacks are found, such as the high harmonic distortion of the output waveform. This drawback is addressed for a better topology called *full bridge* or *H-bridge* (Ginart 2018).

### 2.4.2 Single-Phase Full-Bridge Voltage Source Inverter

This circuit as seen in Figure 2.9, employs four power switches (S1 to S4) for output voltage generation and four anti-parallel thyristors (T1 to T4) to enable reverse voltage conversion from the load to the source. The power switches generate the output voltage  $v_o$  by applying PWM or SPWM signals. Given the increasing implementation of distributed energy resources (DER), storage systems are essential for enhancing stability and resilience in energy conversion within the VSI (Vásquez et al. 2017). These storage systems play a crucial role in compensating for variable solar radiation and fluctuations in MGs, thereby improving the performance of IBMGs. Notably, advancements in electric batteries have boosted energy integration from electric vehicle batteries into the grid, thereby supporting non-conventional electricity generation (Clairand et al. 2019a).



**Figure 2.9:** Single-phase inverter in islanding operation, adapted from (Vásquez et al. 2017).

The proper management of output voltage generation is needed by employing a control algorithm. To ensure precise control, the closed-loop scheme incorporates cascade control for both voltage and current, utilizing output power measurements. At the output stage of the VSI, a low-pass  $LC$  filter is positioned. This filter generates a sinusoidal voltage waveform tailored to meet the operating frequency requirements (50 or 60  $Hz$ ) of the grid where the inverter is connected.

In this context, the waveforms responsible for driving commutations in electronic devices are depicted in Figure 2.10, utilizing two sine waves. The sinusoidal PWM (SPWM) technique compares sine and triangular signals to produce the modulation signal for the power switches in the inverter. The resulting modulated signals over S1 to S4 incorporate a deliberate delay to minimize harmonic content. As a result, the output voltage exhibits a sinusoidal waveform, and efforts are made to ensure that the output current approximates a sinusoidal shape. However, the behavior of the current output will be influenced by the characteristics of the load connected to the VSI.

To generate the proper modulation signals for power switches, the control of VSIs is commonly achieved using cascade control schemes, as described in Shen et al. (Shen et al. 2019). The cascade control structure consists of an internal loop responsible for regulating the current, denoted as  $i_o$ , and an external loop focused on regulating the voltage, represented as  $v_o$ , within the VSI. Various controllers, from classical to advanced algorithms, are utilized at different system stages to accomplish precise control.

Figure 2.11 illustrates the power control scheme employed in VSIs. This scheme requires measurements of the output voltage  $v_o$  and current  $i_o$  at the  $LC$  filter output. The power delivered to the load, considering the impedance of the output connector ( $R_c, L_c$ ), is computed. These power values are then filtered through a filter composed of inductance ( $L_f$ ) and capacitance ( $C_f$ ) to reach the control module.

The control algorithm considers both the active power ( $P_i$ ) and reactive power ( $Q_i$ ) values to regulate the frequency and output voltage of the VSI. The control algorithm receives references for the voltage ( $V_o$ ) and frequency ( $\omega_o$ ), which are used to calculate the voltage reference ( $v_i$ ) for the outer loop of the cascade control. Subsequently, the inner loop utilizes the reference current ( $i_{li}^*$ ) from the outer loop to control the VSI current ( $i_{li}$ ) using an SPWM signal applied at the input of the inverter.

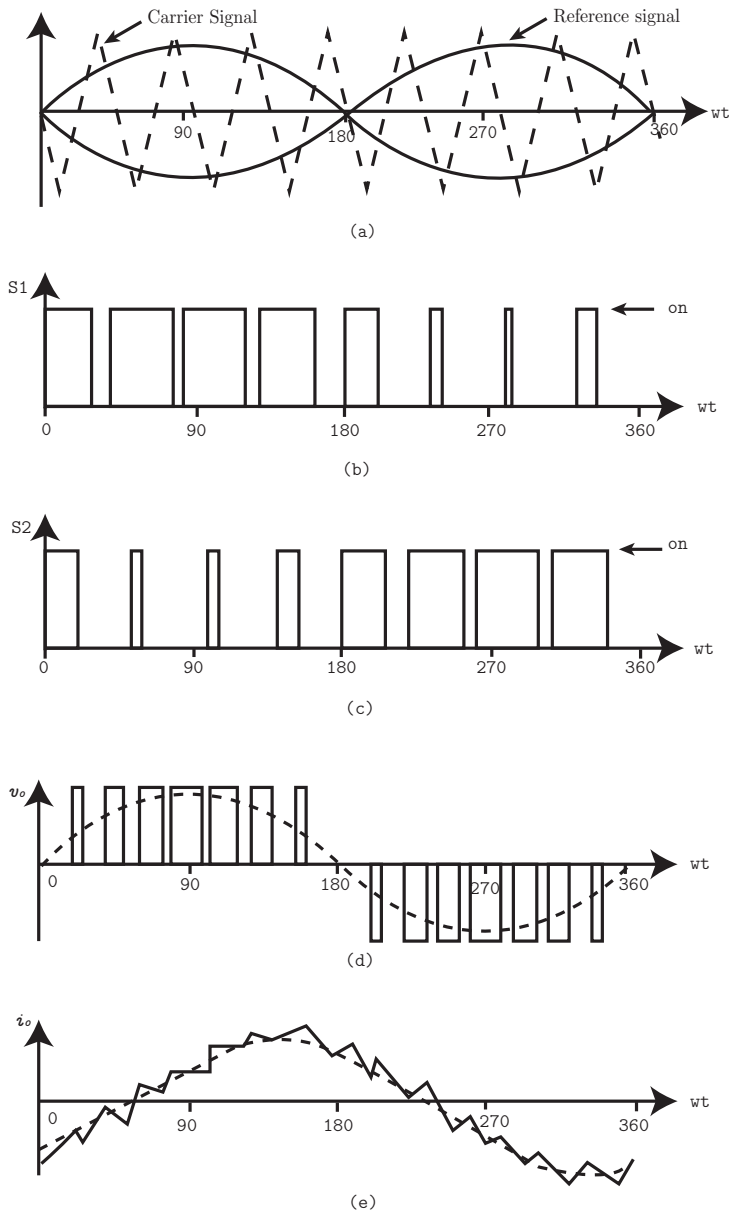


Figure 2.10: SPWM for a single-phase full-bridge inverter, adapted from (Ye et al. 2020).

This cascade control strategy enables precise regulation of the current and voltage within the VSI, ensuring efficient and reliable operation.

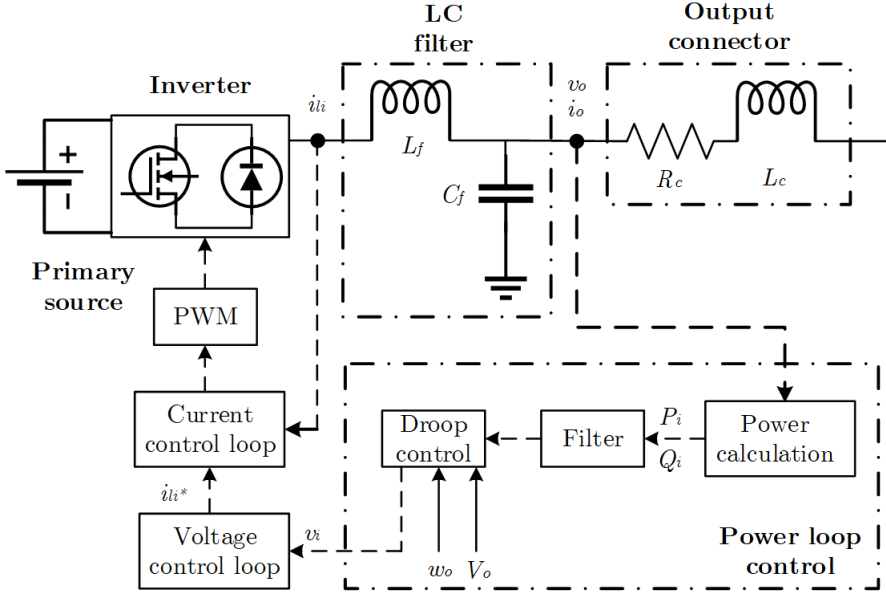


Figure 2.11: Single-phase inverter in islanding operation, adapted from (Shen et al. 2019).

Once the power conversion is understood, the following step is the analysis of the MG integration and the different control schemes employed to ensure operating conditions. These points are seen in the next section.

## 2.5 Microgrid Energy Management

The following sections will describe the main features of MG's structure and energy management.

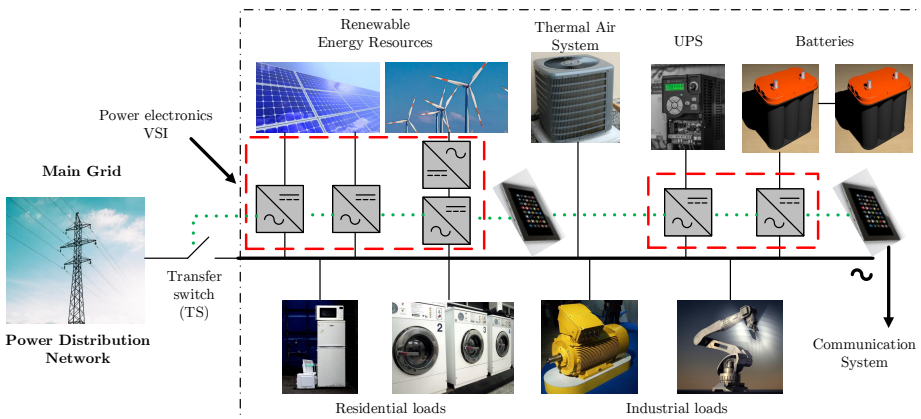
### 2.5.1 Single-phase IBMG energy management approach

As mentioned, MGs are smaller-scale power generation systems than traditional grids. They combine diverse energy resources in parallel, providing reliable and efficient electrical energy. MGs' growth benefits many countries, including competitive investment costs, scalability, and flexible operation (Olivares et al. 2014). In this context, challenges related to energy management,

electrical connectivity, and fossil fuel utilization are overcome. The integration of renewable resources into the traditional grid is addressed through MGs, resulting in a widespread implementation trend and ongoing research on protection schemes and robust closed-loop control. MGs incorporate various power sources such as batteries and renewable or non-renewable energy sources (Miveh et al. 2016), as depicted in Figure 2.12. MGs can operate in conjunction with the main grid or island mode when working independently. MGs represent an additional source of generation that can supply power to both linear and non-linear loads (Arbab-Zavar et al. 2019).

The interface between the MG and the conventional electrical grid is established through electronic power converters (EPCs). The EPCs enable the MG to absorb or inject electrical energy. In the case of the grid operating in a connected state, the frequency and voltage of the grid are standardized values. However, when the MG operates in island mode, the voltage, frequency, and harmonic content exhibit variable values due to the low inertia of the system (Kerdphol et al. 2017). These parameters become unstable and require recalibration of the EPC specifications to ensure the proper operation of equipment and systems (Andishgar, Gholipour, and Hooshmand 2017).

To address this issue, extensive research has been conducted to enhance the stability of MGs operating on-grid or in island mode. One approach involves the application of automatic control methods to EPCs. These methods improve energy exchange during shared load situations, mitigate harmonics generated



**Figure 2.12:** Microgrid scheme from different inverter-based sources adapted from (Miveh et al. 2016).



by non-linear loads, and address the slow dynamic response resulting from the implementation of low-pass filters to measure voltage, current, or power values (Baharizadeh, Karshenas, and Guerrero 2018).

At the regulation level, various inverter topologies are studied to develop appropriate control laws that meet the reliability specifications of a power electrical system (PES). Consequently, research has focused on objectives such as improving hierarchical control structures (Tavakoli et al. 2018) or developing intelligent inverter systems that utilize communication networks among inverters (Arbab-Zavar et al. 2019) regarding the MG's low inertia, regulation schemes presented by (Yang et al. 2019) address voltage and frequency stability.

Stability is crucial in MGs, as electricity production must be maintained within safe operation levels. This aspect becomes critical to the widespread implementation of MGs, as they differ from traditional grid production due to factors such as line impedances. The steady-state variables of the system must satisfy constraints related to voltage, current, and frequency, even when the MG is sharing power or operating in island mode under strong disturbances in the grid (Farrokhhabadi et al. 2019).

On the other hand, efficient management of an islanded microgrid involves control systems that explore alternative approaches to overcome challenges associated with distributed generation (DG). These objectives, continually under development, ensure system stability and reliability. The most significant trends in this field are outlined below (Yoldaş et al. 2017):

- *Control of Output Variables:* The IBMG requires precise control of the output voltage and current variables to track their set points closely. In the presence of disturbances, it is essential to dampen the oscillations of these variables to prevent significant deviations that could impact load performance.
- *Power Flow Control and Protections:* As MGs are increasingly integrated into the utility grid to support electrical generation, it is crucial to prepare systems to accommodate additional electrical generation without overloading their infrastructure. Algorithms have been developed to limit high-line currents due to voltage variations in the utility grid. Furthermore, the IBMG controller must effectively balance power supply and demand, even during sudden load changes. The controller aims to stabilize the IBMG system, accounting for equipment disconnection, integrating RES, and activating electrical protections.

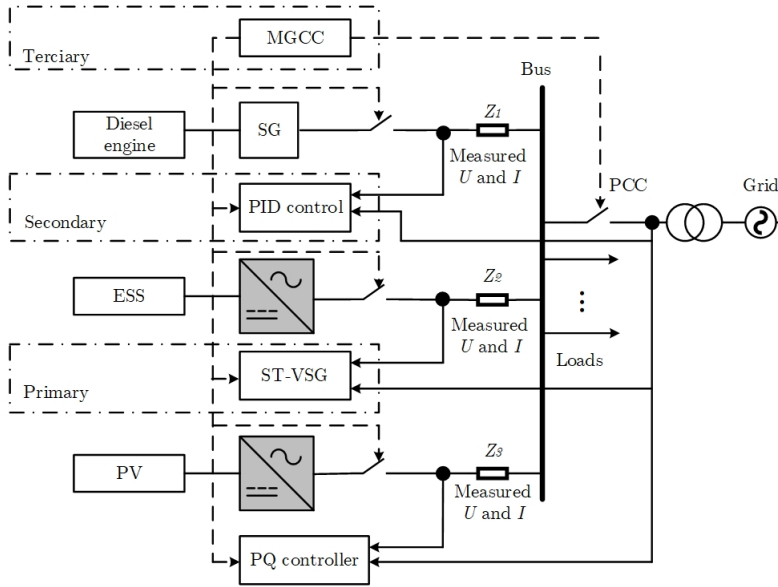
- *Cost-Benefit*: Efficient control of the IBMGs should result in energy and economic benefits for its consumers. These advantages are particularly noticeable in isolated areas that invest in IBMG equipment, as the return on investment is relatively quick. The benefits include lower electricity payments and the sustainable utilization of natural resources.
- *Transition between Operating Modes*: The IBMG can operate in conjunction with the conventional grid for power-sharing purposes or independently in island mode. Smooth transitions between these two states are essential, maintaining stable voltage and frequency variables to ensure transient stability.
- *Controller Tuning*: The performance of controllers can be affected by the variability of process behavior, especially during significant changes in the generation system. In such cases, it may be necessary to re-tune the controller to adapt to the new conditions. Controller tuning works well within specific performance ranges, but it may not effectively address regulation conditions when the distributed generation (DG) system operates outside its linear zone. This issue is mainly studied in the context of high incorporation of nonlinear loads, limited disturbance rejection capability, and communication delays in hierarchical MG control systems.

## 2.5.2 Hierarchical control structure

Hierarchical control in an MG represents a defined term to characterize a standard on DG. This structure means three control levels with other objectives and time scales. In this sense, primary, secondary, and tertiary control structures have been defined (Hou et al. 2018). This structure coordinates the different control levels necessary to manage electricity production. At each level is implemented a control algorithm to manage voltage, frequency, and power, among other MG variables. A typical hierarchical control is seen in Figure 2.13, where authors of (Shi et al. 2018b) implemented a control scheme on a PV-battery-diesel MG.

This scheme implemented a suitable controller aligned with the MG generation objectives. The framework encompasses a range of algorithms, including traditional controllers like PID and inertia regulation techniques derived from the control scheme. However, further research and development are necessary for this domain to meet the reliability goals demanded by MGs effectively.

### 2.5.2.1 Primary Control



**Figure 2.13:** Hierarchical scheme for control a PV-battery-diesel MG, adapted from (Shi et al. 2018b).

The primary control plays a crucial role in adjusting voltage and frequency values to specific rates in the MG. Its primary objective is to ensure the system's reliability by improving local voltage performance and stability. Distributed generation (DG) utilizes this control mechanism for practical power-sharing activities (Kundur, Balu, and Lauby 1994).

The primary control structures possess the following characteristics:

- The regulation of internal voltage and current loops is achieved through linear and non-linear controllers. The objective is to measure and monitor current in inductors and capacitors at the output of a filter. The controller must ensure a fast and stable response to maintain these values.
- The generation of virtual impedance to emulate a physical impedance connected to the system's output is needed.
- The regulation of external control loops for active and reactive power variables. These values govern the primary-level output voltage regulation. Generally, a method called *droop power control* is utilized.

Droop power control is employed at this stage, introducing voltage and frequency variations in the inverter, as expressed in the following equation:

$$\begin{aligned}\omega &= \omega^* - m(P - P^*), \\ E &= E^* - n(Q - Q^*).\end{aligned}\tag{2.4}$$

Where  $\omega^*$  represents the angular frequency,  $E^*$  denotes the amplitude of the no-load output voltage, and  $m$  and  $n$  are coefficients defining the slope of frequency and voltage, respectively. Furthermore,  $P^*$  and  $Q^*$  serve as reference values for active and reactive power  $P$  and  $Q$ , respectively (Rokrok, Shafie-Khah, and Catalão 2018). Droop control has been extensively studied, and various variants have been proposed to enhance the performance of primary control. These include  $P - F/Q - U$  droop control, Modification of  $P - F/Q - U$  droop control, and  $P - U/Q - F$  droop control, as discussed in (Rokrok, Shafie-Khah, and Catalão 2018). Furthermore, works employed a method based on DQ coordinates to address voltage and frequency distortion in systems operating at a fixed frequency (Toub et al. 2019).

### 2.5.2.2 Secondary Control

The secondary control manages the connection between the MG and the main grid. Its objective is to transition from island mode to a conventional generation system. During this process, the closed-loop regulators restore the frequency and amplitude variables to stable values, which may have changed during synchronization. The MG measures the required frequency and amplitude values for continuous feedback control. If a significant difference exists, these values can be restored at that time (Shuai et al. 2018).

### 2.5.2.3 Tertiary Control

The MG facilitates energy flow exchange with the main grid at the tertiary control level. This means that the MG can inject or absorb power based on the requirements of the environment. The manipulated variables at this level are the active power ( $P$ ) and reactive power ( $Q$ ) (Shuai et al. 2018).

Governments and institutions worldwide are developing policies to redefine environmental approaches. These efforts have transformed how fossil fuels are consumed. Microgrids play a crucial role in this transformation, as they have the potential to significantly impact electricity generation from carbon-based sources through the widespread adoption of renewable energy. The next section will show microgrids' environmental concerns in achieving green energy philosophy.

## 2.6 Microgrid's Opportunity on Environmental Concerns

Fossil fuel energy consumption is a global concern, particularly in countries with extensive industrial areas. Continuous emissions of carbon dioxide (CO<sub>2</sub>) into the atmosphere of carbon, coal, and petroleum severely affect our planet. The concentration of greenhouse gases (GHGs) contributes to climate change on a global scale.

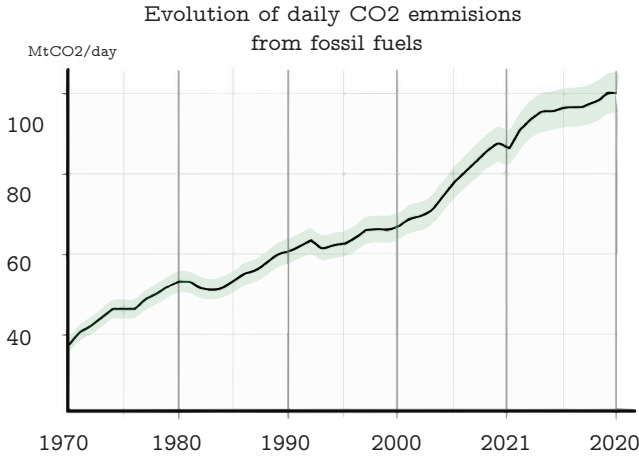
Mitigation has become a widely used term associated with the actions taken to reduce environmental damage to the planet. Renewable resources offer an innovative strategy to address this escalating problem. Using sustainable energy sources such as solar, tidal, and wind power has gained recognition. In contrast, non-renewable resources like oil have finite availability. Microgrids have emerged as an alternative generation method, often incorporating different energy sources to mitigate the effects of concentrated GHGs in the atmosphere.

Fossil fuels originated in the Paleozoic period around 600 million years ago. Coal formation in geological formations takes considerable time, eventually depleting these reserves. This fundamental reason classifies coal as a non-renewable resource. Petroleum, on the other hand, depends on the decomposition of animal and plant matter over time. While petroleum could be considered renewable if the decomposition process continues, it takes many years, indicating an impending shortage.

### 2.6.1 International Environmental Policies

The fragility of our planet has prompted extensive research into remediation methods for diverse ecosystems. Carbon levels have reached alarming heights, and overcoming this problem will require the collaborative efforts of many future generations. Industrial growth since the 1900s, coupled with the impact of CO<sub>2</sub> emissions on Earth's ecosystems, has been exponential. Population growth exacerbates the issue, particularly in Brazil, China, and India. Population density leads to expansion and environmental damage that is challenging to overcome. However, innovative solutions must be devised to address these problems. Energy and the economy are closely interconnected factors. Figure 2.14 illustrates the continuous rise in CO<sub>2</sub> production over the last few decades (Peters et al. 2020).

CO<sub>2</sub> concentrations are approaching critical levels, with values as high as 410 parts per million (ppm). This translates to approximately 100 million tons of CO<sub>2</sub> being released into the Earth's atmosphere daily. The rapid growth



**Figure 2.14:** Global carbon dioxide emissions, adapted from (Peters et al. 2020).

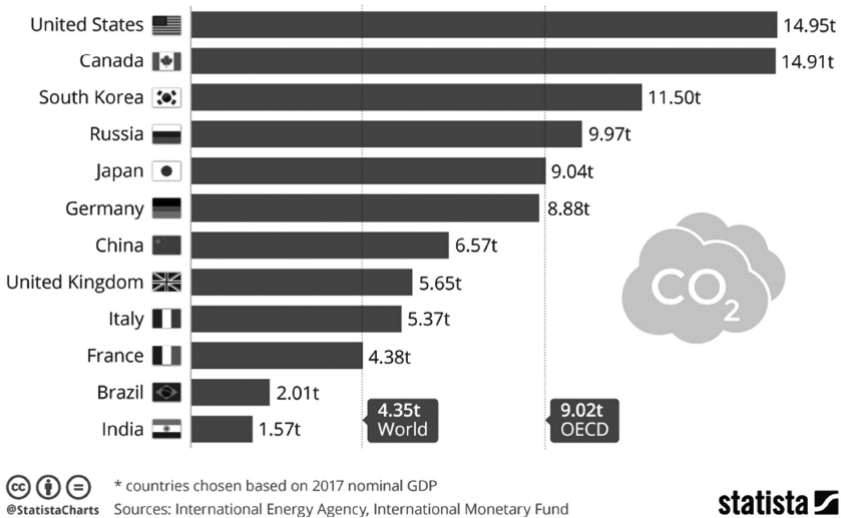
of environmental pollution has caused a temperature increase of  $2^{\circ}C$  to  $3^{\circ}C$ , contributing to rising water levels. The gradual melting of glaciers has raised concerns, leading to increased instances of flooding, such as in Venice, Italy, which were unheard for this place 50 years ago.

The growth of greenhouse gases in the atmosphere has been significant. By the 2000s, CO2 emissions were increasing by 3% annually due to the lack of stringent environmental mitigation policies. By 2030, CO2 emissions will reach 42.9 billion metric tons, raising substantial concerns about the impact on the environment, economy, health, and resources.

Despite the notable advantages of implementing microgrids, there are still lingering questions about the potential environmental impact of widespread adoption. Undoubtedly, this is an essential concern since one of the primary objectives of microgrids is to mitigate the ecological effects. The following section highlights the key environmental considerations that should be addressed in implementing microgrids on a larger scale.

## The Global Disparity in Carbon Footprints

Per capita CO<sub>2</sub> emissions in the world's largest economies in 2016\* (in metric tons)



**Figure 2.15:** Dioxide of carbon emissions per capita by 2016, adapted from (Fuller 2018).

### 2.6.2 The Kyoto and Paris Agreements

Environmental remediation has become a significant challenge in recent years, leading various countries and institutions to propose solutions for reducing CO<sub>2</sub> emissions. The continuous negotiations to reach global consensus have resulted in formulating essential policies, notably the Kyoto and Paris Agreements (Pickering et al. 2018). The Kyoto Protocol, established in 2005, introduced targets for GHG emissions to be balanced at anthropogenic or manufactured levels.

Since the implementation of the Kyoto Protocol, countries such as the United States have made gradual progress in reducing CO<sub>2</sub> production. However, further efforts are required to meet the agreement's targets. One of the main arguments against achieving these objectives is the potential economic repercussions for industrialized nations.

By 2016, the Paris Agreement was signed, representing a more ambitious commitment to global GHG emission reduction and striking a balance between industrial production and environmental priorities. Several industrialized countries have demonstrated their commitment to fulfilling the objectives of the

**Table 2.3:** Study from McKinsey to GHG reductions in USA.

Action	GHG reduction in megatons
CO <sub>2</sub> reduction from electric power production by using alternative energy and CCS technologies	800-1570
Improved energy efficiency in buildings and appliances	710-870
Implementing carbon reduction opportunities in the industrial sector	620-770
Expanding natural carbon sinks to capture and store more carbon	440-590
Increasing vehicular efficiency using less carbon-intensive fuels	340-660

Paris Agreement. Notable examples include Germany, Denmark, Hungary, Switzerland, and Sweden. These countries are dedicated to driving worldwide environmental policy change. Unfortunately, the United States decided to withdraw from the agreement in 2019, posing a setback to the overall goals of the Paris Agreement. The United States justified its withdrawal by arguing that achieving greenhouse gas reduction targets would require exorbitant financial investments in hundreds of trillions or even trillions of dollars.

However, a study conducted by McKinsey ([Seeley and Dhakal 2021](#)) has identified key factors that can contribute to reducing GHG emissions in the United States, as shown in [Table 2.3](#).

In this context, it is estimated that carbon emissions can be reduced approximately from 4400 to 2900 megatons, which translates to a significant decrease from 62% to 40% compared to the emissions in 2005 ([Seeley and Dhakal 2021](#)). The United States has been exploring various alternatives to mitigate greenhouse gas emissions. Areas such as improving electric vehicle efficiency and developing advanced building technologies are being carefully examined. Additionally, reducing electricity demand without significantly impacting industrial production is a viable option for environmental mitigation.

Microgrids have emerged as a part of the solution to address peak energy demands on the grid. By integrating microgrids into the energy infrastructure, it is anticipated that renewable energy sources will gradually surpass coal-fired power plants in electricity generation. This transition will contribute



to reducing carbon emissions and promote the growth of sustainable energy systems.

The climate agreements under analysis present challenges that need to be addressed by MGs. These challenges are a crucial aspect of any distributed generation project. Also, it is essential to the technical agreements that need to be met to implement an MG. These agreements have been implemented in various regions worldwide, considering technical and technological disparities. Some countries have elaborated standards for MGs' safe and productive operation for these reasons. The following section provides a summary of the primary regulation standards of microgrids across the globe.

## 2.7 Microgrid Management and Operation Standards

Environmental policies play a crucial role in shaping the regulations and guidelines for MG implementation. Embracing MGs can enhance electricity generation while contributing to ecological mitigation efforts. However, MGs must supplement traditional electricity generation technologies rather than complement them fully. In many cases, the existing conventional grid can meet the energy demands of its users, with microgrids serving as support systems by integrating alternative generation resources.

Leading global economies such as the United States and China have long-term plans to increase the adoption of microgrids significantly. Similarly, the European Union has set ambitious objectives, as demonstrated by its 20/20/20 program ([Arababadi et al. 2017](#)). While this widespread growth of microgrids presents promising opportunities, it may also pose challenges regarding voltage stability, interconnection capacity, and operability. Over time, existing electrical standards have evolved to shape microgrid policies, drawing from earlier regulations on distributed generation and renewable resource implementation.

Various countries have implemented guidelines and standards to ensure the efficient management of microgrids. These measures aim to maintain power quality standards, prevent failures that could undermine generation capacity, and ensure the stability of electrical appliances. Such policies are crucial for facilitating large-scale electrical energy development and addressing the increasing energy demands of population growth in recent years. In cases where specific microgrid guidelines are not in place, countries have adopted policies from societies with similar electrical grid characteristics. Table 2.4 provides an overview of some key microgrid policies implemented by different countries.

**Table 2.4:** Main energy polices for MG development from 2010 (Ali et al. 2017).

Country	Title	Year
USA	State-level Renewable Portfolio Standards (RPS)	Multiple years
USA	IEEE 1547-2018	2018
Poland	Renewable Energy Law of Poland	2015
Germany	2014 Amendment of the Renewable Energy Sources Act -EEG-	2014
China	Renewable electricity generation bonus	2013
China	The Notice of further improvement of New Energy Demonstration Implementation	2013
Slovakia	Act on Energy and amendments to certain acts (No. 251/2012)	2013
Spain	Royal Decree-Law on urgent measures to guarantee financial stability in the electricity system	2013
UK	Electricity Market Reform (EMR)	2013
Italy	National Energy Strategy	2013
China	China Energy White Paper 2012	2012
China	The Notice on New Energy Demonstration City and Industrial Park	2012
Croatia	Energy Act 2012	2012
Denmark	Regulation on Net-metering for the Producers of Electricity for Own Needs	2012
Luxembourg	Energy performance requirements for residential buildings 2012-2020	2012
Slovakia	Act on Regulatory Office for Network Industries (Act No. 250/2012)	2012
Lithuania	Law on Energy from Renewable Sources	2011
Spain	Regulation of small power plants connected to the electricity grid (Royal Decree 1699/2011)	2011
Slovakia	National Renewable Energy Action Plan (NREAP)	2010
Germany	Energy Concept	2010

Voltage source inverter devices in DG systems serve as the power interface between the MG and the conventional grid. They play a crucial role in power consumption or injection into the grid while providing functions such as power flow control, fault sensing, and connection/disconnection based on load demands. To ensure standardized performance and interoperability, the Institute of Electrical and Electronics Engineers (IEEE) has proposed specifications for IBMG systems, outlined in the IEEE 1547 series (Arbab-Zavar et al. 2019). This series of standards address essential aspects such as power quality, voltage regulation, and MG islanding detection.

For VSIs, the IEEE 1457-2018 standard (Photovoltaics and Storage 2018) incorporates a chapter dedicated to smart VSIs associated with generating facilities and their interconnections, based on the California Electric Tariff Rule 21 (*Rule 21 Interconnection*). This chapter provides guidelines and requirements for the operation of VSIs in IBMGs. Table 2.5 provides an overview of the power quality requirements specified for IBMGs, according to these standards.

The following lines present the microgrid standards in major economic countries and associations adopted worldwide.

The European Union (EU) relies heavily on a centralized power generation structure, which poses economic, environmental, and technical challenges for implementing microgrids. To address these challenges, three key objectives have been identified for the evolution of electricity generation through microgrids: 1. Reduction of greenhouse gas emissions, 2. Enhanced reliability, and 3. Improved competitiveness.

These objectives propose various initiatives, including increased utilization of renewable resources, widespread deployment of distributed generation units, and development of highly efficient microgrids that align with the European Commission's regulations on reducing greenhouse gases. In 2014, the EU established an agreement known as Vision 2030, which aims to achieve efficiency improvements by utilizing renewable resources to account for more than 27% of the energy mix and reducing greenhouse gas emissions by 40%. Furthermore, the EU has set even more ambitious targets to reduce greenhouse gas emissions by 95% by the year 2050.

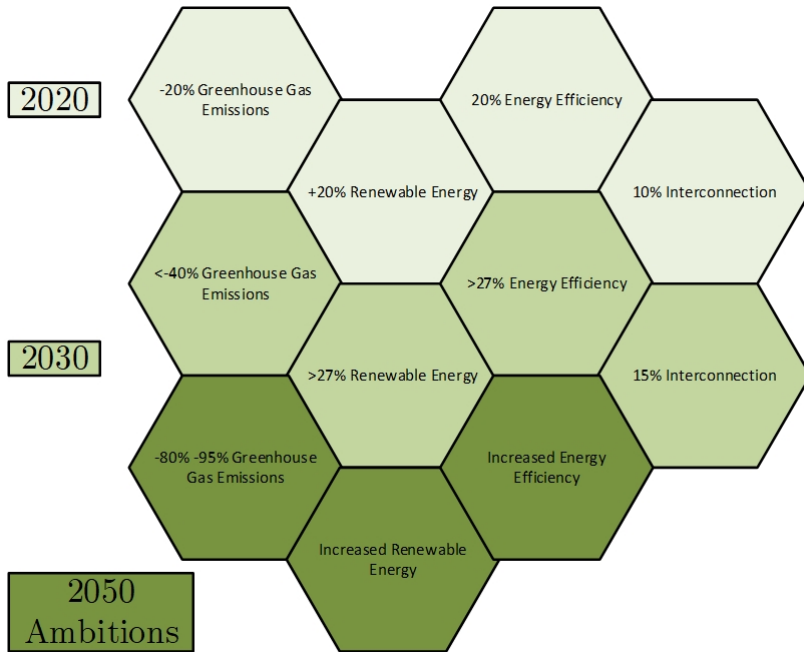
The regulatory landscape for microgrids varies across different regions and countries. In the European Union (EU), although no specific regulations are dedicated solely to microgrids, the European Commission has implemented several regulations about renewable energy generation. These regulations include 2013/347/EC, 2004/8/EC, and 2009/72/EC, as well as initiatives like

**Table 2.5:** Power quality requirements on IEEE Std 1547-2018.

DC injection	DER will not inject more than 0.5% of DC current compared to full rated output current at the reference point of applicability
Voltage fluctuation	<p><i>Rapid voltage changes:</i> DER in PCC at medium voltage must not exceed 3% of nominal voltage and 3% over a period of one second. DER in PCC at low voltage must not exceed 5% of nominal voltage and 5% throughout one second.</p> <p><i>Flicker:</i> Short-term flicker severity evaluated in a time of <math>600s = 0.35</math>. Long-term flicker severity evaluated in a time of <math>2h = 0.25</math>.</p>
Current distortion	<p><i>Odd harmonics:</i> 4% for <math>h &lt; 11</math>, 2% for <math>11 \leq h &lt; 17</math>, 1.5% for <math>17 \leq h &lt; 23</math>, 0.6 for <math>23 \leq h &lt; 35</math>, 0.3% for <math>35 \leq h &lt; 50</math>.</p> <p><i>Even harmonics:</i> 1% for <math>h=2</math>, 2% for <math>h=4</math>, 3% for <math>h=6</math>.</p>
Overvoltage contribution	<p><i>Over one fundamental frequency period:</i> DER must not exceed 138% of nominal frequency value for a duration of one fundamental frequency period. Applicable to the line-to-ground or line-to-line voltage systems.</p> <p><i>On cumulative instantaneous overvoltage:</i> DER instantaneous and cumulative voltage must not exceed acceptable region defined on Std section 7.4.2.</p>

FP5, FP6, and FP7. Over time, these regulations have contributed to the standardization and advancement of microgrid and smart grid technologies. In 2009, the Smart Grids Task Force was established, defining criteria for implementing smart electrical grid systems (Ali et al. 2017).

The EU has made significant strides in promoting renewable energy sources through various policies. In 2001, the European Parliament introduced the Renewable Energy Sources regulation as part of the Internal Electricity Market, which has boosted electricity generation from renewable sources and drove substantial changes in the electricity market. In 2009, the EU implemented



**Figure 2.16:** Targets for renewable energy from 2020 to 2030 in the European Union, adapted from (Liobikienė and Butkus 2017).

the Renewable Energy Directives, prioritizing using renewable energy sources such as photovoltaic panels, wind power, solar thermal energy, geothermal energy, wave energy, and biomass. Subsequently, the Electricity Production from Renewable Energy Sources regulation was formulated to ensure that 20% of the EU's energy consumption will come from renewable resources by 2020.

In 2010, the European Commission proposed a strategy focused on increasing energy efficiency and integrating distributed energies, emphasizing the importance of microgrids and smart grids in achieving sustainability goals. This commitment to smart grids was further recognized by the European Commission in 2011 with the publication of *Smart Grids: from innovation to Deployment*. Other standards that have positively influenced the EU's energy transition include the Energy Efficiency and Energy Service regulation in 2006, the Rules for Electricity Market regulation in 2009, and regulations promoting energy co-generation. These initiatives demonstrate the EU's dedication to transitioning from traditional energy sources to renewable energy.

While the EU sets objectives that member countries must strive to achieve, each country can determine how to meet these goals, considering their national laws and specific circumstances. Despite the differences and particularities among member countries, the EU continues to work towards energy integration and address any barriers that may hinder the achievement of its energy objectives.

With over 60 policies formulated in the renewable energy sector, EU members have used these guidelines to develop new policies supporting distributed generation technologies' growth. These regulations serve as instruments to reinforce policies specifically targeting microgrids.

In the United States, a leading global economy heavily reliant on fossil fuels, energy policies have been driven by the need to diversify energy resources and reduce oil imports, particularly since the oil crisis in the 1970s. The Public Utilities Regulatory Policy Act of 1978 was a significant regulation allowing consumers to access electricity without needing third-party involvement. This policy was updated in the 1990s to incorporate third-party energy transactions under regulated standards. Subsequently, various regulations were introduced to promote renewable energy markets and increase renewable energy consumption across states. These policies include State Policies to Support Renewable Energies, the Energy Policy Act of 2005, the Renewable Portfolio Standard, the Energy Efficiency Resource Standard, and the Renewable Energy Standard, among others. The goals set by these policies include achieving a 20% consumption of renewable energy by 2025, increasing renewable energy generation by 2% annually, and reaching a 20% renewable energy share nationwide within a decade.

The United States has witnessed a significant increase in renewable energy usage and a shift towards distributed generation. The country has made notable progress, with a 5% rise in renewable energy consumption in 2016.

### *2.7.1 U.S. Clean Air Act*

The U.S. Clean Air Act (Gingerich, Zhao, and Mauter 2019) is a regulatory standard established by the United States Environmental Protection Agency (EPA). It defines requirements for the responsible use of fossil fuel-based generation. While microgrids may utilize fossil fuels, they must adhere to specific environmental parameters outlined in this law. The primary objective is to maintain air quality standards and limit the emission of greenhouse gases into the atmosphere. In 2009, the EPA categorized gases like CO<sub>2</sub>, methane, hy-

drofluorocarbons, and perfluorocarbons as priority pollutants that require immediate attention to address significant environmental concerns. The Supreme Court supported this decision in 2007 by recognizing greenhouse gas emissions as threatening human health. Consequently, other federal governments joined this consensus to reduce greenhouse gas emissions and improve air quality.

### ***2.7.2 IEEE Standard 1547-2018 for Interconnection and Interoperability of Distributed Energy Resources with Associated Electric Power Systems Interfaces***

IEEE Standard 1547-2018 (Sadan and Renz 2020), also known as the IEEE 1547 standard, is proposed by the Institute of Electrical and Electronics Engineers (IEEE). It defines the requirements and technical specifications for the interconnection of distributed energy resources with conventional power grids. This standard is crucial as it addresses distributed system design, security, response to abnormal conditions, power quality improvement, and equipment considerations. The development of this standard began in 2003 with the specific goal of establishing technical requirements that can serve as a reference worldwide. It also considers unintentional islanding where environmental conditions may be warranted. Furthermore, it includes measures to ensure the safety of the main power grid during anti-islanding conditions.

### ***2.7.3 IEEE P1547.4-2011 Guide for Design, Operation, and Integration of Distributed Resource Island Systems with Electric Power Systems***

The IEEE P1547.4-2011 standard (Chandak and Rout 2021) guides operators and system integrators involved in distributed generation. It focuses on the intentional islanding of microgrids and the potential impacts on interconnected equipment. The guide covers resource interconnection systems and the involvement of electrical devices. It provides a resource for learning best practices in microgrids' design, operation, and integration.

### ***2.7.4 IEEE P2030.7-2007 Standard for the Specification of Microgrid Controllers***

This standard (Roosa 2020c) pertains to digital microgrid controllers, which are crucial in managing energy systems. It defines a microgrid as an entity that can operate connected and disconnected from the main power grid. It includes the steps for a smooth transition between grid-connected and islanded modes.

The standard focuses on four aspects: interactive control, control supervision, local area functions, and level control devices.

### **2.7.5 IEC 61727 International Electrotechnical Commission's PV System Requirements**

IEC 61727 (Abobakr et al. 2019) is an international standard that addresses the parallel operation of photovoltaic (PV) systems utilizing solid-state devices such as static power converters in MGs. The standard governs these PV systems' connection and disconnection activities within microgrids. It emphasizes the role of inverters in microgrids as the means of power generation during islanded operation, power transfer, and coupling with different loads.

## **2.8 Conclusions of the Chapter**

This chapter provided a comprehensive overview of IBMGs, focusing on the inverter as the central component of energy management in a microgrid. It also discusses the various microgrids applications, their environmental challenges, and relevant regulations.

The significant rise in energy consumption within residential sectors has become increasingly apparent in recent years. Given that most of these consumers use single-phase systems, it is crucial to develop a single-phase system that can effectively meet the energy requirements of these small consumers. This chapter examines the fundamental aspects of inverters, including their role in power electronics, signal filtering, and modulation techniques. One commonly used modulation technique, SPWM (Sinusoidal Pulse Width Modulation), is explored for its ability to reduce harmonic content in the output voltage of inverters.

The chapter introduces microgrids' definitions, structures, types, and applications. It highlights the key components that comprise a microgrid and how each element contributes to the distributed generation scheme. Particular emphasis is given to AC microgrids, which serve as the primary case study in this thesis.

Furthermore, the challenges associated with microgrids are addressed, particularly the objective of reducing environmental pollution in power generation. The chapter also examines the importance of complying with operating standards for grid-connected inverters, which different organizations in each region



or country regulate to ensure safe and environmentally conscious operations in the current era.

However, the widespread adoption of microgrids in low-consumption systems presents particular challenges in energy management. The subsequent chapter delves into the issues and proposed solutions for controlling IBMGs.



## Chapter 3

# State of the Art: Multi-objective Control Approach

### 3.1 Introduction

This chapter provides an in-depth analysis of the multi-objective optimization philosophy, different types of methods, and related works, among other relevant aspects. In MG applications, multi-objective processes play a crucial role by effectively addressing the diverse objectives of the MG operation. These methods can optimize multiple criteria concurrently, such as cost minimization, energy efficiency maximization, and system reliability assurance. To formulate a multi-objective optimization problem, objective functions representing each desired objective are defined. The quality of solutions is then evaluated using performance indicators, including the concept of Pareto efficiency. By employing these approaches, informed and balanced decision-making can be achieved when designing and operating microgrids, considering multiple criteria simultaneously.

Section 3.2 shows the state of the art, proposal developments, and research achieved in the multi-objective optimization of inverter-based microgrids (IBMGs). In addition, different multi-objective and control algorithms are studied to have a criterion for selecting multi-objective algorithms in this work. Section 3.3 analyzes results using performance indexes for multi-objective optimization, and section 3.4 presents typical indexes for evaluating multi-objective algorithms. This chapter concludes with the conclusions generated in section 3.5.

## 3.2 Multi-objective Functions Approach on IBMGs

In Chapter 2, the critical characteristics of an MG were examined. As part of the introduction to the VSI study, a few research proposals were briefly mentioned. This section provides a detailed overview of the works contributing to the VSI control algorithm, addressing various closed-loop regulation challenges within the MG as works related to the state of the art.

Researchers have proposed complex control structures by integrating advanced algorithms to achieve better results than conventional control systems. For instance, (Kerdphol, Rahman, and Mitani 2018) employed model predictive control (MPC) to achieve improved transient response based on dynamic plant models. Addressing uncertainties in the VSI model (Li et al. 2017) focused on control design and filter parameter optimization, leading to enhanced performance in uncertain scenarios. Intelligent methods have also been employed in control algorithm tuning. Particle swarm optimization (PSO) was applied by (Hossain et al. 2019), artificial neural networks (ANN) were utilized by (Shokoohi et al. 2018), and a combination of these methods was explored in (Safari, Babaei, and Farrokhifar 2019).

Numerous studies have been conducted in the field of IBMG control, with various reviews examining different architectures and control schemes. For example, (Miveh et al. 2016) investigated other four-leg VSI structures in MG island mode, highlighting the advantages and disadvantages of applying different reference frames for voltage and frequency control. Hierarchical control in IBMGs was explored in depth by (Rokrok, Shafie-Khah, and Catalão 2018), focusing on the primary control structure. Various schemes, including systems with or without communication methods, were analyzed, with particular emphasis on control droop formulations that cater to a wide range of voltage and frequency regulation through active and reactive powers.

Additionally, (Andishgar, Gholipour, and Hooshmand 2017) delved into the hierarchical control of IBMGs based on island mode control. They analyzed primary, secondary, and tertiary hierarchical regulation structures, addressing objectives such as efficient control for consensus on RES, active and reactive power sharing, load dependency, dynamic stability, and islanding detection. Another study by (Bouziid et al. 2015) surveyed different control schemes used in IBMGs, mainly focusing on the regulation of the DG's internal control loop using various methods such as proportional-integral-derivative (PID) and dead-beat for primary control, linear quadratic regulator (LQR) or model predictive control (MPC) for optimal control, fuzzy logic for experience-based algorithms, and artificial neural networks (ANN) for learning schemes. The study also provided an overview of commercial control software for IBMGs, including HOMER, HOGA, and SOMES.

The studies above address control objectives, including voltage and frequency stability, robustness in the face of load changes, and achieving fast transient responses. However, these features are only partially addressed within a single objective function, considering the constraints of different variables. It is necessary to leverage additional characteristics further to enhance the efficiency of the energy production process. Conversely, there is a need for further research in multi-objective control algorithms. These approaches incorporate multiple regulatory requirements of the grid through mathematical formulations based on various objective functions. This consideration encompasses several aspects aimed at optimizing IBMGs based on the following characteristics:

- Smooth transition between transient states when the voltage source inverter (VSI) interacts with MGs.
- Ensuring stability in steady-state conditions for important variables such as voltage, frequency, and active power.
- Effective control of power flow, whether injected or absorbed, through interactions between the VSI, MGs, and loads.
- Development of an optimal control strategy that adheres to the limitations and constraints of the system.
- Enhancing the robustness of the MG against uncertainties and disturbances in the system models.

However, multi-objective control algorithms have certain drawbacks, including the mathematical complexity of formulating control laws and the significant computational load required for online implementation. The challenges faced

by multi-objective controllers are more extensive than those encountered in conventional control systems due to their focus on specific regulatory targets in IBMGs (Saeed et al. 2021). Mathematical complexity and computational load pose significant challenges when implementing these control schemes. To overcome these challenges, alternative approaches are required to simplify models into concise expressions and facilitate their versatile implementation in hardware systems while ensuring optimal performance. IBMG researchers and energy consumers must address these challenges effectively.

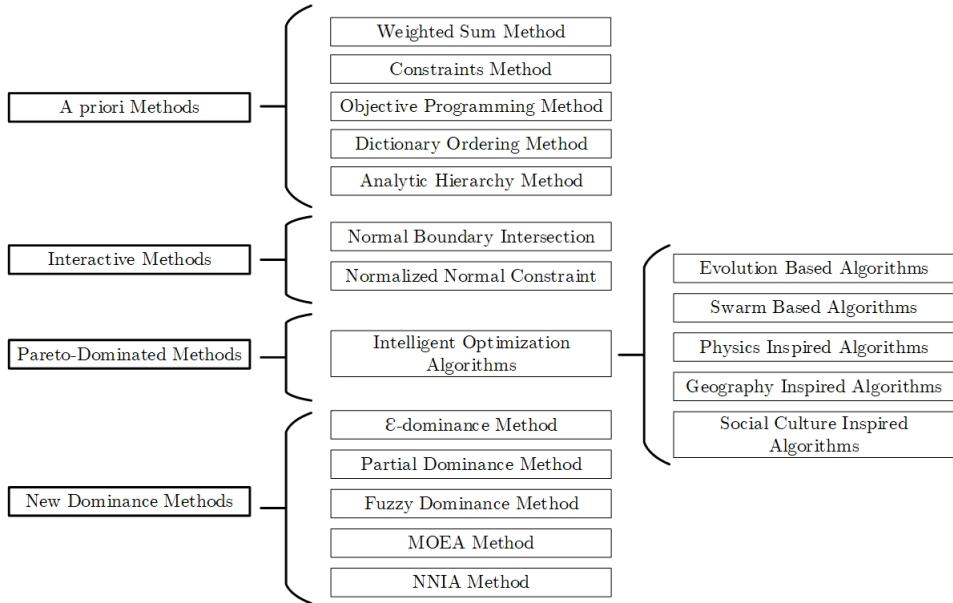
The conventional control approach used in IBMG typically addresses specific objectives by optimizing a single objective function. By considering various variables within constraints, the control law is determined by minimizing a single objective function. Results obtained so far have demonstrated improved energy production and cost optimization performance. However, other essential characteristics still require analysis due to the limitations of control algorithms or conflicts between objectives. For instance, adjusting power references can create a trade-off between achieving a fast response to track new setpoints and maintaining stable voltage and frequency variables in IBMGs. Establishing regulations that ensure both rapid response and system stability while maintaining a balanced operation is desirable.

Existing approaches based on multi-objective algorithms aim to provide optimal solutions that mitigate conflicts between different goals. The choice of a specific optimization method depends on its advantages and the consideration of moderate computational cost. These previous findings have led to various proposals in multi-objective optimization, as depicted in Figure 3.1.

The broad spectrum of multi-objective methods demonstrates the alternatives available to minimize a problem with various objectives, depending on factors such as computational cost, achievements, and the intrinsic concepts of algorithms. This advantage represents an essential source for new proposals and unused methods in IBMGs.

Constant research on MG has been leading to better efficiency results. The predominant AC consumption in residential and industrial applications has highlighted the VSI technology with year-by-year improvements. The main objectives and trends in the widespread introduction of IBMGs consider the following aspects (Ross et al. 2015):

- Energy-cost reduction;
- Reliability of the service;



**Figure 3.1:** Multi-objective trade-off optimization methods, adapted from (Cui et al. 2017).

- Minimizing power fluctuations;
- Reduction in peak loading;
- Mitigation of  $CO_2$  emissions;
- Multi-objective optimization;
- Tuning algorithms.

The optimal solution for two or more conflicting objectives does not yield a single solution; instead, it results in an optimal solution set with a trade-off among objectives, aiming for IBMG optimization. If an objective contributes to IBMG performance, this aspect can be quantified as a mathematical function. Solving these expressions holistically requires advanced methods such as the Pareto-optimal front.

The following concepts describe the main multi-objective approaches with specific features tailored to different controllers. The goals have been classified based on the main characteristics' requirements and the means of achievement

through advanced algorithms. A multi-objective optimization approach is also addressed, where essential works in this area have been reviewed.

### 3.2.1 Energy-cost reduction

Effective operation and maintenance of MGs achieve reduced energy losses and increase system efficiency. This feature is commonly addressed through objective functions under constraints. The objective function that describes the average cost of energy to the loads in MGs is given in (Ross et al. 2015) as follows:

$$v_C(x(t), t) = \sum_{\forall y \in DER} (\pi_y(P_y(t), t)P_y(t)\Delta t). \quad (3.1)$$

Where  $v_C$  is the cost function,  $\pi_y$  is the kilowatt-hour cost of  $P_y$  kilowatts from DER,  $y$  measured in hours, and  $\Delta t$  is the time where the measurements are performed.

Particular features compromise transient and steady-state stability. Changes in output IBMG variables can be adequately achieved with controllers offering fast and accurate responses. However, an inadequate control law might create oscillations that lead to grid instability. During steady-state operation, events such as the connection and disconnection of loads and sources to the grid produce disturbances that affect the performance of MGs. With the increased integration of renewable energy sources (RES), the grid becomes more susceptible to instability due to the low inertia of RES. Grid voltage and frequency variables are particularly sensitive in AC energy production. The following concepts are essential for maintaining stability and producing practical cost functions.

#### 3.2.1.1 Fast response

Controllers act aggressively to achieve fast response by reaching new setpoint values. However, this aggressive performance often leads to undesired oscillations in regulated variables. In (Chang 2018), an SMC was employed to control a VSI. Despite its ability to achieve fast transient response and robustness in steady-state, the SMC suffers from a significant issue known as chattering, which manifests as high-frequency oscillations (Gonzales et al. 2019). Moreover, the mathematical formulation of the SMC can result in the resolution of special functions, posing challenges in generating an adequate control law. To address these problems, an ANFIS structure was utilized. This method is



a neuro-diffuse system of inference rules. As a result, the VSI achieved both a fast transient response and steady-state stability while avoiding generating distinct functions. The ANFIS (adaptive neuro-fuzzy inference system) algorithm guided the SMC to reject unknown disturbances. A similar approach was employed in (Shen et al. 2019), where the SMC and ANN algorithms were combined to eliminate voltage deviation in the primary control of an MG, effectively reducing chattering using the ANN.

In (Das, Gurralla, and Shenoy 2016), an LQR controller was implemented to facilitate a seamless transition of an MG from the primary grid to island mode. The study analyzed the behavior of the MG during severe transient changes. The LQR controller successfully mitigated the transients generated in the voltage and current variables. It exhibited fast dynamics in three different scenarios: direct grid connection with reference variations of P and Q powers, alterations in wind speed, and response to faults resulting in immediate islanding of the MG.

#### *3.2.1.2 Ramps for power setpoint tracking*

Ramps for power rate on DG have been effectively introduced to facilitate smooth changes in the power setpoints of MGs. However, in some instances, it is necessary to control the ramp rate to avoid generating peak values appropriately. In (Nguyen, Khodaei, and Han 2017), peak power ramp minimization is introduced. The authors employ the Nash bargain theory to address the social welfare problem and maximize the efficiency of power consumption from various sources of storage and generation. Depending on local power generation policies, there are possibilities for reimbursement. Another work, such as (Xiao et al. 2018), presents a balanced tie-line power scheduling control approach for MGs. The MG system includes photovoltaic panels, wind turbines, and PV/WT/ESU energy storage units. The power ramp is implemented to achieve precise and smooth transitions between different energy values. Despite the system's complexity, a central control algorithm that considers fluctuations from other sources accomplishes the objective.

#### *3.2.1.3 Voltage and frequency regulation*

Voltage and frequency regulation is a synthesis controller that ensures the robustness of the process variables in a steady state. The formulation of this algorithm requires the optimization of a mathematical function. Its key feature is the rejection of disturbances through a mathematical approach that considers the measurable disturbances in the system. In (Baghaee et al. 2018), the controller was implemented in an MG to track output voltage references. The

system's ability to reject disturbances in nonlinear loads was considered an advantage. Additionally, an environmental conditions model was developed to predict demand parameters in the load.

In a different study (Panda and Ghosh 2020), the authors controlled a power converter using Model Predictive Control (MPC) to maintain output voltage tracking. One advantage of this control method is using a different optimization function that presents a single prediction horizon. This approach minimizes the computational cost associated with the implementation of MPC.

Many control algorithms in MGs are based on the droop controller, commonly employed at the primary control level to stabilize voltage and frequency variables. This controller considers the relationship between frequency and active power, as well as voltage and reactive power. In (Zhang et al. 2019), the droop controller was combined with an Artificial Neural Network (ANN) to enhance the performance of the inverter. The system measures the voltage and current values of the inverter to calculate the output power, enabling the droop controller to obtain voltage and frequency reference values for cascade control. The ANN assists the inverter in preparing for sudden changes, such as when the MG needs to transition from island mode to connect to the traditional grid.

#### 3.2.1.4 Virtual impedance

Virtual impedance is crucial in grid stabilization, particularly when Variable Speed Drives (VSI) are involved. The power flow can change significantly due to variable impedance at the VSI output. Virtual impedance maintains stable VSI operation by emulating a constant virtual value of line impedances. In (Zhu et al. 2019), a shaped control method addressed Power Conversion Center (PCC) voltage issues related to variable impedances. This approach highlighted the importance of considering different impedance values based on various frequency bands. Another study, such as (Samavati and Mohammadi 2019), aimed to enhance energy quality in Islanded MGs by implementing cascade control to regulate local load voltage and current injection into the grid. Using  $H_\infty$  control as an internal control mechanism facilitated a seamless transition between grid connection and island mode.

#### 3.2.1.5 Virtual inertia

In (Kerdphol, Rahman, and Mitani 2018), the integration of a virtual inertia algorithm with Model Predictive Control (MPC) was investigated to stabilize the frequency of the MG, particularly under high penetration of renewable energy. As mentioned earlier, renewable energy sources have lower inertia

compared to conventional grids, which can lead to voltage and frequency instability when integrated. Applying MPC with the virtual inertia algorithm enabled a time-stable and reliable system, effectively addressing uncertainties arising from renewable energy integration, was achieved. The study also compared the results obtained using MPC with a fuzzy algorithm, demonstrating improved stability in frequency.

In (Shi et al. 2018a), the authors combined a virtual inertia algorithm with an adaptive controller. While virtual inertia is a practical algorithm for increasing MG inertia, there are challenges associated with strong electrical coupling and maintaining constant MG variables with high accuracy. The AC signal frequency response was analyzed to enhance system accuracy, particularly from storage devices. The proposed system integrated a cascade Proportional-Integral (PI) algorithm with the droop controller and virtual inertia. The results indicated that the controller effectively handled load variations in the MG while minimizing changes in the operating frequency.

### 3.2.2 Reliability of the service

The reliability of the MG can be assessed by quantifying the non-delivered energy (NDE). The cost associated with NDE varies depending on whether the load is critical or non-critical, as seen in (Sullivan, Mercurio, and Schellenberg 2009). The objective function for calculating NDE is given by:

$$v_R(x(t), t) = \pi_{NDE, noncrit} dP_L(t) \Delta t + \pi_{NDE, crit} (1 - u_{L, crit}) P_{L, crit}(t) \Delta t. \quad (3.2)$$

Here,  $v_R$  is the reliability cost function,  $\pi_{NDE, noncrit}$  is the kilowatts per hour cost,  $dP_L$  represents the total non-critical load,  $u_{L, crit}$  is a binary factor indicating the connection or disconnection of critical loads, and  $P_{L, crit}$  represents the crucial load in kilowatts, and  $\Delta t$  is the time where the measurements are performed.

The reliability of the MG is critical in applications where environmental conditions and system disturbances introduce fluctuations. In the case of an islanded MG (IBMG), common disturbances include voltage and frequency variations. Uncertainties also arise due to weather conditions, unbalanced loads, and unknown load profiles.

### 3.2.3 Uncertainties

In recent years, several proposals have emerged for robust control algorithms such as  $H_2/H_\infty$ . In one study (Li et al. 2017), a cascade structure was employed to control current and voltage. The internal current loop utilized an SMC controller, while the external voltage loop incorporated an  $H_2/H_\infty$  algorithm. This hybrid approach improved inverter performance in system uncertainties, ensuring constant frequency values, low harmonic distortion, robustness against parameter variations, and fast transient response. Importantly, this structure did not require an accurate inverter model. The objectives included steady-state stability analysis, robustness against disturbances, and optimal tuning.

In another study (Fathi, Shafiee, and Bevrani 2018), a  $H_\infty$  controller was implemented to enhance the robustness of an MG, addressing the issue of low inertia. The  $H_\infty$  algorithm was employed to tune the parameters of virtual inertia, considering different scenarios such as step changes in load, disturbances, and system uncertainties. This controller successfully maintained constant voltage and frequency values in the MG.

### 3.2.4 Adaptive schemes

An IBMG implemented an adaptive controller using a combination of MPC and ANN (Amoateng et al. 2017). The objective was to regulate voltage and frequency values. The MPC analyzed the inverter model to establish a control law based on power controller dynamics, and Lyapunov's criterion was incorporated for system stability analysis. To mitigate uncertainties arising from possible errors in the mathematical expression, ANNs were employed to improve the model. The adaptive scheme allowed the controller to adapt to varying process conditions. The effectiveness of this proposal was evaluated through various cases, including sudden load changes, load types, gain variations, and communication delays.

### 3.2.5 Minimizing power fluctuations

Power fluctuations in the electrical power system (EPS) arising from continuous changes in production and demand can be quantified by the difference in firm and variable generation. The following equation in (Sopinka and Pitt 2013) expresses the reduction of power fluctuations:

$$v_D(x(t), t) = \pi_{\Delta P} \frac{|P_{EPS}(t) - P_{EPS}(t - \Delta t)|}{\Delta t}. \quad (3.3)$$

Here,  $v_D$  is the fluctuations cost function,  $\pi_{\Delta P}$  is the kilowatts per hour cost,  $P_{EPS}$  is the active power from the electrical power system, and  $\Delta t$  is the sample time where measurements are performed.

To address this issue, advanced controllers offer several advantages. The Sliding Mode Control (SMC) technique is widely used to stabilize voltage and frequency variables in an MG. It operates in two phases: the first phase aims to quickly reach the reference, while the second phase ensures robust set-point tracking over time. In a study by Baghaee et al. (Baghaee et al. 2017a), SMC was applied to improve voltage regulation and active-reactive power transfer, resulting in a robust design supported by stability analysis using the Lyapunov function. These advantages are particularly beneficial in a hierarchical management system.

Furthermore, Gholami et al. (Gholami, Saha, and Aldeen 2018) addressed the problem of power tracking with a focus on achieving a more robust transient response.

Maintaining a balance between generation and demand is crucial, as different interactions between sources and loads contribute to active and reactive power flow. In an IBMG scenario, Mousavi et al. (Mousavi et al. 2018) implemented a power generation scheme based on voltage and current control modes regulated by droop control. This decentralized scheme effectively managed active and reactive power flow between different sources in island mode. In cases where reactive power support was required, the droop control strategy was modified, as demonstrated in Fani et al. (Fani, Zandi, and Karami-Horestani 2018). The IBMG system accurately shared reactive power by calculating the error of this variable when disturbances were present, thereby overcoming power-sharing issues caused by mismatched line impedances.

### 3.2.6 Reduction in peak loading

Peak power at the Point of Common Coupling (PCC) is a crucial factor in this regard, as reducing peak power can yield significant financial benefits to the grid, as seen in (Sopinka and Pitt 2013). The goal presented in the research was peak power reduction. It was quantified as follows:

$$v_P(x(t), t) = \pi_p P_{EPS}^2(t). \quad (3.4)$$

Here,  $v_P$  is the cost function,  $\pi_p$  represents the cost per kilowatt, and  $P_{EPS}$  is the active power delivered by the electrical power system.

The widespread adoption of power converters has led to a degradation in the power quality of the grid. This degradation is manifested in increased Total Harmonic Distortion (THD) of current, which generates abnormal heat in power wires and reduces the lifespan of electrical machines.

To address this issue, optimal control laws are sought to regulate IBMG variables. The optimal value represents the most desirable option that minimizes a criterion, such as the error in output values. Various control methods employ an objective function to prioritize one or multiple objectives to be achieved through closed-loop regulation.

### ***3.2.7 Minimization of Performance Index***

The Linear Quadratic Regulator (LQR) is an optimal control algorithm that minimizes a control law based on objectives defined in its optimization function.

Accurate measurement of the system's state variables is essential to optimize the cost function and approach a global minimum value. In (Khayat et al. 2018), this algorithm was applied in a non-communication environment within a hierarchical control structure. The LQR served as a secondary controller to regulate the frequency in an autonomous MG. The results demonstrated optimal frequency regulation values close to the system reference, ensuring stability at the second level of control. The system's output filter dynamics were considered state variables in this study.

Based on operator experience, fuzzy control incorporates fuzzy inferences or rules to determine the output control law based on process inputs and states. In (Arcos-Aviles et al. 2016), fuzzy control was applied to an MG, considering parameters such as renewable generation and local load demand. One advantage of the fuzzy controller was the reduced number of inference rules required for this type of process. However, optimization was performed to generate only 25 rules in this study, focusing on power-sharing performance under varying environmental conditions.

### 3.2.8 State Estimation

In (Alyazidi, Mahmoud, and Abouheaf 2018), Artificial Neural Networks (ANNs) were employed as a mathematical estimation technique to observe the dynamics of distributed generation sources. This approach highlighted the benefits of using advanced computing methods for predictions, especially when dealing with complex processes that may be challenging for traditional control algorithms.

Lastly, (Buduma and Panda 2018) presented a robust cascade control scheme combining two optimal algorithms. The external voltage loop controller utilized the  $H_2/H_\infty$  technique, while the internal current loop controller employed LQR. Additionally, a full-state observer was incorporated to estimate non-measurable system variables. The results demonstrated high stability and robustness, even in the presence of uncertainty parameters in the output filter and variable load changes.

### 3.2.9 Constraints

Model Predictive Control (MPC) has gained significant prominence in recent years. One of its key features is the ability to generate anticipatory control actions based on prior knowledge of the system model. This algorithm is also considered optimal due to its cost-function minimization. Its formulation in discrete time characterizes MPC. However, the most notable characteristic of MPC is the incorporation of constraints in the control process. While many controllers utilize saturators to define control signal ranges, MPC seeks to find an optimal control law based on an optimization criterion that considers constraints.

In (Batiyah et al. 2020), power control in an islanded MG was implemented using MPC. The mathematical model of the system was developed as a strategic power management system, and constraints were applied to the storage system, battery, generation, and loads.

### 3.2.10 Harmonic Mitigation

Artificial Neural Networks (ANNs) are mathematical algorithms that emulate the functioning of neurons in the brain. ANNs have inputs, activation functions, and outputs. Like neurons, ANNs can be organized in a network to solve complex problems. These algorithms require training, where the ANN learns the desired result from specific input data through learning mechanisms. In

(Baghaee et al. 2017b), shared power control in an MG with nonlinear loads was achieved. Nonlinear loads introduce harmonics in the voltage output at the point of common coupling (PCC). ANNs were employed to mitigate voltage harmonics, improving the efficiency of active and reactive power flow.

In Benhalima, Miloud, and Chandra 2018, Sliding Mode Control (SMC) was utilized to mitigate output voltage harmonics in an MG. SMC is known for its robustness, fast response, and zero steady-state error. Additionally, it enabled tracking of the maximum power transfer point through the electronic converter.

### 3.2.11 Mitigation of $CO_2$ Emissions

In this context, research proposed a cost function to determine the mitigation of environmental damage. The cost function for  $CO_2$  mitigation can be determined through the carbon cap-and-trade market (Reyna 2014). It can be expressed as follows:

$$v_G(x(t), t) = \pi_{GHG} \sum_{\forall y \in DER} G_y(P_y(t)\Delta t), \quad (3.5)$$

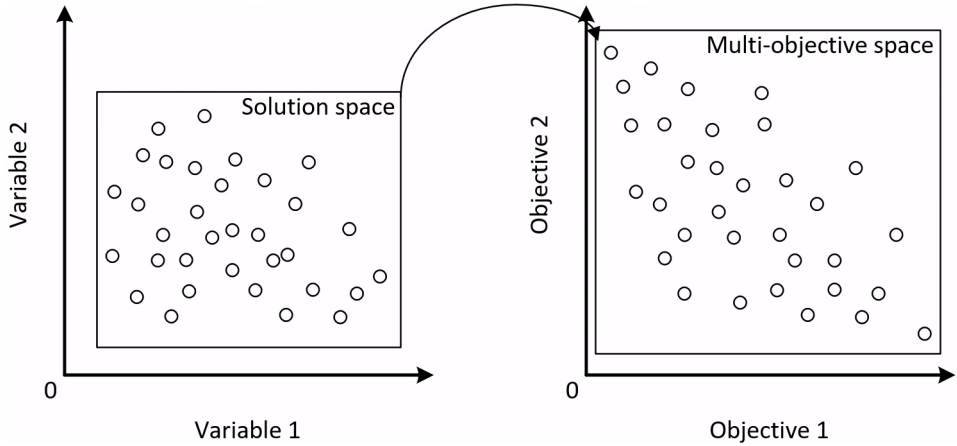
where  $v_G$  is the cost function,  $G_y$  represents the carbon emissions associated with the generation of  $P_y$  kilowatts of power, and  $\pi_{GHG}$  denotes the carbon price per ton of  $CO_2$ .

### 3.2.12 Multi-objective Approaches and Optimization

This section explores the current trends in formulating and optimizing multi-objective approaches for power management control. These approaches incorporate advanced regulation structures and machine-learning techniques like genetic algorithms.

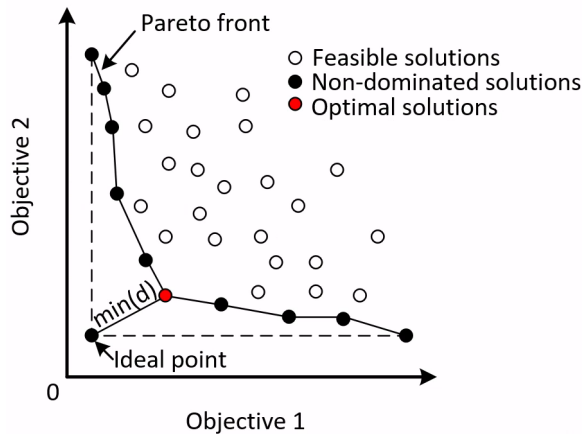
The multi-objective problem involves minimizing multiple interdependent objectives. These objectives are expressed as mathematical functions representing the error or sensitivity of the process's performance. However, finding a unique solution is challenging. Each calculation represents an optimal solution that differs from others regarding the trade-off between objectives. Therefore, finding solutions that achieve regulatory goals is crucial while considering other essential purposes. Figure 3.2 illustrates the evaluation mapping of a multi-objective problem.





**Figure 3.2:** Evaluation mapping of a multi-objective problem, adapted from (Van Veldhuizen, Lamont, et al. 1998).

From Figure 3.2, two perspectives can be identified. First, the solution space encompasses all possible solutions for a given problem. These solutions are then evaluated in the multi-objective space to find optimal solutions that simultaneously optimize multiple objectives. The optimization of multi-objective issues is based on Pareto optimization. Figure 3.3 illustrates the concept of the Pareto front for optimizing two objectives.



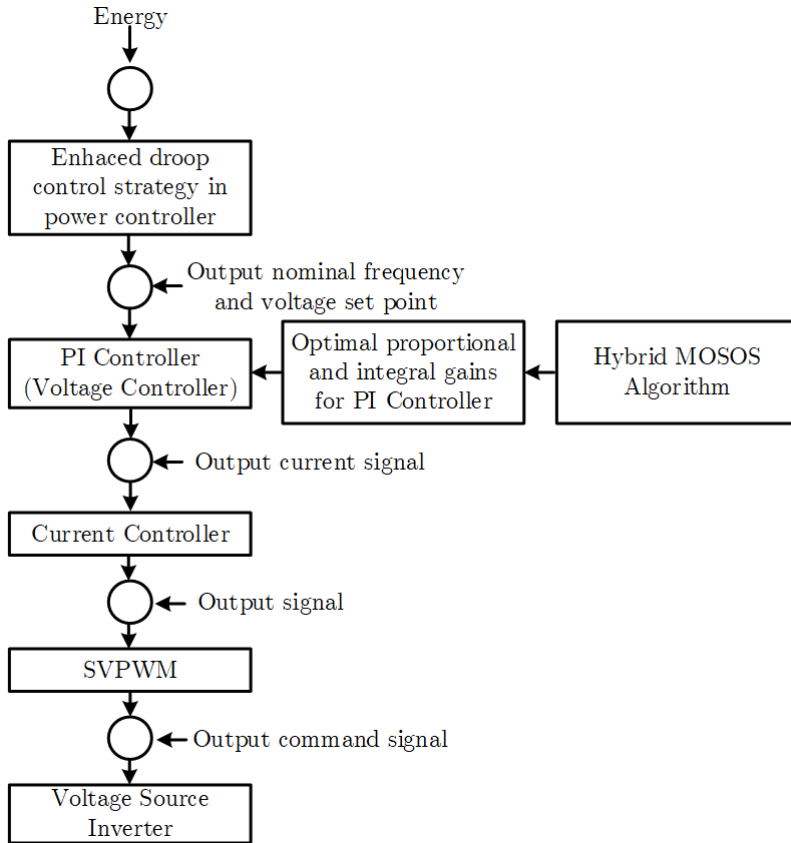
**Figure 3.3:** Pareto front for two objectives, adapted from (Van Veldhuizen, Lamont, et al. 1998).

The Pareto front, also known as the Pareto set or Pareto frontier, is a fundamental concept in multi-objective optimization. It represents a set of solutions where improving one objective can only be achieved by sacrificing performance in at least one objective. The Pareto front showcases the trade-offs between different objectives and highlights the best compromises. The solutions within the Pareto front are referred to as non-dominated solutions, as no other solution in the objective space dominates them. These non-dominated solutions are considered feasible solutions, as they satisfy all the constraints and requirements of the problem. Among these feasible solutions, the optimal ones offer the best overall performance based on specific decision criteria. The search for optimal solutions involves exploring the solution space, evaluating the objective functions, and iteratively improving the solutions until a satisfactory set of Pareto-optimal solutions is achieved. Optimal solutions provide decision-makers with various choices that balance conflicting objectives and enable them to make informed decisions according to their preferences and priorities (Van Veldhuizen, Lamont, et al. 1998).

A multi-objective control proposal for improving power quality in an islanded MG is presented in (Teekaraman, Kuppusamy, and Nikolovski 2019). The authors applied a cascade voltage and current scheme to regulate the voltage and frequency in a three-leg IBMG. They employed a hybrid Multi-objective Symbiotic Organism Search (MOSOS) algorithm to optimize specific objectives, including voltage overshoot, voltage undershoot, rise time, settling time, and tuning of ITAE and PI parameters. The results demonstrated the robustness of the proposed controller under scenarios involving harmonics and fluctuating sources as disturbances in the grid. Figure 3.4 depicts a flow diagram of the proposed method illustrating the control signal on the voltage source inverter (VSI).

The primary objective is to achieve a smooth response by addressing voltage overshoot and undershoot, rise time, settling time, and integral time absolute error. This is accomplished through a cascade regulation structure that combines a PI controller to generate the control signal for Space Vector Pulse Width Modulation (SVPWM) on a Voltage Source Inverter (VSI). The Multi-objective Symbiotic Organism Search (MOSOS) scheme provides a numerical solution for the objectives outlined in this analysis, ensuring effective regulation of voltage and frequency in the MG.

In a study by Zeng et al. (Zeng et al. 2016), a multi-objective control algorithm was proposed to enhance the performance of multi-functional grid-connected inverters. These inverters face challenges in meeting the requirements for in-



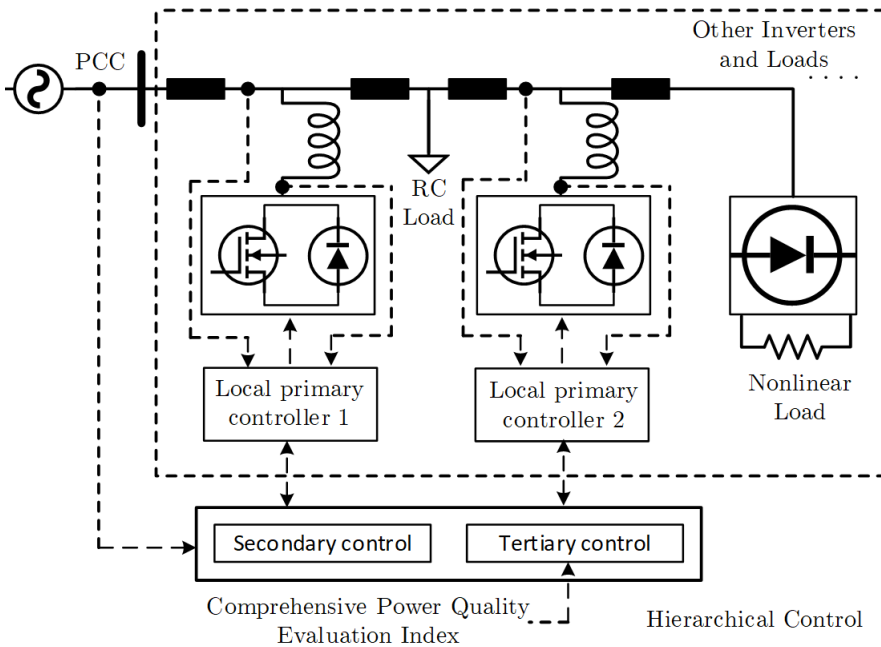
**Figure 3.4:** Flow diagram of MOSOS multi-objective control, adapted from (Teekaraman, Kuppusamy, and Nikolovski 2019).

tegrating renewable energy into the utility grid and providing ancillary power-quality services.

The proposed method involved a cooperative scheme with communication support between the VSIs to address power quality requirements on distribution feeders effectively. Figure 3.5 illustrates the interaction between comprehensive power quality evaluation objectives and hierarchical control for adjusting the electrical power demand in the MG. The management of each Distributed Generation (DG) system was achieved by calculating coefficients required by local controllers to achieve optimal compensation. The control scheme computed the Total Harmonic Distortion (THD) on the utility grid based on voltage and

current measurements at the Point of Common Coupling (PCC). The tertiary control stage solved the Pareto front solution to fulfill the system operator’s requirements.

Figure 3.5 represents the interaction between comprehensive power quality evaluation objectives and hierarchical control in the MG. Overall, this approach presents a comprehensive strategy for addressing power quality issues in grid-connected inverters, considering the interaction between renewable energy integration and ancillary services.

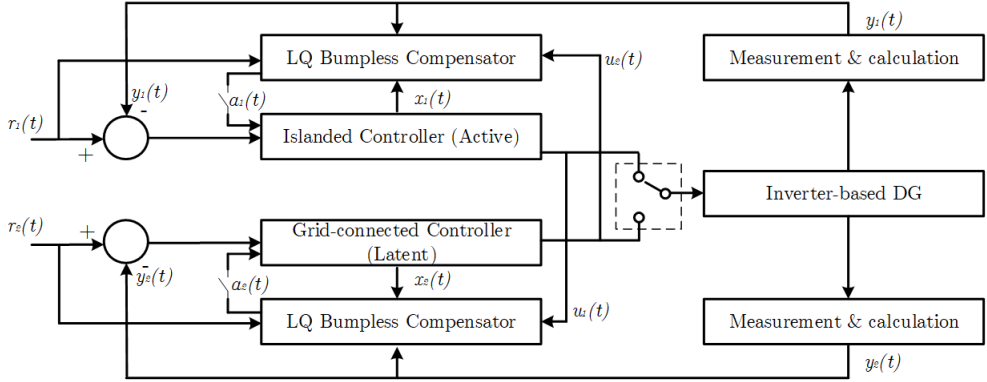


**Figure 3.5:** Multi-objective control on Hierarchical-based micro-grid application, adapted from (Zeng et al. 2016).

The control scheme presented in this study successfully addressed the energy management challenge by optimizing a comprehensive power quality evaluation index. Based on catastrophe decision theory, this index quantified the parameters that enhance power quality in MGs. The results demonstrated the effective utilization of the limited capacity of multi-functional grid-connected inverters to meet the specifications of optimal power quality in MGs.

As discussed earlier, MGs can operate in two modes: supplying energy to the utility grid and functioning independently in island mode. The transi-

tions between these modes introduce transient jumps that can compromise the reliability of the utility grid. Building on this observation, the authors of (Wu et al. 2019) developed a multi-objective control structure based on a linear quadratic-based optimal bumpless controller with two degrees of freedom. Figure 3.6 illustrates the control scheme, which addresses the two operation modes of the MG.



**Figure 3.6:** Bumpless control structure of MGs with two mode controllers, adapted from (Wu et al. 2019).

This control structure enables smooth and seamless transitions between grid-connected and island modes, minimizing the impact on the utility grid during mode changes. Utilizing the linear quadratic-based optimal bumpless controller provides robust performance and ensures the stability and reliability of the MG system.

This strategy involves the measurement of critical parameters in the MG, such as voltage and current, to improve reference and controller tracking errors using a bumpless method. While this approach is innovative for MG regulation, it is based on conventional optimum schemes like linear quadratic controllers. The mathematical structures employed are more fundamental compared to advanced controllers, resulting in quick computing calculations. The proposed approach addresses the requirements of both island mode, including power sharing and circulating current suppression, and grid-connected mode, encompassing active/reactive power flow and voltage/frequency synchronization with the conventional grid.

Some researchers have emphasized the use of multi-objective control to enhance the efficiency of management in islanded MGs. Existing studies involve com-

plex algorithms to perform multi-objective optimization and achieve control objectives.

The main objective of the work presented by (Sedighizadeh, Esmaili, and Eisapour-Moarref 2017) was to control power, voltage, and current values in an islanded MG. Specific objectives considered included overshoot/undershoot, settling time, rise time, and integral time absolute error (ITAE) in the output voltage. A notable advantage of this approach was using fuzzy membership functions to define objective functions. The complex mathematical expressions were solved using a hybrid big bang-big crunch algorithm, which tuned PI regulators to accommodate different changes in load consumption.

The advantages of multivariable Model Predictive Control (MPC) were demonstrated in the study conducted by (Yazdi and Hosseinian 2019). The authors proposed a smart branch method for islanded MGs. This control structure utilized voltage and current measurements at the point of common coupling (PCC) to address various control objectives defined in the MPC performance index. These objectives included adjusting the output transformer impedance, enhancing power quality, and minimizing deviations in current values to reduce harmonics in the grid. To solve this complex problem, multi-objective optimization was employed, with an important characteristic being the incorporation of droop control to tune the weights of the MPC based on variable measurements.

In another study by (Bassey, Butler-Purry, and Chen 2019), a methodology for restoration sequences in distribution MGs was presented. The focus was on the islanded mode, where controlled power quality (PQ) inverters addressed common unbalanced load issues. The control strategy simultaneously optimized energy utilization and dynamic stability. Before developing the control strategy, transient electromagnetic simulations were conducted to analyze the transient behavior of the MG. A multi-objective function, subject to constraints, was then optimized to achieve load restoration and minimize the total restoration time, using an IEEE 123 node test feeder as a reference scenario.

The issue of unbalanced conditions in MG inverters is addressed in work by (Miao, Zhao, and Wan 2020). The study focused on improving the operation of grid-connected inverters by tackling power oscillations and current harmonic suppression problems. A multi-objective coordinated control strategy was proposed, which decoupled the grid voltage into positive and negative sequences. By applying a simplified Fourier transform and reducing mathematical complexity, the computational load was reduced while enhancing power quality in IBMGs under unbalanced grid voltages.

**Table 3.1:** Multi-objective optimization approaches

Method	Advantages	Disadvantages
Pareto optimally	Incorporates scalarization methods and provides a flexible framework for algorithm design	Requires prior knowledge of the Pareto front in objective space, the number of weight vectors grows exponentially with the objective space size The definition of desired goals requires extra computational effort; a solution might be non-dominated if the goals are chosen in a feasible domain and such conditions can limit their applicability
Global criterion	Simplicity and effectiveness because a Pareto ranking procedure is not required	Difficult to determine appropriate weight coefficients when scarce information of the problem is available
Linear combination of weights	Simplicity in implementation, use, and computational efficiency	High computational cost, encoding of objective functions limited for a few objectives
The $\epsilon$ -constraint method	Simple approach have been applied in many areas of engineering	
Multi-objective genetic algorithm (MOGA)	Versatility to find several members of the Pareto optimal set in a single performance of the algorithm	High computational cost
Non-dominated sorting genetic algorithm II (NSGA-II)	No extra diversity control is needed, elitism preserve Pareto-optimal solutions	More members in the first non-dominated set lead place to other Pareto-optimal solutions
Multi-objective evolutionary algorithm (MOEA)	The performance index are integrated as environmental selection, guided search, and continuous optimization of the entire population	Slow convergence, poor performance, and unknown convergence behavior of each non-dominated solution in the Pareto optimal set

Table 3.1 shows a summary of the current trends in multi-objective optimization on MG and compares methods.

### 3.2.13 Tuning algorithms

In the study conducted by (Jain et al. 2017), the issue of low-frequency instability in an MG with active and passive loads was addressed. MGs can experience stability problems when operating in island mode due to their low inertia and susceptibility to small changes in system operating conditions. To mitigate this issue, the researchers designed an LQR-based controller. Additionally, they employed a Kalman filter to estimate the system states. The advantage of using the Kalman filter lies in its ability to predict variable changes without the need for physical sensors or transmitters, relying solely on the mathematical functions of the process. In this work, the Kalman filter served as a state estimator, facilitating the communication system in hierarchical control.

Both the LQR control and Kalman method involved diagonal matrices that required calibration. The researchers employed genetic algorithms (GA), specifically the fast and elitist multi-objective non-dominated sorting genetic algorithm (NSGA-II). The NSGA-II technique within the GA framework allowed efficient tuning of the system's parameters.

In the study by (Dehkordi, Sadati, and Hamzeh 2018), robust stability analysis was performed on an MG with inverters employing a droop controller. The researchers examined situations where oscillatory phenomena occurred within the MG, attributing them to significant load changes, MG reconfiguration, high energy demand, and low frequencies from dominant electrical elements. A two-degree freedom droop controller, consisting of a conventional droop control and a robust transient function, was implemented to address these issues. The authors utilized Kharitonov's mathematical theorem for tuning the system and minimizing variable oscillations. Kharitonov's theorem has been widely employed in MG stability studies, offering a margin for adjusting the droop control gains while maintaining system reliability.

In another study focusing on collective behavior algorithms, (Barik et al. 2019) utilized the Particle Swarm Optimization (PSO) algorithm to optimize a fuzzy PD+I controller for mitigating frequency fluctuations in integrating renewable energy units. The PSO algorithm was employed to tune the gains of the PD+I controller and the fuzzy control parameters.

The controllers discussed in this section share common objectives, including improving transient response, tracking voltage, and frequency references, re-



jecting disturbances, stabilizing voltage in nonlinear loads, and facilitating efficient active and reactive power transfer. However, the subsequent section will explore the advantages of hybrid algorithms, which combine diverse mathematical methods to achieve robustness, fast response, and a broader range of performance with improved efficacy. Table 3.2 presents a list of common objectives various control structures address.

**Table 3.2:** Resume of advanced controllers objectives

Controller	Objective
PID	Voltage and frequency control, grid stabilization, improvement of power quality
LQR	Seamless transition, current control in island mode, frequency regulation, power sharing, mitigation of minor signal instability
MPC	Voltage and frequency control, virtual inertia, dynamic stabilization, power sharing, primary control
Fuzzy	Voltage and frequency control, power AC/DC control, virtual inertia, online tuning, power-sharing, voltage, current control
ANN	Fault detections, adaptive voltage and frequency control, islanding detection, prediction of load demand
SMC	Power flow control, disturbances rejection, voltage and frequency control, robust control for unbalanced load
$H_2/H_\infty$	Robust and optimal control, voltage and frequency control, cascade scheme

These research proposals have yielded significant improvements in a specific objective: reducing the cost of energy. However, the control algorithm approach can be further extended to target other objectives related to power quality. In this evolving field, complex control structures have been developed to achieve superior results compared to their predecessors. These advanced structures integrate different control methods, capitalizing on their inherent capabilities. Table 3.3 analyzes various controllers and the objectives they have successfully addressed in their papers. The presented proposals underscore the immense research potential for designing IBMG algorithms using VSI that surpass conventional regulators, opening up new possibilities for enhanced performance and efficiency.

**Table 3.3:** Objectives presented on IBMG regulation

Method	V/f control	Inertia stability	Fast transient response	Power flow control	THD reduction	Uncertainty rejection	Tuning	Sources
ANN + droop control	✓	✓	✓	✓	—	✓	—	Zhang et al. 2019; Baghaee et al. 2019; Yang et al. 2017
MPC + ANN	✓	—	—	✓	—	✓	—	Amoateng et al. 2017; Bonala and Sandepudi 2018
MPC + VI	✓	✓	✓	✓	—	—	—	Kerdphol et al. 2017
PI + VI + droop control	✓	✓	✓	✓	—	—	—	Shi et al. 2018a
SMC + $H_2/H_\infty$	✓	—	✓	—	✓	✓	✓	Li et al. 2017
$H_\infty$ + VSG	✓	✓	✓	✓	—	✓	✓	Fathi, Shafiee, and Bevrani 2018
LQR + $H_2/H_\infty$	✓	—	✓	—	✓	✓	—	Buduma and Panda 2018; Tran, Yoon, and Kim 2018
SMC + AN-FIS	✓	—	✓	—	✓	✓	—	Chang 2018; Anbarasu, Basha, et al. 2020
SMC + ANN	✓	—	✓	✓	—	—	—	Shen et al. 2019; Kirankumar, Reddy, and Vijayakumar 2017
PSO + droop control	✓	✓	—	✓	—	—	✓	Vinayagam et al. 2018
LQR + Kalman + GA	✓	—	✓	✓	—	✓	✓	Zhang et al. 2019
Droop control + Kharitonov	✓	—	—	✓	—	✓	✓	Dehkordi, Sadati, and Hamzeh 2018
Fuzzy PD + I + PSO	✓	—	—	✓	—	—	✓	Barik et al. 2019

The provided information highlights the advantages of multi-objective control in the context of IBMGs. These control schemes encompass various tasks, such as voltage, frequency, and power regulation. Additionally, they emphasize the importance of achieving fast response, effective disturbance rejection, and robustness against uncertainties. As the field progresses, new challenges arise, including establishing stability through virtual inertia and impedance algorithms, mitigating harmonics from integrating nonlinear loads, and optimizing controller tuning. In specific scenarios, self-tuning approaches can prove advantageous in developing intelligent algorithms that adapt and optimize their performance. These advancements pave the way for smarter control strategies that enhance the operation and efficiency of IBMGs.

All the works presented as part of the state of the art have shown innovative proposals for a multi-objective approach. A key parameter in this research is the formulation of the optimization functions. The following section presents the main concepts of the multi-objective approach.

### 3.3 Multi-objective Optimization Methods

Multi-objective optimization problems (Gunantara 2018) are common in science and engineering research. According to the objectives, these problems can be classified into single and multi-objective optimization. In the case of multi-objective optimization, two or more objective functions need to be optimized simultaneously. In many cases, these objective functions are mutually contradictory. A value must be found to reach a solution, and it can satisfy all the objective functions. If this situation exists, it is stated that there is a feasible solution.

Two approaches are distinguished for solving multi-objective problems: analytical and numerical. In the case of the analytical method, it involves using mathematical equations to obtain an exact solution. However, this approach has limitations in real-life scenarios where mathematical equations can only represent a few characteristics. To overcome this problem, an alternative solution is to find a model that can provide the optimal value for a multi-objective problem. This mathematical expression is iterated multiple times until the solution reaches a tolerable error level. The critical requirement is to define the decision variables of the problem and provide feedback on the objective being pursued. Once the decision variables are defined, this optimization method can be considered a black box problem, where only the inputs are known, and the outputs are measured.

There are several classical optimization methods to solve a single objective. As examples, we can analyze the strategies of Newton-Raphson, the simplex method, and the direct conjugation method, among others. These methods demonstrate high efficiency and fast convergence if they use a suitable initial value for the optimization problem. From this point, the resolution of the issue will depend on successive iterations according to the definition of its gradient. However, these methods have drawbacks for solving gradients that contain multiple terms. If these techniques are applied to multi-objective methods, probably, they can not be efficient, and consequently, they will be trapped in local optimal solutions. In addition, these methods merely find a single solution for each iteration, a problem in multi-objective approaches. This procedure would generate a loss of precision, and convergence would frequently depend on how the initial value of the variables to be optimized has been chosen (Marler and Arora 2004).

Otherwise, intelligent numerical methods have a heuristic nature. They are search algorithms that emulate behaviors of specific present systems in nature. Several investigations have been carried out in this field, so the search algorithms vary. A global classification can be made where four main branches are identified for intelligent numerical algorithms: inspired by biology, inspired by physics, inspired by geography, and inspired by social culture. In the following sections, the most employed methods are described:

### ***3.3.1 Biology inspired algorithms***

Biology-inspired algorithms are based on the activities of different living agents. These agents can represent micro or macro elements, generally modeled as sets of individuals. Evolution-based and swarm-based algorithms are known for these reasons.

#### *3.3.1.1 Evolution based algorithms*

Evolution-based algorithms (EA) are known to be stochastic search processes. They principally refer to the survival of the fittest. The search for these parameters generates individuals who adapt to more adverse environmental conditions and organize themselves to produce better generations. In this area, algorithms such as Evolutionary Strategy (ES), Evolutionary Programming (EP), Membrane Computing (P system), Genetic Algorithm (GA), Harmony Search Algorithm (HSA), and Differential Evolution Algorithm (DE), among others, can be identified.

Some techniques have been included in these algorithms to improve them, such as the case of Jia, where the author explored the neighborhood search mechanism through the chaos theory. In this way, the ability of the search and exploration process was improved from a previous stage to a later stage. Other authors form hybrid organisms, where the combinations of DE with PSO made by Liu can be found. The results showed this scheme was very efficient in solving problems with constraints (Cui et al. 2017).

Other biological algorithms manifest themselves in membrane computing. They are characterized by being non-deterministic algorithms and are ideal to implement in parallel computing devices. Thus, this abstract structure is presented as living cells, and their interaction allows the search algorithms to be generated. In 1988, the publication of this P algorithm with variants began in 2001. Many of the works consisted of forming membranes from cells. In this way, a hierarchical structure is proposed through different regions. As the process runs parallel, its evolution has several advantages over other methods. The applications that have been determined are computer graphics, cryptography, mathematics with biology, ecology with chemistry, and linguistics, among others.

Another method used from evolution-based algorithms is known as HS. Geem developed this method, and initially, only discrete problems were considered. However, with development in later years, its applications were expanded to continuous systems. This algorithm seeks to emulate the behavior of musicians with their different abilities to obtain a goal. Features such as: having a memory on the target and adjusting the pitch are highlighted. In this sense, the search is favored by the harmony presented by the algorithm and evolution mechanisms. These processes strengthen the exploratory ability to reach optimal results (Cui et al. 2017).

### *3.3.1.2 Swarm based algorithms*

In the case of algorithms based on swarms, a variety of them is inspired by the behavior of collectives, populations, or groups in their respective development environments. Different proposals emulate the behavior of ants, bees, wolves, sheep, and birds, among others (Marler and Arora 2004). A particular feature in these algorithms is the cooperation between the different individuals. In nature, cooperation activities are rewarded with survival, protection between individuals, and cooperativity, among others. Examples of these algorithms can be observed in: Artificial Bee Colony Algorithm (ABC), Ant Colony, Artificial Immune System (AIS), Teaching-Learning Based Optimization algorithm (TLBO), Optimization Algorithm (ACO), Firefly Algorithm

(FA), Cuckoo Search algorithm (CS), Pigeon Inspired Optimization (PIO), Bacteria Foraging Optimization algorithm (BFO), among others.

Different works have proposed the concept of artificial life (Cui et al. 2017). This idea was born to represent a natural system through computer processes. Many associated this theory with the dogmas Charles Darwin taught in his evolution theory. In this sense, it is sought that all the agents present in the computational models seek the same objectives as a natural system.

Comparing the classical and evolution methods, the evolution methods can determine a series of advantages that make them most used by the scientific community today. The strengths are the search capacity, greater precision in results, they do not depend on a gradient, and they represent systems that work in parallel and distributed, among others. Thus, these algorithms and large-scale processes that require higher computational costs to solve more complex mathematical functions can be incorporated.

### ***3.3.2 Physics inspired algorithms***

Algorithms inspired by physical systems are also heuristic algorithms. These methods can mimic physical behavior and properties of matter based on properties of physics. The most common algorithms are Chaotic Optimization Algorithm (COA), Gravitational Search Algorithm (GSA), Intelligent Water Drops Algorithm (IWD), Magnetic Optimization, Algorithm (MOA), Simulated Annealing (SA), etc.

One of the most prominent cases is the COA, characterized by its random search technique. The work in this area by Hamzacebi and Kutay generated adaptive algorithms to solve optimization problems heuristically. Other authors, such as Velázquez, used the chaotic sequences for features like randomness, ergodicity, and regularity. An advantage present in chaotic systems is that small changes produced in initial values generate significant differences in the system's behavior (Cui et al. 2017).

### ***3.3.3 Geography inspired algorithms***

These algorithms are heuristic, and they generate random solutions for searching spaces in the optimization process. They are classified as Tabu Search Algorithm (TSA) and Imperialistic Competition Algorithm (ICA). In the case of TS, Glover suggested in 1986 that it be identified as a local search method. This technique explores all feasible solutions in a moving space. A prohibited

class of prohibited movements is analyzed; in this way, the algorithm is ensured not to select a local minimum. While the ICA algorithm is inspired by imperialism, This philosophy is oriented toward implementing a government in a population. There may be many colonies where one empire has authority over others. From various sets, strong empires and weak empires can be detected (Gunantara 2018).

### 3.3.4 Social culture inspired algorithms

Social algorithms are inspired by many of the characteristics that populations have today. These characteristics are: social, economic, and cultural, among others. An example is presented in Moscato's work from 1989. This work introduces how computational algorithms can be implemented to simulate granular systems. One of the characteristics of this method remains the possibility of analyzing a problem through partitions of the same. Its applications are oriented to fuzzy problems, not precious, inconsistent, and with partial values. Other works have implemented intelligent algorithms MOEAs (multi-objective EAs) to optimize social problems have been observed. These problems were focused on: the economy and energy as development, among others. These applications also reached other philosophical sectors, such as reforestation, biomass, micro-grids, distributed generation systems, and hybrid renewable energy systems (Cui et al. 2017).

Several other methods have been developed with their respective variants, including a vital component of genetic algorithms (GA). The best-known methods are VEGA, MOGA, SPEA, SPEA2, NSGA, NSGA-II, PESA, PESA-II, NPGA, and NPGA2. These algorithms have had good results in some sectors, such as the type design of distribution transformers, complex industrial processes, or processes that integrate renewable energies (Gunantara 2018).

In summary, new methods are still being developed to help solve multi-objective problems. Many of these methods are known as hybrids because they combine some techniques to improve their results. Classical optimization methods are also considered, which need to be more robust. In recent years, the application of these energy methods and systems and their optimization has been strengthened with several applications that seek to improve the effectiveness of the processes.

### 3.4 Evaluation Indexes on Multi-objective Optimization

In multi-objective optimization is desired a set of effective values based on the Pareto optimal. After that, the evaluation of these functions depends on the following:

- Convergence: The best solutions are approximated to the Pareto optimal.
- Uniformity: Good solutions are placed along the Pareto optimal.
- Distribution: All the solutions cover the Pareto optimal.

To evaluate the effectiveness of the multi-objective approach, indexes are used. The following sections will describe some indexes to understand their performance.

#### 3.4.1 Interactive methods

These methods (Gunantara 2018) leverage decision-makers' prior knowledge and experiences. They utilize iterative approaches that incorporate decision-makers' preferences for optimizing each objective. The scalarization method is also employed to generate the Pareto optimal front.

Two widely applied interactive methods for multi-objective problems are the Normal Boundary Intersection (NBI) and Normalized Normal Constraint (NNC).

The NBI method solves multi-objective problems from an intuitive geometric perspective. This technique considers the convex hull of individual minima (CHIM) to construct lines normal to the plane. The intersection of the CHIM normal lines with the edges of the feasible targets near the origin generates the set of Pareto optimal values. This method offers the advantage of developing evenly spaced values throughout the Pareto set. It is particularly advantageous in solving non-convex and multidimensional problems, distinguishing it from classical methods.

The NNC method shares many similarities with NBI in its applications. However, NNC incorporates constraints to minimize the most significant objective among the set of goals in a problem. The remaining objectives are handled by integrating them as inequalities in the mathematical approach. To elaborate further, the NNC method constructs the utopia hyperplane using all normalized values of individual minima and distributed points. The points in this hyperplane can vary based on the weights assigned to each. Hyperplanes are perpendicular to another set of planes constructed for each objective function.



### 3.4.2 Pareto-dominated methods

Pareto-front methods (Cui et al. 2017) have evolved through intelligent algorithm techniques. The pioneering work in this field was performed by the NSGA method, which aimed to obtain solution values based on the Pareto front. Subsequently, more research has focused on determining non-dominated solutions on the Pareto front. A non-dominated solution is a value that benefits all possible objectives in a multi-objective optimization problem. Such solutions are among the best options for improving all objectives in a multi-optimization approach.

One advantage of this approach is the utilization of hybrid algorithms. These combine intelligent optimization techniques with swarm-based methods to enhance the robustness of solving multi-objective problems. This integration, known as hybrid optimization, enables a vast search space exploration while reducing convergence time.

Originating from economic problems, the concept of Pareto solutions extends to multi-variable systems where specific solutions may benefit some components without adversely affecting others. The optimization methodology aims to identify solutions that help all members within an economic system, thereby maximizing overall performance.

The Pareto front is designed to optimize various objectives while avoiding conflicts. The potential solutions generated by this method represent an improvement across all objectives in the best possible manner.

The Pareto-front method and its hybrid algorithms have applications in diverse science and technology areas (Gonzales-Zurita et al. 2020). This technique offers an efficient approach to solving complex real-life problems. However, one main drawback is the computational cost of some intelligent algorithms, which may require many iterations to achieve high efficiency. Therefore, adequate hardware resources are essential for performing Pareto-front optimization effectively.

### 3.4.3 New dominance methods

While the Pareto method offers advantages, its computational cost can challenge achieving convergence across multiple objectives. Some authors proposed the  $\epsilon$ -dominance method (Cui et al. 2017). Unlike the Pareto front, which formulates the optimization process on hyper grids in the space, the new dominance methods introduce an  $\epsilon$  vector whose length is proportional to the hyper

grids. This approach generates values related to the Pareto front's geometrical shape.

These algorithms can also incorporate hybrid proposals, combining classical methods with intelligent algorithms to tackle multi-objective problems.

Multi-objective optimization finds applications in various fields of science and technology. For instance, in the environmental domain, these algorithms aim to minimize pollutant emissions, maximize energy efficiency, and optimize economic profits. Power management presents explicit challenges due to the involvement of multiple stakeholders, each with their objectives and perspectives. Moreover, these electrical systems must adhere to specific regulations and policies, further complicating the mathematical problem.

To address these challenges, efficient methods must be developed to cater to diverse requirements. The different models presented in this chapter provide practical approaches to achieve a trade-off between objectives, highlighting the convergence of the problem and the results obtained through these approaches. Control designers must evaluate their solutions and determine the best option based on the performance of each system.

#### 3.4.4 *A posteriori methods*

*A posteriori* methods (Marler and Arora 2004) in multi-objective optimization are techniques used to obtain a representative set of Pareto-optimal solutions after optimization. These methods focus on post-processing the obtained solutions to filter out the non-dominated ones and provide decision-makers with a range of trade-off solutions.

One widely used *a posteriori* method is the non-dominated sorting approach. It categorizes solutions into different Pareto fronts based on their dominant relationship with one another. Solutions that are not dominated by any other solution form the first Pareto front, while subsequent fronts consist of solutions that are dominated only by the solutions from previous fronts.

Another popular *a posteriori* method is the evolutionary algorithm-based approach, such as the NSGA-II (Non-dominated Sorting Genetic Algorithm II). These algorithms use a population-based search process to generate diverse solutions iteratively. The solutions are then ranked based on their dominance relationship, and the non-dominated solutions are selected as the final Pareto front.

A posteriori methods allow for a flexible exploration of the Pareto front without needing a predefined grid or reference points. They can handle complex and high-dimensional problems efficiently. However, the obtained solutions may only cover part of the Pareto front, and the density of solutions may vary across different regions.

### ***3.4.5 No-preference methods***

No-preference methods (Gunantara 2018) in multi-objective optimization are techniques used when there is no clear preference or priority among the conflicting objectives. These methods aim to explore the solution space without making assumptions or imposing preferences on the objectives.

One commonly used no-preference method is the weighted sum approach. It involves assigning weights to each objective and transforming the multi-objective problem into a single-objective problem by summing the weighted objectives. By varying the weights, different trade-offs between objectives can be explored. However, this method assumes linear relationships between objectives and may not capture the true trade-off surface.

Another no-preference method is the  $\epsilon$ -constraint approach. It involves solving a series of single-objective optimization problems, where each problem constrains one objective to a specific value and maximizes the other objectives. By varying the constraint value, different trade-offs can be examined. This method allows more flexibility in capturing the trade-off surface but can be computationally expensive.

No preference methods provide decision-makers with comprehensive solutions without requiring explicit preferences. They allow for a broad exploration of the trade-off space and offer a range of feasible solutions. However, they may not capture complex non-linear relationships among objectives and may require additional analysis to select the most preferred solution.

## **3.5 Conclusions of the Chapter**

This chapter provides a comprehensive review of multi-objective algorithms and control techniques. Various algorithms, their optimization processes, and performance metrics have been examined.

The reviewed control algorithms offer proposals for enhancing the control of IBMGs, focusing on optimizing energy management. However, it is observed

that the application of multi-objective algorithms in the context of microgrids, particularly in renewable energy generation, is still an area under active development.

The formulation of optimization indices enables the development of methodologies for algorithm optimization. These indices can be designed as composite or multiple cost functions, depending on the specific goals, computational cost, and the chosen approach for simultaneously applying a single composite index or several simple indices in the optimization process.

Furthermore, performance evaluation indices for multi-objective algorithms have been explored. These indices consider various criteria, with the Euclidean distance between points on the Pareto front being the most common measure. While different approaches exist for these evaluation indices, they share the common objective of providing a numerical value that quantifies the effectiveness of multi-objective algorithms.

Having analyzed the two main aspects of this thesis, namely the MG structure and closed-loop control, the subsequent chapters will focus on developing efficient approaches for applying multi-objective methods in managing energy within IBMGs.

# New Methodology: Multi-objective Approach for Optimizing the Closed-loop Control of Active Power in Inverter-based Microgrids

### 4.1 Introduction

The previous chapters explored the general aspects of microgrids and their control methods. The main components of microgrids and their function in the system's operation were analyzed in Chapter 2. The inverter, as the primary element for energy management, was examined. Furthermore, valuable information about state-of-the-art control in inverter-based microgrids was obtained in Chapter 3. The objectives and performance indices that evaluate the effectiveness of the controllers were observed.

Once the background and state of the art are known, the control algorithm for improving IBMGs is needed. One commonly used method for inverter microgrid control is the Proportional-Integral (PI) regulator (Serban and Ion 2017). It is favored for its simplicity and effectiveness. However, certain issues regarding its precision and stability have yet to be identified. If PI is not properly calibrated, the controller often leads to oscillations and may need more robustness when facing sudden system changes.

On the other hand, multi-objective methods can be employed in two approaches. Multiple objectives can be combined into a single cost function, or the optimization of cost functions can be individually focused on various objectives. These multi-objective methods are utilized to improve the performance of closed-loop control in terms of speed, stability, and reliability, among others. This chapter analyzes these two approaches, providing an innovative methodology that demonstrates the advantages of this technique compared to traditional controllers in inverters. A non-conventional controller, such as the Second order sliding mode control (SMC-2), is proposed, and the values of its constants are optimized using multi-objective methods.

Finally, the performance of the proposed controllers is determined numerically, evaluating how they enhance their performance compared to the traditional controller through performance indices.

Examining these topics, this chapter contributes to understanding microgrid control methods based on inverters. Exploring multi-objective approaches and introducing innovative techniques aims to improve microgrids' overall performance and overcome traditional controllers' limitations. This research provides valuable insights into optimizing microgrid control and showcases the potential benefits of utilizing non-conventional controllers and multi-objective optimization in microgrid systems.

This chapter addresses various topics related to the new methodology applied to inverter-based microgrid control. Section 4.2 explains how the inverter dynamic variables interact with the microgrid. Section 4.3 shows the proposal of a non-conventional sliding mode controller for active power regulation in the microgrid. Section 4.4 presents the solution to an active power regulation problem with multiple objectives by optimizing a single cost function. Section 4.5 analyzes the active power optimization of a problem with multiple objectives in a microgrid, considering more than one optimization function. Section 4.6 shows the equations of performance indexes considered to evaluate numerically the new methodology presented in this thesis. Finally, section 4.7 provides the chapter's conclusions.

## 4.2 Microgrid Modelling

As discussed in Chapter 2, the voltage source inverter plays a crucial role in microgrids. It facilitates the conversion of direct current (DC) energy into alternating current (AC), enabling modification of the active power. During this transformation process, various interactions occur among the inverter's variables. These interactions necessitate a sophisticated strategy where the controller perceives the inverter as a black box. By receiving input signals, the controller can execute appropriate corrective actions to modify the process output.

This thesis focuses on studying microgrids that incorporate controllers for single-phase inverters. With the growing adoption of residential electricity generation in recent years, challenges have emerged concerning the speed and stability of power generation in single-phase microgrids. This section presents the dynamic model of a microgrid's single-phase voltage source inverter. Subsequent sections provide an overview of different topologies and types of converters employed in generating single-phase inverters for microgrids.

### 4.2.1 Topologies of Single-phase inverter-based microgrids

As mentioned, a single-phase voltage source inverter (SPVSI) generates AC voltage from a DC voltage source. The H-bridge is the most commonly used topology among the various hardware implementation options. The selection of this scheme can be attributed to several reasons. Firstly, the maximum AC voltage value equals the maximum value of the DC bus voltage, denoted as  $V_{DC}$ . The converter operates with three output levels:  $+V_{DC}$ , 0, and  $-V_{DC}$ . Additionally, the sizing of each semiconductor component is determined by the maximum inverse voltage of the DC bus (Xu et al. 2019). This circuit configuration comprises two branches, each containing two power switches. The switches alternate between open and closed states based on a modulation signal generated by the control circuit. The Sinusoidal Pulse Width Modulation (SPWM) technique is widely used for the control signal due to its ability to minimize harmonic content at the load. Table 4.1 provides an overview of the switch states in the SPVSI.

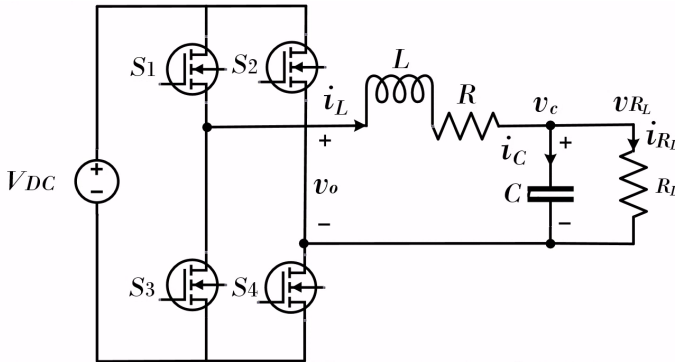
The performance of the single-phase voltage source inverter (SPVSI) is closely tied to the configuration in which it is connected to the grid. Therefore, it is crucial to analyze the following schemes to understand their operation and capabilities.

**Table 4.1:** States of power switches on the SPVSI.

$S_1$	$S_2$	$S_3$	$S_4$	$v_o$
1	0	0	1	$V_{DC}$
0	1	1	0	$-V_{DC}$
1	1	0	0	0
0	0	1	1	0

### 4.2.2 The Stand-alone SPVSI scheme

The SPVSI utilizes sinusoidal pulse width modulation (SPWM) to generate a high-frequency sinusoidal output voltage. To mitigate the presence of harmonics, a low-pass filter is incorporated at the output of the circuit. Figure 4.1 illustrates the SPVSI scheme with the output filter.



**Figure 4.1:** SPVSI scheme.

The output voltage  $v_o$  is represented as:

$$v_o = u \cdot V_{DC}, \quad (4.1)$$

where  $v_o = -V_{DC}$  for  $u = -1$ ,  $v_o = 0$  for  $u = 0$ , and lastly  $v_o = V_{DC}$  for  $u = 1$ .

Kirchhoff's voltage and current equations are employed to describe the dynamic behavior of the SPVSI. The analysis encompasses the relationship between the output voltage of the SPVSI, the filter components, and the load, which can be expressed as follows:



$$v_o(t) = v_L(t) + v_R(t) + v_c(t), \quad (4.2)$$

$$i_L(t) = i_c(t) + i_{R_L}(t). \quad (4.3)$$

Where:

$$v_o(t) = L \cdot \frac{di_L(t)}{dt} + i_L(t) \cdot R + v_c(t), \quad (4.4)$$

$$i_L(t) = C \cdot \frac{dv_c(t)}{dt} + \frac{v_c(t)}{R_L}. \quad (4.5)$$

The low-pass filter, consisting of the  $L$ ,  $R$ , and  $C$  elements, attenuates the high-order harmonics generated by the SPWM modulation. This filter operates with a cut-off frequency, above which signals are effectively blocked from reaching the load. The specific cut-off frequency depends on the frequency of the grid system (e.g., 50  $Hz$  or 60  $Hz$ ) in a given region. Additionally, the resistive load  $R_L$  represents the electrical consumption of the system.

The final equations that show the dynamical states of the SPVSI are presented below:

$$\frac{di_L(t)}{dt} = \frac{1}{L} \cdot [v_o(t) - i_L(t) \cdot R - v_c(t)], \quad (4.6)$$

$$\frac{dv_c(t)}{dt} = \frac{1}{C} \cdot \left[ i_L(t) - \frac{v_c(t)}{R_L} \right]. \quad (4.7)$$

In addition, the state space representation is formulated as seen in [Ogata 2010](#). The state space variables are depicted as  $\dot{x} = Ax + Bu$ , where  $\dot{x}$  denotes the derivatives of state variables,  $x$  is used to represent the set of state variables,  $u$  is the input variable,  $A$  and  $B$  are the state matrix and input matrix respectively. The set of state variables and their derivatives are presented as follows:

$$x(t) = [i_L(t), v_c(t)]^t, \quad (4.8)$$

$$\dot{x}(t) = \left[ i_L(t), v_c(t) \right]^t. \quad (4.9)$$

The letter  $t$  at the end of each vector represents the transpose operation. The next expression shows the state variables model of the SPVSI:

$$\dot{x} = \begin{bmatrix} -\frac{R}{L} & -\frac{1}{L} \\ \frac{1}{C} & -\frac{1}{R_L C} \end{bmatrix} x + \begin{bmatrix} \frac{V_{DC}}{L} \\ 0 \end{bmatrix} u. \quad (4.10)$$

### 4.2.3 The Grid-tied SPVSI scheme

The dynamic equations of the SPVSI undergo a slight modification when the grid is included in the system. This modified model is illustrated in Figure 4.2.

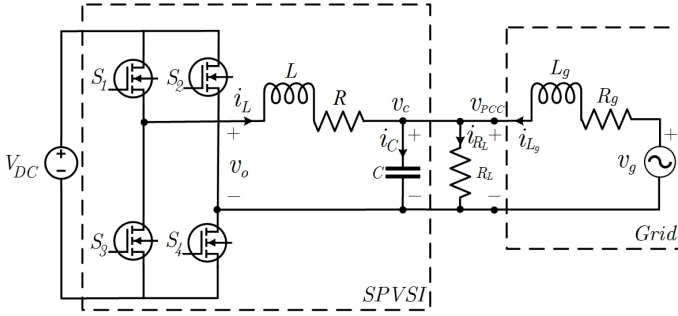


Figure 4.2: Grid connected SPVSI scheme.

Once again, Kirchhoff's voltage and current equations are applied, this time incorporating the voltage and impedance of the grid. As a result, the voltage across the load is now referred to as the Voltage of the Point of Common Coupling (PCC) ( $v_{PCC} = v_c$ ).

The equations are:

$$v_o(t) = v_L(t) + v_R(t) + v_{PCC}(t), \quad (4.11)$$

$$v_g(t) = v_{Lg}(t) + v_{Rg}(t) + v_{PCC}(t), \quad (4.12)$$

$$i_L(t) + i_{Lg}(t) = i_C(t) + i_{R_L}(t), \quad (4.13)$$

where:

$$v_o(t) = L \cdot \frac{di_L(t)}{dt} + i_L(t) \cdot R + v_c(t), \quad (4.14)$$

$$v_g(t) = L_g \cdot \frac{di_{L_g}(t)}{dt} + i_{L_g}(t) \cdot R_g + v_c(t), \quad (4.15)$$

$$i_L(t) + i_{L_g}(t) = C \cdot \frac{dv_c(t)}{dt} + \frac{v_c(t)}{R_L}. \quad (4.16)$$

where  $i_L(t)$ ,  $i_{L_g}(t)$  and  $v_c(t)$  are the states of the SPVSI. The new representation of these states is considered as follows:

$$\frac{di_L(t)}{dt} = \frac{1}{L} \cdot [v_o(t) - i_L(t) \cdot R - v_c(t)], \quad (4.17)$$

$$\frac{di_{L_g}(t)}{dt} = \frac{1}{L_g} \cdot [v_g(t) - i_{L_g}(t) \cdot R_g - v_c(t)], \quad (4.18)$$

$$\frac{dv_c(t)}{dt} = \frac{1}{C} \cdot \left[ i_L(t) - \frac{v_c(t)}{R_L} + i_{L_g}(t) \right]. \quad (4.19)$$

The set of state variables and their derivatives are presented as follows:

$$x(t) = [i_L(t), i_{L_g}(t), v_c(t)]^t, \quad (4.20)$$

$$\dot{x}(t) = [i_L \dot{(t)}, i_{L_g} \dot{(t)}, v_c \dot{(t)}]^t. \quad (4.21)$$

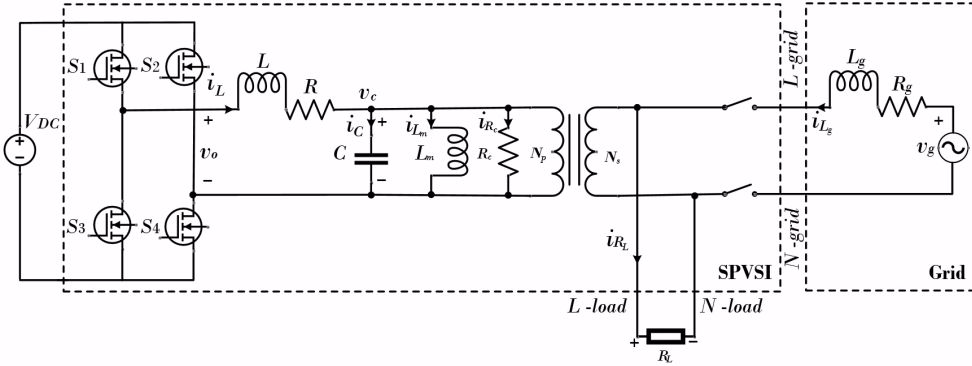
The next expression shows the state variables model of the SPVSI:

$$\dot{x} = \begin{bmatrix} -\frac{R}{L} & 0 & -\frac{1}{L} \\ 0 & -\frac{R_g}{L_g} & -\frac{1}{L_g} \\ \frac{1}{C} & \frac{1}{C} & -\frac{1}{R_L C} \end{bmatrix} x + \begin{bmatrix} \frac{V_{DC}}{L} \\ 0 \\ 0 \end{bmatrix} u + \begin{bmatrix} 0 \\ \frac{v_g}{L_g} \\ 0 \end{bmatrix}, \quad (4.22)$$

where  $\begin{bmatrix} 0 & \frac{v_g}{L_g} & 0 \end{bmatrix}^t$  is an extended vector due to the effect of the external variable  $v_g$  from the grid.

#### 4.2.4 The Grid-tied step-up transformer SPVSI scheme

The dynamic equations of the SPVSI with step-up transformer need an analysis of new parameters. This modified model is illustrated in Figure 4.3.



**Figure 4.3:** Grid connected SPVSI with step-up transformer scheme.

To derive the dynamical equations of the SPVSI, a simplified model of the inverter-based microgrid is utilized. In this model, one component that can be disregarded is the step-up transformer, which connects the output voltage of the filter to the point of common coupling between the grid and the load. The step-up transformer is characterized by the ratio  $N$  between the primary ( $N_P$ ) and secondary ( $N_S$ ) windings, given by:

$$N = \frac{N_S}{N_P}. \quad (4.23)$$

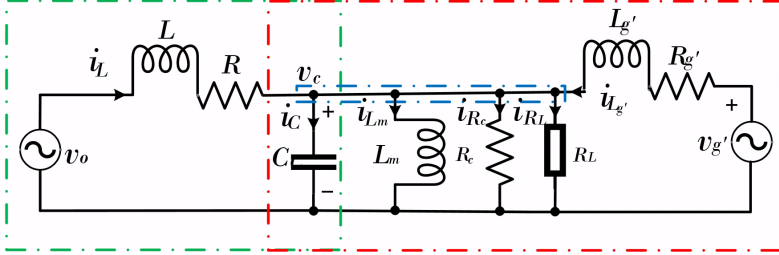
The following parameters were transformed from the high-voltage side to the low-voltage side to obtain a reduced circuit:

$$v_{gt} = \frac{v_g}{N}, \quad (4.24)$$

$$R_{gt} = \frac{R_g}{N^2}, \quad (4.25)$$

$$L_{g'} = \frac{L_g}{N^2}. \quad (4.26)$$

Figure 4.4 shows the equivalent circuit with all parameters located in the low voltage side of the step-up transformer:



**Figure 4.4:** Reduced equivalent circuit of an inverter-based microgrid.

The following steps are taken to determine the state variables model of the SPVSI, allowing for a mathematical understanding of the power converter's function.

First, applying Kirchhoff's voltage law in the first mesh of green color:

$$v_o(t) = R \cdot i_L(t) + L \frac{di_L(t)}{dt} + v_C(t), \quad (4.27)$$

Applying Kirchhoff's voltage law in the second mesh of red color:

$$v_{g'}(t) = R_{g'} \cdot i_{L_{g'}}(t) + L_{g'} \frac{di_{L_{g'}}(t)}{dt} + v_C(t). \quad (4.28)$$

Applying Kirchhoff's current law in the node of blue color:

$$i_L(t) + i_{L_{g'}}(t) = i_C(t) + i_{L_m}(t) + i_{R_c}(t) + i_{R_L}(t), \quad (4.29)$$

$$i_L(t) + i_{L_{g'}}(t) = C \frac{dv_C(t)}{dt} + i_{L_m}(t) + \frac{v_C(t)}{R_c} + \frac{v_C(t)}{R_L}. \quad (4.30)$$

Finally, the equation of the voltage of  $L_m$  is also considered:

$$v_{L_m}(t) = v_C(t) = L_m \frac{di_{L_m}(t)}{dt}. \quad (4.31)$$

The dynamic states of the last equations are presented as follows:

$$\frac{di_L(t)}{dt} = -\frac{Ri_L(t)}{L} - \frac{v_C(t)}{L} + \frac{v_o(t)}{L}, \quad (4.32)$$

$$\frac{di_{L_{g'}}(t)}{dt} = -\frac{R_{g'}i_{L_{g'}}(t)}{L_{g'}} - \frac{v_C(t)}{L_{g'}} + \frac{v_{g'}(t)}{L_{g'}}, \quad (4.33)$$

$$\frac{dv_C(t)}{dt} = \frac{i_L(t)}{C} - \frac{v_C(t)}{R_c C} - \frac{v_C(t)}{R_L C} + \frac{i_{L_{g'}}(t)}{C} - \frac{i_{L_m}(t)}{C}, \quad (4.34)$$

$$\frac{di_{L_m}(t)}{dt} = \frac{v_C(t)}{L_m}. \quad (4.35)$$

The state-space variables for the SPVSI and its derivatives are:

$$x(t) = [i_L(t), i_{L_{g'}}(t), v_c(t), i_{L_m}(t)]^t, \quad (4.36)$$

$$\dot{x}(t) = [\dot{i}_L(t), \dot{i}_{L_{g'}}(t), \dot{v}_c(t), \dot{i}_{L_m}(t)]^t. \quad (4.37)$$

The next expression shows the state variables model of the SPVSI:

$$\dot{x} = \begin{bmatrix} -\frac{R}{L} & -\frac{1}{L} & 0 & 0 \\ 0 & -\frac{1}{L_{g'}} & -\frac{R_{g'}}{L_{g'}} & 0 \\ \frac{1}{C} & -\frac{1}{R_L C} - \frac{1}{R_m C} & \frac{1}{C} & -\frac{1}{C} \\ 0 & \frac{1}{L_m} & 0 & 0 \end{bmatrix} x + \begin{bmatrix} \frac{V_{DC}}{L} \\ 0 \\ 0 \\ 0 \end{bmatrix} u + \begin{bmatrix} 0 \\ \frac{v_{g'}}{L_{g'}} \\ 0 \\ 0 \end{bmatrix}, \quad (4.38)$$

where  $\begin{bmatrix} 0 & \frac{v_{g'}}{L_{g'}} & 0 & 0 \end{bmatrix}^t$  is an extended vector due to the effect of the external variable  $v_g$  from the grid side.

The system represented by the state variables relies on the transformer for converting energy from the primary to the secondary side. During this energy conversion process, the magnetization components of the transformer generate energy in the secondary winding. In the absence of saturation, the voltage level required for coupling with the microgrid can be attained.

The observed mathematical modeling for different implementations of the inverter demonstrates how its variables interact dynamically. This shows us how a control system should be implemented and which variables should be considered. The power management control proposal for the inverter is outlined in the following section.

### 4.3 Sliding Mode Controller Approach

Nowadays, closed-loop control algorithms have become indispensable for effectively regulating output variables in various processes. These algorithms provide a mathematical framework to achieve regulatory objectives. In the context of inverter-based microgrids, one crucial objective is closed-loop active power control. By implementing an appropriate control method, achieving faster and more stable responses becomes possible, thereby enhancing the efficiency of active power generation in the inverter.

Among the various closed-loop control methods available, sliding mode control has gained significant attention recently due to its robustness and rapid response characteristics. However, it should be noted that commercially available industrial-grade inverters currently do not incorporate sliding mode controllers. Nevertheless, the motivation behind employing sliding mode control in inverters is to improve the efficiency of active power generation.

In the upcoming sections, this thesis will delve into the fundamental principles of sliding mode control and propose an innovative approach to designing the controller. By introducing this novel perspective, the field is anticipated to advance, leading to improved performance of inverter-based microgrids.

### 4.3.1 Controller formulation

In this section Sliding Mode Control (SMC) is presented as the algorithm for closed-loop regulation of active power. This method allows for controlling non-linear processes with high accuracy and robustness against disturbances (Yu, Feng, and Man 2021). Besides the various advantages of this method, there is one key disadvantage in its implementation, known as the chattering effect. Due to physical limitations, this feature consists of high-frequency signals that electromechanical elements cannot follow. An alternative to overcome this drawback is High-Order Sliding Mode Controller (HOSMC) (Fridman and Levant 2002). The following lines will provide a brief review and the formulation of the HOSMC.

First, any dynamical system can be expressed in function of their states as follows:

$$\dot{x} = \frac{dx(t)}{dt} = f(t, x, u) \in \mathbb{R}, u = u(t, x) \in \mathbb{R}, \quad (4.39)$$

where  $x$  represents the states variables,  $u$  is the input signal,  $f(t, x, u)$  represents the derivative function of the state variables, and  $u(t, x)$  is a time varying function of the control signal. The state variables for the grid-tied SPVSI are  $i_L(t)$ ,  $i_{Lg}(t)$ ,  $v_c(t)$  and they are written in a vector  $x(t) = [i_L(t), i_{Lg}(t), v_c(t)]^t$ , where  $t$  represents the transpose matrix.

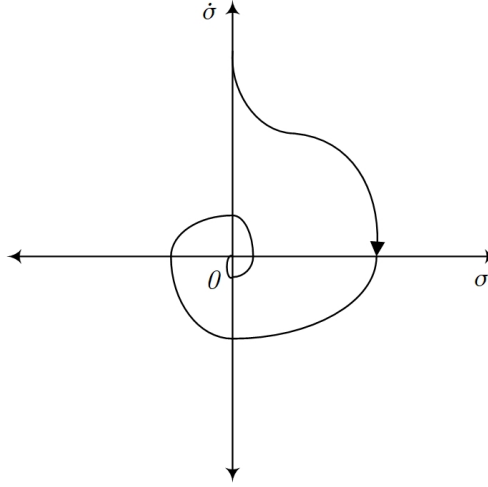
The actions of the SMC are performed on a hyperplane represented by a term called sliding surface. The main purpose of the SMC is to maintain the state trajectory as close as possible to the sliding surface until its path ends near zero. The sliding surface is defined by  $\sigma = \sigma(t, x) \in \mathbb{R}$ .

In Figure 4.5, the path of any state in the sliding surface can be seen.

The HOSMC control law incorporates techniques to select a control action that achieves the desired objectives while mitigating the chattering effects. These techniques include twisting, sub-optimal, drift, and an algorithm with a prescribed convergence law known as the super-twisting algorithm. Among these alternatives, the super-twisting algorithm has gained recognition in the control field due to its advantages, such as a relative degree of 1 and sliding surface trajectories that orbit around the origin.

In the super-twisting algorithm, the control law consists of two terms. The first term is defined by its continuous time derivative, while the second term represents a continuous function of the sliding variable.





**Figure 4.5:** Super-twisting phase trajectory.

In HOSMC, the relative degree of a system indicates the order of the control law. HOSMC typically has orders greater than 1. Therefore, the relative degree of a system can be determined by:

$$r \geq 2 \Leftrightarrow \frac{\partial}{\partial u} \sigma^{(i)} = 0, (i = 1, 2, \dots, r - 1), \frac{\partial}{\partial u} \sigma^{(r)} \neq 0, \quad (4.40)$$

where  $i$  constitutes the  $i$ -esime derivative until reaching a determinate relative degree. Classical variable structure systems define the control variable  $u(t)$  as a relay output.

The following lines explain how to set up the control law for HOSMC with super-twisting criterion.

Assume that parameters such as  $t$ ,  $u(t)$ ,  $\sigma(t, x)$ , and the sign of the time derivative of  $\sigma$  are known. The control law of a HOSMC steers  $\sigma$  to zero in finite time.

In this sense,  $\mathcal{U} = \{u : |u| \leq U_M\}$  is defined and assume that:

- There exists  $u_1 \in (0, 1)$  for any continuous function  $u(t)$  with  $|u(t)| > u_1$ . There is a  $t_1$ , such that  $\sigma(t) u(t) > 0$  for each  $t > t_1$  and the control law  $u(t) = -\text{sign}[\sigma(t_0)]$ , where  $t_0$  is the initial time that the control law hitting the sliding surface in finite time.

- There are positive constants  $\sigma_0, u_0 < 1, \Psi_m, \Psi_M$  such that if  $|\sigma(t, x)| < \sigma_0$  then:

$$0 < \Psi_m \leq \frac{\partial}{\partial u} \dot{\sigma}(t, x, u) \leq \Psi_M, \forall u \in \mathcal{U}, x \in \mathcal{X}, \quad (4.41)$$

and the inequality  $|u| > u_0$  entails  $\dot{\sigma}u > 0$ . Here  $\dot{\sigma}(t, x, u)$  represents the total time derivative of the sliding variable  $\sigma(t, x)$ .

- There is a  $0 \leq \Phi \in \mathbb{R}$  in the region defined by  $|\sigma| < \sigma_0$  such that

$$\left| \frac{\partial}{\partial t} \dot{\sigma}(t, x, u) + \frac{\partial}{\partial x} \dot{\sigma}(t, x, u) f(t, x, u) \right| \leq \Phi. \quad (4.42)$$

The above conditions define that  $u(t)$  is stable no matter the state variable's starting point.

To mitigate the chattering effect, the super-twisting algorithm is selected. This algorithm is particularly effective for systems with a relative degree of one. It employs a technique where the state of a function orbits around the origin while the objective is to drive the sliding surface and its derivatives to zero. The continuous representation of the control law is expressed as:

$$u(t) = \int_0^t \dot{u}_1(t) + u_2(t), \quad (4.43)$$

where:

$$\dot{u}_1(t) = \begin{cases} -u & \text{if } |u| > 1, \\ -W \text{sign}(\sigma) & \text{if } |u| \leq 1, \end{cases} \quad (4.44)$$

$$u_2(t) = \begin{cases} -\lambda |\sigma_0|^\rho \text{sign}(\sigma) & \text{if } |\sigma| > \sigma_0, \\ -\lambda |\sigma|^\rho \text{sign}(\sigma) & \text{if } |\sigma| \leq \sigma_0. \end{cases} \quad (4.45)$$

The conditions for finite time convergence of the sliding surface are defined as (Elyoussef et al. 2012):

$$W > \frac{\Phi}{\Psi_m}, \quad (4.46)$$

$$\lambda^2 \geq \frac{4\Phi \Psi_M(W + \Phi)}{\Psi_m^2 \Psi_m(W - \Phi)}, \quad (4.47)$$

$$0 < \rho \leq 0.5, \quad (4.48)$$

where  $W$ ,  $\lambda$ , and  $\rho$  represent the gains of the super-twisting algorithm. These values will be determined using a metaheuristic algorithm called Particle Swarm Optimization (PSO). PSO is an intelligent optimization process originally developed by Kennedy and Eberhart (Lee et al. 2018) to mimic the behavior of biological systems. The details of the algorithm will be discussed in the following section.

Before selecting a specific order for HOSMC, it is necessary to determine the relative degree. Since the grid side maintains a constant voltage of  $230V_{rms}$ , the active power error is obtained by subtracting the actual output current value. The control error for the current is expressed as follows<sup>1</sup>:

$$e(t) = i_L(t) - i_{Lref}. \quad (4.49)$$

The derivative of the error is  $\dot{e}(t) = \dot{i}_L(t)$ , where  $\dot{i}_L(t)$  is given in (4.17). Conventional sliding surface is a linear plane:  $\sigma(t) = e(t) + \lambda \dot{e}(t)$ . In this Chapter, the sliding surface  $\sigma$  is a PI hyperplane which is expressed as follows:

$$\sigma(t) = K_p e(t) + K_i \int_0^t e(t). \quad (4.50)$$

This type of sliding surface reaches the error softly by the integral action. The derivative of (4.50) is:

$$\dot{\sigma}(t) = K_p \left( \frac{1}{L} \cdot [v_o(t) - i_L(t) \cdot R - v_c(t)] \right) + K_i (i_L(t) - i_{Lref}). \quad (4.51)$$

Using the relative degree  $r$  of the system:

$$\frac{\partial}{\partial u} \dot{\sigma}(t) = \frac{K_p}{L} \neq 0. \quad (4.52)$$

---

<sup>1</sup>Note that  $e(t, x)$  is denoted as  $e(t)$  to evaluate the function at a specific time. The same convention applies to  $\sigma(t, x)$ .

As a consequence, the dynamical equations of the SPVSI have a relative degree  $r = 1$ , and the Second-Order SMC (SMC-2) is chosen<sup>2</sup>. A simplified model (Fridman and Levant 2002) for Equation 4.43 that is linearly dependent is:

$$u_{SMC-2}(t) = -\lambda|\sigma|^\rho \text{sign}(\sigma) + \int_0^t \dot{u}_1(t), \quad (4.53)$$

where

$$\dot{u}_1(t) = -W \text{sign}(\sigma). \quad (4.54)$$

Compared to other SMC alternatives, one advantage of the super-twisting algorithm is that it does not require knowledge of  $\dot{\sigma}$ , the time derivative of the sliding surface.

This proposal utilizes the DQ reference frame to achieve independent, active power control in the SPVSI. Also, this method is known as the Park transformation and converts the complex time-domain system into a DC equivalent (Xu et al. 2020). As this work focuses on an SPVSI, it is necessary to obtain the orthogonal alpha-beta (AB) reference frame to transform the single-phase signal into its stationary orthogonal values. Subsequently, the stationary reference frame is further transformed into a non-stationary reference frame defined by the D and Q axes.

A first-order low-pass filter is employed twice to achieve a 90-degree phase shift (45° for each stage). This process allows for obtaining the missing orthogonal component with a gain of 2 to compensate for the amplitude attenuation in the beta signals, which is approximately  $\frac{1}{\sqrt{2}}$  at each filtering stage. The low-pass filter is applied to both  $i_L$  and  $v_g$  signals (Gonzales-Zurita, Clairand, and Escrivá-Escrivá 2022).

$$i_{L_a} = \frac{2}{(\tau_S + 1)^2} i_{L_b}, \quad (4.55)$$

$$v_{g_a} = \frac{2}{(\tau_S + 1)^2} v_{g_b}, \quad (4.56)$$

---

<sup>2</sup>The control variable  $u_{HOSMC}$  showed in Equation 4.43 is now defined as  $u_{SMC-2}$

where  $i_{Lb} = i_L$  and  $v_{gb} = v_g$ . The time constant  $\tau$  is set based on the grid's frequency, and  $s$  represents a pole in the frequency domain. The SPVSI equivalent in AB coordinates is presented as follows:

$$u_a(t) = L \frac{di_a(t)}{dt} + Ri_a(t) + v_a(t), \quad (4.57)$$

$$u_b(t) = L \frac{di_b(t)}{dt} + Ri_b(t) + v_b(t). \quad (4.58)$$

After getting the AB components, the DQ components can be calculated as follows:

$$\begin{bmatrix} X_d(t) \\ X_q(t) \end{bmatrix} = T_{DQ} \begin{bmatrix} X_a(t) \\ X_b(t) \end{bmatrix}, \quad (4.59)$$

where  $X$  represents any value of voltage and current of the SPVSI, and  $T_{DQ}$  is given by:

$$T_{DQ} = \begin{bmatrix} \cos \omega t & \sin \omega t \\ -\sin \omega t & \cos \omega t \end{bmatrix}. \quad (4.60)$$

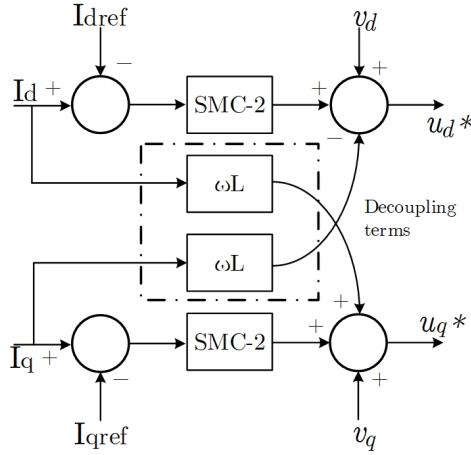
Where the angular velocity  $\omega$  and the time  $t$  produce the rotation angle  $\theta$  ( $\theta = \omega t$ ). The rotation angle is applied to the DQ reference frame to synchronize the SPVSI and grid voltages through an algorithm known as a phase-locked loop (PLL) (Sultani 2013).

The transformation is applied to voltage and current values from the VSI (Sultani 2013). The current controller uses the current of the DQ coordinate frame. These expressions could be expressed as:

$$u_d(t) = L \frac{di_d(t)}{dt} - \omega Li_q(t) + Ri_d(t) + v_d(t), \quad (4.61)$$

$$u_q(t) = L \frac{di_q(t)}{dt} + \omega Li_d(t) + Ri_q(t) + v_q(t). \quad (4.62)$$

The DQ model of the SPVSI presents coupled values that need to be solved to apply a control algorithm. Figure 4.6 shows the controller used to avoid coupled expressions.



**Figure 4.6:** Decoupling model for SPVSI control.

The decoupled expressions are:

$$u_{d^*}(t) = u_{SMC-2}(t) - \omega L i_q(t) + v_d(t), \quad (4.63)$$

$$u_{q^*}(t) = u_{SMC-2}(t) + \omega L i_d(t) + v_q(t). \quad (4.64)$$

These new equivalent expressions are replaced in Equations 4.61 and 4.62.

$$u_{SMC-2}(t) = L \frac{di_d(t)}{dt} + R i_d(t), \quad (4.65)$$

$$u_{SMC-2}(t) = L \frac{di_q(t)}{dt} + R i_q(t). \quad (4.66)$$

As presented in Equation 4.53, the parameter  $\rho = 0.5$  provides maximal realization for SMC-2 (Fridman and Levant 2002). The control law can be re-written as:

$$u_{SMC-2}(t) = -\lambda |\sigma|^{0.5} \text{sign}(\sigma) - \int_0^t W \text{sign}(\sigma). \quad (4.67)$$

Where  $\lambda$  and  $W$  represent the gains on the SMC-2 algorithm, an advantage of the super-twisting method is that it does not need the derivative of the sliding surface  $\dot{s}$  required for other SMC approaches. This control law will be applied to each axis in the DQ reference frame through the variables  $u_{SMC-2d}$  and  $u_{SMC-2q}$ .

#### 4.3.2 New Sliding Surface and Stability through Lyapunov's function

Lyapunov's criteria for dynamical systems stability considers the following candidate function:

$$V^* = \frac{\sigma^2}{2}. \quad (4.68)$$

Then,

$$\dot{V}^* = \sigma \dot{\sigma} < 0. \quad (4.69)$$

This thesis proposes an unconventional (new) sliding surface  $\sigma$  for HOSMC from error signal  $e$  is chosen as a PI function in DQ coordinates. This analysis considers the same control algorithm for both coordinates as follows:

$$\sigma_{d/q} = K_{pd/q} e_{d/q} + K_{id/q} \int_0^t e_{d/q}, \quad (4.70)$$

Therefore, Lyapunov's criterion must be satisfied in the surfaces in D and Q, respectively. Thus, in the  $D$  axis, the following expression is obtained:

$$\sigma_d(K_{pd}\dot{e}_d(t) + K_{id}e_d(t)) < 0, \quad (4.71)$$

where

$$e_d(t) = i_d(t) - i_{dref}, \quad (4.72)$$

And the error derivative is calculated as follows:

$$\dot{e}_d(t) = \dot{i}_d(t) \quad (4.73)$$

Hence, (4.71) changes to:

$$\sigma_d(K_{pd}\dot{i}_d(t) + K_{id}(i_d(t) - i_{dref})) < 0. \quad (4.74)$$

Using (4.61) and taking the values  $u_d$  and  $u_{SMC-2}$  from (4.63) and (4.53), respectively the following expression is obtained:

$$\sigma_d \left( \frac{K_{pd}}{L} (u_{SMC-2d} - Ri_d(t)) + K_{id}(i_d(t) - i_{dref}) \right) < 0, \quad (4.75)$$

$$\begin{aligned} \sigma_d \dot{\sigma}_d = \sigma_d \left[ \frac{K_{pd}}{L} (-\lambda |\sigma_d|^{0.5} \text{sign}(\sigma_d) - \int_0^t W \text{sign}(\sigma_d) - Ri_d(t)) \right. \\ \left. + K_{id}(i_d(t) - i_{dref}) \right] < 0. \end{aligned} \quad (4.76)$$

Due to the fact that  $i_{dref}(t) > i_d(t)$ , from (4.72)  $e(t) < 0$  and therefore  $\int_0^t e(t)dt < 0$  for all  $t > 0$ , then  $\sigma_d < 0$ . This result implies that to show that the inequality (4.76) is true, it is necessary to show that:

$$\frac{K_{pd}}{L} \lambda |\sigma_d|^{0.5} + \frac{K_{pd}}{L} \int_0^t W dt > \frac{K_{pd}}{L} Ri_d(t) - K_{id}(i_d(t) - i_{dref}), \quad (4.77)$$

where the condition  $\text{sign}(\sigma_d) = -1$  is used. Since  $i_{dref}(t) > i(t)$  and  $Ri_d > 0$ , both sides of the previous inequality are positive, and therefore they provide a bound that has to be satisfied  $W$  and  $\lambda$  simultaneously. Thus, for a fixed  $W$ , a  $\lambda$  is obtained, which is bounded from below. The condition (4.77) leads to a constraint that has to be satisfied by  $\lambda$  and  $W$  simultaneously. It provides different scenarios. The right member of the inequality (4.77) is always a positive number; therefore, for a given  $\lambda$ , a bound for  $W$  from below will be obtained and vice versa. Thus, for a given  $\lambda_o < 0$  the value for  $W$  must satisfy

$$\int_0^t W dt > Ri_d(t) - K_{id} \frac{L}{K_{pd}} (i_d(t) - i_{dref}) - \lambda_o |\sigma_d|^{0.5}. \quad (4.78)$$

The right-hand side of (4.78) is a positive number. Therefore,  $W$  must also be a positive number. If  $\lambda_o > 0$  then two options exist, if:

$$Ri_d(t) - K_{id} \frac{L}{K_{pd}} (i_d(t) - i_{dref}) > |\lambda_o| |\sigma_d|^{0.5}, \quad (4.79)$$



then the bound for  $W$  is a positive number, and therefore  $W$  is a positive number. On the other side, if

$$Ri_d(t) - K_{id} \frac{L}{K_{pd}} (i_d(t) - i_{derf}) < |\lambda_o| |\sigma_d|^{0.5}, \quad (4.80)$$

then the bound from below is a negative number; therefore,  $W$  can take negative values. In any case, for big enough positive values of  $\lambda$  and  $W$ , the system will satisfy (4.69) being a stable system according to the Lyapunov criterion.

At this point, the controller has been formulated to regulate active power. The controller is characterized by its determined constants,  $\lambda$  and  $W$ . However, one common challenge in closed-loop controllers is tuning these constants. Typically, this process involves heuristic tuning, where the constants are adjusted based on the individual's system knowledge.

Employing these multi-objective optimization techniques can overcome the limitations of heuristic tuning, leading to a more systematic and robust tuning process. This approach allows for exploring various trade-offs and balancing different control objectives. Ultimately, it improves the controller's performance in regulating power.

This research proposes a multi-objective optimization approach to generate optimal tuning constants for the controller. By considering one or multiple cost functions, the aim is to find the best constants that meet the desired performance criteria. The following sections outline these approaches and present the results obtained from their implementation.

## 4.4 Single Function Optimization Approach

The multi-objective approach encompasses many philosophies and techniques to optimize multiple cost functions simultaneously. One option within this approach is to formulate a single composite cost function incorporating multiple objectives. This offers the advantage of simplifying the algorithmic solution to the problem. This section will outline the strategy for tuning the controller using a single cost function.

The Particle Swarm Optimization (PSO) algorithm is employed as an intelligent search process to identify the optimal point that minimizes an objective function. In our case study, the objective function minimizes the error between the reference value of active power and the actual active power produced by

the SPVSI. PSO operates by utilizing a swarm of multiple particles, which collaborate to minimize the objective function. Initially, a set of  $N$  particles is randomly distributed throughout the solution space. The position of each particle, denoted as  $Xp_i$ , is defined as:

$$Xp_{i(k)} = (xp_{i1(k)}, xp_{i2(k)}, \dots, xp_{iD(k)}). \quad (4.81)$$

Each particle moves with a velocity  $Vp_i$ :

$$Vp_{i(k)} = (vp_{i1(k)}, vp_{i2(k)}, \dots, vp_{iD(k)}). \quad (4.82)$$

The iterative process is performed when each particle in the swarm updates its position and velocity. The movement of each particle in the swarm is affected by its best position, which optimizes the objective function.

$$Xp_{i(k+1)} = Xp_{i(k)} + Vp_{i(k+1)}\Delta t. \quad (4.83)$$

The calculation of a new velocity value is updated in each iteration based on three components: inertia, cognitive and social parameters of the swarm. In each iteration, the position and velocity variables have uniform distribution:

$$Vp_{i(k+1)} = \Omega Vp_{i(k)} + c_1 r_{1(k)} (Xp_{ipbest(k)} - Xp_{i(k)}) + c_2 r_{2(k)} (Xp_{inbest(k)} - Xp_{i(k)}), \quad (4.84)$$

The sample time in the presented equation is  $\Delta t = 1$ .  $Xp_{ipbest(k)}$  represents the previous best position of each particle in the swarm, while  $Xp_{inbest(k)}$  denotes the previous best global position of any particle in the swarm. The learning coefficients,  $c_1$  and  $c_2$ , are constants that govern the influence of personal and global best positions on the particle's velocity update. The variables  $r_{1(k)}$  and  $r_{2(k)}$  are random numbers uniformly distributed between 0 and 1, and  $\Omega$  represents the inertial constant, which typically takes values between 0.1 and 0.9.

The PSO search process can be summarized as follows. Initially, a set of particles is randomly initialized in the search space. Each particle possesses its position and velocity, which are iteratively updated based on its own historical experience and the collective knowledge of the entire swarm.

In each iteration, the particles adjust their velocity and position by considering two key factors: their individual best position (personal best) and the overall best position found by any particle in the swarm (global best). These two values influence the direction and magnitude of each particle's movement.

Throughout the search process, the particles actively explore different regions of the search space, adapting their movement to approach the optimal solution. The algorithm continues iterating until a termination condition is satisfied, such as reaching a maximum number of iterations or achieving a desired level of convergence.

The particle swarm algorithm effectively combines global exploration and local exploitation. The particles can explore new areas of the search space through their velocities while also benefiting from the collective knowledge of the swarm to guide them toward better solutions.

This study utilized the fitness function  $J$  to minimize the tracking error of active power generation in the SPVSI. The calculation of this fitness function is as follows:

$$J = \sum_{k=1}^{i_t} e_k^2 = \sum_{k=1}^{i_t} (P_k - P_{ref})^2. \quad (4.85)$$

The objective function is minimized by considering the square value of the tracking error, denoted as  $e_k$ . This error is calculated as the difference between the active power of the SPVSI, represented by  $P_k$ , and the reference power value, denoted as  $P_{ref}$ . This calculation is performed for each iteration  $k$  within a maximum number of iterations  $i_t$ , while the PSO algorithm updates the position and velocity values of the particles. By using the square value of the error, the algorithm aims to find the optimal tuning constants for SMC-2 by identifying the minimum point of optimization.

The personal and best positions of the particles in the swarm represented a two-dimensional search space for  $\lambda$  and  $W$  as seen in (4.81) to (4.84):

$$Xp_{(k)} = (\lambda_{(k)}, W_{(k)}), \quad (4.86)$$

$$Xp_{best(k)} = (\lambda_{best(k)}, W_{best(k)}). \quad (4.87)$$

The updates in particle positions, denoted as  $Xp_{(k)}$ , lead to the generation of a new best position, which is stored in  $Xp_{best(k)}$  until a better optimization result is achieved. Additionally, calculating a new position involves determining a new velocity value, enabling the algorithm to proceed with its recursive optimization process. This iterative process continues according to the predefined configuration of the PSO parameters, specifying the timing of the updates.

The control algorithm with the tuning process is presented in the following diagram considering the topology and structure of SPVSI (Figure 4.7).

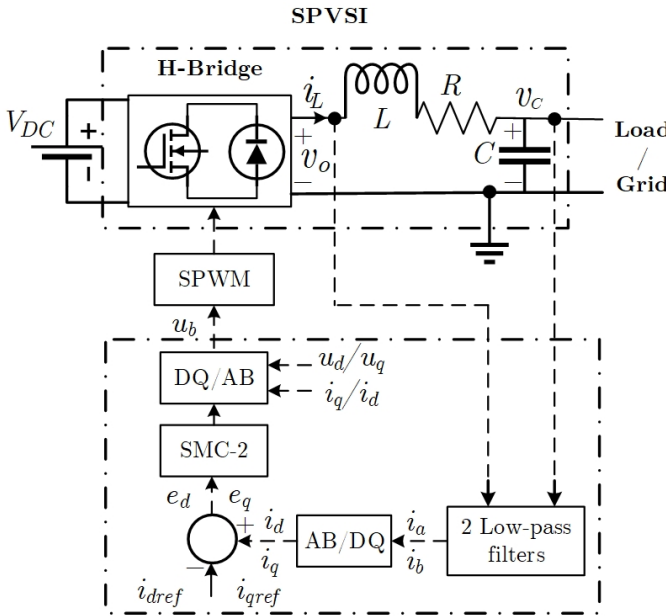


Figure 4.7: SPVSI control scheme.

The measurements considered in the system are the voltage at the output of the filter and the current at the input of the SPVSI filter. These measurements enable the calculation of the power generated by the inverter. These signals are passed through low-pass filters to obtain the orthogonal components required for the AB to DQ coordinate transformation. The resulting values are then fed into the SMC-2, which generates the control signal based on the optimization process of the tuning constants using the PSO algorithm. Subsequently, the control signal is passed through the DQ to AB coordinate transformation block to generate the SPWM modulation signal, which determines the on/off state of the power switches in the SPVSI.

Given that the control of the SPVSI focuses solely on active power, the reference value for the Q axis is set to zero. As previously mentioned, the active power generation is associated with the D axis, while the reactive power is related to the Q axis. This implies that the voltage and current signals from the microgrid should not exhibit a phase difference. The upcoming section will detail the design of the controller based on the HOSMC methodology.

Algorithm 1 outlines the criterion for tuning the SMC-2 during the iteration process carried out by PSO. The objective of the search is to identify the optimal values of  $\lambda$  and  $W$  that effectively tune the SMC-2.

---

**Algorithm 1:** Pseudocode for PSO/SMC-2 tuning.

---

- 1 **Input:** N-particles population;
  - 2 **Output:** Optimal output value;
  - 3 *Initialisation* : position and velocity of each particle for  $\lambda$  and  $W$ ;
  - 4 *LOOP Process*
  - 5 **for** *Fitness value calculation to minimize error tracking ( $J$ ); do*
  - 6 Update personal and global best ( $Xp_{(k)}$  and  $Xp_{best(k)}$ );
  - 7 Meeting stopping criterion;
  - 8 **Return** Optimal output value;
- 

The pseudocode outlines the steps this proposal employs to tune the SMC-2 effectively. The optimization objective is to determine the values of  $\lambda$  and  $W$  that enable the generation of an optimal control law by the SMC-2.

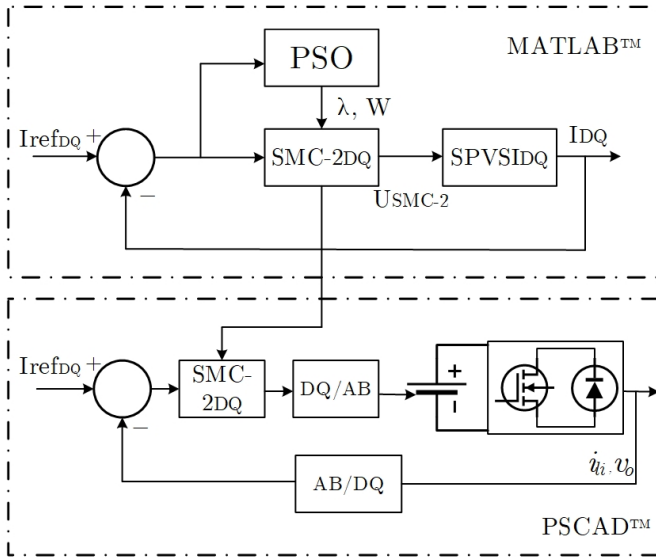
The optimization begins by initializing random values for  $\lambda$  and  $W$ . As the PSO iterations progress, these values are updated iteratively. In each iteration, the particles aim to find their best positions while searching for the best global position. The position and velocity vectors are adjusted during this process, allowing the particles to explore the solution space more effectively.

The optimization process continues until the maximum number of PSO iterations is predetermined before executing the algorithm. At this point, the algorithm terminates, and the final values of  $\lambda$  and  $W$  are obtained, representing the optimized solution for the SMC-2 tuning.

The utilization of the PSO algorithm facilitates an efficient search for the optimal values of  $\lambda$  and  $W$  in the SMC-2 controller. The iterative nature of the algorithm enables continuous refinement of the control parameters, thereby improving the performance of the SMC-2 and enhancing its ability to generate an optimal control law. Incorporating randomized initial values and the

exploration-exploitation balance of the particle swarm contribute to a comprehensive search of the solution space, resulting in improved tuning outcomes.

In this approach, the PSO demands higher computational costs. The SPVSI was modelled in MATLAB<sup>TM</sup>. The simulation of the scenarios was performed in PSCAD<sup>TM</sup> with the tuning values received by MATLAB<sup>TM</sup> as seen in Figure 4.8.



**Figure 4.8:** Scheme for controller's tuning.

In MATLAB<sup>TM</sup>, an offline tuning process is conducted to optimize the controller parameters of the SMC-2 based on the microgrid model. The objective is to find optimal values that enhance performance and stability. The tuning process involves iterative simulations and parameter adjustments until satisfactory results are attained.

Once the tuning process is finalized, the obtained parameters are implemented in the PSCAD<sup>TM</sup> environment, a widely used simulation tool for power system analysis. By integrating the optimized SMC-2 controller into PSCAD<sup>TM</sup>, the microgrid's performance can be assessed under various operating conditions and scenarios.

The offline tuning approach ensures a systematic and efficient optimization of the SMC-2 controller, considering the specific characteristics and dynamics of

the microgrid model. By accurately capturing the microgrid's behavior and fine-tuning the controller parameters, the system can achieve improved control over voltage and current, resulting in enhanced power generation, stability, and overall performance.

Having discussed this optimization approach, the following section presents the multi-objective approach. This methodology considers more than one objective to regulate active power in the inverter from an optimization perspective using more complex algorithms.

## 4.5 Multiple Function Optimization Approach

Multi-objective problems pose a complex challenge that requires careful consideration and effective resolution strategies. One contemporary approach to tackle these problems is by employing diverse cost functions. This method enables the simultaneous optimization of multiple objectives, even when they conflict. The inherent conflict arises from the fact that improving one objective may lead to the deterioration of others, necessitating a delicate balance.

To find a satisfactory solution, it is crucial to identify a negotiation point where multiple objectives can be optimized without causing significant harm to the remaining ones. As a result, multi-objective methods have emerged as viable solutions, providing a logical framework for selecting the most suitable solution that maximizes the benefits of conflicting objectives. These methods are designed to facilitate selecting an optimal trade-off solution that achieves the best compromise among competing objectives. The following proposals outline the principles of the multi-objective approach.

### 4.5.1 Basic definitions of multi-objective problems (MOPs)

#### **Definition 1: Single-objective optimization problems**

Optimizing a single function  $J(x)$  subjected to constraints depends on some conditions. These constraints constitute equality functions such as  $h_i(x) = 0$ ,  $i = \{1, \dots, m\}$  and/or inequality functions such as  $g_j(x) \leq 0$ ,  $j = \{1, \dots, p\}$ . The values of  $x$  belong to some universe  $\Psi$  and represent all possible solutions that satisfy an evaluation of  $J(x)$  and its constraints.

#### **Definition 2: General MOPs**

The approach of MOPs is to optimize simultaneously  $k$  objective functions known as:  $J_1(x), J_2(x), \dots, J_k(x)$  considered in a vector function  $J(x)$ :

$$J(x) = \begin{bmatrix} J_1(x) \\ J_2(x) \\ \vdots \\ J_k(x) \end{bmatrix}. \quad (4.88)$$

### Definition 3: Multi-objective optimization problems

The optimization of MOPs considers the objective function set as  $J(x) = (J_1(x), \dots, J_k(x))$  subjected to a series of constraints. These constraints constitute equality functions such as  $h_i(x) = 0$ ,  $i = \{1, \dots, m\}$  and/or inequality functions such as  $g_j(x) \leq 0$ ,  $j = \{1, \dots, p\}$ . The values of  $x$  belong to some universe  $\Psi$  and represent all possible solutions that satisfy an evaluation of  $J(x)$  and its constraints.

### Definition 4: Pareto optimality

A solution  $x \in \Psi$  is said to be Pareto optimal if and only if there is no  $x' \in \Psi$  for which  $\nu = J(x') = (J_1(x'), \dots, J_k(x'))$  dominates  $\mu = J(x) = (J_1(x), \dots, J_k(x))$ .

### Definition 5: Pareto dominance

A vector  $\mu = (\mu_1, \dots, \mu_k)$  dominates another vector  $\nu = (\nu_1, \dots, \nu_k)$  (denoted by  $\mu \preceq \nu$ ) if and only if  $\mu$  is partially less than  $\nu$ , i.e.,  $\forall i \in \{1, \dots, k\}, \mu_i \leq \nu_i \wedge \exists i \in \{1, \dots, k\} : \mu_i < \nu_i$ .

### Definition 6: Pareto optimal set

The Pareto optimal set for a given MOP  $J(x)$  is defined as:

$$\mathcal{P}^* := \{x \in \Psi \mid \exists x' \in \Psi J(x') \preceq J(x)\}. \quad (4.89)$$

Pareto optimal solutions correspond to a set of solutions that can not improve all variables simultaneously.

### Definition 7: Pareto front

The Pareto front for an optimal set  $\mathcal{P}^*$ , and a given MOP  $J(x)$  is defined as:



$$\mathcal{PF}^* := \{u = J(x) \mid x \in \mathcal{P}^*\}. \quad (4.90)$$

$\mathcal{P}^*$  is a subset of some solution set where its evaluated objective vectors form  $\mathcal{PF}^*$ , of which each is non-dominated concerning all objective vectors produced by evaluating every possible solution in  $\Psi$ .

**Definition 8: True Pareto front**

The true Pareto front  $\mathcal{PF}$  refers to the complete and definitive set of optimal or non-dominated solutions. In practice, it can be difficult or even impossible to know all the optimal solutions due to the complexity of the problems, the limitation of available resources for an exhaustive exploration of all possibilities, and the ideal solutions that still need to be reached in practice.

**Definition 9: Multi-objective global minimum**

Given a function  $J : \Psi \subseteq \mathbb{R}^n \rightarrow \mathbb{R}^k, \Psi \neq \emptyset, k > 2$ , for  $x \in \Psi$  the set  $\mathcal{PF}^* \triangleq J(x_i^*) > (-\infty, \dots, \infty)$  is called the global minimum if and only if:

$$\forall x \in \Omega : J(x_i^*) \preceq J(x). \quad (4.91)$$

Then,  $x_i^*, i = 1, \dots, n$  is the global minimum solution set (i.e.,  $\mathcal{P}^*$ ),  $J$  is the multiple objective function, and the set  $\Psi$  is the feasible region. Determining the global minimum solution set is called the multi-objective global optimization problem.

**4.5.2 Problem formulation**

In this section, the optimization of the SPVSI is described as the MOO approach. The optimization problem is formed through the formulation of the MG, the formulation of cost functions, and the use of the MOO for minimizing both objectives, as seen in Algorithm 2.

The pseudocode shows the optimization process of the SMC-2 that is focused on improving the performance of the SPVSI. Optimization is done through the MOO approach, employing the libraries by (Oldenhuis 2022) developed into MATLAB for MOO. First, the voltage and current values are obtained by integrating the SPVSI and the grid to determine the active power measurement. These values go into first-order filters to obtain their respective orthogonal components. The result of signal filtering establishes an equivalent

---

**Algorithm 2:** Pseudocode for MOO of SPVSI.

---

```
1 Input: Output active power.
2 Output: Optimal values.
3 //Initialization Initial conditions of the SPVSI.
4 Initial tuning parameters of the SMC-2.
5 //Optimization of the performance of the SPVSI
6 for 1 To Max Iterations do
7     MOO optimization for generation of tuning values.
8     for 1 To Population do
9         Testing each member of the solution space.
10        Obtaining the active power value from SPVSI.
11        Applying first-order filters.
12        Obtaining alpha and beta components.
13        Synchronization to the grid through the PLL.
14        Obtaining D and Q components.
15        Determining overshoot and rising time.
16        Calculating the difference between the reference and the measure.
17        Obtaining alpha and beta components.
18        SPWM generation for commutation of power electronic devices.
19        Updating the members of the population.
20    end
21    Updating the calculation of optimum values.
22 end
23 Return optimal values.
```

---

of the single-phase system in the time domain to a system in Alpha and Beta coordinates (AB). Employing a Phase-Locked Loop (PLL), the synchronization angle is calculated. This angle determines the rotation of a new coordinate system according to the grid's frequency. The components are generated in a rotary system DQ by applying the transform from AB to DQ. In this new coordinate system, the measurements of the maximum overshoot and rise time of the current response of the SPVSI are established. These values are also taken as process feedback, which enters the closed-loop control algorithm described by the SMC-2 scheme. The discrepancy between the reference and the feedback is established to calculate the control signal to minimize the difference between the reference and the measurement of the current value. Subsequently, the inverse transformation of DQ coordinates to AB is performed so that the control signal adopts a sinusoidal form. This signal goes into an SPWM modulation block that compares the sinusoidal signal (modulator) with a triangular

signal (carrier). This comparison process results in the generation of pulses for switching the power semiconductors in the SPVSI. The MOO algorithm updates the tuning parameters of the SMC-2 to continue with the iterative optimization process until a response is obtained. An adequate response can improve the proposed control objectives without prioritizing one over the other.

### 4.5.3 Optimization variables

The optimization variables are parameters that change iteratively to achieve the objectives defined in the performance indexes. These variables in the SMC-2 are the parameters  $\lambda$  and  $W$  that lead the controller to perform active power tracking.

### 4.5.4 Cost functions

The cost functions constitute the design objectives to be minimized by the MOO. The objective functions used in this research are the rising time and the maximum overshoot. The mathematical expressions of the performance indexes are described as follows:

$$J_1 = t_{90} - t_{10}, \quad (4.92)$$

$$J_2 = (y_{max} - y_{ref})^2. \quad (4.93)$$

Rise time can be expressed as the interval between the moment the process reaches 10% of its total response and the instant it reaches 90% of said response. The objective function  $J_1$  aims to minimize this difference.

Similarly, overshoot is defined as the difference between the maximum value reached by a process during its transient response ( $y_{max}$ ) and the corresponding steady-state value achieving the reference objective ( $y_{ref}$ ). The objective function  $J_2$  aims to reduce this difference.

#### 4.5.5 Proposed MOO algorithms for IBMG active power control

The algorithms selected to perform the MOO are the Multi-objective genetic algorithm (MOGA), Multi-objective differential evolution (MODE), and Multi-objective artificial sheep algorithm (MOASA). The algorithms selected are handy for research applications. They have been chosen for their effectiveness in works such as (Costa-Carrapico, Raslan, and González 2020). A brief description of the mathematical method used by each chosen MOO method will be explained, recalling that their theoretical description was reviewed in Chapter III.

In addition, MATLAB is used for MOP resolution. Employing the GODLIKE library for MOO (Oldenhuis 2022), the operation of the SPVSI is optimized using the three multi-objective algorithms mentioned above.

Since the three algorithms rely on evolution processes, a pseudocode is presented that describes in a general way the application of these three techniques that will be used to tune the SMC-2, as shown in Algorithm 3, where:

- $N_P$  is the total number of particles in a population.
- $lb$  is the lower bound of search.
- $ub$  is the upper bound of search.
- $G$  is the generation that represents the evolution stage of a population.
- $X_{opt}$  are the optimum particle values from MOO process.
- $J_{opt}$  are the optimum cost function values from MOO process.
- $P_0$  is the initial population.
- $X_n$  represents each member of the initial population from  $1 \leq n \leq N_P$ .
- $P_{parent}$  is the precedent or parent population.
- $J_0$  is the initial set of cost functions.
- $J_{parent}$  is the precedent or parent set of cost functions.
- $P_{child}$  is the consequent or child population.
- $J_{child}$  is the consequent or child set of cost functions.
- $X_{childn}$  represents each member of the child population from  $1 \leq n \leq N_P$ .

**Algorithm 3:** Multi-objective optimization process

---

```

1 Input:  $N_P, lb, ub, G$ .
2 Output:  $X_{opt}, J_{opt}$ .
3 //Initialization
4 //Generation of the initial population from random decision variables in
  the range of  $lb$  to  $ub$ 
5    $P_0 = \{X_1, X_2, X_3, \dots, X_{N_P}\}$ 
6    $P_{parent} \leftarrow P_0$ 
7 //Evaluate initial cost function
8    $J_0 = f(P_0)$ 
9    $J_{parent} \leftarrow J_0$ 
10 for  $i = 1$  To  $G$  do
11   //From  $P_{parent}$ , two decision variables are chosen as parents to
    generate two children's decision variables
12    $P_{child} = \{X_{child1}, X_{child2}, X_{child3}, \dots, X_{childN_P}\}$ 
13   for  $j = 1$  To  $N_P$  do
14     // Calculate the new cost function
15      $J_{child(j)} = f(P_{child(j)})$ 
16     if  $J_{parent(j)} < J_{child(j)}$  then
17        $X_{opt} \leftarrow P_{parent(j)}$ 
18        $J_{opt} \leftarrow J_{parent(j)}$ 
19     end
20     else
21        $X_{opt} \leftarrow P_{child(j)}$ 
22        $J_{opt} \leftarrow J_{child(j)}$ 
23     end
24   end
25    $P_{parent} \leftarrow P_{child}$ 
26    $J_{parent} \leftarrow J_{child}$ 
27 end
28 return  $(X_{opt}, J_{opt})$ 

```

---

The values required in this multi-objective optimization are the number of particles ( $N_P$ ) in the population, the upper ( $ub$ ) and lower ( $lb$ ) search bounds, and the evolutionary generations ( $G$ ).

The process begins by initializing the optimization with randomly generated optimal values in  $P_0$ . Each population member  $X_n$  from  $1 \leq n \leq N_P$  represents one solution to the optimization problem, where  $X_n = [\lambda_n, W_n]^t$ . These values

are evaluated using the corresponding cost functions  $J_1$  and  $J_2$ . The cost functions are evaluated based on the population members through  $J_0 = [J_1, J_2]^t$ .

In each iteration, new population members are generated ( $P_{child}$ ), which generate new values when evaluating the cost functions ( $J_{child}$ ). The algorithm is recursive and executed in two parts. First, it repeats until all population members have been iterated. Then, it continues until the algorithm's iterations determine the number of generations. The initial population  $P_0$  is the parent population, and the new generation is the child population. In each iteration, the child populations become the parent populations, giving way to new child populations through evolution. Once all the iterations are completed, the program delivers the optimal values  $X_{opt}$  and the minimization  $J_{opt}$  functions generated with these values. The optimal values are selected from the Pareto front to determine a final solution to the optimization problem.

The preceding pseudocode describes the optimization process performed by the MOO algorithms of the GODLIKE library for MATLAB. The algorithm requires input arguments such as the maximum number of members in a population, the number of generations, and the minimum and maximum limits. The last parameters bound the values of new members in the search space for each new generation.

Each member's population evaluates the objective in their respective generations to find the best optimization option on the Pareto front. The child generations that replace the members of the parent population are obtained through MOGA, MODE, and MOASA algorithms. If the new generations present a more satisfactory resolution of objectives than their predecessors, these values will be saved as optimal; otherwise, the best values generated by the members of the previous population will be maintained.

The proposals presented in the last sections will be implemented in the microgrid to observe the improvements in active power control. One way to numerically evaluate these algorithms' results is by applying the performance indexes discussed in the following section.

## 4.6 Performance Indexes

This section will present the indexes for evaluating control proposals for active power management in SPVSI systems. These mentioned indices provide numerical results that allow for an objective evaluation of control actions. Firstly, this experiment considered four performance indexes to evaluate each controller's performance. These indexes are known as the Integral of Absolute Error (IAE), the Integral of Square Error (ISE), the Integral of Time and Absolute Error (ITAE), and the Integral of Time and Square Error (ITSE) (Huaman Loayza and Pérez Zuñiga 2019).

The IAE index is calculated by integrating the absolute values of the errors between the system's response and the desired reference over time. It measures the magnitude of errors the control system makes but does not consider their duration.

On the other hand, the ISE index calculates the integral of the squared errors over time. This means that larger errors have a more significant impact on the index. The ISE measures the magnitude and duration of errors but can be sensitive to outliers or transient errors.

The ITAE index considers both the magnitude and duration of errors by weighting them with the absolute time of the error. This means that long-duration errors have a more significant impact on the index. The ITAE is particularly useful for systems where it is essential to minimize transient errors quickly.

Lastly, the ITSE index combines the magnitude and duration of errors by weighting them with the squared time of the error. This gives greater importance to persistent long-term errors, as they are multiplied by the square of time. The ITSE is especially useful when aiming to minimize transient and steady-state errors in the long term.

These indexes provide valuable insights into the system's performance and can be used to identify areas for improvement. The equations of the performance indexes are shown as follows:

$$IAE = \int_0^t |e(t)| dt, \quad (4.94)$$

$$ISE = \int_0^t e(t)^2 dt, \quad (4.95)$$

$$ITAE = \int_0^t t |e(t)| dt, \quad (4.96)$$

$$ITSE = \int_0^t te(t)^2 dt. \quad (4.97)$$

Furthermore, the Inverse Generational Distance (IGD) index assesses multi-objective methods. This index quantifies the distance between the points of the obtained Pareto front and the true Pareto front, aiming to observe the dispersion of points in the search space. In other words, the IGD is a crucial indicator for evaluating the quality of solutions obtained by a MOO algorithm (Lai et al. 2019). It helps researchers and designers identify areas for improving their algorithm's performance. The IGD index is calculated through:

$$IGD = \frac{\sum_{\vartheta \in \mathcal{PF}^*} d(\vartheta, \mathcal{PF})}{|\mathcal{PF}^*|}. \quad (4.98)$$

Where  $\mathcal{PF}$  is the Pareto front obtained so far,  $\mathcal{PF}^*$  is a set of uniformly distributed points on the true-Pareto front,  $|\mathcal{PF}^*|$  stands for the number of agents in the Pareto front, and  $d(\vartheta, \mathcal{PF})$  is the Euclidean distance between the points on the true-Pareto front (ideal and not reachable points) and its closest point in  $\mathcal{PF}^*$ .

## 4.7 Conclusions of the Chapter

This study presents the design of the SMC-2 for a microgrid to enhance the performance of existing industrial SPVSI that utilize a PI regulator. The primary control objective was to regulate active power generation to align with the demand of the load or inject spare active power into the grid.

The SMC-2 utilizes the super-twisting algorithm to effectively prevent chattering without sacrificing algorithm robustness regarding conventional SMC proposals. In addition, a non-conventional sliding surface in a PI form enhanced the controller's accomplishment of objectives.

The PSO algorithm was utilized to determine the optimal parameter values for tuning the SMC-2. These values were calculated using the Lyapunov stability criterion, offering an effective alternative to traditional heuristic tuning methods for SMC controllers. In addition, the use of PSO for tuning the SMC-2



algorithm demonstrates the versatility of this method to adjust the SMC-2 applied to a different circuitry in the SPVSI over other processes that require a more heuristic analysis.

The MOO methods (MOGA, MODE and MOASA) considered conflicting objectives such as rise time and overshoot. The optimization process to enhance the SMC-2 performance will define the best option to improve both objectives without majorly decreasing the results on one of them to manage active power in the microgrid with SPVSI.

The following performance evaluation indexes were described to determine the effectiveness of the SMC-2 under the PSO and MOO tuning: IAE, ISE, ITAE, and ITSE. The indexes will show the different approaches between PSO and MOO methods to determine numerically the effectiveness of the new methodology.



# Case Study: Analysis of an Experimental Inverter-based Microgrid for Active Power Management

### 5.1 Introduction

The previous chapters explored the general aspects of microgrids and their control methods. The main components of microgrids and their function in the system's operation were analyzed in Chapter 2. The inverter, as the primary element for energy management, was examined. Furthermore, valuable information about state-of-the-art control in inverter-based microgrids was obtained in Chapter 3. The objectives and performance indices that evaluate the effectiveness of the controllers were observed.

The Universitat Politècnica de València possesses suitable infrastructure and equipment for energy management research. The university has a fully functional microgrid equipped with necessary components such as photovoltaic

panels, battery banks, charge regulators, inverters, and various loads. Also, the microgrid is equipped with software components that enable data logging and analysis through a SCADA system, allowing the examination of voltage, current, and power values at different stages.

Within this setup, various energy management tests will be conducted in a case study to propose a multi-objective optimization methodology to enhance energy management within the microgrid. By analyzing the technological infrastructure at Universitat Politècnica de València, the fundamental components required for developing a microgrid at the Universidad de Las Américas in Quito, Ecuador, have been identified.

This thesis created a microgrid at Universidad de Las Américas to facilitate future research projects in microgrids. The implemented microgrid includes all the essential elements for its operation, whether connected to the main power grid or operating autonomously. It is also open to incorporating various enhancements to improve its performance and generate future research opportunities in energy generation.

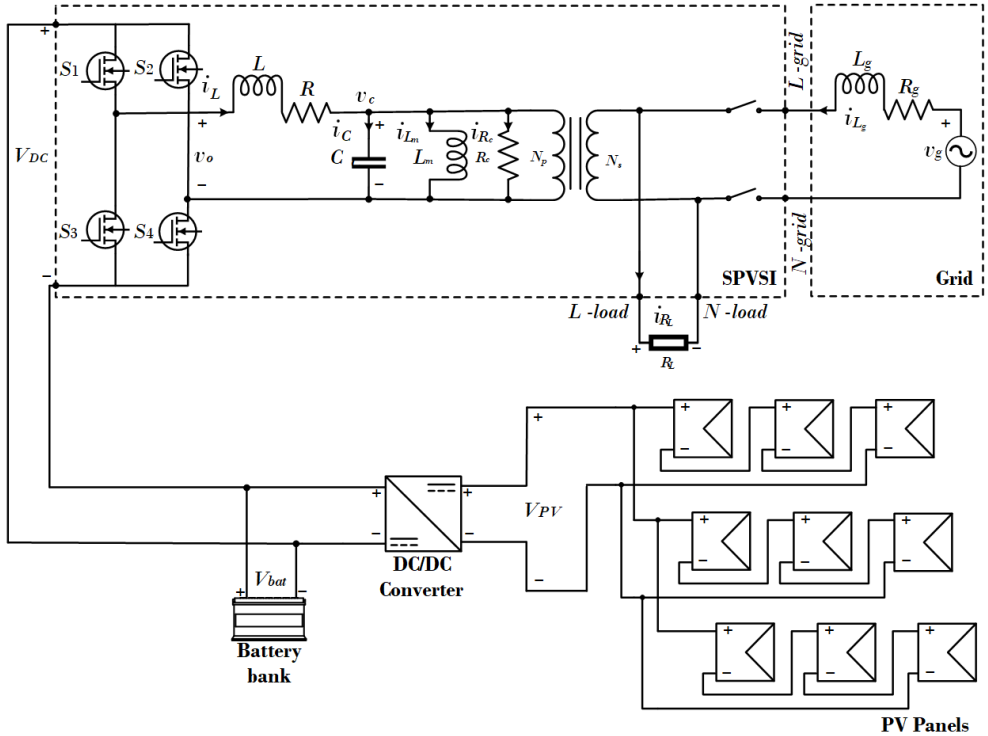
The microgrid sector in Ecuador is gradually growing in both academia and industry. However, most universities in the country need microgrid laboratories, which hinders this area's technological and research potential. The microgrid established at Universidad de Las Américas was designed through user and functionality analysis to promote energy research and strengthen the university's research position in the near future. Undoubtedly, achieving this microgrid is a significant accomplishment, serving as a foundation for future innovation projects in energy management.

Section 5.2 describes an analysis of the inverter-based microgrid at Universitat Politècnica de València, section 5.3 determines the meteorological data needed for experimentation and, section 5.4 shows a proposal for an inverted-based microgrid at Universidad de Las Américas in Ecuador. Finally, section 5.5 concludes the work with some remarks.

## **5.2 Experimental Microgrid at Universitat Politècnica de València**

After having determined the effectiveness of the PSO-tuned SMC-2 control over the traditional PI control, it is proposed to apply this methodology to a microgrid located at the Universitat Politècnica de València. In this system, a set of elements should have been considered in the initial proposal for active

power control for a microgrid. These elements include photovoltaic panels, DC/DC converters, and interface switches in the SPVSI. For this reason, a clear recognition of these elements is carried out, starting with a diagram of the real system of the microgrid, which is shown in Figure 5.1.



**Figure 5.1:** Microgrid system at Universitat Politècnica de València.

It is observed that the inverter acts as an intermediary between the load and the grid. In scenarios where the load needs to be connected only to the grid, the inverter will activate its internal contacts and operate as a bypass, allowing the energy from the source to flow directly to the load. Conversely, depending on the experimental needs, the inverter will operate connected to the grid and/or the load.

A description of the system parameters of Figure 5.1 is presented in Table 5.1:

**Table 5.1:** Parameters of the inverter-based microgrid at Universitat Politècnica de València.

Parameter	Symbol	Value
Output filter		
Capacitor	$C$	$25.97\mu F$
Inductor	$L$	$244\mu H$
Resistor	$R$	$1m\Omega$
Grid		
Frequency	$f$	$50Hz$
Rated RMS voltage	$V_g$	$230V$
Inductor	$L_g$	$4.35mH$
Resistor	$R_g$	$1m\Omega$
SPVSI		
Rated power output	$P_o$	$5.5kW$
Rated output voltage	$v_o$	$230V$
Switching frequency	$f_s$	$20kHz$
Switching signal	$u_s$	Depends on SPWM
Rated DC bus voltage	$V_{DC}$	$44V$
PV panels		
Rated maximum voltage	$V_{PV}$	$132V$
Panel rated maximum current	$I_{PV}$	$9.08A$
Panel rated maximum power	$P_{max}$	$310W$
Number of panels	$n$	$9$
Step-up transformer		
Magnetization inductor	$L_m$	$0.1pu$
Core losses resistor	$R_c$	$0.1pu$
Base apparent power	$S_b$	$2.5kVA$
Base voltage line-line	$VLL_b$	$230V$
Turns ratio	$N = N_s/N_p$	$6.76$
Batteries		
Rated voltage	$V_{bat}$	$48V$
Capacity	$C_{bat}$	$300Ah$
Load		
Rated maximum power	$P_L$	$2kW$
Resistor	$R_L$	Variable

The images of the main components from this microgrid are found in Appendix A. One of the main parameters that must be considered for power generation is incident solar radiation. Currently, global applications allow obtaining ra-

diation data based on the geolocation of a specific location. The following section demonstrates how solar radiation data is obtained for the microgrid at Universitat Politècnica de València.

## 5.3 Meteorological Data

In this section, the steps taken to emulate the microgrid of the Universitat Politècnica de València are summarized. The procedure closely resembles the one conducted in the preceding chapter. However, it incorporates adjustments aimed at effectively managing the active power of the microgrid. These modifications are informed by actual data extracted from the microgrid itself.

### 5.3.1 Model adaptation

Implementing some elements outside the microgrid described in the previous chapter has been considered. These elements are described below.

Electricity generation was reinforced through photovoltaic panels (**PV panels**) along with a battery bank for energy storage. In the previous chapter, energy generation was performed solely through a battery bank connected to the input terminals of the inverter. The solar energy incident on the solar panels was consulted through the data provided by NASA's web page: <https://power.larc.nasa.gov/data-access-viewer/>.

This free and online tool can access various data on climatic variables (such as radiation, temperature, humidity, and wind pressure, among others) in a user-selected location on the planet. To select the desired data, Figures 5.2 and 5.3 describe the main steps, and details about it are summarized as follows:

1. In the search bar at the top of the screen, the location of the site of interest is specified. This research selected the location of the Universitat Politècnica de València.
2. On the left side of the screen, a data configuration menu called **POWER Single Point** appears. The Renewable Energy alternative is selected in the **Choose a User Community** option.
3. In the **Choose a Temporal Average** option, the temporal frequency of the desired data is selected. In this research, the data is **daily**.

- In the **Enter Lat/Lon or Add a Point to Map** option, a cursor is chosen to locate a more specific place at Universitat Politècnica de València can be defined with greater accuracy. This option places a marker dragged by the user to the desired location on the map.
- In the **Select Time Extent** option, select the dates of climatological data. For this purpose, 5-year data from 2017 to 2021 in the fall season (October-December) are considered. The data for the year 2022 is not available on the platform yet. Therefore, the selected time can provide an approximation for validating the radiation data obtained in the laboratory in 2022.
- In the **Select Output File Format** option, the file extension for selected data is chosen. In this case, the CSV option allows the reading and processing of the exported data in Excel.
- In the **Select Parameter** option, the desired data is chosen and displayed by a set of folders. In the **Solar Fluxes and Related** folder, the **All Sky Surface Photosynthetically Active Radiation (PAR) Total** alternative is selected.
- In the **Temperatures** folder, the **Temperature at 2 Meters** alternative is chosen. Finally, these data are generated and exported once the **Submit** option is selected at the end of the POWER Single Point panel.

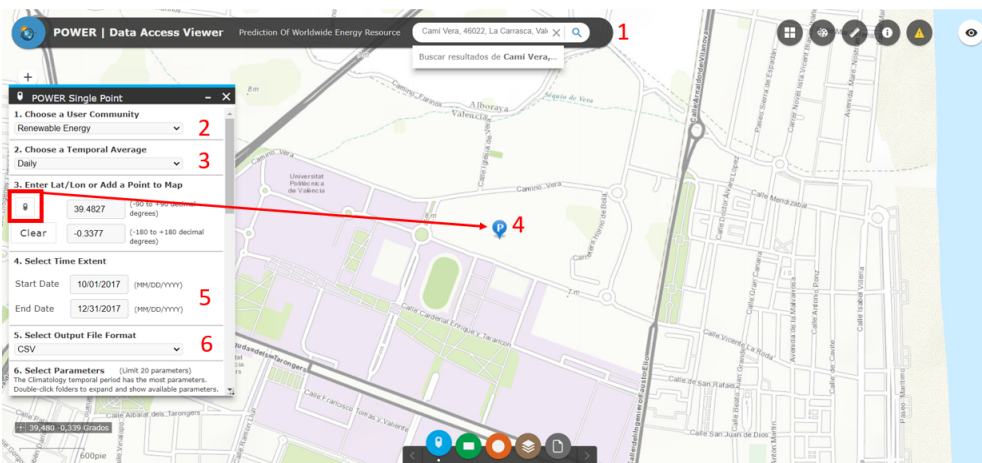


Figure 5.2: Setting the place and time for climatology data.



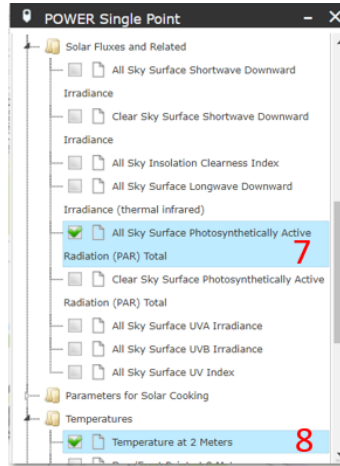


Figure 5.3: Getting the radiation and temperature data.

The data obtained on radiation and temperature exhibit the changes of these variables throughout the fall season in 5 years from 2017 to 2021. The historical values of these variables are depicted in Figures 5.4 and 5.5.

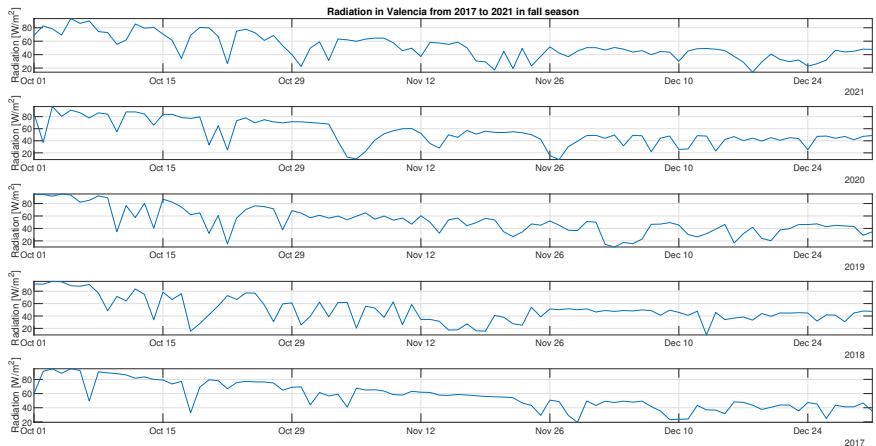
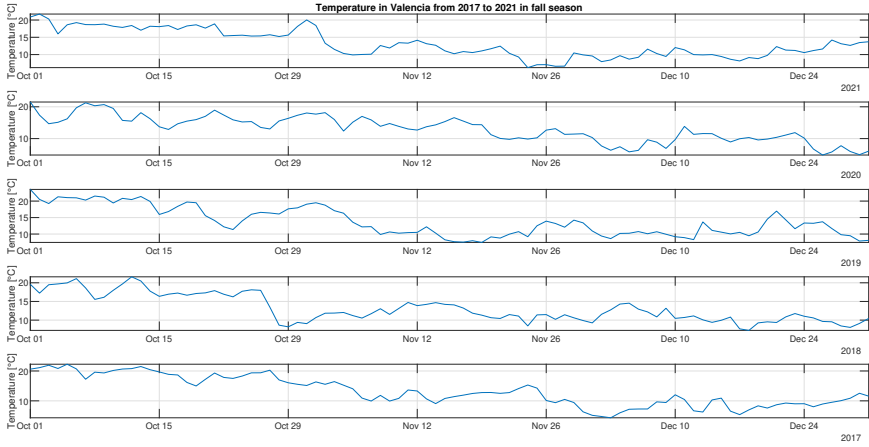


Figure 5.4: Radiation in fall season from 2017 to 2021 in València city.



**Figure 5.5:** Temperature in fall season from 2017 to 2021 in València city.

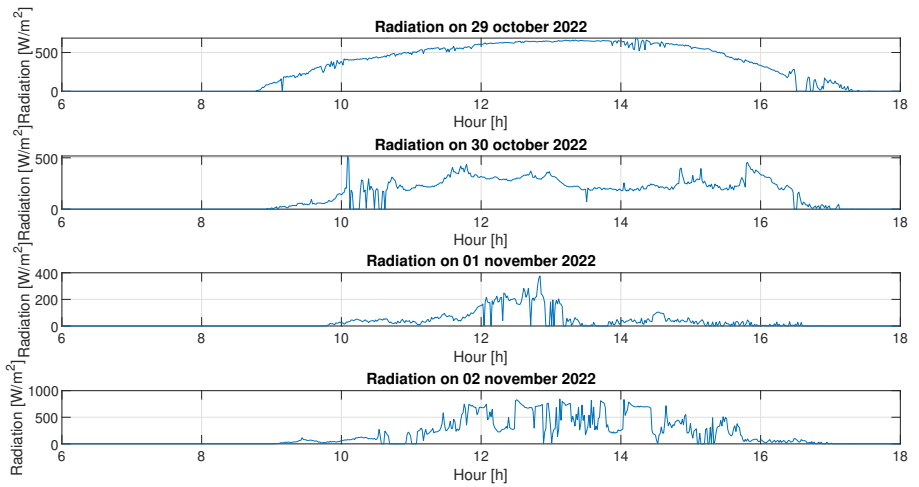
The data obtained on radiation and temperature show changes in these variables throughout the fall season in the mentioned period of 5 years, from 2017 to 2021. The data obtained from NASA’s weather application allow for validation of the radiation data collected in the microgrid at Universitat Politècnica de València. This radiation data was calculated considering the power generation records from the PV panels in the microgrid’s Supervisory Control And Data Acquisition (SCADA). To calculate the incident radiation, the PV panel efficiency ratio in Equation 5.1 is used (Warren 2022):

$$\eta [\%] = \frac{P_{max}}{E \cdot l \cdot w} \cdot 100\%. \quad (5.1)$$

Where  $\eta$  is the efficiency in percentage,  $P_{max}$  is the maximum power per panel in watts ( $W$ ),  $E$  is the incident radiation at  $1000W/m^2$ ,  $l$  is the length of each PV panel in meters ( $m$ ) and  $w$  is the width of each PV panel in meters ( $m$ ). All these parameters are considered for an environmental temperature of  $25^{\circ}C$ . From (ENF Ltd), the electrical and mechanical characteristics are selected, such as  $\eta = 18.23\%$ ,  $l = 1.623m$ , and  $w = 1.04m$ . These values with the electrical power registers from SCADA from the microgrid can calculate the incident radiation changing Equation 5.1 to Equation 5.2.

$$E = \frac{P_{max}}{n\eta [\%] \cdot l \cdot w} \cdot 100\%. \quad (5.2)$$

The value of the number of panels  $n$  has been added to calculate the radiation received by each PV panel from the total solar power recorded in the SCADA system of the microgrid. The calculations graphically display the following radiation values (Figure 5.6).



**Figure 5.6:** Radiation in Valencia from 29 October to 02 November 2022.

Finally, a comparative level of radiation calculated at the Universitat Politècnica de València and measured using the NASA application for result validation has been established. Table 5.2 displays the average per day values for the year 2022 and the maximum average per day in each year from 2017 to 2021.

**Table 5.2:** Radiation data validation

Parameter	Data from oct/nov 2022				Fall season from 5 years				
	Oct-29	Oct-30	Nov-01	Nov-02	2021	2020	2019	2018	2017
Average/day	157.62	70.17	16.41	90.13	93.96	96.66	95.34	95.83	95.02

The data demonstrate a correlation between the calculated and platform-presented data. The only exception was observed on October 29, 2022, a clear day with higher incident radiation than the others, as seen in Figure 5.6.

It is well-known that energy generation from photovoltaic panels is not constant due to different environmental conditions that disrupt direct sunlight radiation on the surface of the PV panels. For instance, cloud cover or the Earth's position relative to the sun minimizes the solar radiation on PV panels producing non-constant energy throughout the day. In this sense, a battery charger is used, which is derived from a DC/DC converter. This device delivers the available energy from the PV panels to the battery bank, which becomes a medium of energy storage. The battery charger searches for the maximum power point (MPP), and maximum power point tracking (MPPT) is performed by an algorithm called perturb and observe (P&O) as seen in Algorithm 4.

---

**Algorithm 4:** P&O process

---

```
1 Input:  $P_{PV}, V_{PV}, p_{PV}, v_{PV}, d$ .
2 Output:  $D$ .
3 //Initialization
4      $dP = P_{PV} - p_{PV}$ 
5      $dV = V_{PV} - v_{PV}$ 
6      $dd = 0.001$ 
7 //Perturb and observe active power generation from PV panels
8 if  $dP > 0$  then
9     if  $dV < 0$  then
10    |  $D = d + dd$ 
11    end
12    else
13    |  $D = d - dd$ 
14    end
15 end
16 else
17    if  $dV < 0$  then
18    |  $D = d + dd$ 
19    end
20    else
21    |  $D = d - dd$ 
22    end
23 end
24 return ( $D$ )
```

---

The main idea of the algorithm is to obtain the maximum power available from converting solar energy into electricity from PV panels. A DC/DC converter processes this electrical energy by increasing or decreasing the duty cycle  $D$  in values of 0.001. If  $D$  increases, the system will be perturbed in one direction of energy flow, verifying that the active power  $P_{PV}$  has increased in value. If this does not happen, the system will be perturbed in the other direction of energy flow by decreasing  $D$ , repeating the process described above until a point is found where the active power  $P_{PV}$  no longer increases and then, the process is reinitialized by increasing  $D$  again.

The microgrid observed at the Universitat Politècnica de València provides the conditions for implementing various experimental proposals. It is undoubtedly a model that deserves to be replicated in other institutions. For this reason, it is proposed to create a microgrid at the Universidad de Las Americas in Ecuador with a structure similar to the one already analyzed, aiming to foster research and innovation projects in microgrids.

## 5.4 Proposal of a Microgrid at Universidad de Las Américas

In this section, the fundamental components of the inverter-based microgrid are sized based on local installation requirements and the purpose of this thesis. After evaluating different conditions, the proper equipment is selected. The following items describe each component analysis.

### 5.4.1 *The House of Quality (HOQ)*

This method considers the technical characteristics in the design process of a final product. The main purpose of this activity is to satisfy end-users' requirements. The HOQ benefits are listed below:

- Creates a product based on the end-user's requirements.
- Reduce the processing time over traditional planning methods.
- Utilize methods of concurring engineering.
- Improves quality establishing priority requirements.

The HOQ employed for the inverted-based microgrid is seen in Appendix B. The HOQ employs The following steps:

- **Step 1: End-user requirements:** The first step considers the main features that will be analyzed before building the testing module. These characteristics look for end-user satisfaction.
- **Step 2: End-user importance:** This parameter uses a scale from 1 to 10 to rate each requirement based on its importance.
- **Step 3: End-user competitive assessment:** The main objective in this step is to compare the different commercial alternatives to the construction of the testing module. In this scenario, some advantages, disadvantages, and opportunities can be found.
- **Step 4: Functional requirements:** This step considers the attributes the test module must contain to determine product specification.
- **Step 5: Direction of improvement:** The features considered in the functional requirements can be analyzed with their technical descriptors.
- **Step 6: Relationship matrix:** This section determines the relationship between the different end-user requirements. The relationship can be strong, moderate, or weak.
- **Step 7: Technical importance rating:** This parameter presents the rating of each element functionality. The element that employs more functions and is most important is the PLC.
- **Step 8: Relative weight:** This parameter presents the percentage of importance of each element in the project with a base value of 100%.
- **Step 9: Correlation matrix:** This feature presents the correlation between the different elements of the final product. The correlations are categorized as positive, negative, and no.
- **Step 10: Technical competitive assessment:** The final step determines the advantages and disadvantages of the proposal in constructing the test module between our proposal and other possible solutions numerically.

Once the main features and elements are identified, the following step is to determine a set of solutions for each component to choose the most suitable solution. This concept is explained in the next section.

### 5.4.2 Morphological chart

A morphological chart is a design method that explores different components that will be included in a final product. This method starts by considering the proper product functionality and alternatives that achieve those features. There is more than one solution for each element that complies with specific functionality. Table 5.3 is presented the morphological chart considering the most suitable solutions to achieve a testing module of an inverter-based microgrid:


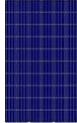





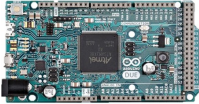


The name's components highlighted in green represent the most suitable solutions for each microgrid component.

Summarizing, the advantages of the chosen components over their counterparts are listed below:

- The efficiency of a monocrystalline PV panel has a typical range between 15% to 21% while the efficiency range in the polycrystalline PV panel considers values between 13% to 16%.
- The charge controller with the MPPT technique offers high efficiency because it employs the maximum power available in PV panels. The PWM charge controller uses the energy available in the operating point of the PV panel based on actual incident solar irradiation.
- The hybrid inverter contains more facilities. Its operations methods include on-grid and off-grid modes. On the other hand, the on-grid inverter only considers the integration with the grid.
- The PLC excels in characteristics over the microcontroller-based hardware. The PLC is more robust against electrical disturbances and is widely employed in industrial applications.
- The energy analyzer represents a complete platform for measuring electrical magnitudes at industrial levels. The voltage and current sensors need an integration interface in the PLC that constitutes more expansion modules.

The following subsections explain the sizing of elements and their main features.

**Table 5.3:** Morphological chart of the inverted-based microgrid

Function	Solutions	
	Option 1	Option 2
Solar generation	 Monocrystalline PV panel	 Polycrystalline PV panel
Charge controller	 PWM	 MPPT
Inverter	 On grid	 Hybrid
Controller	 PLC	 Microcontroller
Feedback	 Voltage and current sensors	 Energy analyzer

### 5.4.3 PV panels

The energy demand determines the number of PV panels in the microgrid. Additionally, important data to be considered are the technical characteristics of the PV panel as well as the nominal voltage of the storage system.



The maximum daily energy consumption ( $E_{max}$ ) calculation considers the load profile connected to the microgrid to obtain the needed number of PV panels  $n$  in the microgrid (Alonso 2022).

$$n = \frac{E_{max} \cdot f_s}{PSH \cdot P_{max}}, \quad (5.3)$$

Where:

- $E_{max}$ : Energy consumed daily.
- $f_s$ : Safety factor (1.3)
- $PSH$ : Peak of Solar Hours determined by the geographical location of the installation.
- $P_{max}$ : Peak power value of PV panels.

Local device supplier introduces 365  $Wp$  24  $V$  monocrystalline PV panels.

$$n = \frac{4000Wh \cdot 1.3}{3.5h \cdot 365W} = 4.07 \text{ PV panels} \approx 4 \text{ PV panels}. \quad (5.4)$$

#### 5.4.4 Batteries

The number of batteries in the installation comes from an arrangement that must meet the energy requirements of the demand. The demand has a high value for a single-phase home. Therefore 48V batteries will be selected. The capacity of the battery bank is given by (Alonso 2022):

$$C_{bat} = \frac{E_{max}}{V_t}. \quad (5.5)$$

Where:

- $E_{max}$ : Maximum demand of energy
- $V_t$ : Terminal voltage of the battery arrangement.

$$C_{bat} = \frac{4000Wh}{48V} = 83.33Ah. \quad (5.6)$$

The battery bank's capacity ( $CB$ ) allows a fixed number of days of autonomy to be obtained. Therefore, considering that the objective is ten days of autonomy in the case of daily energy consumption.

$$CB = \frac{\#Days \cdot C_{bat}}{0.7}. \quad (5.7)$$

Where:

- $CB$ : Capacity of the power bank
- $\#Days$ : Number of days of autonomy (10 days).
- 0.7: Variation of efficiency due to climate conditions.

The capacity of the battery bank is  $CB = 1190.47Ah$ .

#### 5.4.5 Charge controller

The charge controller is a device that regulates the proper charge of the battery bank. This device is essential if you want to have a long battery life. The chosen device is the *Variotrack VT-80* of the *Studer* brand (Figure 5.7). This device has been selected because It achieves peak power values of up to 5  $kWp$ . It can charge the battery bank with a maximum current of 80  $A$ . It can perform charge management and adjust battery parameters directly inside the equipment.



**Figure 5.7:** Variotrack VT-80 (Fadlallah and Benhadji Serradj 2020)

The main functionalities of Variotrack VT-80 are listed below:

- Optimal energy production
- Tracking efficiency: >99%
- Conversion efficiency: >99%
- 4 step charger for longer battery life
- 8 predefined battery charge curves as standard
- Low self-consumption: <1W in night mode
- Protection against incorrect wiring and reverse polarity
- IP54 enclosure protection
- Communication with Xcom-LAN, Xcom-GSM, Xcom-SMS.

#### 5.4.6 Voltage source inverter

This device belongs to the Studer brand as well as the charge controller. The XTM 4000-48 inverter is also a battery charger with multiple features (Figure 5.8). It combines the functions of an inverter, battery charger, transfer system, and source assistance. Once these tasks can be combined, the optimal available energy management is obtained.



**Figure 5.8:** Studer XTM-4000 (Stanev and Nakov 2020)

The programmable auxiliary contacts allow interconnection between the inverter and the present systems to achieve extended functions.

The remote control can adjust all inverter parameters. Software technology is permanently evolving, updating features and adding new functionalities. It is

possible to arrange several units in parallel to increase power generation. Up to nine inverters can be combined in the array to extend power capacity.

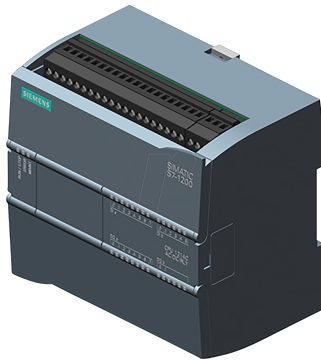
A list of the main functionalities of the Xtender 4000-48 is presented below:

- Battery rated voltage: 48 V
- Input voltage range: 38 - 68 V
- Continuous power at 25C: 3500 VA
- Power up to 30 min. at 25C: 4000 VA
- Power up to 5 sec. at 25C: 10.5 kVA
- Maximum load: Up to short circuit
- Load detection (stand-by): 2 to 25 W
- Peak Yield: 96%
- Consumption OFF/Stand-by/ON: 1.8 W/2.1 W/14 W
- Pure sinusoidal output voltage: 230 V<sub>AC</sub> / optional 120 V<sub>AC</sub>
- Output frequency: 50 Hz / optional 60 Hz
- Overload and short circuit protection
- Automatic disconnection with three restart attempts
- Over temperature protection: Alarm before the cut-off and automatic restart
- 6-stage battery charger: Modifiable with RCC-02 (optional)
- Maximum charging current: 50A
- Temperature compensation: With BTS-01 or BSP 500/1200
- Power Factor Corrector (PFC): EN 61000-3-2
- Input voltage range: 150 to 265 V<sub>AC</sub> / 50 to 140 V<sub>AC</sub>
- Input frequency: 45 - 65 Hz
- Max. input current / max. output current: 50 A / 56 A

- Transfer time (UPS): <15ms
- Multifunctional contacts Module ARM-02 with 2 contacts, optional
- Weight: 22.29g
- Dimensions W x H x L (mm.): 133 x 322 x 466
- Protection index: IP20
- Working temperature range: - 20 to 55 °C
- Operating relative humidity: 95% non-condensing
- Ventilation: Forced from 55 °C
- Acoustic level: <40dB

#### 5.4.7 Programmable Logic Controller (PLC)

The CPU of this PLC allows the automation of simple but very precise tasks (Figure 5.9). This device has integrated digital and analog inputs. Despite its small size, its computational performance is high. The PLC belongs to the Siemens brand, the 1214C AC/DC/RLY model. Its main characteristics are listed below:



**Figure 5.9:** Siemens S7-1200 CPU 1214C AC/DC/RLY (Santos and da Silva 2021)

- Supply voltage: 24 VDC
- Consumption (nominal value): 500 mA, CPU only
- With built-in memory: 100 kByte

- Number of digital inputs: 14
- Number of digital outputs: 10
- Number of analog inputs: 2
- PROFINET interface (open Ethernet standard)
- Supports web servers
- Dimensions: 110 x 100 x 75mm

#### 5.4.8 Energy analyzer

The energy analyzer is a device that measures different parameters in any electrical circuit. The calculation of these parameters is based on measures of voltages and currents. Other measures include active power, reactive power, and total harmonic distortion.

The chosen energy analyzer is the model SENTRON PAC 3220 from SIEMENS (Figure 5.10).



Figure 5.10: Sentron PAC 3220 (Sarmiento Paute 2020).

This device has the following features:

- Basic to advanced metering up to 200 parameters
- Load profile and event logging

- Automation integration
- Basic metering up to 50 parameters
- Digital input  $24 V_{DC} / 0.7 mA$
- Digital Output  $12-24 V_{DC} / 10-27 mA$

#### 5.4.9 Fuses

The calculation of the fuses is the maximum current that can manage the charge controller. Internally this device incorporates a 125A/80V fuse or can have an equivalent of 4 30A/80V fuses. Additionally, fuses have been added to the input of the energy meters and the control circuit. In the first case, the position of the fuses is recommended by the manufacturer's manual at a value of 1A/250V for very low-voltage devices. In the case of the control circuit, the value of the fuse is also 1A/250V considering the consumption of the powered devices such as the PLC and the industrial switch.

#### 5.4.10 Thermomagnetic switches

These protections take into account overcurrent values that can occur in a circuit. The maximum power criterion is utilized to calculate the current value of the thermomagnetic switch. The inverter can be overloaded in a short period, up to 4000W.

$$P = V \cdot I, \quad (5.8)$$

$$4000W = 120V \cdot I, \quad (5.9)$$

$$I = 33.33A. \quad (5.10)$$

Where  $P$  is the active power,  $V$  is the voltage, and  $I$  is the current, all parameters are based on the load characteristics. The current of the protection device ( $I_{th}$ ) must be sized with 140% of the calculated value:

$$I_{th} = 1.4 \cdot 33.33A = 46.66A. \quad (5.11)$$

Therefore, the thermomagnetic switch with a maximum current capacity of 50A is chosen.

### 5.4.11 Communication System

The microgrid should handle different tasks to establish a closed-loop control. All elements involved in this module have a specific function for the operating state of the microgrid, as seen in the flow diagram of Figure 5.11.

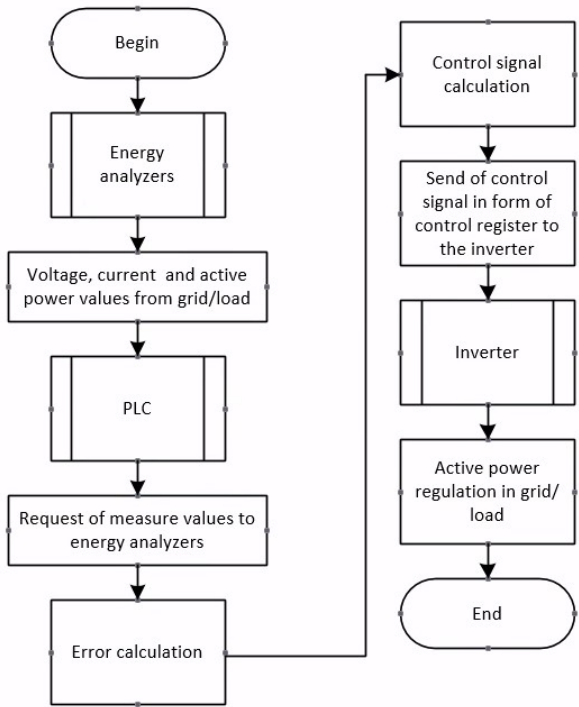
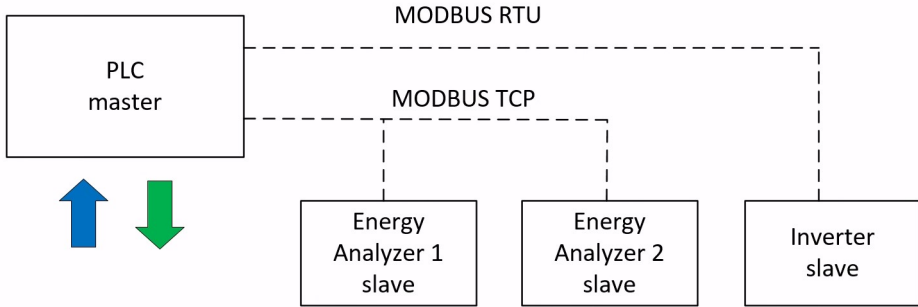


Figure 5.11: Flow diagram of the closed-loop regulation.

There are some differences in the communication protocols of the energy analyzers and the inverter. Both of them use MODBUS. Nevertheless, the energy analyzers apply MODBUS/TCP, and the inverter uses the MODBUS RTU module. This drawback can be solved by programming adequately each protocol with the architecture presented in Figure 5.12:





**Figure 5.12:** Flow diagram of the closed-loop regulation.

The energy analyzers communicate using the MODBUS TCP protocol. For connecting the slave device, which is the inverter in this case, MODBUS RTU communication is employed. However, the selected PLC for this project lacks a built-in communication port for the MODBUS RTU protocol. Hence, it is necessary to integrate an expansion module that supports the mentioned protocol to establish the connection.

#### 5.4.12 Justification of the implemented topology

The diagram of the final product that represents the implementation of the inverter-based microgrid is seen in Figure 5.13.

The different reasons for achieving this final product are explained as follows:

The primary purpose for sizing and implementing the inverter-based microgrid is to create an experimental plant for testing advanced control techniques. Most renewable applications contain some challenges related to energy management to be approached by advanced control techniques.

The microgrid module contains the necessary elements to conduct tests to regulate active power management. The different parts constitute a closed-loop system, such as the feedback signals through energy analyzers, the controllers through the PLC, and actuators through the inverter. The implemented microgrid is seen in Appendix C.

Although Quito (the capital of Ecuador) is in a privileged geographical position to receive solar radiation, its climatic variability represents a challenge for microgrids. There are days when the change from a clear sky to a rainy sky

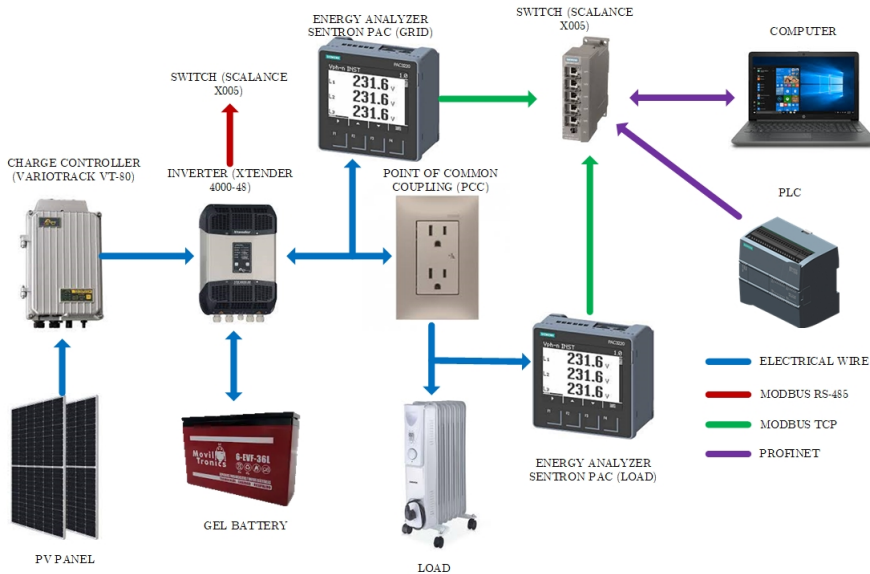


Figure 5.13: Implemented topology of an inverter-based microgrid

originates in a few hours. These events represent less energy that batteries can store in PV installations.

Multi-objective control on inverter-based microgrids represents a novel strategy that prioritizes the balance between different variables on the inverter. In control systems theory, the objective seeks to improve the response of a system to a given reference. For this reason, one or more aspects must be sacrificed to achieve one objective, such as the settling time, overshoot, and steady-state error, among others. Another solution is using complex algorithms that can cover several needs or objectives of the system but represent a challenge for microcontrollers because the processing time increases dramatically and affects the speed response of the control system.

In this sense, inverter manufacturers can analyze an alternative for the control schemes implemented in their converters' chips. In this way, the efficiency of energy production in systems connected to the electricity grid can be improved. Microgrids can offer better performance which improves the market of these systems.

For forthcoming projects in renewable energy in Ecuador, the grid can benefit from the contribution of energy from different microgrids. Ecuador is a coun-

try that depends primarily on hydroelectric production and fossil fuels. This country seeks to reduce oil consumption and its derivatives by promoting electricity production from non-contaminant sources. In this context, the massive implementation of microgrids based on proper regulation parameters is needed to manage energy production efficiently.

## **5.5 Conclusions of the Chapter**

In this chapter, the different components of the experimental microgrid were analyzed. Essential elements were observed, such as the nominal operating values of the photovoltaic panels, battery bank, charge controller, and inverter. The controller considered These parameters for effective management of closed-loop active power. The analysis also involved examining meteorological data to obtain incident radiation using power measurements recorded in the microgrid's database.

Furthermore, a microgrid proposal was developed and implemented for the Universidad de Las Américas, drawing inspiration from the microgrid in Valencia. This implementation explores potential research applications for renewable energy projects in Ecuador. By studying the Valencia microgrid and its successful utilization, valuable insights were gained for the design and operation of the microgrid in Ecuador. The implemented microgrid at the Universidad de Las Américas is a valuable learning tool and provides opportunities for research and development in the field of renewable energies.

The analysis of the microgrid's components, consideration of operational parameters, utilization of meteorological data, and the implementation of the microgrid at the Universidad de Las Américas collectively contribute to the advancement of research and application of renewable energy systems.



# Results of Multi-objective Approach for Active Power Management on Microgrids

### 6.1 Introduction

This chapter presents the results obtained in the active power management of the microgrid using the different multi-objective proposed algorithms. The process begins by constructing a simulation scheme of the microgrid using PSCAD<sup>TM</sup>. An optimization approach employing multi-objective algorithms is then performed using MATLAB<sup>TM</sup>. Experimental data from the Universitat Politècnica de València microgrid is utilized to generate a control algorithm tailored to the specific needs of this microgrid. Once a model is developed that enhances the performance of an industrial inverter, various operating scenarios are considered where the inverter, grid, and load exhibit differences in energy absorption or generation within the microgrid.

Subsequently, criteria are established for evaluating the new control proposals over the microgrid using the multi-objective algorithms selected in the previous chapter. Throughout this chapter's development, the controllers' performance

is evaluated using performance indexes that numerically demonstrate the value of the newly implemented control proposals.

Each stage of this chapter's development involves assessing the controllers' performance and utilizing performance indexes that quantitatively illustrate the effectiveness of the implemented control strategies. The results provide valuable insights into the capabilities and improvements achieved by applying the proposed algorithms in the microgrid.

The rest of the chapter is structured in the following manner: Section 6.2 provides detailed results of the SMC-2+PSO method applied to the SPVSI. 6.3 focuses on the analysis and results of the proposal of SMC-2+PSO to improve the experimental plant. In section 6.4, the SMC-2 results proposed by the multi-objective optimization proposal are shown. Lastly, Section 6.5 emphasizes the key conclusions and contributions of the chapter.

## 6.2 Simulation Proposal Under SMC-2 + PSO Method

In this section, the detailed results are presented from a simulated model that approximates the conditions of the experimental microgrid. This initial step was taken to establish the fundamental criteria for the microgrid configuration through simulation. As described in the following sections, these proposals were implemented in PSCAD<sup>TM</sup> and MATLAB<sup>TM</sup> environments.

Furthermore, the active power transfer ramps required by the IEEE Std 1547-2018 standard for connecting microgrids to the grid were generated. The proposed control model generated active power ramps. Also, the reference tracking for different load conditions is presented. Finally, different analyses determine the effectiveness of the new control proposals over the common and traditional regulation method known as PI (Serban 2011).

### 6.2.1 Active power transfer between SPVSI and the grid

The first step in this section is to determine the parameter values of the PSO algorithm used for the optimal tuning of the SMC-2. Several tests were performed, resulting in multiple outcomes. These outcomes were compared to identify a single configuration that produces precise results for active power tracking.

The PSO algorithm was fine-tuned by several trial-and-error actions to achieve a functional response based on the following parameters, as illustrated in Table 6.1:

**Table 6.1:** PSO scenario for tuning the control method.

Parameter	Value
Population	10
No. of iterations	50
$c_1 = c_2$	2
$\Omega$	1

The final parameters found by the tuning algorithm are presented in Table 6.2:

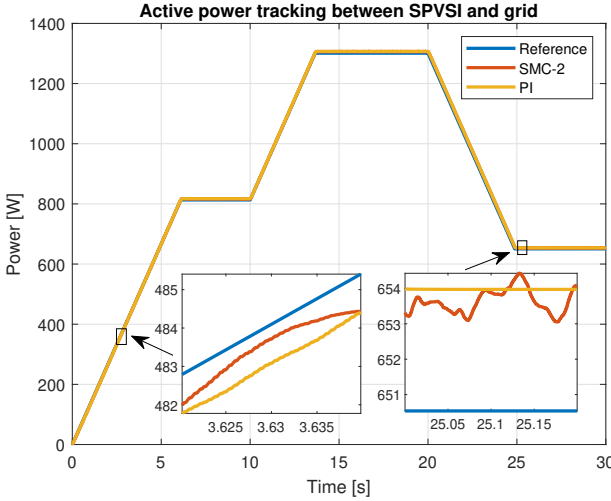
**Table 6.2:** SMC-2 tuning based in PSO.

SMC-2 parameters	Value
$K_{pd} = K_{pq}$	10
$K_{id} = K_{iq}$	100
$\lambda$	-98
$W$	8

The non-conventional PI sliding surface is designed with an integral constant value ten times greater than the proportional constant value to prioritize dynamical tracking. This configuration prioritizes the convergence of variables to the sliding surface. Furthermore, based on the results obtained from the PSO optimization process, the constant  $W$  is set to a higher value than the constant  $\lambda$ . This choice aligns with the Lyapunov criterion discussed earlier, ensuring the stability of the SPVSI during its interaction with the microgrid.

By the regulations outlined in (Rosewater et al. 2016), the active power transfer between the SPVSI and the grid must adhere to specific requirements. In this standard, the ramp rate is 20% per minute of the maximum available active power. To determine the magnitude of the active power ramp, the following procedure is performed: the battery bank voltage and capacity are respectively set as  $V_{bat} = 400V$  and  $C_{bat} = 100Ah$ . The available active power is  $P_{tot} = 40000W = 40kW$ . Therefore, the rate of the active ramp can be defined as:

$$r_r = 0.2P_{tot} \frac{W}{min} = 8000 \frac{W}{min} = 133.33 \frac{W}{s}. \quad (6.1)$$



**Figure 6.1:** Active power rate tracking.

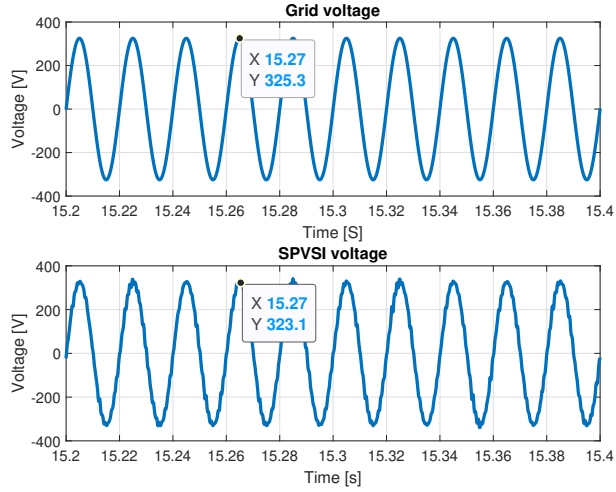
In Figure 6.1, two sections have been zoomed in to analyze and compare the response of the PI controller and the SMC-2 controller tuned by PSO. It is observed that the SMC-2 controller, after tuning, demonstrates superior performance in achieving the ramp reference compared to the PI controller tuned with values of  $k_p = 50$  and  $k_i = 6.67$  obtained as the best response from trial-and-error approach.

The SMC-2 controller closely tracks the reference ramp in the first zoomed-in section, exhibiting a tighter and more accurate response. The SMC-2 controller displays a closer approach to the constant reference signal in the second zoomed-in section, resulting in a reduced error value. It is worth noting that the ramp rate is specified in watts per second, representing the rate at which energy is produced or received by the SPVSI.

The grid and the SPVSI voltages are shown in Figure 6.2.

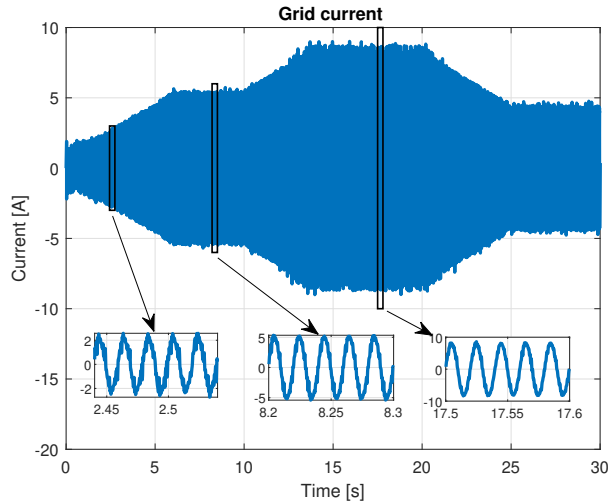
Both signals in Figure 6.2 exhibit synchronized magnitudes and frequencies, facilitating active power exchange. The peak voltage value is approximately 325 V, while the frequency is 50 Hz for both signals. This synchronization ensures a smooth and coordinated power flow between the grid and the SPVSI.





**Figure 6.2:** Grid and SPVSI voltages in the time domain.

Figure 6.3 visually represents the current flowing between the grid and the SPVSI.

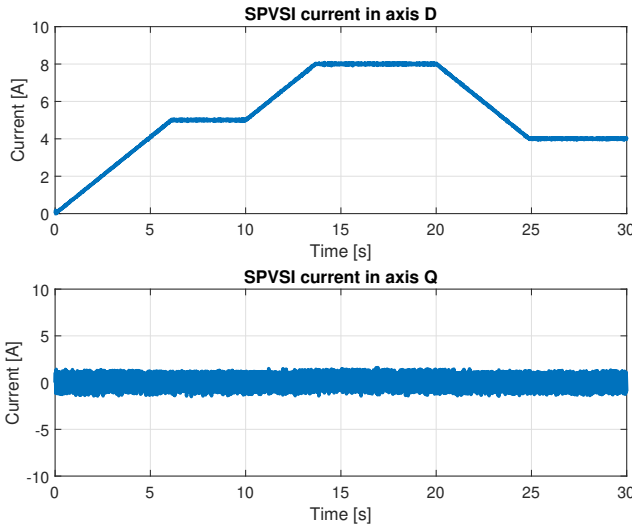


**Figure 6.3:** Grid current in the time domain.

The current values between the grid and the SPVSI are identical in magnitude. However, there is a difference in the current direction: the current flowing from the SPVSI is positive, while the current flowing from the grid is negative. This is illustrated in Figure 6.3.

Three specific segments are selected in Figure 6.3 to highlight the current variations over time. These segments correspond to moments when the ramp rate for active power transfer reaches values of  $2A$ ,  $5A$ , and  $8A$ . By examining these segments, we can observe the changes in current about the ramp rate.

Since a stationary reference frame is used, the D and Q components of the grid currents are presented in Figure 6.4.

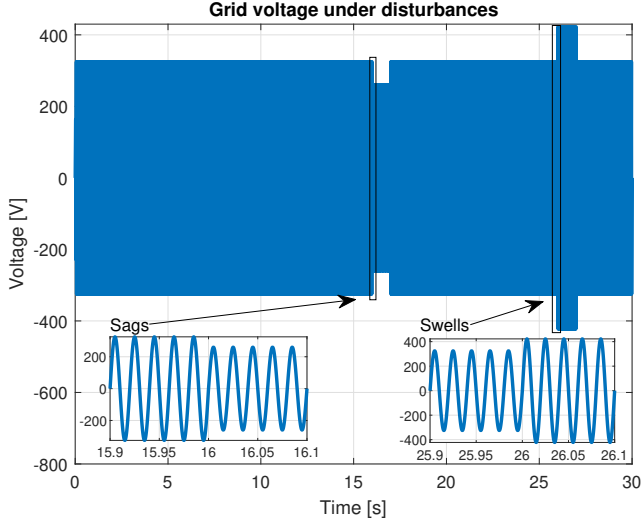


**Figure 6.4:** SPVSI currents in axes D and Q.

The current in the D axis exhibits changes in response to the ramp rate reference, while the mean value of the current in the Q axis converges to zero with slight oscillations around this point. The SPVSI maintains stable current values of  $5A$ ,  $8A$ , and  $4A$ , ensuring the trade-off of active power without generating reactive power.

To evaluate the robustness of the control proposal, a scenario is introduced to test its performance in the presence of external disturbances. The following disturbances are considered in this test:

- Overcurrent in the grid of 23 A at 3 s.
- Voltage sags in the grid of 20% of  $V_g$  between 16 to 17 s.
- Voltage swells in the grid of 30% of  $V_g$  between 26 to 27 s.



**Figure 6.5:** Scenario of sag and swell disturbances on the grid.

Figure 6.5 shows the sag and swell disturbances on the grid. This phenomenon can be observed in the power and current figures shown below in the overcurrent case.

In Figure 6.6, the impact of disturbances on the power transfer process between the grid and the SPVSI is depicted. In section A, at 3 seconds, the SMC-2 achieves a power peak of approximately 2 kW, whereas the PI controller exhibits a value of 2.194 kW.

In section B, at 16 seconds, the SMC-2 demonstrates a lower tracking error than the PI controller during voltage sag. Similarly, in section C, at 17 seconds, the SMC-2 outperforms the PI controller in mitigating the effects of voltage swells.

In Figure 6.7, the response of the current on the D axis to external disturbances is depicted. This particular parameter was chosen as it directly relates to active power generation. In section A, at time  $t=3$  seconds, it is evident that an overcurrent disturbance has a more pronounced effect on the PI controller,

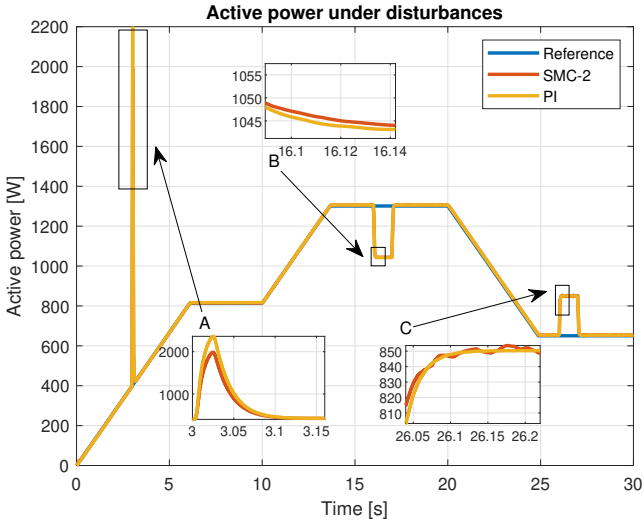


Figure 6.6: Scenario of active power tracking with disturbances.

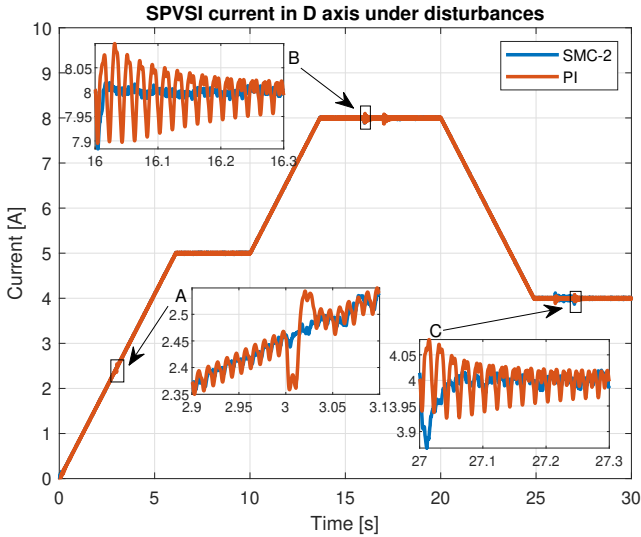


Figure 6.7: Scenario of active power response against disturbances in axis D.

resulting in a more significant current distortion. On the other hand, the SMC-2 exhibits a more robust response with less distortion in the current.

Sections B and C, occurring at times  $t = 16$  seconds and  $t = 27$  seconds, respectively, demonstrate the response of the controllers to voltage sag and swell disturbances. In both cases, the PI controller exhibits oscillatory behavior and takes longer to recover to the reference than the SMC-2. The SMC-2, on the other hand, showcases greater resilience to disturbances, maintaining stability without sustained oscillations.

To further evaluate the performance of each controller, a load is introduced between the SPVSI and the grid, as shown in Figure 4.2. The figures depict the reference value represented by the load derived from a load profile of a low-voltage consumption household. The load data correspond to various home appliances, including a fridge, induction cooktop, and heater, as illustrated in Figure 6.8.

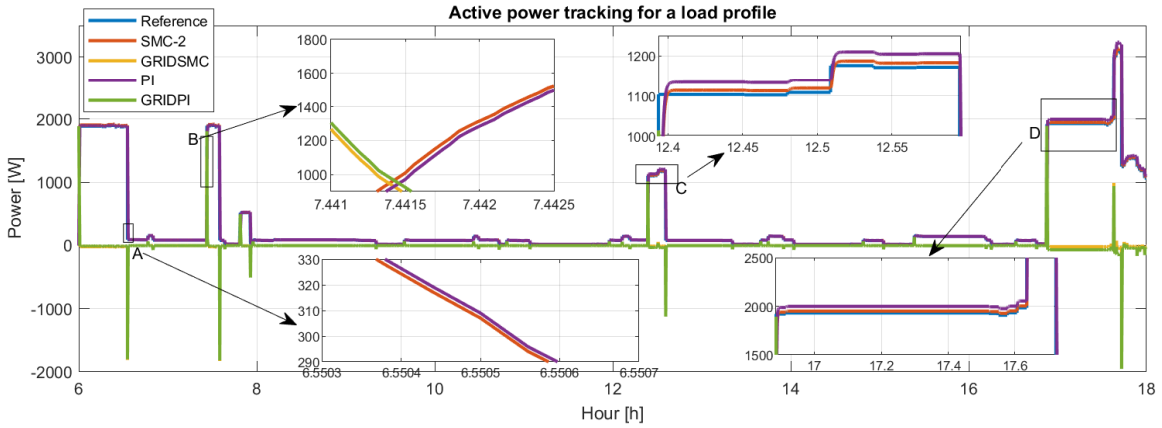


Figure 6.8: Load profile tracking.

The performance of the SPVSI system is analyzed over 12 hours, specifically from 6:00 to 18:00 hours. Four close-up sections (A, B, C, and D) have been examined in the simulation to assess the system's behavior under different conditions.

In close-ups A and B, the response of the SMC-2 controller is observed to be faster than that of the PI controller when there are changes in the reference due to load connections or disconnections. The rising time  $t_r$  is used as a parameter to evaluate the speed of response. It measures the time taken for the output response to start from 10% and reach 90% of its final value. For close-ups A and B, the SMC-2 controller achieves  $t_r = 0.003508h$  and  $t_r = 0.003188h$ , respectively, while the PI controller achieves  $t_r = 0.003512h$  and  $t_r = 0.003196h$ , respectively.

In close-ups C and D, the SMC-2 controller demonstrates lower steady-state errors in dynamic tracking than the PI controller. The relative error  $e_r$  is used to evaluate the steady-state error, quantifying the controller response deviation from the reference and measurement values in percentage.

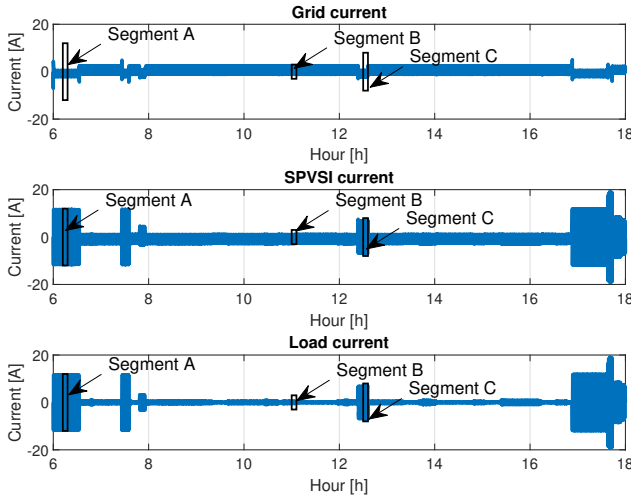
$$e_r = \frac{|reference - measurement|}{reference} \cdot 100\% \quad (6.2)$$

For close-ups C and D, the SMC-2 controller achieves  $e_r = 0.99\%$  and  $e_r = 0.93\%$ , respectively, while the PI controller achieves  $e_r = 2.81\%$  and  $e_r = 3.47\%$ , respectively.

In this scenario, the voltages of the grid, SPVSI, and load exhibit synchronized magnitudes and frequencies to facilitate the trade-off of active power. As depicted in Figure 6.2, these signals reach peak values of  $325V$  and a frequency of  $50Hz$  due to their synchronized operation. The SPVSI generates output signals in accordance with the load demands, ensuring efficient power delivery.

Figure 6.9 illustrates the currents flowing through the grid, SPVSI, and load. These currents are crucial components in the power transfer process. The grid current represents the power exchange with the external grid, the SPVSI current reflects the energy generation/consumption from the PV panels, and the load current signifies the power consumption of the connected devices. Together, these currents play a vital role in maintaining balance and stability within the system.

The current values from the SPVSI exhibit variations based on the load requirements. The SPVSI dynamically adjusts its output current to meet the



**Figure 6.9:** Grid, SPVSI, and load currents in the time domain.

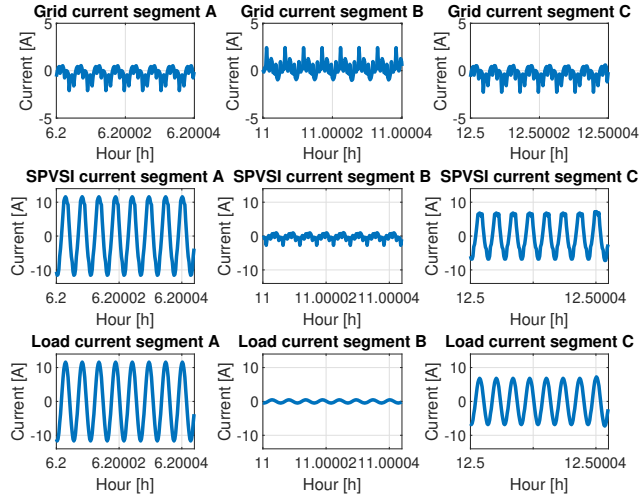
load’s demand, effectively reducing the need for current supply from the grid. To examine this behavior more closely, three close-ups (A, B, and C) have been selected at specific time intervals, representing the currents flowing through the grid, SPVSI, and load, as shown in Figure 6.10.

In these close-ups, the segments highlight the generation of current values corresponding to the load demands. Segment A demonstrates a current generation of 11A by the SPVSI, indicating a high load demand that requires a significant power supply. Segment B represents a lower load demand, resulting in a reduced current value of approximately 0.5A from the SPVSI. Finally, segment C illustrates the SPVSI generating a current of approximately 8A in response to moderate load requirements.

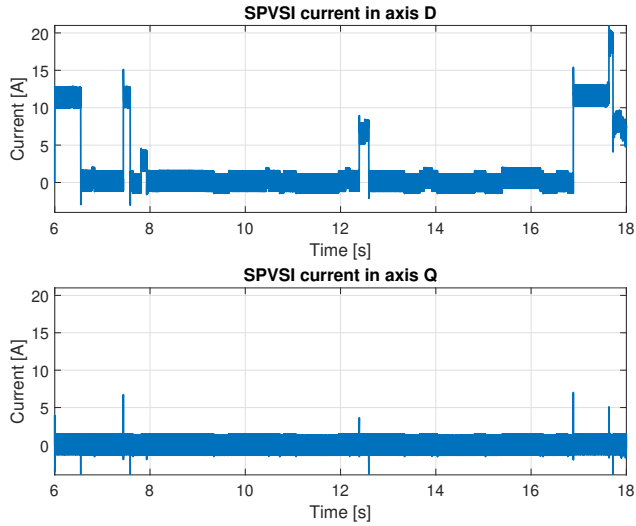
Figure 6.11 shows the D and Q currents from the grid.

The current flowing through axis D responds to the load demand, adjusting its value accordingly. Meanwhile, the current in the Q axis exhibits minor oscillations around a mean value of zero, ensuring the trade-off of active power without generating reactive power. The maximum current consumption reaches 20A. These characteristics highlight the effectiveness of the controllers in maintaining active power generation while minimizing deviations in reactive power.





**Figure 6.10:** Grid, SPVSI, and load current segments in the time domain.



**Figure 6.11:** SPVSI currents in axes D and Q with load demand.

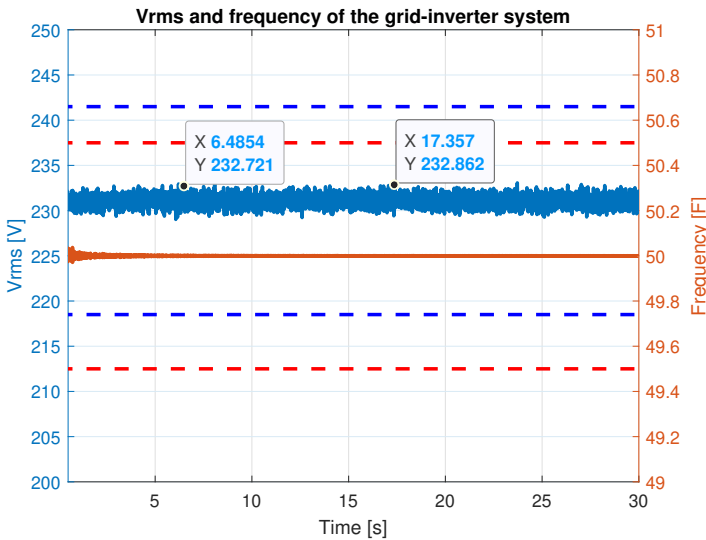
Table 6.3 presents the calculated indexes IAE (Integral of Absolute Error) and ISE (Integral of Squared Error) for evaluating the performance of the PI and

SMC-2 controllers. These indexes are computed using the equations outlined in Chapter 4, allowing for a comprehensive assessment of the controllers’ effectiveness in achieving desired power transfer values.

**Table 6.3:** Performance comparison between SMC-2 and PI.

Scenario	SMC-2		PI	
	IAE	ISE	IAE	ISE
Active power ramp rates	0.1143	0.6182	0.1236	0.7109
Load consumption	1.2149	575.4860	1.5474	616.3820
Disturbances	0.6031	161.7740	0.6264	193.5810

The IEEE Std 1547-2018 standard sets specific requirements for inverter-based microgrids, including voltage range specifications. The system described in this work belongs to Category A, specifically addressing reactive power capability and voltage regulation. The proposed design meets the minimum performance capabilities required for electric power systems, especially in scenarios with limited distributed generation (DG), by adhering to the standard (Enayati 2019). Refer to Figure 6.12 for a visual representation of the system’s compliance with the standard.



**Figure 6.12:**  $V_{rms}$  voltage and frequency on the grid for SMC-2 controller.

The root-mean-square voltage ( $V_{rms}$ ) value is required to not surpass values between  $0.95V_N$  to  $1.05V_N$ , where  $V_N$  represents the nominal value of 230V. The results depicted in Figure 6.8 demonstrate effective control of the voltage generated by the SPVSI, as the values remain within the acceptable limits defined by the IEEE Std 1547-2018. The maximum value reached is 232.9V, indicating compliance with the standard's requirements.

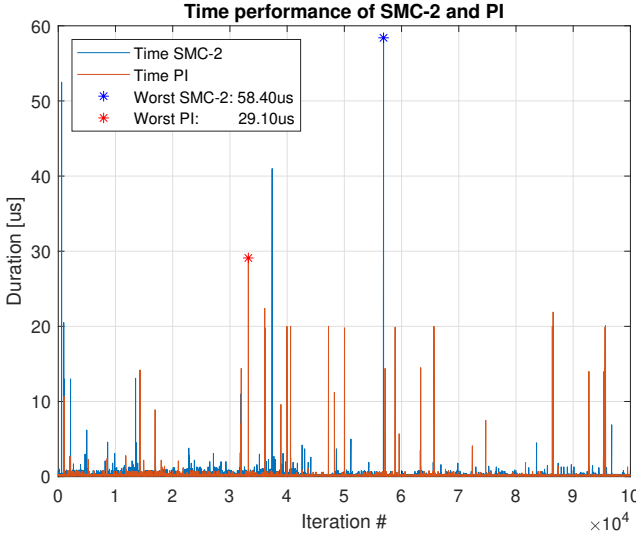
Regarding abnormal performance categories, the IEEE Std 1547-2018 categorizes the system as Category I, applicable to installations involving minimal bulk power systems. This classification ensures reliable operation for all commonly used distributed resources (Enayati 2019).

The acceptable deviation limits for the frequency operation of IBMGs are defined as  $\pm 0.5 Hz$ . The DQ algorithm successfully synchronizes with the grid frequency in less than 1 second, as demonstrated in Figure 6.12. Despite ramp active power references, the SPVSI maintains a stable frequency of 50 Hz. The slight variations observed in the frequency do not lead the MG to instability. These oscillations are dependent on the synchronization of the DQ reference frame.

In addition, this study also includes measuring the time required for the algorithm to calculate its control law. This time measurement approaches two key points: the error signal generation (the starting point) and the control signal generation, which passes through the inverse DQ to AB coordinate transformation (the endpoint). Figure 6.13 presents the time measurements of calculating the control law for tracking active power ramps.

The results depicted in Figure 6.13 reveal no significant differences in the time required by each algorithm to generate the control signal. The average calculation time for the PI algorithm is  $0.18\mu s$ , while for the SMC-2 algorithm, it is  $0.27\mu s$ , resulting in a ratio of 0.68:1. The maximum time taken by the PI algorithm to calculate the control law is  $29.10\mu s$ , whereas, for the SMC-2 algorithm, the time is  $58.40\mu s$ , resulting in a ratio of 0.49:1. On the other hand, for the minimum time, both algorithms have equal times of  $0.10\mu s$ , as evident from the results presented in Table 6.4.

These findings demonstrate that the SMC-2 algorithm does not impose a significant computational burden for its implementation in electronic power converters. Industrial inverters are equipped with high-quality electronic processors, typically DSP-based microcontrollers with clock frequencies around  $60MHz$  ( $0.016\mu s$ ) (Wang et al. 2022), thus capable of accommodating the computational requirements of the SMC-2 algorithm.



**Figure 6.13:** Calculation time performance of the control law.

**Table 6.4:** Time performance comparison between SMC-2 and PI.

Time algorithm	SMC-2	PI
Minimum	0.10 $\mu s$	0.10 $\mu s$
Average	0.27 $\mu s$	0.18 $\mu s$
Maximum	58.40 $\mu s$	29.10 $\mu s$

### 6.2.2 Discussion

The control of the SPVSI is of utmost importance in microgrids, considering that most ordinary home appliances consume AC energy. This study’s control criterion is based on technical specifications derived from the IEEE Std 1547-2018 standard. The objective of managing the energy flow between the grid and the SPVSI is accomplished through a well-designed closed-loop control system.

The control algorithm employed in voltage source inverters (VSIs) plays a critical role in the overall performance of closed-loop control. Traditionally, the PI regulator has been widely used as the control algorithm in most SPVSIs. This algorithm is known for its simplicity and efficiency in achieving control

objectives such as fast response and reduced steady-state error. Due to these advantages, most manufacturers rely on the PI algorithm. However, this work highlights the potential benefits of alternative control structures that may be more complex but offer significant advantages compared to the PI.

In this work, the authors have introduced a novel control structure known as SMC-2+PSO, which shares some similarities with the traditional PI regulator regarding parametrization. The SMC-2 control structure incorporates a PI-type sliding surface, which brings additional advantages in target reachability compared to conventional linear sliding surfaces. This innovative approach expands the possibilities for improved control performance in SPVSI systems based on the SMC algorithm with different sliding surfaces.

Nowadays, the reliability of electrical systems is a crucial factor in providing a satisfactory experience for end-users. It has been demonstrated in this study that enhanced reliability can be achieved through the superior performance of the SPVSI when controlled by the SMC-2 algorithm. The SMC-2 algorithm outperformed the traditional PI control regarding response time for ramp rate references and load tracking tests. Furthermore, the stability exhibited throughout the performance of the SPVSI demonstrated that the closed-loop controller successfully achieved objectives such as synchronization, accurate active power trade-off, and the maintenance of desired voltage and current levels.

Improving energy management in microgrids through advanced control algorithms enhances microgrid operations' efficiency. These efforts can significantly benefit small-scale consumers, mainly where distributed generation sources are scarce.

As highlighted in the introduction, voltage source inverters (VSIs) represent a technology trend that aligns with the continuous evolution of microgrids. These electronic devices encompass advancements in control, communication, and electrical protection. Studies like this one support the development of innovative proposals in the VSIs field and contribute to the ongoing research in microgrid systems.

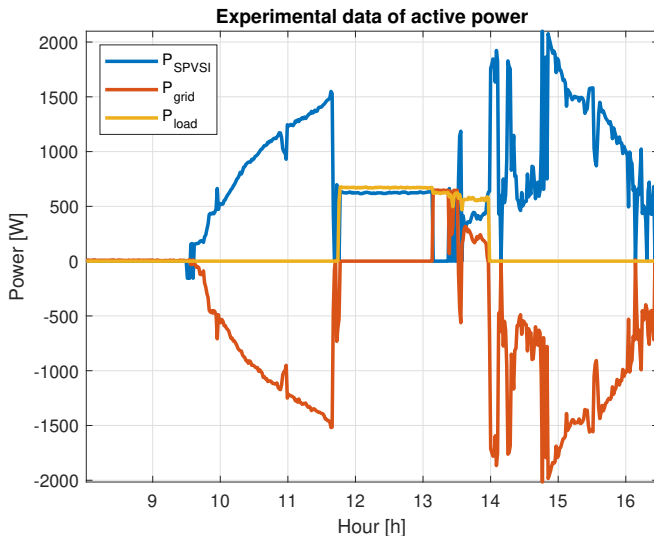
Future works in this area could explore the application of other intelligent algorithms for tuning the SMC-2 controller. While the Particle Swarm Optimization (PSO) algorithm was used in this study, numerous other metaheuristic algorithms are available for optimization. Leveraging different methods could lead to novel proposals. Also, online tuning approaches for the SMC-2 algorithm could enhance the controller's performance and adaptability.

### 6.3 Experimental Microgrid Improvement Under SMC-2 + PSO Methodology

This section presents the experimental results obtained from an inverter-based microgrid. The initial phase involved taking measurements from an experimental microgrid setup. To ensure compatibility with the microgrid converter model provided by the manufacturer, modifications were made to the PSCAD<sup>TM</sup> configuration. The converter model incorporates hardware interfaces with automatic switches, facilitating the seamless connection and disconnection of the SPVSI to the grid or load. This configuration allows for various scenarios, manipulating the interaction between the SPVSI, grid, and load based on different experimental criteria.

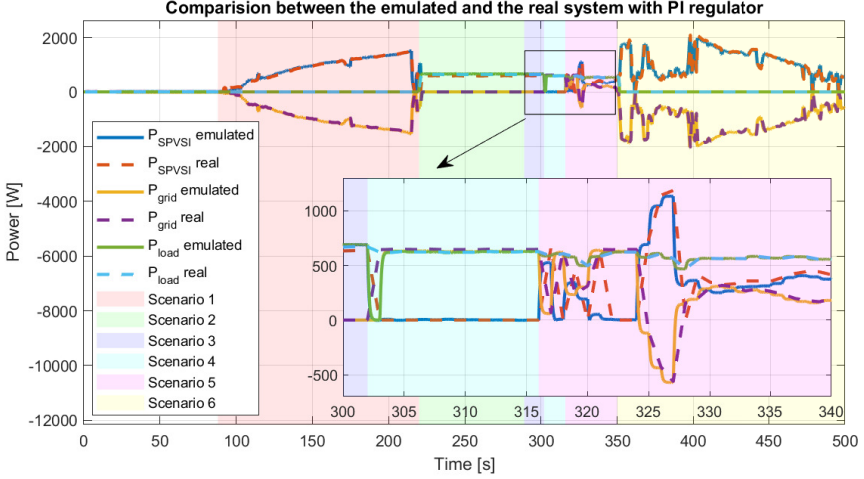
#### 6.3.1 Active power control for various management scenarios at experimental microgrid

The primary data collected for analysis included solar irradiation, active power in the grid, active power in the load, and active power from the solar photovoltaic system. These significant parameters are depicted in Figure 6.14.



**Figure 6.14:** Experimental data from an inverter-based microgrid at Universitat Politècnica de València.

Subsequently, the collected experimental data were utilized in a simulation scheme in PSCAD to replicate the experimental model. The PI controller parameters for the SPVSI were adjusted to  $k_p = 180.47$  and  $k_i = 23.67$ , resulting in the response shown in Figure 6.15.



**Figure 6.15:** Comparison between the real and emulated model.

The relative error is calculated using Equation 6.3 to determine the difference between actual and simulated data.

$$\varepsilon\% = \frac{1}{N_{data}} \sum_{k=1}^{N_{data}} \frac{|V_{real}(k) - V_{sim}(k)|}{V_{real}(k)} \cdot 100\%. \quad (6.3)$$

Where  $N_{data}$  represents the number of samples in both data sources,  $V_{real}$  denotes the values obtained from the experimental SPVSI, and  $V_{sim}$  corresponds to the values obtained from the SPVSI model. All values are calculated iteratively at each discrete instant  $k$ . After data processing, the relative error obtained was  $\varepsilon\% = 2.1\%$ . This value indicates a close approximation and demonstrates that the simulated system accurately reproduces the behavior of the real SPVSI under its operating conditions, as observed in the experimental data.

The load in the system exhibited varying values, and different consumption scenarios were defined for the interactions between the grid and the load. These scenarios are detailed in Table 6.5.

**Table 6.5:** Performance scenarios of the inverter-based microgrid

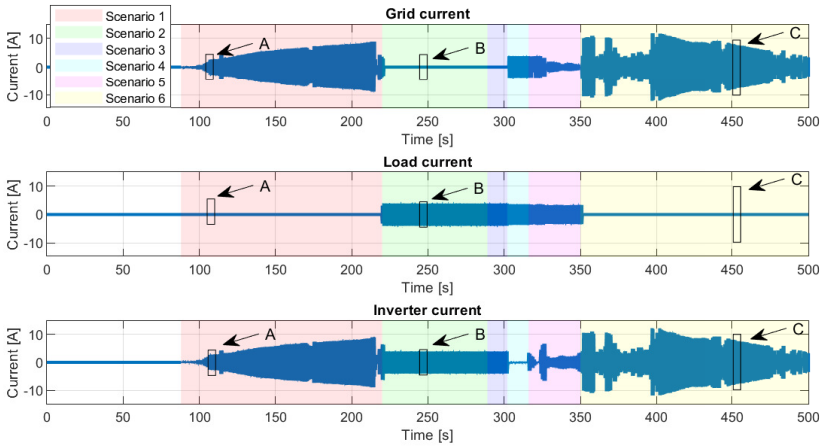
Scenario	Hour	Simulation time	Actions
0	08:00 to 09:27	1 to 88	Equipment off
1	09:28 to 11:39	89 to 220	The solar panels supply energy to the charger. The charger then charges the batteries. If there is no load, the inverter delivers energy to the grid as it maintains a constant voltage in the battery. The grid is disconnected and a load is connected.
2	11:40 to 12:49	221 to 289	There is solar energy available, and the charger continues to charge the batteries while this takes place.
3	12:49 to 13:13	290 to 302	The solar panels are disconnected. The system remains disconnected from the grid and continues to operate with a load. The battery discharges as a result.
4	13:13 to 13:27	303 to 316	The grid is connected while the solar panels remain disconnected. A load is present, which is powered by the inverter's bypass from the grid.
5	13:27 to 14:00	317 to 350	The solar panels are connected, and the charger charges the batteries. The excess energy is supplied to the grid if the battery reaches its charging limit.
6	14:00 to 16:30	351 to 500	The load is removed. Since the solar panels are connected, the charger delivers energy to the batteries. Since the batteries are fully charged, the excess energy is supplied to the grid by the SPVSI.

To optimize the simulation time, the large real-time data was escalated employing the following relation:

$$1 \text{ second of simulation} = 61.2 \text{ seconds of real-time data} \quad (6.4)$$

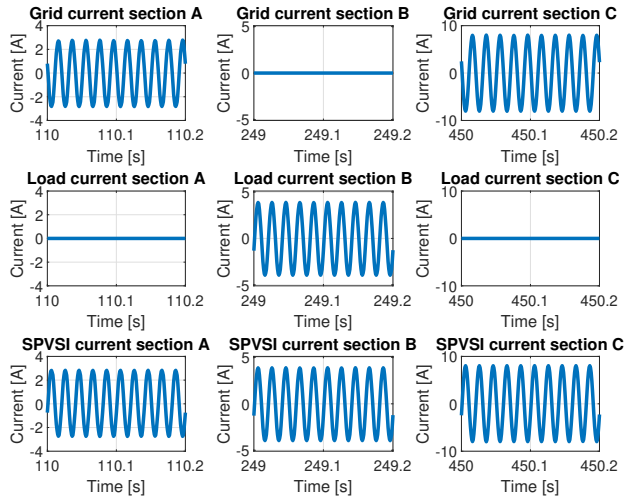
The SMC-2 control was fine-tuned using the Particle Swarm Optimization (PSO) algorithm to achieve active power regulation in the microgrid. The optimal tuning constants obtained were  $\lambda = -104.02$  and  $W = 9.14$ . The resulting currents from the grid, the load, and the SPVSI are depicted in Figure 6.16:





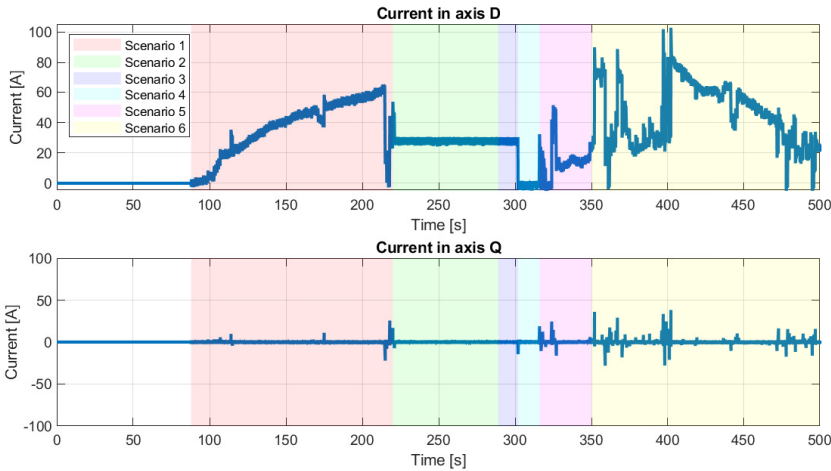
**Figure 6.16:** Current values of the grid, load, and SPVSI.

The SPVSI becomes an energy source for the grid, the load, or both. Peak current consumption reached up to 12A on the grid and 4A on the load.



**Figure 6.17:** Sections under the analysis of currents from the grid, load, and SPVSI.

The different operating modes of the MG described in Table 6.5 allow for distinct scenarios to be observed. Figure 6.17 provides a closer look at specific sections of the currents, allowing for better identification and analysis. The different sections demonstrate that the SPVSI supplies energy to both the grid and the load, depending on the specific scenario of the microgrid’s operation. Figure 6.18 illustrates the equivalent currents from the SPVSI in the D and Q axes.



**Figure 6.18:** Currents in DQ reference frame of SPVSI.

The results clearly show that power generation is active, as indicated by the current’s Q component being close to zero. This phenomenon becomes evident in various scenarios where the current in the D axis reaches the necessary values to fulfill the requirements for grid injection and load supply.

Furthermore, in compliance with the guidelines specified in standard IEEE Std 1547-2018, the voltage and frequency responses of the SPVSI at the point of common coupling are examined. Figure 6.19 presents the reaction of the SPVSI under the SMC-2 controller for the proposed experimental scenarios. This figure provides an evaluation of the performance of the inverter-based microgrid. In scenarios 1 and 6, where the inverter is solely connected to the grid, there is slightly greater distortion compared to the other scenarios where the inverter is connected to the load or both, the grid and load simultaneously. In particular, the values of  $V_{rms}$  and  $f$  remain well within the  $\pm 5\%$  limits specified by the IEEE standard.

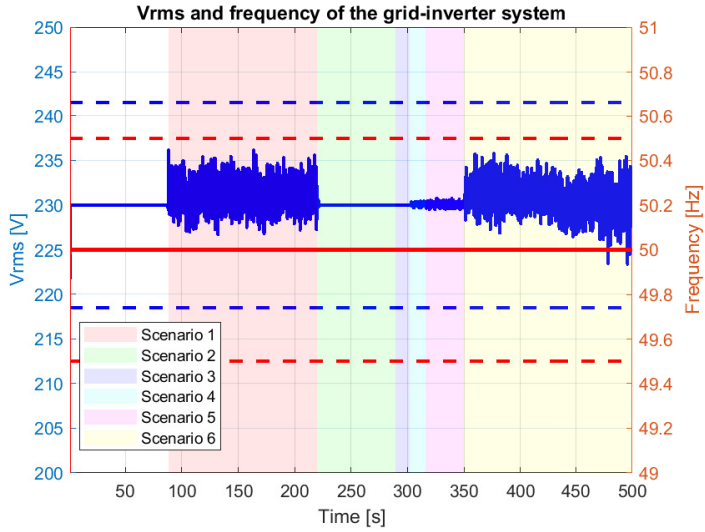


Figure 6.19:  $V_{rms}$  voltage and frequency on the grid for the SMC-2 controller.

Finally, a comparison of active power performance between the SMC-2 and PI control is shown in Figure 6.20.

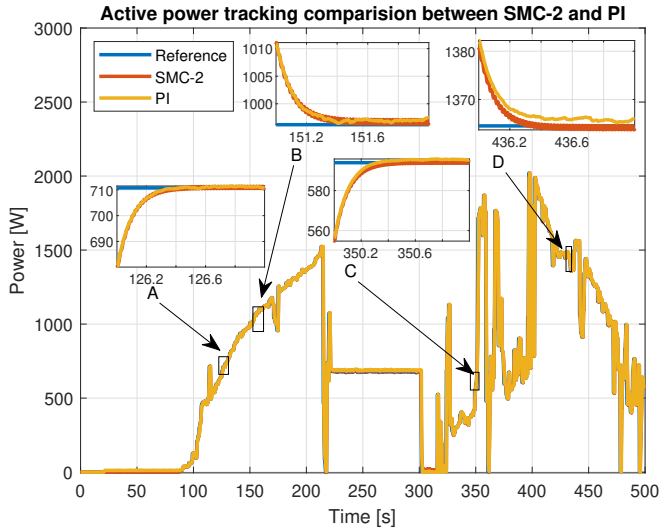


Figure 6.20: Active power performance comparison between SMC-2 and PI.

Both controllers exhibit comparable performance in meeting the transient regime and steady-state operation requirements in sections A and B.

However, the distinction between the two responses can be quantified numerically using performance indexes. Sections C and D highlight the superior performance of the SMC-2 controller in terms of steady-state values compared to the PI controller.

The effectiveness of each control method is evaluated based on the calculated values of IAE (Integral of Absolute Error), ISE (Integral of Squared Error), ITAE (Integral of Time-weighted Absolute Error), and ITSE (Integral of Time-weighted Squared Error). These values provide valuable insights into the performance of each controller and are presented in Table 6.6.

**Table 6.6:** Performance indexes values between SMC-2 and PI

Controller	Performance indexes							
	IAE	<i>Pct</i> [%]	ISE	<i>Pct</i> [%]	ITAE	<i>Pct</i> [%]	ITSE	<i>Pct</i> [%]
SMC-2	7.613683		0.001067	93.51	2481.463712	82.89	0.386907	95.38
PI	10.203392	74.62	0.001141		2993.611660		0.405629	

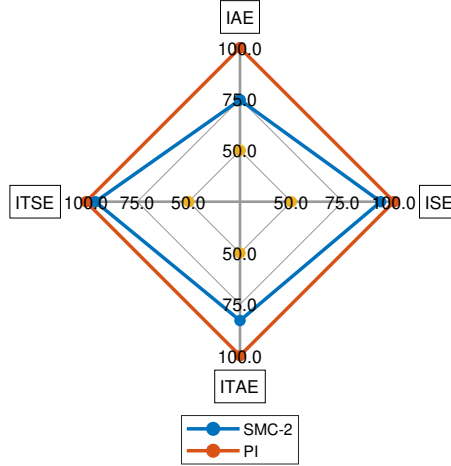
Additionally, percentage values (*Pct*) have been calculated to highlight the differences between the performance indexes of each controller, ranging from 0% to 100%.

The values for the PI controller are represented as 100%, and the values for the SMC-2 controller are expressed as a percentage equivalent to the PI values. As an example, Equation 6.5 demonstrates how these values are calculated:

$$Pct = \frac{IAE (SMC - 2)}{IAE (PI)} \cdot 100\% \tag{6.5}$$

More detailed information about the performance indices can be seen in Figure 6.21, which displays a radar chart with the parameters of the performance indices in percentages values:

Comparison in percentage of performance indexes between SMC-2 and PI



**Figure 6.21:** Active power performance comparison between SMC-2 and PI.

The results obtained from the SMC-2 controller demonstrate superior performance compared to those achieved with the PI controller. Moreover, the SMC-2 controller exhibits lower values for various performance indexes than the PI controller.

### 6.3.2 Discussion

Currently, there is a need to align laboratory-level prototypes of SPVSI with industrial inverters, as these prototypes are typically designed for specific research objectives. It is essential to emulate industrial SPVSI to facilitate the development of large-scale solutions. In this research, a dependable SPVSI model was developed to supply energy to various household consumption conditions. This model enabled the analysis of active power generation scenarios, including power generation directed towards the load, the grid, and both the grid and load simultaneously.

The accuracy of the emulated model compared to real microgrid data was approximately 2.1%. This level of accuracy is acceptable considering that measuring instruments have tolerance ranges from  $\pm 0.5\%$  in balanced conditions to  $\pm 5\%$  under unbalanced conditions (Electric 2023). Additionally, the measured data obtained from the microgrid needed to undergo processing due

to certain values not aligning with the anticipated operating trends of SPV-SIs. These inconsistencies, such as zero or negative values, were attributed to electromagnetic interference that disrupted the normal data transmission from the measurement equipment to the control center.

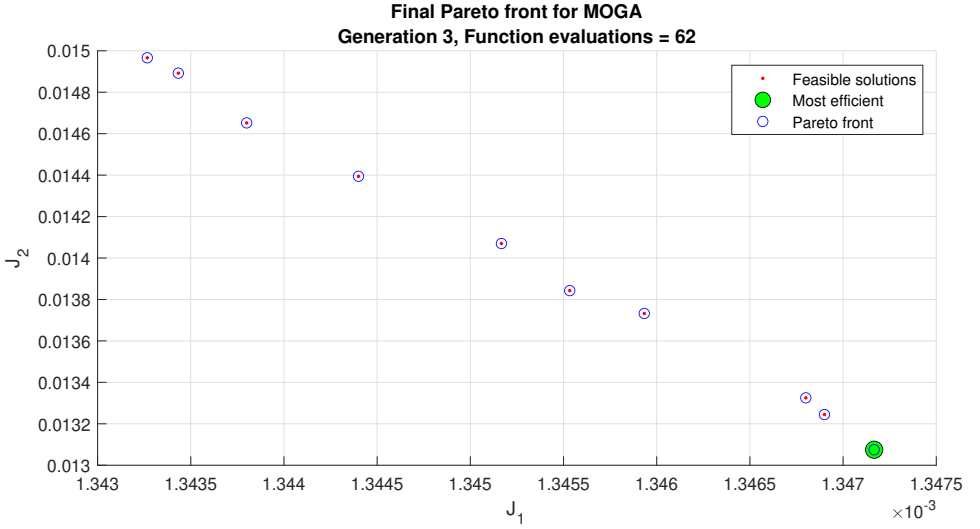
Considering that the experimental SPVSI's maximum active power generation can reach  $5.5 \text{ kW}$ , the approximations made in this research yielded promising results that can contribute to enhancing microgrid performance through smart inverters. The differences observed in the performance indexes of each control algorithm ranged from 5% for the ITSE index to 25% for the IAE index. These results indicate significant improvements, with a minimum enhancement of 5% and a substantial improvement of 25%. Such modifications can be crucial in utilizing energy from microgrids with limited renewable sources.

## 6.4 Experimental Microgrid Improvement Under SMC-2 + MOO Methodology

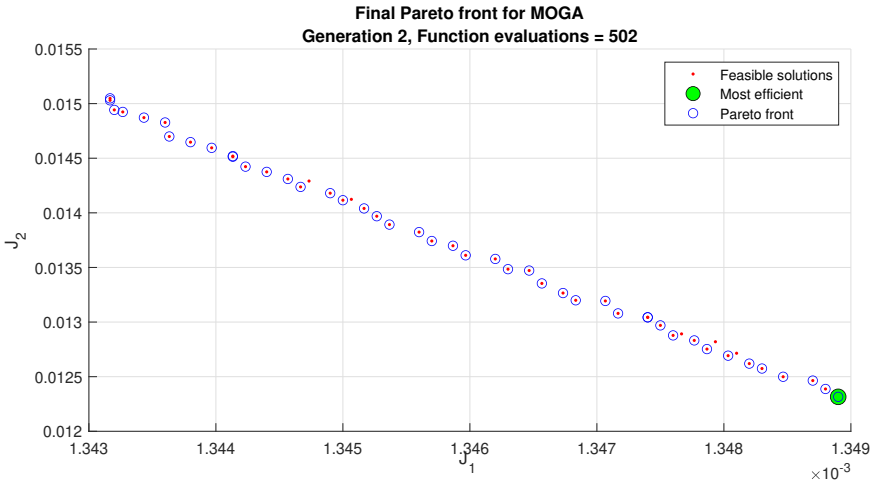
This section provides a detailed overview of the multi-objective optimization methods employed to enhance the performance of the SPVSI. These methods are compared with the PSO-based approach to identify their advantages and disadvantages.

### 6.4.1 *Multi-objective methods applied to the SPVSI for active power management*

This section generates Pareto fronts for the three selected MOO strategies (MOGA, MODE, and MOASA). For each MOO method, three simulations with different population sizes are conducted. Simulation #1 includes 10 particles, simulation #2 consists of 50 particles, and simulation #3 contains 100 particles. To differentiate each simulation for the three MOO algorithms, this research established that simulation #1 corresponds to the individual simulation of the three algorithms using 10 particles, simulation #2 corresponds to the individual simulation of the three algorithms using 50 particles, and simulation #3 corresponds to the individual simulation of the three algorithms using 100 particles. Consequently, the nomenclatures MOGA 1, MODE 1, and MOASA 1 are used for simulation #1, MOGA 2, MODE 2, and MOASA 2 for simulation #2, and MOGA 3, MODE 3, and MOASA 3 for simulation #3.



**Figure 6.22:** Pareto front from MOGA in simulation #1.



**Figure 6.23:** Pareto front from MOGA in simulation #2.

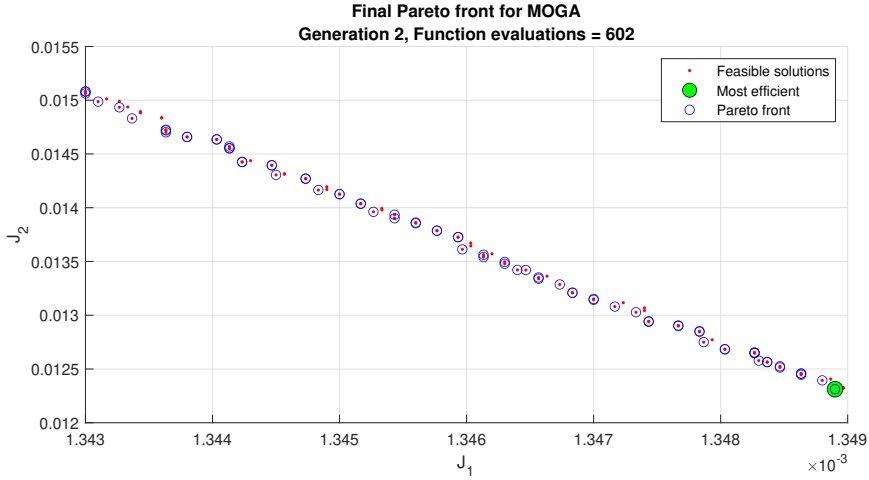


Figure 6.24: Pareto front from MOGA in simulation #3.

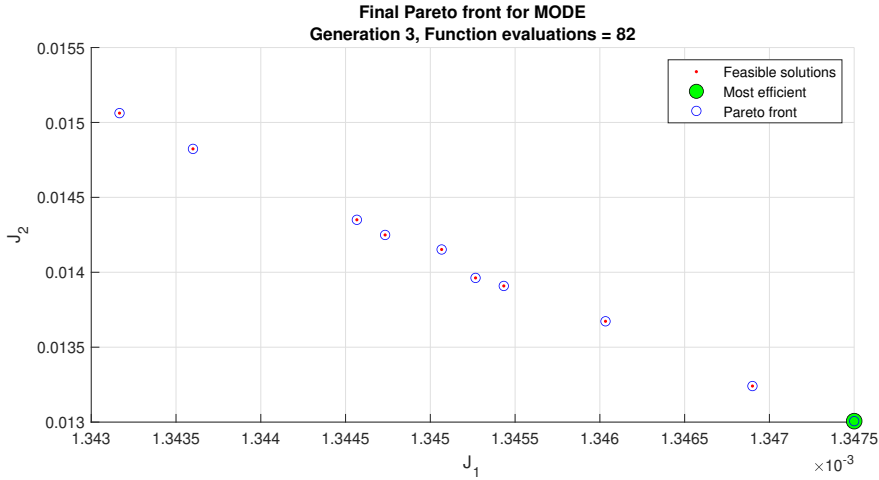


Figure 6.25: Pareto front from MODE in simulation #1.



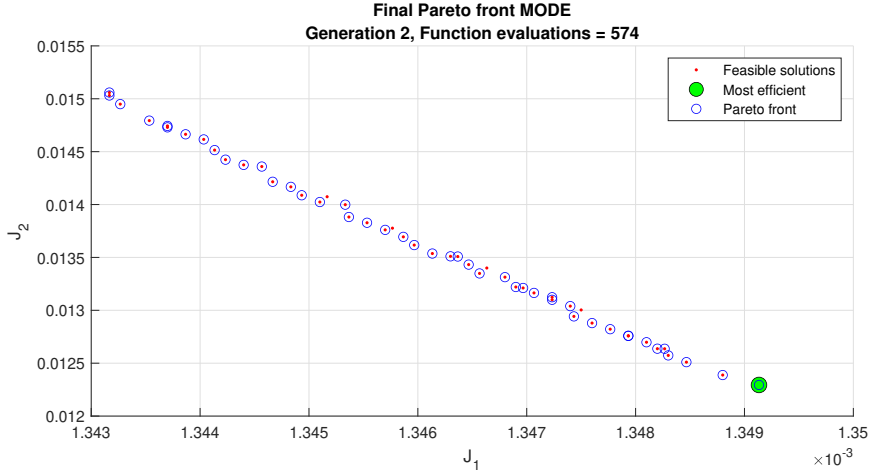


Figure 6.26: Pareto front from MODE in simulation #2.

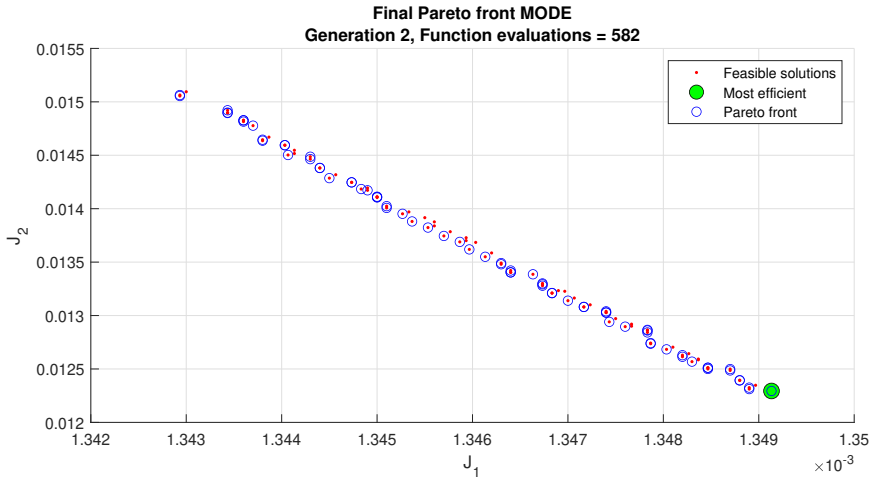
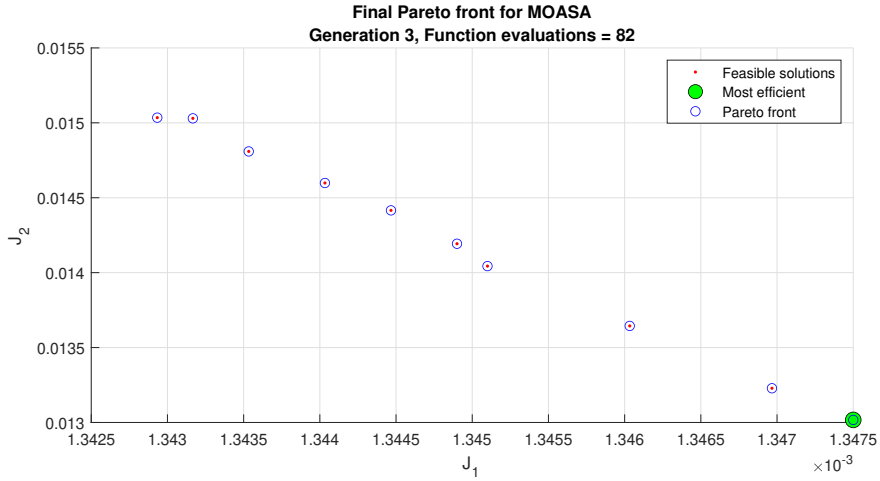
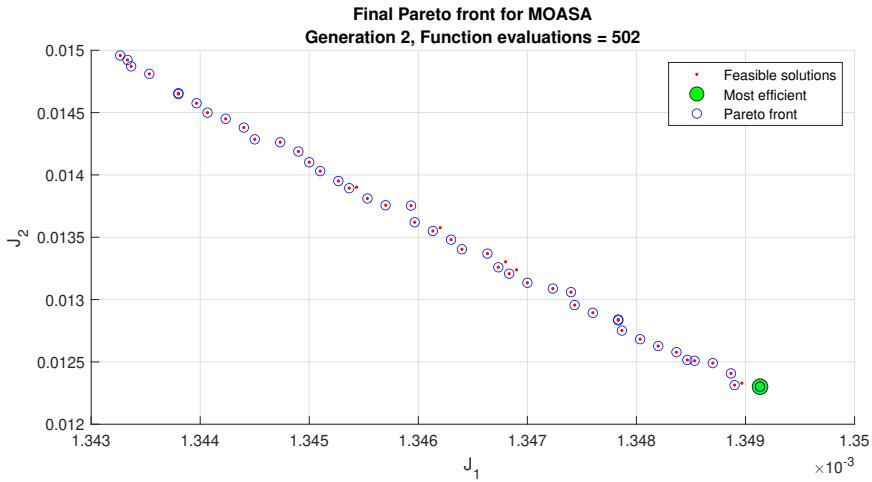


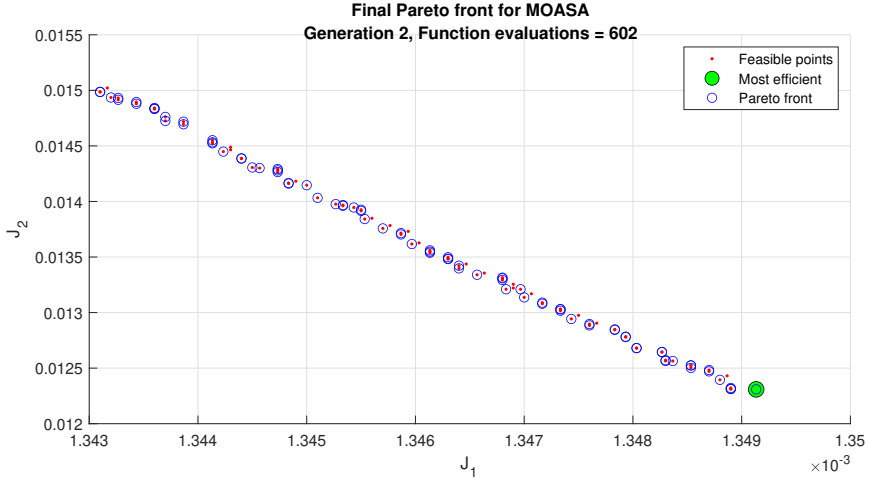
Figure 6.27: Pareto front from MODE in simulation #3.



**Figure 6.28:** Pareto front from MOASA in simulation #1.



**Figure 6.29:** Pareto front from MOASA in simulation #2.



**Figure 6.30:** Pareto front from MOASA in simulation #3.

Table 6.7 summarizes the parameters generated for each simulation case.

**Table 6.7:** Parameters for MOO simulations

		Parameters		
		Number of particles	Generations	Evaluated functions
Simulation #1	MOGA 1	10	3	62
	MODE 1	10	3	82
	MOASA 1	10	3	82
Simulation #2	MOGA 2	50	2	502
	MODE 2	50	2	574
	MOASA 2	50	2	502
Simulation #3	MOGA 3	100	2	602
	MODE 3	100	2	582
	MOASA 3	100	2	602

The term *number of particles* refers to the count of agents in each group for their MOO method. *Generations* signify the quantity of new particles generated through mating or mutation of parents. The "Evaluated functions" parameter indicates how frequently the algorithm attempts to discover the optimal solution for the optimization problem, reflecting the level of effort exerted by the algorithm in its quest for the best solution.

It can be observed that reducing the population size increases the number of generations required to reach a given termination criterion. This phenomenon can be explained through the theory of natural selection: a smaller population leads to greater genetic variability and, therefore, greater search space exploration. In practical terms, reducing the population size can be useful if one wants to improve the performance of a genetic algorithm. However, it should be noted that a smaller number of particles also implies a smaller number of objective functions evaluated during the optimization process. Therefore, reducing the population must be balanced with obtaining high-quality solutions reasonably.

On the other hand, Table 6.8 displays the values generated during the optimization process of SMC-2. These values show the quantities adopted by  $\lambda$  and  $W$  for each simulation of SMC-2.

**Table 6.8:** SMC-2 parameters from MOO methods

		SMC-2 parameters	
		$\lambda$	$W$
Simulation #1	MOGA 1	-88.64	9.18
	MODE 1	-99.69	1.49
	MOASA 1	-99.64	7.62
Simulation #2	MOGA 2	-89.63	2.21
	MODE 2	-99.87	8.09
	MOASA 2	-99.96	5.35
Simulation #3	MOGA 3	-89.47	5.43
	MODE 3	-99.93	4.56
	MOASA 3	-99.74	2.60

The values are very similar for the simulations with 50 and 100 particles per population, while for 10 particles, there is a more significant difference. This allows for evaluating the SMC-2 algorithm with the premise of obtaining different results in the controller evaluation process.

In all simulation cases, the Pareto fronts show a more pronounced minimization of the rise time compared to the overshoot. Electric systems have very fast response dynamics compared to other physical systems with slower responses, such as temperature control processes. Loading and unloading actions of electric energy storage elements like inductors and capacitors contrast sharply with thermal storage elements with longer response times.

On the other hand, overshoot response indicates that an inherently fast process oscillates due to the system's strong response to input signal requirements. This also contrasts with slow dynamics processes that mostly do not have overshoots because they are represented as a first-order transfer function.

The inverted generational distance (IGD) seen in Chapter 4 will be employed to evaluate the performance of the multi-objective optimization (MOO) algorithms. The IGD measures how well a set of solutions from the Pareto front approximates the true Pareto front. When the IGD value is small, the MOO algorithm has achieved adequate convergence, and the obtained solutions are well-distributed in the search space. In other words, the approximate solution set is closer to the true Pareto front, meaning the algorithm has found high-quality solutions.

The IGD index allows the thesis' approach for statistical comparisons regarding the positioning of each solution in the Pareto front. The following values are considered: mean, median, best, worst, and standard deviation (SD), to determine how dispersed the solutions found by each group of particles are in their search space. The results obtained are shown in Table 6.9.

**Table 6.9:** IGD results from MOO simulations

IGD	Solution #1			Solution #2			Solution #3		
	MOGA	MODE	MOASA	MOGA	MODE	MOASA	MOGA	MODE	MOASA
Average	0.9449m	1.0368m	1.1847m	1.3561m	1.3297m	1.2055m	1.3942m	1.2881m	1.3053m
Median	0.8814m	1.0508m	1.2872m	1.3394m	1.2293m	1.1408m	1.4144m	1.2264m	1.2347m
Best	3.9000u	4.3333u	4.5667u	5.7333u	5.9667u	5.8667u	5.9000u	6.2000u	6.0333u
Worst	1.8912m	2.0558m	2.0174m	2.7328m	2.7645m	2.6568m	2.7689m	2.8004m	2.7129m
SD	0.6897m	0.6383m	0.7169m	0.8275m	0.7750m	0.8113m	0.8447m	0.8065m	0.8101m

Based on the results in Table 6.9, it can be determined that algorithms with a lower number of particles have a lower IGD value, indicating that their dispersion through the search space is lower than other simulation methods. Better dispersion indicates the particle group moving collectively towards the optimal solution for solving the MOP.

From this data, simulations are carried out for a step input of current in axis D. Since the SPVSI is represented in a DQ reference frame, the current in axis D has a direct impact on the active power that is desired to be generated in the microgrid, as previously discussed in earlier chapters. Therefore, 10A energy transfer between the grid and the SPVSI has been taken as a step input. Since the power switches of the SPVSI are placed on the primary side of the step-up transformer, a value of approximately 67.51A must be generated on the

primary side of the SPVSI. The graphs of the responses of each of the MOO methods to a step input are shown in Figures 6.31, 6.32 and 6.33:

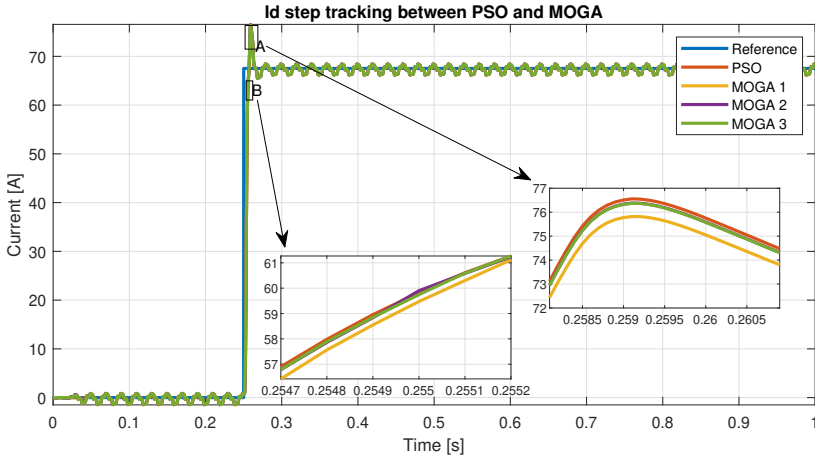


Figure 6.31: Step response for MOGA simulations.

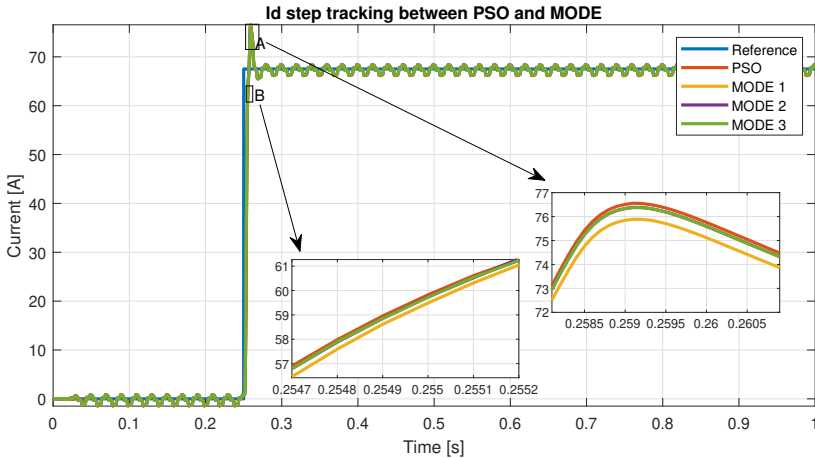
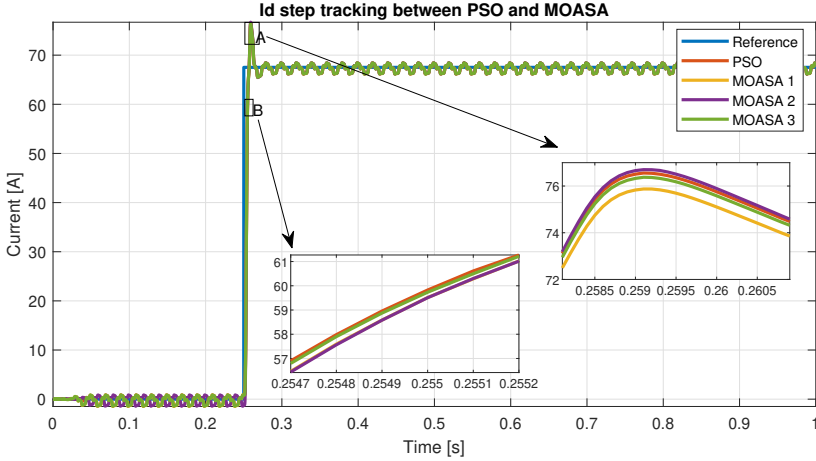


Figure 6.32: Step response for MODE simulations.



**Figure 6.33:** Step response for MOASA simulations.

The numerical results of these simulation cases are shown in Table 6.10:

**Table 6.10:** Response parameters from MOO simulations for a step input

Algorithm		Overshoot [%]	Rising time [ms]	IAE	ISE	ITAE	ITSE
MOGA	Solution #1	12.2911	2.8575	6.9260	2.2638	1.4593	4.5757
	Solution #2	13.1270	2.8457	6.9305	2.2645	1.4598	4.5785
	Solution #3	13.1085	2.8492	6.9305	2.2645	1.4598	4.5784
MODE	Solution #1	12.3932	2.8636	6.9267	2.2639	1.4594	4.5761
	Solution #2	13.1336	2.8562	6.9306	2.2645	1.4598	4.5785
	Solution #3	13.1142	2.8545	6.9305	2.2645	1.4598	4.5784
MOASA	Solution #1	12.3736	2.8650	6.9265	2.2639	1.4594	4.5760
	Solution #2	13.5995	2.8454	6.9298	2.2643	1.4597	4.5782
	Solution #3	13.1171	2.8607	6.9305	2.2645	1.4598	4.5785

On the other hand, the radar plots are shown in Figures 6.34, 6.35 and 6.36 for each of the simulations to understand the performance to understand the pros and cons of each MOO method presented.

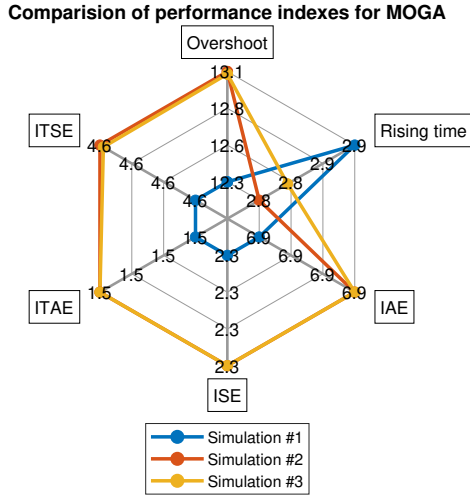


Figure 6.34: Radar plot for MOGA simulations.

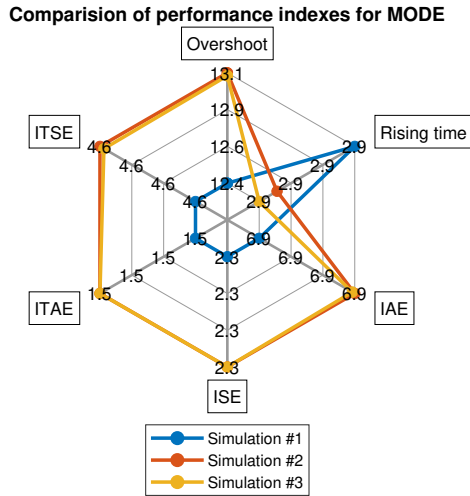
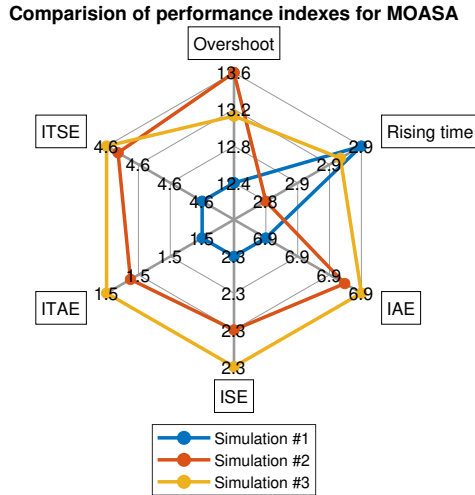


Figure 6.35: Radar plot for MODE simulations.





**Figure 6.36:** Radar plot for MOASA simulations.

The radar chart shows that the responses generated for the first experiment had better results than the other two options. The algorithm's search area for optimal tuning constants will greatly impact the results. Using more particles only sometimes leads to better results because the processing time can negatively affect the algorithm's convergence. Additionally, it can be challenging to choose the appropriate search area for the algorithm because it depends on the designer's experience with specific process control, in this scenario, the SPVSI control.

The responses of each MOO method are presented as follows:

#### 6.4.2 MOGA responses

The following figures will show the different details showing the response of the SMC-2 controller tuned by the MOGA algorithm.

The reference tracking of the power reference is observed in Figure 6.37.

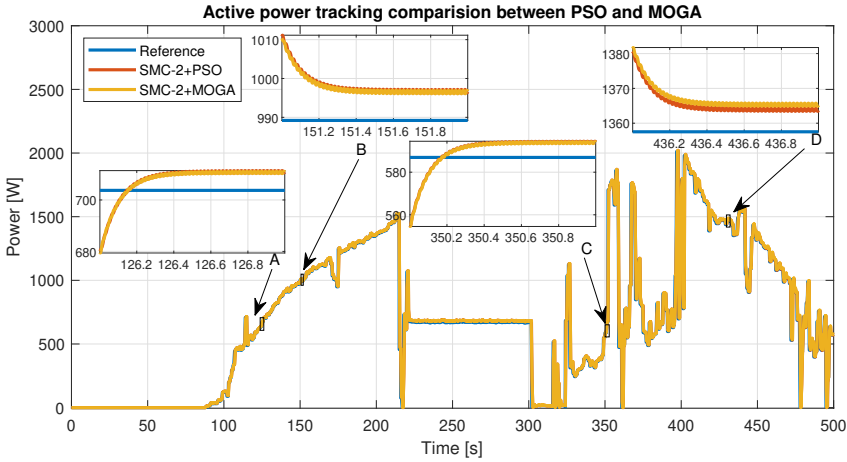


Figure 6.37: Comparison between PSO and MOGA applied to SMC-2.

Sections A, B, C, and D present the differences in power reference tracking that compare the SMC-2 controller tuned by the PSO and MOGA. For low active power values ranging from 580W (panel C) to 700W (panel A), the performance of the 2 tuning algorithms is similar. On the other hand, at high values such as 990W (panel B), a favorable trend to PSO is seen, which increases at higher power values such as 1360W (panel D).

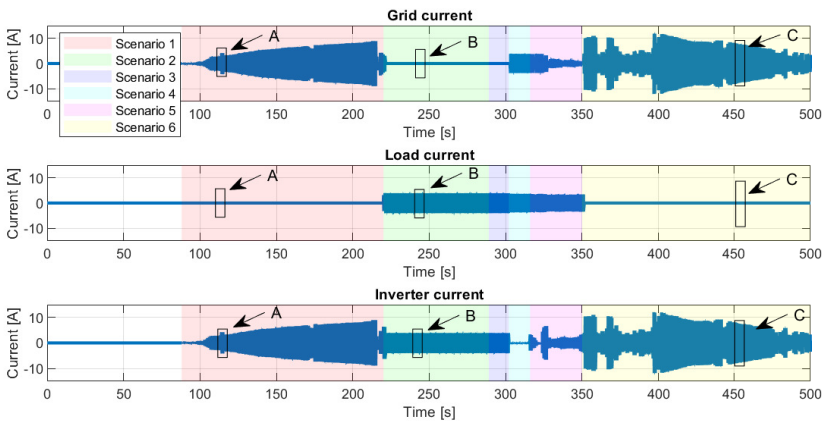


Figure 6.38: Current values of the grid, load, and SPVSI.

Figure 6.38 shows the currents generated in the grid, the load, and the SPVSI; while the detailed analysis of MG's currents is seen in Figure 6.39.

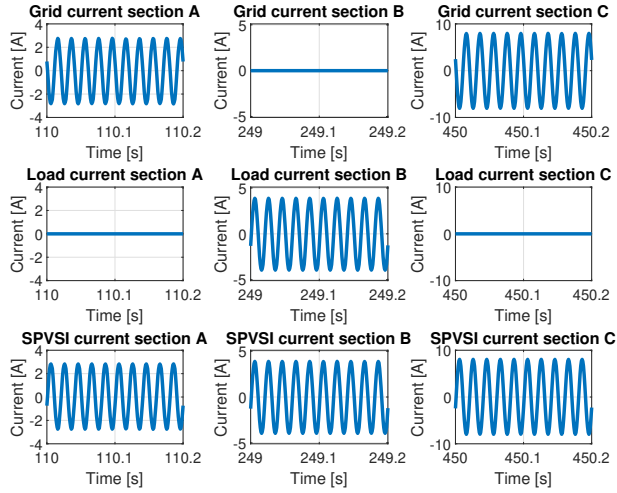


Figure 6.39: Sections under the analysis of currents from the grid, load, and SPVSI.

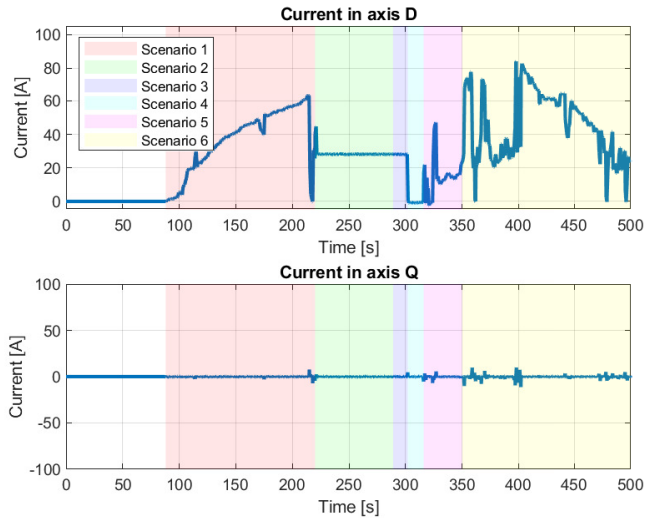
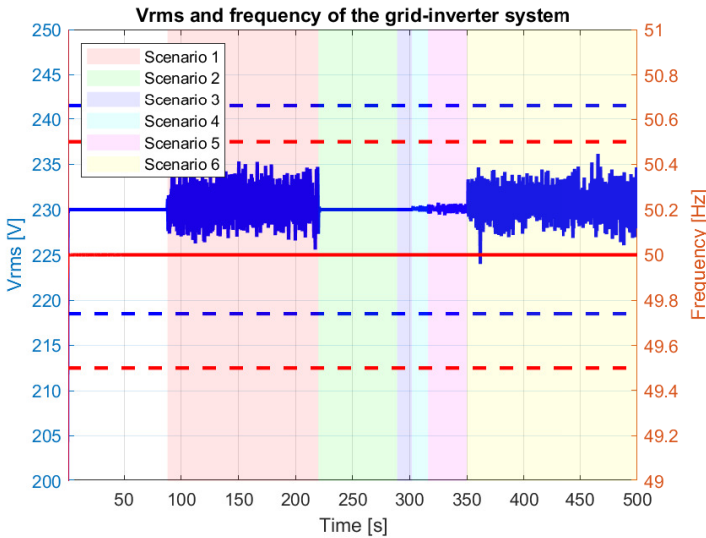


Figure 6.40: Currents in DQ reference frame of SPVSI.

The values presented in sections A, B, and C align with the aforementioned discussion, where grid and load currents exhibit changes directly associated with the SPVSI current.

Moving on to Figure 6.40, we can observe the D and Q currents variations. The changes in the D current correspond to the desired current values that the SPVSI needs to generate within the microgrid to produce active power. As for the Q current, it remains close to zero, except for instances of sudden reference changes, where deviations occur.

Finally, the SPVSI  $V_{rms}$  voltage and frequency values are shown in Figure 6.41.



**Figure 6.41:**  $V_{rms}$  voltage and frequency on the grid for SMC-2+MOGA controller.

These values are maintained within limits set by the IEEE Std 1547-2018 standard, which stipulates that voltage and frequency values should remain within approximately  $\pm 5\%$  of their nominal values of  $230V$  and  $60Hz$ . It is worth noting that a higher degree of distortion is observed in scenarios where the SPVSI is connected to the grid compared to scenarios where it is connected directly to the load.

### 6.4.3 MODE responses

The following figures show the SMC-2 controller's response to the MODE tuning. The reference tracking of the power reference is observed in Figure 6.42 and the MG's currents in Figure 6.43.

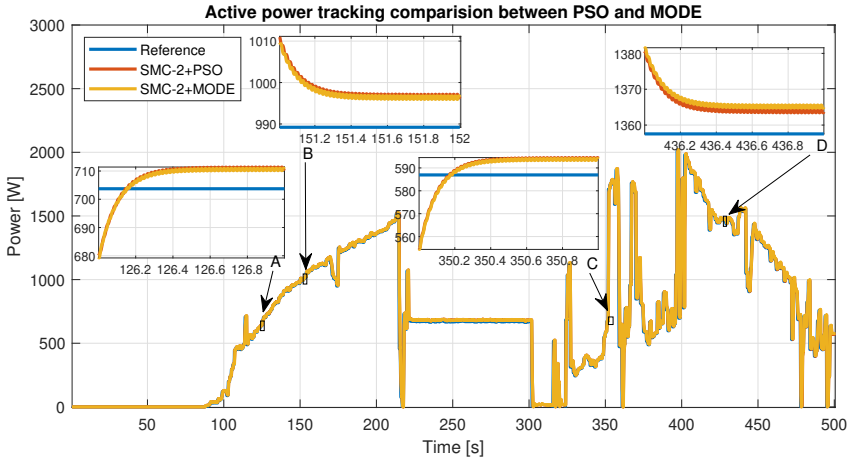


Figure 6.42: Comparison between PSO and MODE applied to SMC-2.

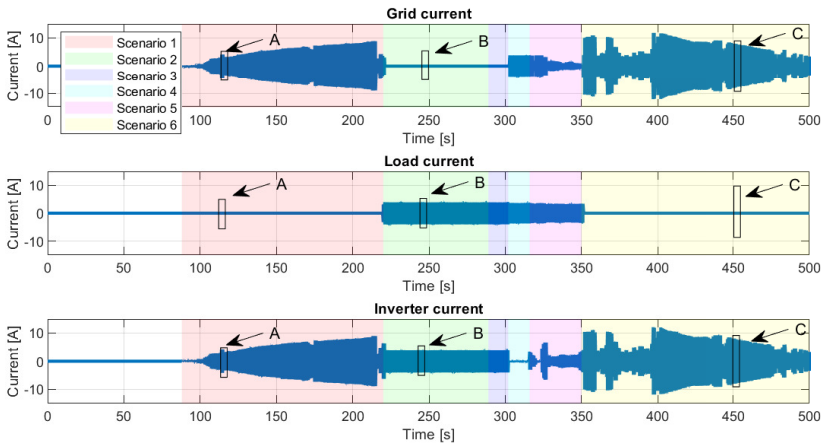
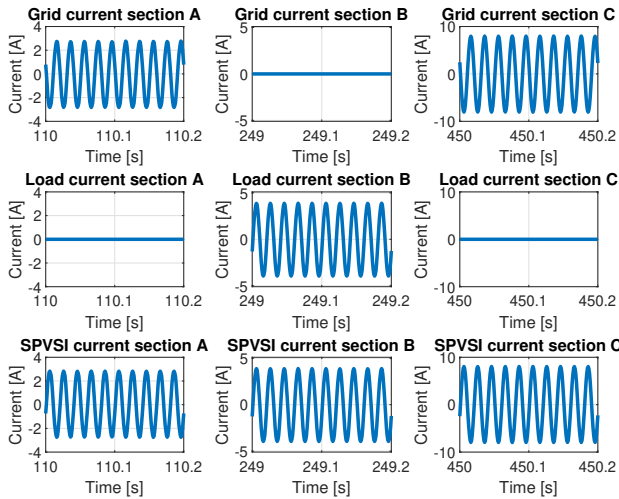


Figure 6.43: Current values of the grid, load, and SPVSI.

Sections A, B, C, and D present the differences in power reference tracking that compare the SMC-2 controller tuned by the PSO and MODE. For low power values, parity is observed between the PSO and MODE methods (panels A and C). In panel B, a slight advantage of MODE is observed; in panel D, PSO shows a better response for higher active power values than MODE.

Meanwhile, the currents presented in Figure 6.43 comprehensively represent the dynamic changes in the SPVSI, grid, and load currents throughout the MODE experiment. These current values offer valuable insights into the performance and behavior of the system under study. Examining these currents makes it possible to assess to understand the interaction between the SPVSI, grid, and load.

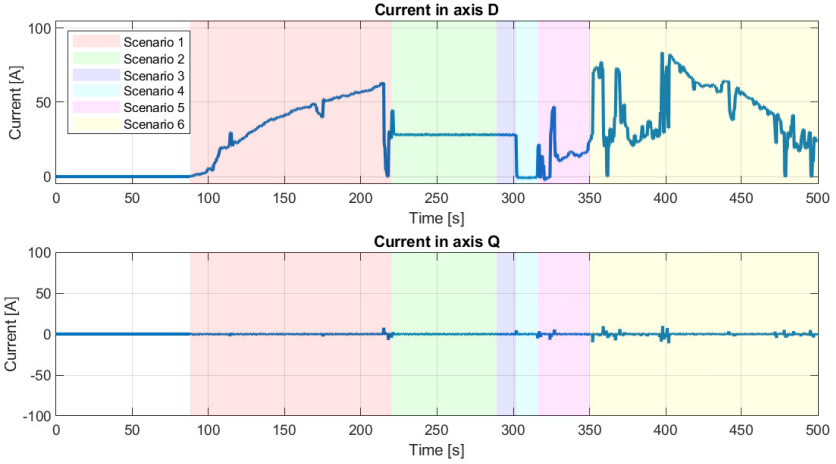
For further observations, an enlarged and detailed analysis of the grid, load, and SPVSI current values is shown in Figure 6.44.



**Figure 6.44:** Sections under the analysis of currents from the grid, load, and SPVSI.

As mentioned earlier, the values shown in sections A, B, and C are correlated between the grid, load, and SPVSI. It means the SPVSI current is obtained by adding the grid current to the load current.

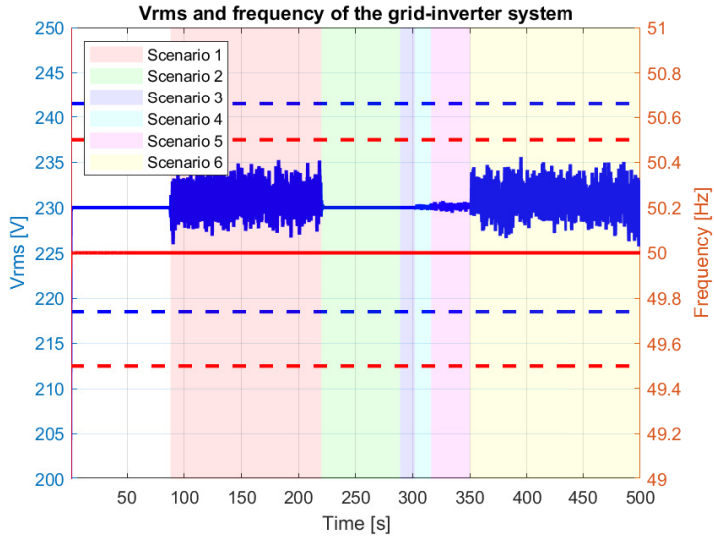
The changes in the currents of axes D and Q are shown in Figure 6.45.



**Figure 6.45:** Currents in DQ reference frame of SPVSI.

The currents on axes D and Q change, as mentioned earlier.

Finally, the SPVSI  $V_{rms}$  voltage and frequency values are shown in Figure 6.46.



**Figure 6.46:**  $V_{rms}$  voltage and frequency on the grid for SMC-2+MODE controller.

These values are kept within limits established by the IEEE Std 1547-2018 standard, as mentioned earlier.

#### 6.4.4 MOASA responses

The upcoming figures will present an in-depth analysis of the response exhibited by the SMC-2 controller when tuned using the MOASA algorithm. These figures provide comprehensive details and insights into the system’s performance and behavior.

Specifically, Figure 6.47 focuses on active power reference tracking. This figure shows how well the controller tracks the desired power reference, offering valuable information regarding the system’s stability and accuracy.

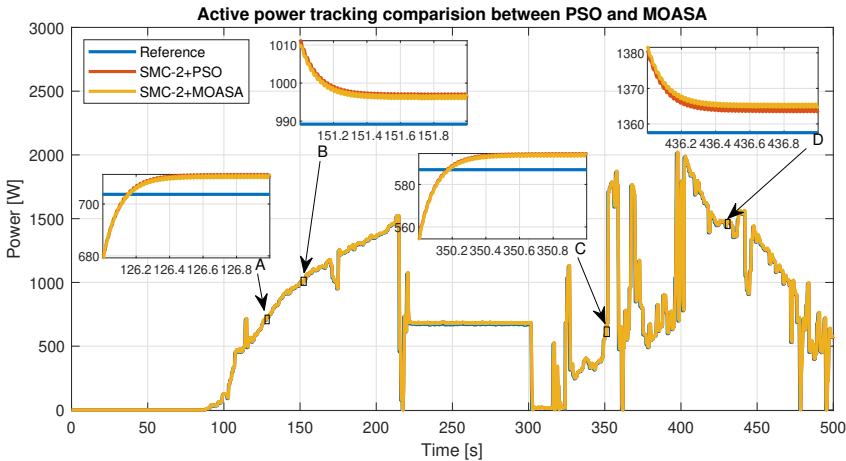
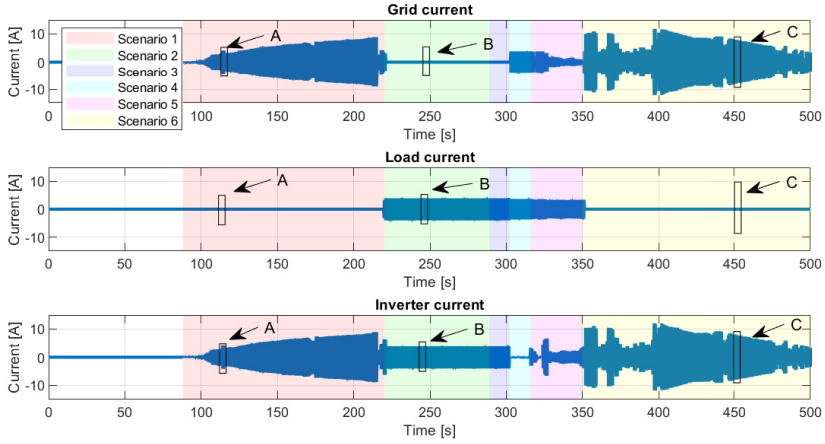


Figure 6.47: Comparison between PSO and MOASA applied to SMC-2.

Sections A, B, C, and D highlight the disparities in power reference tracking between the SMC-2 controller tuned by the PSO and the MOASA methods. The responses observed for all panels exhibit similarities to those described in the MODE scenario, further supporting the findings.

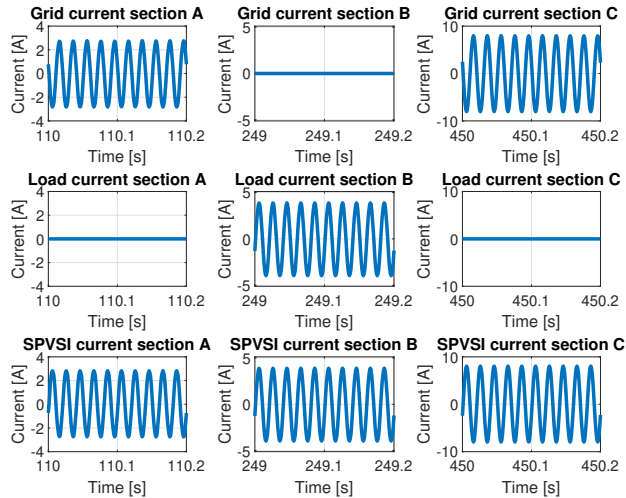
Additionally, Figure 6.48 provides a graphical representation of the currents generated in the grid, load, and SPVSI. This visual depiction aids in visualizing the variations and dynamics of these currents throughout the experimental process.





**Figure 6.48:** Current values of the grid, load, and SPVSI.

An enlarged and detailed analysis of the grid, load, and SPVSI currents values is shown in Figure 6.49.



**Figure 6.49:** Sections under the analysis of currents from the grid, load, and SPVSI.

In addition, the D and Q currents are shown in Figure 6.50 and the  $V_{rms}$  in SPVSI and frequency values in Figure 6.51.

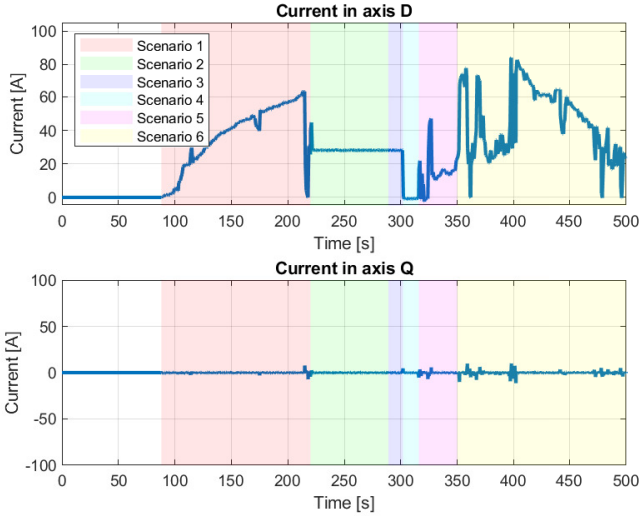


Figure 6.50: Currents in DQ reference frame of SPVSI.

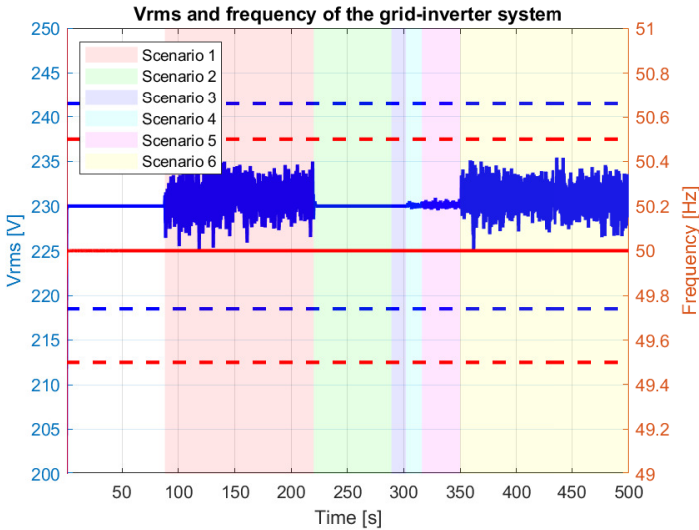


Figure 6.51:  $V_{rms}$  voltage and frequency on the grid for SMC-2+MOASA controller.

These values are kept within limits established by the IEEE Std 1547-2018 standard, as mentioned earlier.

Once the values to be compared with the PSO have been identified, simulations of the various SMC-2 tuning methods for active power management in the microgrid are carried out, as observed in Chapter 6. The results of each of these cases are shown in Table 6.11:

**Table 6.11:** Performance indexes between PSO and MOO methods for various scenarios of SPVSI

Algorithm	IAE	ISE	ITAE	ITSE
PSO	7.613683	0.001067	2481.463712	0.386907
MOGA	7.607168	0.001069	2493.755679	0.388170
MODE	7.562280	0.001068	2481.472717	0.387879
MOASA	7.564328	0.001068	2482.016041	0.387846

The results show performances that differ in minor values between the proposals implemented to control SPVSI. This implies that the multi-objective approach can be addressed by simultaneously optimizing a cost function or multiple cost functions. Applying one or the other optimization strategy will depend on the design criteria, available resources, and objectives desired in the microgrid.

The results of Table 6.11 are interpreted in the radar graphs presented in Figure 6.52.

The results shown in Figure 6.52 present a deviation approach implemented in the previous chapter. The baseline is the response of the SPVSI with the PI controller, representing a value of 100%. The values generated by the SMC-2 and its respective tuning algorithms are fractions of the baseline value. The difference between these values and the baseline represents the improvement of each proposed method. In this regard, Figure 6.52 shows that the improvement in the IAE parameter represents a value of 0.5%. In contrast, the values for the other parameters have not been significantly improved and range from 0.2% to 0.4%. However, it is worth noting that none of the analyzed approaches, whether multi-objective in a cost function or multiple cost functions, performs worse than the traditional PI, as they all perform better than the latter.

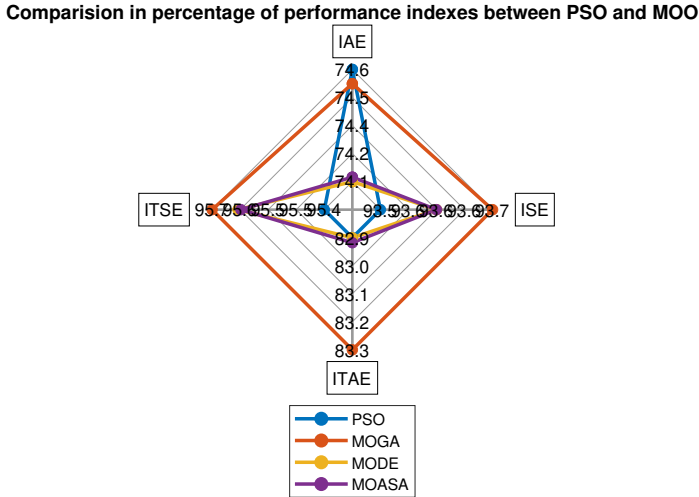


Figure 6.52: Radar plot between MOO algorithms and PSO.

### 6.4.5 Discussion

In this section, a broad approach is presented on the use of MOO algorithms, which aim to improve the performance of the SPVSI for effective active power management. The results showed some nuances where grouping multiple objectives can yield better results than having a single objective. This analysis has considered various aspects, such as the number of particles, the SMC-2 controller constants, and operating values. Therefore, the main elements of this chapter are detailed below.

In this research, the rise time and overshoot characteristics of the SPVSI have been considered conflicting objectives that directly affect the controller’s performance. While a more significant number of objectives may allow for a more detailed analysis to achieve more ambitious control objectives, it also entails a more complex algorithm and high computational cost. Care must be taken in the approach and number of objectives desired.

This research established a maximum of 100 members per population to achieve better results. It was observed that while more agents can help find an optimal solution, this largely depends on where the particles are located in the search space. A higher number of agents was not chosen because the optimization

process would take considerable time, given that the process involves rapid changes such as the modulation frequency of  $20kHz$ .

As observed in the results, increasing the number of population members will only sometimes produce better outcomes. Another factor that can help the algorithm achieve optimal results in less time is the algorithm's search zone. In this sense, one option is to leverage the expertise of someone who knows the process, which can assist the algorithm in searching in a delimited area near the optimal point. Otherwise, a search without a reference point can be performed with a larger population, resulting in a longer processing time for achieving the results.

The optimized goals, rise time and overshoot, are correlated and have been improved to the extent that one is not harmed more than the other. As mentioned earlier, these goals conflict, which means that improving one necessarily worsens the other and vice versa. As the SPVSI is a system composed of electronic components that are naturally fast, it tends to have a critical goal regarding overshoot. However, the cost function evaluation results showed that the overshoot needed to reach a minimum as low as the rise time.

The Pareto front showed a linear trend with relative closeness among all its points. While the optimal point was mainly focused on the rise time objective, the same trend was not observed in the overshoot objective. This is because the SPVSI includes electronic components that are naturally fast and generate oscillations due to aggressive responses. In this situation, MOO algorithms have located the most appropriate optimization points for these operational circumstances.

Based on what has been observed in the controller evaluation stage, it is possible to propose different closed-loop regulations that can be optimized using MOO methods. In these new control laws, other objectives can be considered that may produce optimal optimization constants. However, generating more objectives to be optimized may increase mathematical complexity and computational load.

## 6.5 Conclusions of the Chapter

This study presents the design and implementation of the SMC-2 for a microgrid-based SPVSI to enhance the performance of existing industrial SPVSI that utilize a PI regulator. The primary control objective was to regulate active power generation to align with the demand of the load or inject spare active power into the grid. The active power, based on parameters of the electrical regulations IEEE Std 1547-2018, is produced and received in the SPVSI. Tracking active power reference values complies with voltage and frequency stability values on standard IEEE Std 1547-2018. These approaches still need to be covered for advanced algorithms.

The SMC-2 utilizes the super-twisting algorithm to effectively prevent chattering without sacrificing algorithm robustness regarding conventional SMC proposals. In addition, a non-conventional sliding surface in a PI form enhanced the controller's accomplishment of objectives. The SMC-2 dealt with the coupled model of the SPVSI in the DQ reference frame. The robustness of the SMC-2 surpasses the model uncertainties presented by parasite capacitance on the SPVSI.

The results reveal that the SMC-2+PSO demonstrated a reduced steady-state error for tested active power reference values compared to the PI algorithm. This can be attributed to the linear characteristics of the PI algorithm, which can difficult its performance in non-linear systems such as the SPVSI. Instead, the SMC-2 demonstrated no such limitations.

Using real-data parameters from both the microgrid components and the environmental weather conditions allows for proposed improvements in the control system of the SPVSI to enhance the efficiency of active power management in low-power domestic applications, with potential application to high-power systems.

The different application scenarios applied in the microgrid showed the robustness of the SMC-2+PSO method under various operating conditions. The SPVSI can supply power to the grid, the load, or both simultaneously, expanding the applications of microgrids to meet the demands of low-power residential systems in the integration of a renewable energy perspective.

The MOO methods considered conflicting objectives such as rise time and overshoot. The PSO results were compared with the MOO proposals to establish improvement criteria. The obtained results revealed that, for tested active power reference values, the SMC-2 could be improved by PSO or MOO

depending on the context of tuning. The results were exposed and analyzed to review the advantages of PSO and MOO methods.

To determine the effectiveness of the SMC-2, the following performance evaluation indexes were employed: IAE, ISE, ITAE, and ITSE. The indexes show numerically the better results obtained from the SMC-2 with a multi-objective approach over the traditional PI.

Finally, both PSO and MOO algorithms significantly improve tuning the SMC-2 controller in areas such as rise time and overshoot compared to the widely-used PI controller in industrial inverters. It has been verified that implementing these approaches is feasible as the SMC-2 controller does not impose an excessive computational burden, and the control algorithm tuning is performed offline. Therefore, modern microprocessors can adopt these alternatives to enhance current industrial inverters and achieve results that further drive the advancement of efficient power production applications in MGs.





## Chapter 7

# Thesis Conclusions

The focus of this chapter is to emphasize the primary findings of the thesis, identify potential topics for future research based on the present study, and provide a list of publications made during the Ph.D. studies.

### 7.1 Conclusions of the Dissertation

This thesis dissertation presented new strategies for the MOO applied to inverter-based microgrids. The new strategies were evaluated and validated in different scenarios of active power regulation.

In Chapter 2, a comprehensive summary of microgrids, their types, and components was presented. In particular, it begins by analyzing one of the main components of microgrids: the voltage source inverter (VSI). Specific cases for inverters connected to single-phase electrical systems are studied. These power converters' topology, closed-loop regulation schemes, and modulation types are analyzed. Likewise, the microgrid as a whole is addressed. The different types of inverter-based microgrids, the elements contributing to their topology, environmental policies, and regulations for their regulation were analyzed.

In Chapter 3, the definition of multi-objective control is presented. A summary of different control proposals to solve multi-objective problems and an

overview of the main closed-loop regulation methods for VSI control are provided. Subsequently, some works focused on multi-objective control are presented, which still face challenges. As the chapter progresses, some proposals focused on multi-objective control are unveiled, but challenges on this topic are addressed.

In Chapter 4, the SMC-2 control method is proposed as an improved control strategy for an inverter-based microgrid under the multi-objective approach. The design of the control algorithm included an innovative proposal to generate a PI sliding surface to improve existing sliding surfaces on SMC controllers.

The control law employed the super-twisting method suitable for first-order systems. A strategy involving first-order filters was performed to generate orthogonal components in the time domain for a single-phase system. The measurement and processing of voltage and current data from the microgrid configuration were applied to the orthogonal components. Subsequently, these components have been transformed into a rotating reference frame known as DQ.

The DQ system is synchronized with the power grid using a phase-locked loop scheme. Independent power control is performed once the DQ system's microgrid signals are measured and calculated. The main objective was prioritizing active power generation in the D-axis using a consumption reference signal while discarding reactive power production using a reference of zero value in the Q-axis.

The SMC-2 control law optimization of the SPVSI was carried out using PSO, MOGA, MODE, and MOASA algorithms. Before tuning the controller, the allowable values of the SMC-2 constants were determined based on the Lyapunov stability criterion. The multi-objective algorithms generated tuning constants that complied with the Lyapunov criterion.

In Chapter 5, the components of the experimental microgrid were detailed. This section described the characteristics of the different elements and equipment of the microgrid, considering the voltage, current, and operating power values. Furthermore, climate data on radiation was collected to establish the parameters for adjusting the proposed methods to improve the SPVSI's performance in active power generation. Finally, the Universitat Politècnica de València microgrid was considered to present a project at the Universidad de Las Américas in Ecuador. The objective is to leverage the institution's potential and foster future projects that develop other techniques in the field of microgrids and generate valuable research for academia. This collabora-

tion will facilitate exploration and advancement in microgrids, promoting the generation of significant and valuable knowledge for the academic community.

In Chapter 6, the results of the controllers developed in Chapter 4 are presented. The established control proposals were tested using PSCAD<sup>TM</sup> simulation software, while the multi-objective algorithms were implemented in MATLAB<sup>TM</sup>. The components of the laboratory microgrid were analyzed to adapt the PSCAD<sup>TM</sup> schemes and create an accurate simulation model compatible with the PI algorithm.

Real microgrid data was incorporated through various experiments, generating scenarios that involved interactions among the grid, load, and SPVSI. The SPVSI operated in different modes, supplying power to the load or feeding excess power back to the grid, depending on the experimental scenario. Voltage and current values of the microgrid elements, such as photovoltaic panels, charge controller, battery bank, SPVSI, and load, were analyzed.

This chapter provides insights into the microgrid's behavior under the multi-objective strategy using the PI and SMC-2 control methods. Performance indices, including IAE, ISE, ITAE, and ITSE, were used to evaluate the controllers' numerical performance.

This chapter's comprehensive analyses and evaluations contribute to a better understanding of the controllers' performance and suitability for specific applications. The findings offer valuable guidance for selecting the most appropriate control method for microgrid systems, aiding in decision-making processes and facilitating the optimization of microgrid operation.

Considering the case studies and based on all these conclusions, it is crucial to note that industrial SPVSIs can be improved from the perspective of closed-loop regulation. These inverters and their applications on residential microgrids will benefit from this research as the local consumption for small users is increasing yearly. The SMC-2 is a versatile algorithm that can be programmed on industrial inverters without affecting the processing time, as seen in (Gonzales-Zurita et al. 2023). The potential applications, as seen in (Escrivá-Escrivá et al. 2023) and its applications, can produce significant advances in microgrid trends in the following years.

## 7.2 Main Contributions

During the development of this thesis, the following contributions were accomplished:

- The design of the HOSMC is proposed for use in a fast dynamic system such as the SPVSI. In such converters, several authors have implemented the conventional SMC. The use of the HOSMC has been shown in the literature to avoid the effect of chattering on the control signal.
- To offer a wider path for tracking the active power reference, the sliding surface for the HOSMC has a new PI form. This new form leads to an increase in the robustness and stability of the SPVSI. It overcomes the problem of non-linearity presented in the dynamical equivalents of the SPVSI.
- An intelligent algorithm such as particle swarm optimization (PSO) tuned the parameters of the HOSMC. This approach offers a more efficient solution over heuristic methods, which are used in many SMC applications that do not consider optimal values for the controller's constants.
- The MOO techniques, such as MOGA, MODE, and MOASA, employed an optimization process of two conflicting objectives: rise time and overshoot. The optimum tuning constants of SMC-2 were obtained, considering the most suitable trade-off between both objectives.
- The establishment of a microgrid at Universidad de Las Américas will facilitate future research projects in the field of energy management. The basic components necessary for the microgrid's operation, whether connected to the main power grid or operated independently, have been integrated. Additionally, the microgrid is open to considering various improvements that could enhance its performance to produce future research in the energy generation field.
- The ramp reference values for active power generation in the grid-connected scheme are applied following the standard IEEE Std 1547-2018. Most works employ step references that do not consider the voltage and frequency stability in the grid for sudden changes in the power reference.

### 7.3 Future Developments

This thesis dissertation opens the gate to some future research developments that are suggested:

- Implementing other control methods for non-linear plants and fast dynamic conditions. In this way, other alternatives can be determined that may effectively regulate active power in microgrids. In this sense, varied MOO methods can also be used to consider another mathematical optimization approach. The MOO approach is comprehensive and is constantly being updated by considering improvements in the formulation and execution process. It should also be considered that with the computational advances of recent years, we are in the process of a technological revolution that generates equipment with advanced processors that can face the difficulties involved in solving a complex computational model.
- When applying other control methods, their stability analysis must also be reformulated. In this way, the tuning constants can be determined through multi-objective methods. In this subject, other alternatives can be seen that can set the stability conditions of the SPVSI together with its ability to face external phenomena, such as disturbances or uncertainties present in the microgrid.
- Also, alternatives can be considered to combine other objectives without making the algorithm more complex. Some approaches, such as PSO, group multiple objectives into a single mathematical formulation. This approach has its advantages and disadvantages, like multi-objective formulation methods. However, performance indices can be determined to evaluate whether single or multiple objective proposals are valid in improving electric power management in the microgrid.
- There are applications where reactive power management allows compensating for certain deficiencies in the energy management of the grid. These generators can inject reactive power to determine safe operating conditions in the grid, such as the voltage and frequency levels that must remain in a secure operating range without being affected by the different demand conditions presented by electricity consumers in a microgrid.
- From the different perspectives in this thesis, some future trends in microgrids are found: renewable energy integration, advances in energy storage, community microgrids or interconnection of microgrids, and energy management and control. The last one can be approached for works like the

one in this thesis to optimize the performance and efficiency of microgrids. In the future, more advanced software tools for energy management are expected to be developed, including artificial intelligence algorithms and machine learning.

## 7.4 Publications

During the development of this thesis, some of the results have been published or submitted in the following journals and conferences:

- Oscar Gonzales-Zurita, Jean-Michel Clairand, Elisa Peñalvo-López and Guillermo Escrivá-Escrivá, "Review on Multi-Objective Control Strategies for Distributed Generation on Inverter-Based Microgrids". In *MDPI Energies* (published on May 25th, 2020).
- Oscar Gonzales-Zurita, Jean-Michel Clairand, Guillermo Escrivá-Escrivá. "PSO Tuning of a Second Order Sliding Mode Controller to Adjust Active Standard Power Levels on a Single-Phase Voltage Source Inverter". In *2022 IEEE Power & Energy Society General Meeting* (published on July 17th, 2022).
- Oscar Gonzales-Zurita, Oscar Lasso Andino, Jean-Michel Clairand and Guillermo Escrivá-Escrivá. "PSO Tuning of a Second-Order Sliding Mode Controller for Adjusting Active Standard Power Levels for Smart Inverter Applications". In *IEEE Transactions on Smart Grid* (published on March 9th, 2023).
- Guillermo Escrivá-Escrivá, Oscar Gonzales-Zurita, Jean-Michel Clairand and Xavier Serrano-Guerrero. "Design and optimal tuning of a high-order sliding mode control for improving active power generation in microgrids based in single-phase inverters". In *International Meet on Power Electronics and Applications PEAMEET 2023* (accepted and presented on April 17th, 2023).
- Oscar Gonzales-Zurita, Guillermo Escrivá-Escrivá, Jean-Michel Clairand and Xavier Serrano-Guerrero. "Designing and Fine-Tuning a Second Order Sliding Mode Control to Enhance Conventional PI Control for Active Power Generation on Single-Phase Inverter-Based Microgrids". (*In progress*).

## Appendix A

# Microgrid at Universitat Politècnica de València

This section shows the microgrid's main components implemented at the Universitat Politècnica de València. The most representative features are shown as follows. Figure A.1 presents the battery's bank.



**Figure A.1:** Battery bank.

The battery bank comprises an array that produces 48 V and 300 Ah, as explained in Chapter 5. The charge controller of this array is presented in Figure A.2.



**Figure A.2:** Charge controller.

The charge controller was sized for the battery bank array. In addition, the PV panels are also connected to the charge controller, and they are shown in Figure A.3.

The PV panel array comprises nine units that produce 132 V, as explained in Chapter 5. Finally, the inverter *Xantrex* from *Schneider Electric company* is shown in Figure A.4.

The inverter's electrical data was also detailed in Chapter 5.





**Figure A.3:** PV panels.



**Figure A.4:** Inverter.



## Appendix B

# HOQ for microgrid implementation

This section shows the electrical scheme of HOQ followed to implement a microgrid at Universidad de Las Américas. The scheme is visualized in [Figure B.1](#).

QFD: Quality Function Deployment  
 Project: Development of a inverter-based microgrid  
 Revision: 01  
 Date: 01/05/2022

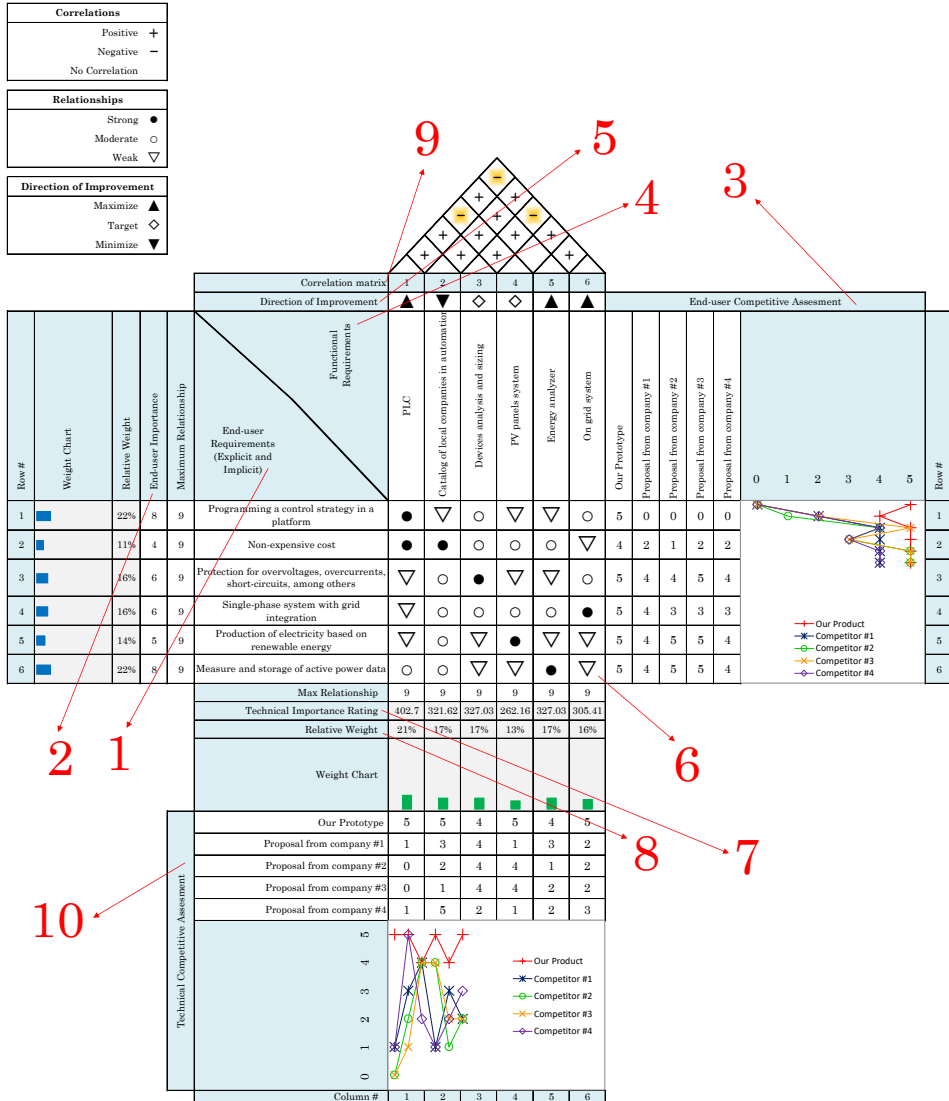


Figure B.1: HOQ of the inverted-based microgrid project

## Appendix C

# Microgrid at Universidad de Las Américas

This section shows the electrical scheme and photographs of the microgrid implemented at the Universidad de Las Américas. The electrical scheme is visualized in [Figure C.1](#).

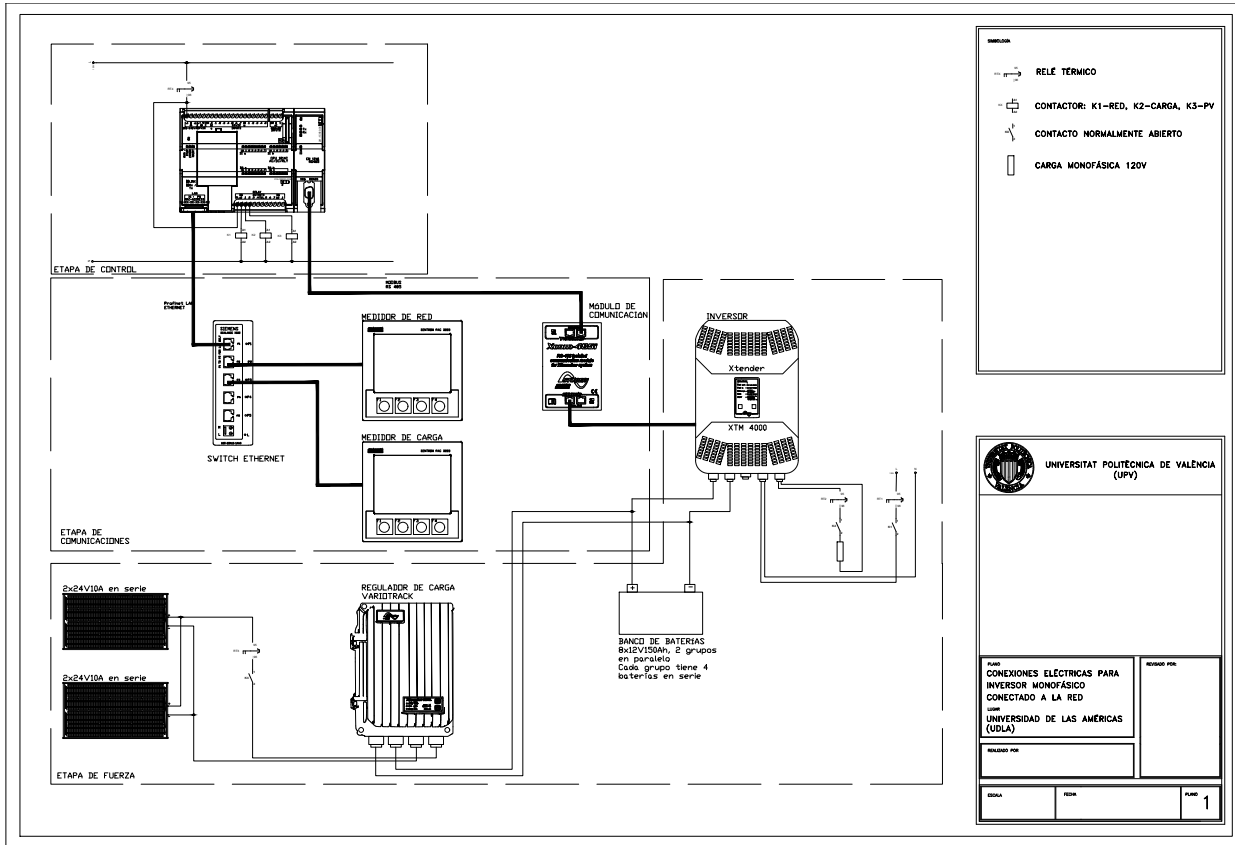
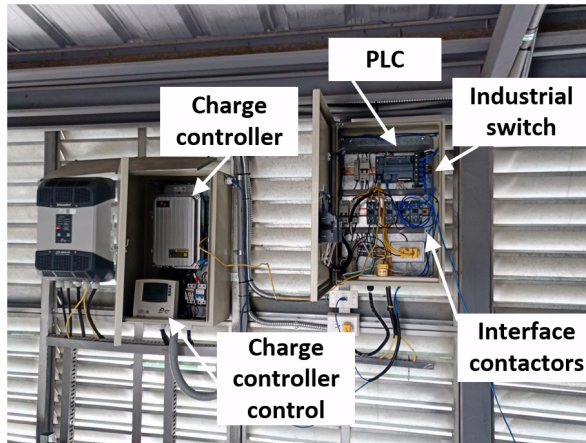


Figure C.1: Elements from the SPVSI scheme at Universidad de Las Américas.

---

Below are the images presenting the successful implementation of a microgrid on the Universidad de Las Américas terrace. These images in Figures C.2, C.3, and C.4 offer a comprehensive glimpse into the various components that constitute this microgrid. Notably, essential elements are observed such as the inverter, charge controller, controller (PLC), and a range of distinct connection interfaces, all contributing to the microgrid's robust functionality.



**Figure C.2:** Elements from the SPVSI part 1.

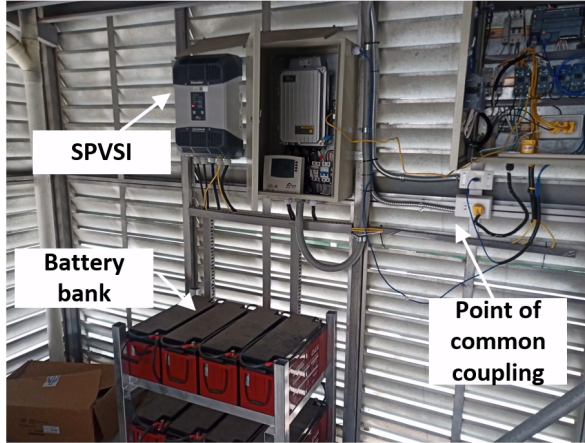


Figure C.3: Elements from the SPVSI part 2.

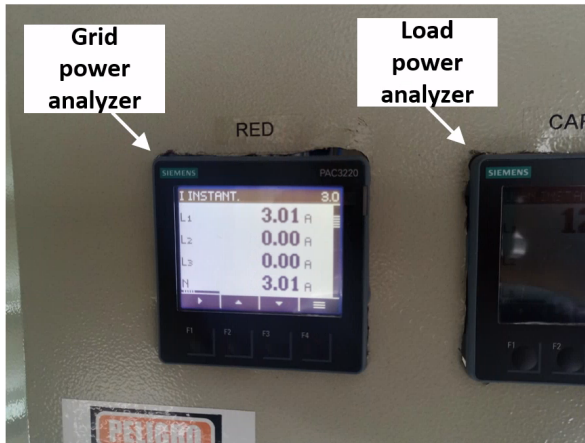


Figure C.4: Elements from the SPVSI (power meters).



# Bibliography

- Abhinav, Shankar et al. (2017). “Optimization-based AC microgrid synchronization”. In: *IEEE Transactions on Industrial Informatics* 13.5, pp. 2339–2349 (cit. on p. 12).
- Abobakr, Hossam et al. (2019). “Comparison of Egyptian standards for grid-connected photovoltaic power plants with IEC and IEEE standards: A case study in Egypt”. In: *Int. J. Adv. Sci. Technol.* 28.16, pp. 856–870 (cit. on p. 50).
- Akinyele, Daniel, Juri Belikov, and Yoash Levron (2018). “Challenges of microgrids in remote communities: A STEEP model application”. In: *Energies* 11.2, p. 432 (cit. on p. 12).
- Al-Ismail, Fahad Saleh (2021). “DC microgrid planning, operation, and control: A comprehensive review”. In: *IEEE Access* 9, pp. 36154–36172 (cit. on p. 15).
- Ali, Amjad et al. (2017). “Overview of current microgrid policies, incentives and barriers in the European Union, United States and China”. In: *Sustainability* 9.7, p. 1146 (cit. on pp. 44, 46).
- Alonso, Jose Alfonso (Jan. 2022). *Instalación Fotovoltaica Aislada*. es. <https://www.sfe-solar.com/noticias/articulos/calculo-sistema-fotovoltaico-aislado/>. Accessed: 2023-9-1 (cit. on p. 139).
- Alyazidi, Nezar M, Magdi S Mahmoud, and Mohammed I Abouheaf (2018). “Adaptive critics based cooperative control scheme for islanded microgrids”. In: *Neurocomputing* 272, pp. 532–541 (cit. on p. 65).
- Amoateng, David Ofori et al. (2017). “Adaptive voltage and frequency control of islanded multi-microgrids”. In: *IEEE Transactions on Power Systems* 33.4, pp. 4454–4465 (cit. on pp. 62, 76).

- Anbarasu, Elango, Adam Raja Basha, et al. (2020). “An improved power conditioning system for grid integration of solar power using ANFIS based FOPID controller”. In: *Microprocessors and Microsystems* 74, p. 103030 (cit. on p. 76).
- Andishgar, Mohammad Hadi, Eskandar Gholipour, and Rahmat-allah Hooshmand (2017). “An overview of control approaches of inverter-based microgrids in islanding mode of operation”. In: *Renewable and Sustainable Energy Reviews* 80, pp. 1043–1060 (cit. on pp. 13, 34, 55).
- Anoh, Kelvin et al. (2019). “Energy peer-to-peer trading in virtual microgrids in smart grids: A game-theoretic approach”. In: *IEEE Transactions on Smart Grid* 11.2, pp. 1264–1275 (cit. on p. 17).
- Arababadi, Reza et al. (2017). “Energy policy assessment at strategic, tactical, and operational levels: Case studies of EU 20-20-20 and US Executive Order 13514”. In: *Energy Policy* 109, pp. 530–538 (cit. on p. 43).
- Arbab-Zavar, Babak et al. (2019). “Smart inverters for microgrid applications: a review”. In: *Energies* 12.5, p. 840 (cit. on pp. 34, 35, 45).
- Arcos-Aviles, Diego et al. (2016). “Fuzzy logic-based energy management system design for residential grid-connected microgrids”. In: *IEEE Transactions on Smart Grid* 9.2, pp. 530–543 (cit. on p. 64).
- Baghaee, H. R. et al. (2018). “A Decentralized Robust Mixed  $H_2/H_\infty$  Voltage Control Scheme to Improve Small/Large-Signal Stability and FRT Capability of Islanded Multi-DER Microgrid Considering Load Disturbances”. In: *IEEE Systems Journal* 12.3, pp. 2610–2621 (cit. on p. 59).
- Baghaee, Hamid Reza et al. (2017a). “Decentralized sliding mode control of WG/PV/FC microgrids under unbalanced and nonlinear load conditions for on-and off-grid modes”. In: *IEEE Systems Journal* 12.4, pp. 3108–3119 (cit. on p. 63).
- Baghaee, Hamid Reza et al. (2017b). “Nonlinear load sharing and voltage compensation of microgrids based on harmonic power-flow calculations using radial basis function neural networks”. In: *IEEE systems journal* 12.3, pp. 2749–2759 (cit. on p. 66).
- Baghaee, HR et al. (2019). “OC/OL Protection of Droop-Controlled and Directly Voltage-Controlled Microgrids using TMF/ANN-based Fault Detection and Discrimination”. In: *IEEE Journal of Emerging and Selected Topics in Power Electronics* (cit. on p. 76).
- Baharizadeh, Mehdi, Hamid Reza Karshenas, and Josep M Guerrero (2018). “An improved power control strategy for hybrid AC-DC microgrids”. In: *International Journal of Electrical Power & Energy Systems* 95, pp. 364–373 (cit. on p. 35).
- Barik, Amar Kumar et al. (2019). “Optimal Load-Frequency Regulation of Demand Response Supported Isolated Hybrid Microgrid Using Fuzzy PD+ I Controller”. In: *International*

- 
- Conference on Innovation in Modern Science and Technology*. Springer, pp. 798–806 (cit. on pp. 74, 76).
- Bassey, Ogonnaya, Karen L Butler-Purry, and Bo Chen (2019). “Dynamic Modeling of Sequential Service Restoration in Islanded Single Master Microgrids”. In: *IEEE Transactions on Power Systems* (cit. on p. 72).
- Batiyah, Salem et al. (2020). “An MPC-based power management of standalone DC microgrid with energy storage”. In: *International Journal of Electrical Power & Energy Systems* 120, p. 105949 (cit. on p. 65).
- Benamar, Abdelkarim et al. (2020). “Non-Linear Control of a DC Microgrid for Electric Vehicle Charging Stations”. In: *International Journal on Advanced Science, Engineering and Information Technology* 10.2, pp. 593–598. ISSN: 2088-5334. DOI: 10.18517/ijaseit.10.2.10815. URL: [http://ijaseit.insightsociety.org/index.php?option=com\\_content&view=article&id=9&Itemid=1&article\\_id=10815](http://ijaseit.insightsociety.org/index.php?option=com_content&view=article&id=9&Itemid=1&article_id=10815) (cit. on p. 12).
- Benhalima, Seghir, Rezkallah Miloud, and Ambrish Chandra (2018). “Real-time implementation of robust control strategies based on sliding mode control for standalone microgrids supplying non-linear loads”. In: *Energies* 11.10, p. 2590 (cit. on p. 66).
- Bhutto, Ghulam Mustafa, Claus Leth Bak, and Ehsan Ali (2017). “Controlled operation of the islanded portion of the international council on large electric systems (CIGRE) low voltage distribution network”. In: *Energies* 10.7, p. 1021 (cit. on p. 11).
- Bonala, Anil Kumar and Srinivasa Rao Sandepudi (2018). “Centralised model-predictive decoupled active–reactive power control for three-level neutral point clamped photovoltaic inverter with preference selective index-based objective prioritisation”. In: *IET Power Electronics* 12.4, pp. 840–851 (cit. on p. 76).
- Bouزيد, Allal M et al. (2015). “A survey on control of electric power distributed generation systems for microgrid applications”. In: *Renewable and Sustainable Energy Reviews* 44, pp. 751–766 (cit. on p. 55).
- Buduma, Parusharamulu and Gayadhar Panda (2018). “Robust nested loop control scheme for LCL-filtered inverter-based DG unit in grid-connected and islanded modes”. In: *IET Renewable Power Generation* 12.11, pp. 1269–1285 (cit. on pp. 65, 76).
- Chandak, Sheetal and Pravat K Rout (2021). “The implementation framework of a microgrid: A review”. In: *International Journal of Energy Research* 45.3, pp. 3523–3547 (cit. on p. 49).
- Chang, En-Chih (2018). “Study and Application of Intelligent Sliding Mode Control for Voltage Source Inverters”. In: *Energies* 11.10, p. 2544 (cit. on pp. 58, 76).
- Chang, Kuo-Chi et al. (2021). “Standalone and minigrid-connected solar energy systems for rural application in Rwanda: an in situ study”. In: *International Journal of Photoenergy* 2021, pp. 1–22 (cit. on p. 16).

- Charles, Rhys G et al. (2019). “Sustainable energy storage for solar home systems in rural Sub-Saharan Africa—A comparative examination of lifecycle aspects of battery technologies for circular economy, with emphasis on the South African context”. In: *Energy* 166, pp. 1207–1215 (cit. on p. 23).
- Clairand, Jean-Michel et al. (2019a). “Long-Term Electric Vehicle Planning in a Microgrid”. In: *2019 IEEE Innovative Smart Grid Technologies-Asia (ISGT Asia)*. IEEE, pp. 3467–3472 (cit. on pp. 12, 30).
- Clairand, Jean-Michel et al. (2019b). “Microgrids as Electrification Alternatives for the Amazon Region in Ecuador”. In: *2019 IEEE Innovative Smart Grid Technologies-Asia (ISGT Asia)*. IEEE, pp. 4286–4291 (cit. on p. 11).
- Comission, California Public Utilities. *Rule 21 Interconnection*. Available online: <https://www.cpuc.ca.gov/Rule21/> (accessed on 28 April 2020) (cit. on p. 45).
- Costa-Carrapico, Ines, Rokia Raslan, and Javier Neila González (2020). “A systematic review of genetic algorithm-based multi-objective optimisation for building retrofitting strategies towards energy efficiency”. In: *Energy and Buildings* 210, p. 109690 (cit. on p. 118).
- Cubas, Javier, Santiago Pindado, and Carlos De Manuel (2014). “Explicit expressions for solar panel equivalent circuit parameters based on analytical formulation and the Lambert W-function”. In: *Energies* 7.7, pp. 4098–4115 (cit. on pp. 21, 22).
- Cui, Yunfei et al. (2017). “Multi-objective optimization methods and application in energy saving”. In: *Energy* 125, pp. 681–704 (cit. on pp. 57, 79–81, 83).
- Das, Dibakar, Gurunath Gurralla, and U Jayachandra Shenoy (2016). “Linear quadratic regulator-based bumpless transfer in microgrids”. In: *IEEE Transactions on Smart Grid* 9.1, pp. 416–425 (cit. on p. 59).
- Dehkordi, Nima Mahdian, Nasser Sadati, and Mohsen Hamzeh (2018). “Robust tuning of transient droop gains based on Kharitonov’s stability theorem in droop-controlled microgrids”. In: *IET Generation, Transmission & Distribution* 12.14, pp. 3495–3501 (cit. on pp. 74, 76).
- Electric, Schneider (Feb. 2023). *PowerLogic™ PM5000 series Technical Datasheet*. [https://download.schneider-electric.com/files?p\\_Doc\\_Ref=PLSED310052EN\\_Web&p\\_enDocType=Technical+leaflet&p\\_File\\_Name=PLSED310052EN\\_%28Web%29.pdf](https://download.schneider-electric.com/files?p_Doc_Ref=PLSED310052EN_Web&p_enDocType=Technical+leaflet&p_File_Name=PLSED310052EN_%28Web%29.pdf). Accessed: 2023-4-7 (cit. on p. 175).
- Elyoussef, Ebrahim Samer et al. (2012). “Super-twisting sliding modes tracking control of a nonholonomic wheeled mobile robot”. In: *IFAC Proceedings Volumes* 45.22, pp. 429–434 (cit. on p. 100).
- Enayati, Babak (2019). *Power Quality and Voltage Regulation in IEEE Std 1547-2018*. IEEE (cit. on pp. 164, 165).

- 
- ENF Ltd. *ENF Ltd.* <https://es.enfsolar.com/pv/panel-datasheet/crystalline/35238>. Accessed: 2023-4-2 (cit. on p. 132).
- Escrivá-Escrivá, Guillermo et al. (2023). “Design and Optimal Tuning of a High-Order Sliding Mode Control for Improving Active Power Generation in Micro Grids Based in Single-Phase Inverters”. In: *International Meet on Power Electronics and Applications PEAMEET 2023*, pp. 12–13 (cit. on p. 205).
- Fadlallah, Sulaiman O. and Djamal Eddine Benhadji Serradj (2020). “Determination of the optimal solar photovoltaic (PV) system for Sudan”. In: *Solar Energy* 208, pp. 800–813. ISSN: 0038-092X. DOI: <https://doi.org/10.1016/j.solener.2020.08.041>. URL: <https://www.sciencedirect.com/science/article/pii/S0038092X20308793> (cit. on p. 140).
- Fani, Bahador, Farshad Zandi, and Alireza Karami-Horestani (2018). “An enhanced decentralized reactive power sharing strategy for inverter-based microgrid”. In: *International Journal of Electrical Power & Energy Systems* 98, pp. 531–542 (cit. on p. 63).
- Farrokhabadi, Mostafa et al. (2019). “Microgrid stability definitions, analysis, and examples”. In: *IEEE Transactions on Power Systems* 35.1, pp. 13–29 (cit. on p. 35).
- Fathi, Abdolwahhab, Qobad Shafiee, and Hassan Bevrani (2018). “Robust frequency control of microgrids using an extended virtual synchronous generator”. In: *IEEE Transactions on Power Systems* 33.6, pp. 6289–6297 (cit. on pp. 62, 76).
- Fontenot, Hannah and Bing Dong (2019). “Modeling and control of building-integrated microgrids for optimal energy management—a review”. In: *Applied Energy* 254, p. 113689 (cit. on pp. 18, 28).
- Fridman, Leonid and Arie Levant (Jan. 2002). “Higher-Order Sliding Modes”. In: vol. 11, pp. 53–101. ISBN: 0-8247-0671-4. DOI: 10.1201/9780203910856.ch3 (cit. on pp. 98, 102, 104).
- Fuller, Sara (2018). “Configuring climate responsibility in the city: carbon footprints and climate justice in Hong Kong”. In: *Routledge handbook of climate justice*. Routledge, pp. 290–298 (cit. on p. 41).
- Gholami, Sasan, Sajeeb Saha, and Mohammad Aldeen (2018). “Robust multiobjective control method for power sharing among distributed energy resources in islanded microgrids with unbalanced and nonlinear loads”. In: *International Journal of Electrical Power & Energy Systems* 94, pp. 321–338 (cit. on p. 63).
- Ghosh, Subhrasankha and Souvik Chattopadhyay (2020). “Three-Loop-Based Universal Control Architecture for Decentralized Operation of Multiple Inverters in an Autonomous Grid-Interactive Microgrid”. In: *IEEE Transactions on Industry Applications* 56.2, pp. 1966–1979 (cit. on p. 13).

- Ginart, Antonio (2018). *Fault diagnosis for robust inverter power drives*. Institution of Engineering & Technology (cit. on p. 30).
- Gingerich, Daniel B, Yifan Zhao, and Meagan S Mauter (2019). “Environmentally significant shifts in trace element emissions from coal plants complying with the 1990 Clean Air Act Amendments”. In: *Energy Policy* 132, pp. 1206–1215 (cit. on p. 48).
- Gonzales, Oscar et al. (2019). “Sliding Mode Controller Applied to a Synchronous DC/DC Power Converter”. In: *The International Conference on Advances in Emerging Trends and Technologies*. Springer, pp. 121–130 (cit. on p. 58).
- Gonzales-Zurita, Oscar, Jean-Michel Clairand, and Guillermo Escrivá-Escrivá (2022). “PSO Tuning of a Second Order Sliding Mode Controller to Adjust Active Standard Power Levels on a Single-Phase Voltage Source Inverter”. In: *2022 IEEE Power & Energy Society General Meeting (PESGM)*, pp. 1–5. DOI: 10.1109/PESGM48719.2022.9917055 (cit. on p. 102).
- Gonzales-Zurita, Oscar et al. (2023). “PSO Tuning of a Second-Order Sliding Mode Controller for Adjusting Active Standard Power Levels for Smart Inverter Applications”. In: *IEEE Transactions on Smart Grid*, pp. 1–1. DOI: 10.1109/TSG.2023.3254908 (cit. on p. 205).
- Gonzales-Zurita, Óscar et al. (2020). “Review on Multi-Objective Control Strategies for Distributed Generation on Inverter-Based Microgrids”. In: *Energies* 13.13. ISSN: 1996-1073. DOI: 10.3390/en13133483. URL: <https://www.mdpi.com/1996-1073/13/13/3483> (cit. on p. 83).
- Groppi, Daniele et al. (2021). “A review on energy storage and demand side management solutions in smart energy islands”. In: *Renewable and Sustainable Energy Reviews* 135, p. 110183 (cit. on p. 16).
- Guerra, Noemi et al. (2018). “Operation and physics of photovoltaic solar cells: an overview”. In: *I+ D Tecnológico* 14.2, pp. 84–95 (cit. on p. 19).
- Gunantara, Nyoman (2018). “A review of multi-objective optimization: Methods and its applications”. In: *Cogent Engineering* 5.1, p. 1502242 (cit. on pp. 77, 81, 82, 85).
- Hariprakash, B et al. (Mar. 2001). “Ceria-Supported Platinum as Hydrogen-Oxygen Recombinant Catalyst for Sealed Lead-Acid Batteries”. In: *Electrochemical Solid State Letters* 4. DOI: 10.1149/1.1346537 (cit. on pp. 24, 25).
- Hossain, Md Alamgir et al. (2019). “Modified PSO algorithm for real-time energy management in grid-connected microgrids”. In: *Renewable energy* 136, pp. 746–757 (cit. on p. 54).
- Hou, Xiaochao et al. (2018). “Distributed hierarchical control of AC microgrid operating in grid-connected, islanded and their transition modes”. In: *Ieee Access* 6, pp. 77388–77401 (cit. on p. 36).

- Huaman Loayza, Alex Smith and Carlos Gustavo Pérez Zuñiga (2019). “Design of a Fuzzy Sliding Mode Controller for the Autonomous Path-Following of a Quadrotor”. In: *IEEE Latin America Transactions* 17.06, pp. 962–971. DOI: 10.1109/TLA.2019.8896819 (cit. on p. 121).
- Jain, Trapti et al. (2017). “Robust optimal centralized controller to mitigate the small signal instability in an islanded inverter based microgrid with active and passive loads”. In: *International Journal of Electrical Power & Energy Systems* 90, pp. 225–236 (cit. on p. 74).
- Katircioğlu, Salih et al. (2019). “Volatility of the alternative energy input prices and spillover effects: a VAR [MA]-MGARCH in BEKK approach for the Turkish economy”. In: *Environmental Science and Pollution Research* 26.11, pp. 10738–10745 (cit. on p. 11).
- Kerdphol, Thongchart, Fathin Saifur Rahman, and Yasunori Mitani (2018). “Virtual inertia control application to enhance frequency stability of interconnected power systems with high renewable energy penetration”. In: *Energies* 11.4, p. 981 (cit. on pp. 13, 54, 60).
- Kerdphol, Thongchart et al. (2017). “Virtual inertia control-based model predictive control for microgrid frequency stabilization considering high renewable energy integration”. In: *Sustainability* 9.5, p. 773 (cit. on pp. 34, 76).
- Khatibzadeh, Ahmadali et al. (2017). “Multi-agent-based controller for voltage enhancement in AC/DC hybrid microgrid using energy storages”. In: *Energies* 10.2, p. 169 (cit. on p. 12).
- Khayat, Yousef et al. (2018). “Decentralized optimal frequency control in autonomous microgrids”. In: *IEEE Transactions on Power Systems* 34.3, pp. 2345–2353 (cit. on p. 64).
- Kirankumar, B, YV Siva Reddy, and M Vijayakumar (2017). “Multilevel inverter with space vector modulation: intelligence direct torque control of induction motor”. In: *IET Power Electronics* 10.10, pp. 1129–1137 (cit. on p. 76).
- Kong, Xiaobing et al. (2019). “Hierarchical distributed model predictive control of stand-alone wind/solar/battery power system”. In: *IEEE Transactions on Systems, Man, and Cybernetics: Systems* 49.8, pp. 1570–1581 (cit. on p. 23).
- Kundur, Prabha, Neal J Balu, and Mark G Lauby (1994). *Power system stability and control*. Vol. 7. McGraw-hill New York (cit. on p. 37).
- Lai, Xinjie et al. (2019). “A multi-objective artificial sheep algorithm”. In: *Neural Computing and Applications* 31, pp. 4049–4083 (cit. on p. 122).
- Lakshmi, M and S Hemamalini (2017). “Nonisolated high gain DC–DC converter for DC microgrids”. In: *IEEE Transactions on Industrial Electronics* 65.2, pp. 1205–1212 (cit. on p. 12).

- Lee, Jin Hwan et al. (2018). “Particle Swarm Optimization Algorithm With Intelligent Particle Number Control for Optimal Design of Electric Machines”. In: *IEEE Transactions on Industrial Electronics* 65.2, pp. 1791–1798. ISSN: 1557-9948. DOI: 10.1109/TIE.2017.2760838 (cit. on p. 101).
- Lee, Munsu et al. (2020). “An analysis of battery degradation in the integrated energy storage system with solar photovoltaic generation”. In: *Electronics* 9.4, p. 701 (cit. on p. 24).
- Lenhart, Stephanie and Kathleen Araújo (2021). “Microgrid decision-making by public power utilities in the United States: A critical assessment of adoption and technological profiles”. In: *Renewable and Sustainable Energy Reviews* 139, p. 110692 (cit. on p. 10).
- Li, Baojie et al. (2021). “Evaluation and improvement of IEC 60891 correction methods for IV curves of defective photovoltaic panels”. In: *Solar Energy* 216, pp. 225–237 (cit. on p. 22).
- Li, Zhongwen et al. (2017). “Control of a Grid-Forming Inverter Based on Sliding-Mode and Mixed H<sub>2</sub>/H Control”. In: *IEEE TRANSACTIONS ON INDUSTRIAL ELECTRONICS* 64.5 (cit. on pp. 54, 62, 76).
- Liobikienė, Genovaitė and Mindaugas Butkus (2017). “The European Union possibilities to achieve targets of Europe 2020 and Paris agreement climate policy”. In: *Renewable Energy* 106, pp. 298–309 (cit. on p. 47).
- Luo, Fang Lin and Hong Ye (2017). *Advanced DC/AC inverters: applications in renewable energy*. Crc Press (cit. on pp. 27, 28).
- Marler, R Timothy and Jasbir S Arora (2004). “Survey of multi-objective optimization methods for engineering”. In: *Structural and multidisciplinary optimization* 26, pp. 369–395 (cit. on pp. 78, 79, 84).
- Miao, Ai Qin, Min Zhao, and Decheng Wan (2020). “CFD-based multi-objective optimisation of S60 Catamaran considering Demihull shape and separation”. In: *Applied Ocean Research* 97, p. 102071 (cit. on p. 72).
- Miveh, Mohammad Reza et al. (2016). “Control techniques for three-phase four-leg voltage source inverters in autonomous microgrids: A review”. In: *Renewable and Sustainable Energy Reviews* 54, pp. 1592–1610 (cit. on pp. 34, 54).
- Mohapatra, Soumya Ranjan and Vivek Agarwal (2019). “Model Predictive Control for Flexible Reduction of Active Power Oscillation in Grid-tied Multilevel Inverters under Unbalanced and Distorted Microgrid Conditions”. In: *IEEE Transactions on Industry Applications* (cit. on p. 13).
- Mousavi, Seyyed Yousef Mousazadeh et al. (2018). “Autonomous control of current-and voltage-controlled dg interface inverters for reactive power sharing and harmonics compensation in islanded microgrids”. In: *IEEE Transactions on Power Electronics* 33.11, pp. 9375–9386 (cit. on p. 63).



- Murty, VVSN and Ashwani Kumar (2020). “Multi-objective energy management in microgrids with hybrid energy sources and battery energy storage systems”. In: *Protection and Control of Modern Power Systems* 5.1, pp. 1–20 (cit. on p. 11).
- Nguyen, Hung Khanh, Amin Khodaei, and Zhu Han (2017). “Incentive mechanism design for integrated microgrids in peak ramp minimization problem”. In: *IEEE Transactions on Smart Grid* 9.6, pp. 5774–5785 (cit. on p. 59).
- Ogata, Katsuhiko (2010). *Modern control engineering fifth edition* (cit. on p. 91).
- Oldenhuis, Rody (2022). *GODLIKE - A robust single- $\ell_3$  multi-objective optimizer* (<https://github.com/ro-oldenhuis/GODLIKE/releases/tag/v1.5>), *GitHub*. URL: <https://la.mathworks.com/matlabcentral/fileexchange/24838-godlike-a-robust-single-multi-objective-optimizer> (cit. on pp. 115, 118).
- Olivares, Daniel E et al. (2014). “Trends in microgrid control”. In: *IEEE Transactions on smart grid* 5.4, pp. 1905–1919 (cit. on pp. 11, 33).
- Panda, Sambit Kumar and Arnab Ghosh (2020). “A Computational Analysis of Interfacing Converters with Advanced Control Methodologies for Microgrid Application”. In: *Technology and Economics of Smart Grids and Sustainable Energy* 5.1, pp. 1–18 (cit. on p. 60).
- Patarroyo-Montenegro, Juan F, John E Salazar-Duque, and Fabio Andrade (2018). “LQR Controller with Optimal Reference Tracking for Inverter-Based Generators on Islanded-Mode Microgrids”. In: *2018 IEEE ANDESCON*. IEEE, pp. 1–5 (cit. on p. 13).
- Periyamayagam, Madasamy et al. (2020). “A modified high voltage gain quasi-impedance source coupled inductor multilevel inverter for photovoltaic application”. In: *Energies* 13.4, p. 874 (cit. on p. 28).
- Peters, Glen P et al. (2020). “Carbon dioxide emissions continue to grow amidst slowly emerging climate policies”. In: *Nature Climate Change* 10.1, pp. 3–6 (cit. on pp. 39, 40).
- Photovoltaics, Distributed Generation and Energy Storage (2018). “IEEE standard for interconnection and interoperability of distributed energy resources with associated electric power systems interfaces”. In: *IEEE Std*, pp. 1547–2018 (cit. on p. 45).
- Pickering, Jonathan et al. (2018). “The impact of the US retreat from the Paris Agreement: Kyoto revisited?”. In: *Climate policy* 18.7, pp. 818–827 (cit. on p. 41).
- Reyna, Emily (2014). *California Carbon Market Watch: A Comprehensive Analysis of the Golden State’s Cap-and-Trade Program, Year One-2012-2013*. Available online: <https://www.issuelab.org/resource/california-carbon-market-watch-a-comprehensive-analysis-of-the-golden-state-s-cap-and-trade-program-year-one-2012-2013.html>(accessed on 21 May 2020) (cit. on p. 66).

- Rodrigues, Yuri R, AC Zambroni de Souza, and PF Ribeiro (2018). “An inclusive methodology for Plug-in electrical vehicle operation with G2V and V2G in smart microgrid environments”. In: *International Journal of Electrical Power & Energy Systems* 102, pp. 312–323 (cit. on p. 13).
- Rokrok, Ebrahim, Miadreza Shafie-Khah, and João PS Catalão (2018). “Review of primary voltage and frequency control methods for inverter-based islanded microgrids with distributed generation”. In: *Renewable and Sustainable Energy Reviews* 82, pp. 3225–3235 (cit. on pp. 38, 54).
- Roosa, Stephen A (2020a). *Fundamentals of Microgrids: Development and Implementation*. CRC Press (cit. on p. 14).
- (2020b). “Introduction to Microgrids”. In: *Fundamentals of Microgrids*. CRC Press, pp. 1–16 (cit. on p. 17).
- (2020c). “Microgrid Architecture and Regulation”. In: *Fundamentals of Microgrids*. CRC Press, pp. 71–90 (cit. on p. 49).
- Rosewater, David Martin et al. (2016). *SIRFN Draft Test Protocols for Advanced Battery Energy Storage System Interoperability Functions*. Tech. rep. Sandia National Lab.(SNL-NM), Albuquerque, NM (United States) (cit. on p. 153).
- Ross, Michael et al. (2015). “Multiobjective optimization dispatch for microgrids with a high penetration of renewable generation”. In: *IEEE Transactions on Sustainable Energy* 6.4, pp. 1306–1314 (cit. on pp. 56, 58).
- Sadan, Nachum and Bruce Renz (2020). “New DER Communications Platform Enables DERMS and Conforms with IEEE 1547–2018 Requirements”. In: *2020 IEEE/PES Transmission and Distribution Conference and Exposition (T&D)*. IEEE, pp. 1–5 (cit. on p. 49).
- Saeed, Muhammad Hammad et al. (2021). “A review on microgrids’ challenges & perspectives”. In: *IEEE Access* 9, pp. 166502–166517 (cit. on p. 56).
- Safa, Ahmed et al. (2018). “A robust control algorithm for a multifunctional grid tied inverter to enhance the power quality of a microgrid under unbalanced conditions”. In: *International Journal of Electrical Power & Energy Systems* 100, pp. 253–264 (cit. on p. 13).
- Safari, Amin, Farshad Babaei, and Meisam Farrokhifar (2019). “A load frequency control using a PSO-based ANN for micro-grids in the presence of electric vehicles”. In: *International Journal of Ambient Energy*, pp. 1–13 (cit. on p. 54).
- Saha, Sajeeb et al. (2022). “A comparative study of commonly used batteries in household rooftop solar battery systems based on test data of commercial batteries”. In: *Sustainable Energy Technologies and Assessments* 52, p. 102252 (cit. on p. 24).

- Samavati, E and HR Mohammadi (2019). “Simultaneous voltage and current harmonics compensation in islanded/grid-connected microgrids using virtual impedance concept”. In: *Sustainable Energy, Grids and Networks* 20, p. 100258 (cit. on p. 60).
- Santos, Adriano A. and Ant3nio Ferreira da Silva (2021). “Simulation and Control of a Cyber-Physical System under IEC 61499 Standard”. In: *Procedia Manufacturing* 55. FAIM 2021, pp. 72–79. ISSN: 2351-9789. DOI: <https://doi.org/10.1016/j.promfg.2021.10.011>. URL: <https://www.sciencedirect.com/science/article/pii/S2351978921002080> (cit. on p. 143).
- Sarmiento Paute, Alex Fabricio (2020). “Adquisici3n y visualizaci3n de par3metros el3ctricos de un motor trif3sico mediante el uso de un m3dulo de internet industrial de las cosas”. B.S. thesis. Universidad del Azuay (cit. on p. 144).
- Sedighzadeh, Mostafa, Masoud Esmaili, and Amir Eisapour-Moarref (2017). “Voltage and frequency regulation in autonomous microgrids using Hybrid Big Bang-Big Crunch algorithm”. In: *Applied Soft Computing* 52, pp. 176–189 (cit. on p. 72).
- Seeley, Christopher Charles and Shobhakar Dhakal (2021). “Energy Efficiency Retrofits in Commercial Buildings: An Environmental, Financial, and Technical Analysis of Case Studies in Thailand”. In: *Energies* 14.9, p. 2571 (cit. on p. 42).
- Serban, Emanuel (Feb. 2011). “Ac connected modules with line frequency or voltage variation pattern for energy control”. Pat. 2011022265:A1 (cit. on p. 152).
- Serban, Ioan and Catalin Petrea Ion (2017). “Microgrid control based on a grid-forming inverter operating as virtual synchronous generator with enhanced dynamic response capability”. In: *International Journal of Electrical Power & Energy Systems* 89, pp. 94–105 (cit. on p. 88).
- Shaikh, M. S. (2017). “A Review Paper on Electricity Generation from Solar Energy”. In: *International Journal for Research in Applied Science and Engineering Technology*, pp. 1884–1889 (cit. on p. 18).
- Shen, Xueqiang et al. (2019). “Distributed secondary voltage control of islanded microgrids based on RBF-neural-network sliding-mode technique”. In: *IEEE Access* 7, pp. 65616–65623 (cit. on pp. 31, 33, 59, 76).
- Shi, Kai et al. (2018a). “Virtual inertia control strategy in microgrid based on virtual synchronous generator technology”. In: *IEEE Access* 6, pp. 27949–27957 (cit. on pp. 61, 76).
- Shi, Rongliang et al. (2018b). “Self-tuning virtual synchronous generator control for improving frequency stability in autonomous photovoltaic-diesel microgrids”. In: *Journal of Modern Power Systems and Clean Energy* 6.3, pp. 482–494 (cit. on pp. 36, 37).

- Shokoohi, Shores et al. (2018). “Intelligent secondary control in smart microgrids: an on-line approach for islanded operations”. In: *Optimization and Engineering* 19.4, pp. 917–936 (cit. on p. 54).
- Shuai, Zhikang et al. (2018). “Hierarchical structure and bus voltage control of DC microgrid”. In: *Renewable and Sustainable Energy Reviews* 82, pp. 3670–3682 (cit. on p. 38).
- Sood, Vijay K and Haytham Abdelgawad (2019). “Microgrids architectures”. In: *Distributed Energy Resources in Microgrids*. Elsevier, pp. 1–31 (cit. on p. 11).
- Sopinka, Amy and Lawrence Pitt (2013). “British Columbia Electricity Supply Gap Strategy: A Redefinition of Self-Sufficiency”. In: *The Electricity Journal* 26.3, pp. 81–88 (cit. on pp. 62, 63).
- Stanev, Rad and Kamen Nakov (2020). “Power System Stabilizers for Inverter Dominated Future Power Systems”. In: *2020 21st International Symposium on Electrical Apparatus Technologies (SIELA)*, pp. 1–8. DOI: 10.1109/SIELA49118.2020.9167134 (cit. on p. 141).
- Steiner, Marc and Gerald Siefer (2023). “Translation of outdoor tandem PV module I–V measurements to a STC power rating”. In: *Progress in Photovoltaics: Research and Applications* (cit. on p. 20).
- Sullivan, Michael J, Matthew Mercurio, and Josh Schellenberg (2009). *Estimated value of service reliability for electric utility customers in the United States*. Tech. rep. Lawrence Berkeley National Lab.(LBNL), Berkeley, CA (United States) (cit. on p. 61).
- Sultani, Jasim Farhood (2013). “Modelling, Design and Implementation of DQ Control in Single-Phase Grid-Connected Inverters for Photovoltaic Systems used in Domestic Dwellings.” In: (cit. on p. 103).
- Tavakoli, Mehdi et al. (2018). “A two stage hierarchical control approach for the optimal energy management in commercial building microgrids based on local wind power and PEVs”. In: *Sustainable Cities and Society* 41, pp. 332–340 (cit. on p. 35).
- Teekaraman, Yuvaraja, Ramya Kuppasamy, and Srete Nikolovski (2019). “Solution for voltage and frequency regulation in standalone microgrid using hybrid multiobjective symbiotic organism search algorithm”. In: *Energies* 12.14, p. 2812 (cit. on pp. 68, 69).
- Toub, Mohamed et al. (2019). “Droop control in DQ coordinates for fixed frequency inverter-based AC microgrids”. In: *Electronics* 8.10, p. 1168 (cit. on p. 38).
- Tran, Thuy Vi, Seung-Jin Yoon, and Kyeong-Hwa Kim (2018). “An LQR-based controller design for an LCL-filtered grid-connected inverter in discrete-time state-space under distorted grid environment”. In: *Energies* 11.8, p. 2062 (cit. on p. 76).

- Van Veldhuizen, David A, Gary B Lamont, et al. (1998). “Evolutionary computation and convergence to a pareto front”. In: *Late breaking papers at the genetic programming 1998 conference*. Citeseer, pp. 221–228 (cit. on pp. 67, 68).
- Vásquez, Virgilio et al. (2017). “Comparison of methods for controllers design of single phase inverter operating in island mode in a microgrid”. In: *Renewable and Sustainable Energy Reviews* 76, pp. 256–267 (cit. on pp. 29, 30).
- Vinayagam, Arangarajan et al. (2018). “Intelligent control strategy in the islanded network of a solar PV microgrid”. In: *Electric Power Systems Research* 155, pp. 93–103 (cit. on p. 76).
- Wang, Lizhi et al. (2020). “Software-defined microgrid control: The genesis of decoupled cyber-physical microgrids”. In: *IEEE Open Access Journal of Power and Energy* 7, pp. 173–182 (cit. on p. 27).
- Wang, Yao et al. (2022). “A DC series arc fault detection method based on a lightweight convolutional neural network used in photovoltaic system”. In: *Energies* 15.8, p. 2877 (cit. on p. 165).
- Warren (Apr. 2022). *Don't settle for less: Calculate solar panel efficiency*. en. <https://heliushub.com/solar-panel-efficiency-calculation/>. Accessed: 2023-4-2 (cit. on p. 132).
- What is a microgrid?* (Jan. 2015). en. <https://neosun.com/what-is-a-microgrid/>. Accessed: 2023-6-13 (cit. on p. 11).
- Wu, Ying et al. (2019). “Bumpless Optimal Control over Multi-Objective Microgrids with Mode-Dependent Controllers”. In: *Energies* 12.19, p. 3619 (cit. on p. 71).
- Xiao, Zhao-xia et al. (2018). “Flat tie-line power scheduling control of grid-connected hybrid microgrids”. In: *Applied Energy* 210, pp. 786–799 (cit. on p. 59).
- Xu, Jinming et al. (2019). “Harmonics and Stability Analysis of Single-Phase Grid-Connected Inverters in Distributed Power Generation Systems Considering Phase-Locked Loop Impact”. In: *IEEE Transactions on Sustainable Energy* 10.3, pp. 1470–1480. ISSN: 1949-3037. DOI: 10.1109/TSTE.2019.2893679 (cit. on p. 89).
- Xu, Litong et al. (2020). “Dual synchronous rotating frame current control of brushless doubly fed induction generator under unbalanced network”. In: *IEEE Transactions on Power Electronics* 36.6, pp. 6712–6724 (cit. on p. 102).
- Yang, Fangfang et al. (2020). “State-of-charge estimation of lithium-ion batteries using LSTM and UKF”. In: *Energy* 201, p. 117664 (cit. on p. 25).
- Yang, Li et al. (2019). “Adjustable virtual inertia control of supercapacitors in PV-based AC microgrid cluster”. In: *Electric Power Systems Research* 173, pp. 71–85 (cit. on p. 35).

- Yang, Qingqing et al. (2017). “New ANN method for multi-terminal HVDC protection relaying”. In: *Electric Power Systems Research* 148, pp. 192–201 (cit. on p. 76).
- Yang, Yongheng et al. (2018). *Advances in grid-connected photovoltaic power conversion systems*. Woodhead Publishing (cit. on pp. 18–20).
- Yazdi, F and SH Hosseini (2019). “A novel “Smart Branch” for power quality improvement in microgrids”. In: *International Journal of Electrical Power & Energy Systems* 110, pp. 161–170 (cit. on p. 72).
- Ye, Jie et al. (2020). “Accurate harmonic calculation for digital SPWM of VSI with dead-time effect”. In: *IEEE Transactions on Power Electronics* 36.7, pp. 7892–7902 (cit. on p. 32).
- Yoldaş, Yeliz et al. (2017). “Enhancing smart grid with microgrids: Challenges and opportunities”. In: *Renewable and Sustainable Energy Reviews* 72, pp. 205–214 (cit. on p. 35).
- Yu, Xinghuo, Yong Feng, and Zhihong Man (2021). “Terminal Sliding Mode Control – An Overview”. In: *IEEE Open Journal of the Industrial Electronics Society* 2, pp. 36–52. DOI: 10.1109/OJIES.2020.3040412 (cit. on p. 98).
- Zeng, Zheng et al. (2016). “Multi-objective control of multi-functional grid-connected inverter for renewable energy integration and power quality service”. In: *IET Power Electronics* 9.4, pp. 761–770 (cit. on pp. 68, 70).
- Zhang, Liang et al. (2019). “Research on the Operation Control Strategy of a Low-Voltage Direct Current Microgrid Based on a Disturbance Observer and Neural Network Adaptive Control Algorithm”. In: *Energies* 12.6, p. 1162 (cit. on pp. 60, 76).
- Zhu, Kunlong et al. (2019). “Frequency-Division Virtual Impedance Shaping Control Method for Grid-Connected Inverters in a Weak and Distorted Grid”. In: *IEEE Transactions on Power Electronics* (cit. on p. 60).
- Ziouani, Islam et al. (2018). “Hierarchical control for flexible microgrid based on three-phase voltage source inverters operated in parallel”. In: *International Journal of Electrical Power & Energy Systems* 95, pp. 188–201 (cit. on p. 13).